VOLUME 116 NUMBER 3

THE ASTROPHYSICAL JOURNAL

AN INTERNATIONAL REVIEW OF SPECTROSCOPY AND ASTRONOMICAL PHYSICS

NOVEMBER 1952

THE LIFETIME OF THE $2S_{1/2}$ STATE OF HYDROGEN IN AN IONIZED ATMOSPHERE
E. M. Purcell 457
INHOMOGENEOUS STELLAR MODELS. II. MODELS WITH EXHAUSTED CORES IN GRAVITATIONAL CONTRACTION . . . . . *A. R. Sandage and M. Schwarzschild* 463
THE TRANSFER OF RADIATION BY AN EMITTING ATMOSPHERE *Henry G. Hertz* 477
TRANSFER THEORY FOR PURELY PRESSURE-BROADENED BAND SPECTRA
Jean I. King 491
THE LOW-TEMPERATURE SPECTRUM OF HD 45910 . . . . . *Paul W. Merrill* 498
MEASUREMENTS IN THE SPECTRA OF TEN SHELL STARS *Paul W. Merrill* 501
OSCILLATIONS IN THE SHELL STAR HD 33232 . . . . . *Paul W. Merrill* 516
SPECTROGRAMS OF TEN HIGH-VELOCITY Me VARIABLE STARS *Paul W. Merrill* 523
INTENSITIES OF ATOMIC ABSORPTION LINES IN THE SPECTRA OF LONG-PERIOD VARIABLE STARS . . . . . *William Buscombe and Paul W. Merrill* 525
A NEW SPECTRUM VARIABLE OF SHORT PERIOD, HD 124224 . . *Armin J. Deutsch* 536
NOTES ON THE SPECTRUM OF GAMMA URSAE MINORIS . . . *Harold P. Wemer* 541
RADIAL VELOCITIES OF 31 CYGNI DURING ATMOSPHERIC ECLIPSE
Dean B. McLaughlin 546
THE SOLAR SPECTRUM FROM 7μ to 13μ *J. H. Shaw, M. L. Oxholm, and H. H. Claassen* 554
STATISTICS OF STELLAR COLOR EXCESSES. I . . . . . *Guido Münch* 575
DETERMINATIONS OF COLOR CLASSES FOR 204 STARS OF LARGE PROPER MOTION . . . . . *E. F. Carpenter, A. J. Deutsch, and W. J. Luyten* 587
STELLAR SPECTRA AND COLORS IN CYGNUS AT GALACTIC LATITUDE $+16°$
Donald A. Mackie 592
SPECTRAL-TYPE, MAGNITUDE, AND COLOR-INDEX RELATIONS IN THE GALACTIC STAR CLUSTER IN COMA BERENICES . . . . . *Harold F. Weaver* 612
PRAESEPE: MAGNITUDES AND COLORS . . . . . *Harold L. Johnson* 640
NOTES
THE REACTION RATE OF THE PROTON-PROTON CHAIN . . . . . *E. E. Salpeter* 649
THE MOTIONS OF HIGH-VELOCITY INTERSTELLAR CLOUDS . . . . . *Leonard Searle* 650
A NEW INFRARED BAND SYSTEM OF *FeO* . . . . . *A. M. Bass and W. S. Benedict* 652
RADIAL VELOCITIES OF Z SCULPTORIS, ξ PHOENICIS, AND β CRUCIS
Jorge Sahade and Julio Altamirano 654
ERRATA 656
INDEX 657

THE UNIVERSITY OF CHICAGO PRESS
CHICAGO, ILLINOIS, U.S.A.

November 1952 Vol. 116, No. 3

THE ASTROPHYSICAL JOURNAL

AN INTERNATIONAL REVIEW OF SPECTROSCOPY AND ASTRONOMICAL PHYSICS

Published in Collaboration with the American Astronomical Society

S. CHANDRASEKHAR
Managing Editor

GERARD P. KUIPER
Associate Editor

Yerkes Observatory of the University of Chicago

EDITORIAL BOARD

O. HERZBERG (1951-56)
National Research Council, Ottawa

C. D. SHANE (1952-58)
Lick Observatory, University of California

FRED L. WHIPPLE (1951-56)
Harvard College Observatory

LYMAN SPITZER, JR. (1951-57)
Princeton University Observatory

PAUL W. MERRILL (1952)
Mount Wilson Observatory of the Carnegie Institution of Washington

---

The Astrophysical Journal is published bimonthly by the University of Chicago at the University of Chicago Press, 5750 Ellis Avenue, Chicago 37, Illinois, during January, March, May, July, September, and November. ¶Two volumes are published per year, one beginning with the January issue and the other beginning with the July issue. The subscription price is $6.00 per volume or $12.00 per year; the price of single copies is $3.00. (Orders for service of less than a volume will be charged at the single copy rate.) ¶Postage is prepaid by the publishers on all orders from the United States and its possessions. No extra charge is made for postage to countries in the Pan American Postal Union. ¶Postage is charged extra as follows: for Canada, 20 cents per volume, 40 cents per year (total $6.20 per volume, $12.40 per year); on single copies 5 cents (total $3.05); for all other countries in the Postal Union, 40 cents per volume, 75 cents per year (total $6.40 per volume, $12.75 per year), on single copies 10 cents (total $3.10). ¶Subscriptions are payable in advance. Please make all remittances payable to The University of Chicago Press, in United States currency or its equivalent by postal or express money orders or bank drafts.

The following is an authorized agent:

For the British Empire, except North America and Australasia: The Cambridge University Press, Bentley House, 200 Euston Road, London, N.W. 1, England. Prices of yearly subscriptions and of single copies may be had on application.

Claims for missing numbers should be made within the month following the regular month of publication. The publishers expect to supply missing numbers free only when losses have been sustained in transit, and when the reserve stock will permit.

Business correspondence should be addressed to The University of Chicago Press, Chicago 37, Illinois. Communications for the editors and manuscripts should be addressed to: S. Chandrasekhar, Editor of THE ASTROPHYSICAL JOURNAL, Yerkes Observatory, Williams Bay, Wisconsin.

Line drawings and photographs should be made by the author, and all marginal notes such as co-ordinates, wave lengths, etc., should be included in the cuts. It will not be possible to set up such material in type.

One copy of the corrected galley proof should be returned as soon as possible to the editor, Yerkes Observatory, Williams Bay, Wisconsin. Authors should take notice that the manuscript will not be sent to them with the proof.

The cable address is "Observatory, Williamsbay, Wisconsin."

The articles in this journal are indexed in the *International Index to Periodicals*, New York, N.Y.

Applications for permission to quote from this journal should be addressed to The University of Chicago Press, and will be freely granted.

Microfilms of complete journal volumes are available to regular subscribers only and may be obtained at the end of the year. Orders and inquiries should be addressed to University Microfilms, 313 North First Street, Ann Arbor, Michigan.

Notice to subscribers: If you change your address, please notify us and your local postmaster immediately.

Entered as second-class matter, July 21, 1900, at the Post-Office at Chicago, Ill., under the Act of March 3, 1879.

Acceptance for mailing at special rate of postage provided for in United States Postal Act of October 3, 1917, Section 1103, amended February 28, 1925.

[illegible]

THE ASTROPHYSICAL JOURNAL

AN INTERNATIONAL REVIEW OF SPECTROSCOPY AND ASTRONOMICAL PHYSICS

VOLUME 116 NOVEMBER 1952 NUMBER 3

THE LIFETIME OF THE $2^2S_{1/2}$ STATE OF HYDROGEN IN AN IONIZED ATMOSPHERE

E. M. PURCELL

Lyman Laboratory, Harvard University

Received July 7, 1952

ABSTRACT

The probability of the transitions $2^2S_{1/2} \rightarrow 2^2P_{1/2}$ and $2^2S_{1/2} \rightarrow 2^2P_{3/2}$ resulting from collisions of hydrogen atoms in $2^2S_{1/2}$ state with electrons *and* positive ions is calculated. The dominant effect of the protons is shown. The population of the 2S state under chromospheric conditions is found to be substantially lower than the estimates of Giovanelli, and the appearance of the line $2^2S_{1/2} \rightarrow 2^2P_{3/2}$ in absorption is improbable.

Wild has discussed in a recent paper[1] the possibility of detecting in the microwave radiation from the chromosphere the transition $2^2S_{1/2} \rightarrow 2^2P_{3/2}$ in atomic hydrogen. These are the levels involved in the well-known experiments of Lamb and Retherford,[2] who found that the $2^2S_{1/2}$ level lies 9882 Mc/sec below the $2^2P_{3/2}$ level and 1062 Mc/sec above the $2^2P_{1/2}$ level. The $2^2S_{1/2}$ state is metastable, and one might suppose that because of this the state would be heavily populated, compared to the 2P states, and that the line $2^2S_{1/2} \rightarrow 2^2P_{3/2}$ would appear in absorption. Wild estimates that the line should be just observable if there are about 10^4 atoms in the $2^2S_{1/2}$ state, per cubic centimeter, in the regions of the chromosphere accessible to 10,000 Mc/sec radiation. Neglecting any compensating stimulated emission from the $2^2P_{3/2}$ state, he finds that a density as high as this would lower the apparent antenna temperature at the maximum of the line by 50°, compared to the background. Wild refers to Giovanelli's theoretical investigation[3] of the population of the hydrogen levels under various assumed chromospheric conditions, which led to estimates ranging from 1 to 10^8 per cubic centimeter for the population of the $2^2S_{1/2}$ state. Giovanelli's estimates were made with the explicit assumption that the cross-section for "elastic" collisions which transfer an atom from the 2S to a 2P state is not abnormally large compared to ordinary excitation and de-excitation cross-sections, and his conclusions were presented with the reservation, "while we may feel justified for the present in neglecting these collisions, it is clear that their importance still remains an open question, which will be answered only after a reliable estimate of the cross-section becomes available."[4] It is the purpose of this note to show that this cross-section is, in fact, so large as to reduce very drastically the estimates of the population of the 2S level.

[1] *Ap. J.*, **115**, 206, 1952. I am indebted to Dr. Wild for the opportunity to read this paper before publication. The $2S \rightarrow 2P$ transition is only one of several topics treated in Wild's paper, which is concerned with the general problem of line emission in radioastronomy.

[2] *Phys. Rev.*, **79**, 549, 1950, and **81**, 222, 1951.

[3] *Australian J. Sci. Res.*, **A1**, 289, 1948.

[4] *Ibid.*, p. 297.

The effect of collisions in inducing transitions between the 2S and 2P states was first treated by Breit and Teller.[5] They considered only collisions with electrons. Ordinarily, the electron component of an ionized atmosphere is reponsible for most of the collisionally induced transitions. In this unusual case, however, the dominant effect is that of collisions with positive ions. The formula of Breit and Teller was modified by Spitzer and Greenstein and applied to the problem of continuous emission from planetary nebulae.[6] Spitzer and Greenstein likewise over ooked the contribution of the positive ions, so that some quantitative modification of their results is called for.[7] We present here an independent derivation of the probability of transitions resulting from collision with electrons *and* positive ions.

We are concerned with a hydrogen atom in the $2^2S_{1/2}$ state in a highly ionized atmosphere containing, say, N electrons per cubic centimeter and an equal number of positive ions, mostly protons. The process of interest can be described as follows. A charged particle passes near the hydrogen atom, with relative speed v, causing a brief "pulse" of electric field at the location of the atom. Similar passages by other ions, at random times, give rise to a randomly fluctuating electric field, which will have a certain spectral intensity at each of the angular frequencies ω' and ω'' connecting the $2^2S_{1/2}$ level with the $2^2P_{1/2}$ level and with the $2^2P_{3/2}$ level, respectively. This fluctuating field will induce transitions to $2P_{1/2}$ and $2P_{3/2}$ at an average rate that we now proceed to compute.[8]

We locate the hydrogen atom at the origin of co-ordinates x, y, and z, and consider, first, the passage of an ion of charge e, which moves with speed v along the path $x = 0$, $z = r$. Let t_i be the instant of closest approach, the ion then being at 0, 0, and r. The electric field at the atom is given by

$$E_x = 0\ ; \quad E_y = e\,v\,(t-t_i)\,[r^2 + v^2\,(t-t_i)^2]^{-3/2}\ ; \quad E_z = e\,r\,[r^2 + v^2\,(t-t_i)^2]^{-3/2}\ . \tag{1}$$

Now consider a random sequence of such events, differing only in respect to t_i, and occurring at the average rate ν sec^{-1}. We are interested in the average intensity in the Fourier spectrum of the resulting electric field, at two frequencies $\omega' = 2\pi \times 1062$ Mc/sec and $\omega'' = 2\pi \times 9882$ Mc/sec.

The Fourier transforms of the functions $E_y(t)$ and $E_z(t)$ can be expressed[9] in terms of Hankel functions, of order 0 and 1, respectively, of the argument $i\omega r/v$. We can thus find the intensity in the spectrum of E. For a given r and v, the average value of E^2 in an angular frequency range $d\omega$ is[10]

$$\overline{E^2} \text{ in } d\omega = \frac{\pi\nu\,e^2\omega^2}{v^4}\left\{\left|H_0^{(1)}\left(\frac{i\omega r}{v}\right)\right|^2 + \left|H_1^{(1)}\left(\frac{i\omega r}{v}\right)\right|^2\right\}d\omega\,. \tag{2}$$

If we regard ν as the number of passages per second with speed v and distance of closest approach r, but now without regard to direction, the disturbance described by equation (2) is equivalent to an isotropic unpolarized radiation field of energy density ρ_ω, given by

$$\rho_\omega d\omega = \frac{1}{4\pi}(\overline{E^2} \text{ in } d\omega) = \frac{\nu\,e^2\omega^2}{4\,v^4}\left\{\left|H_0^{(1)}\left(\frac{i\omega r}{v}\right)\right|^2 + \left|H_1^{(1)}\left(\frac{i\omega r}{v}\right)\right|^2\right\}d\omega\,. \tag{3}$$

[5] *Ap. J.*, **91**, 215, 1940. [6] *Ap. J.*, **114**, 407, 1951.

[7] According to Professor Greenstein (private correspondence), the effect, although appreciable, does not alter very significantly the conclusion reached in *Ap. J.*, **114**, 407, 1951. I am indebted to Professor Greenstein for calling earlier work on this problem to my attention.

[8] A discussion of the effect of *static* fields on the lifetime of the metastable $2S_{1/2}$ state, and references to earlier work on the same problem, can be found in n. 2.

[9] W. Magnus and F. Oberhettinger, *Special Functions of Mathematical Physics* (New York: Chelsea Publishing Co., 1949), p. 118.

[10] See, e.g., S. O. Rice, *Bell Syst. Tech. J.*, **43**, 282, 1944.

For $\omega r/v \ll 1$ the dominant term in the brackets in equation (3) is $|H_1^{(1)}(i\omega r/v)|^2$ which is then approximately $4v^2/(\pi^2 r^2 \omega^2)$, so that in this limit the spectrum reduces to

$$\rho_\omega \approx \frac{e^2}{\pi^2 r^2 v^2}. \tag{4}$$

As it should be, this is just the spectral-energy density corresponding to a random sequence of narrow pulses, each of area

$$\int_{-\infty}^{\infty} E dt = \int_{-\infty}^{\infty} E_z dt = \frac{2e}{rv}.$$

We consider, first, the transition $2^2S_{1/2} \rightarrow 2^2P_{1/2}$. The frequency is ω', and the square of the dipole moment connecting these states is[11] $9e^2a_0^2$. The transition probability w' is given, as usual, by

$$w' = \frac{4\pi^2}{3\hbar^2} 9 e^2 a_0^2 \rho_\omega (\omega'). \tag{5}$$

Substituting expression (3) for ρ_ω, we have

$$w' = \nu \frac{3\pi^2 e^4 a_0^2 \omega'^2}{\hbar^2 v^4} \left\{ \left| H_0^{(1)}\left(\frac{i\omega' r}{v}\right)\right|^2 + \left| H_1^{(1)}\left(\frac{i\omega' r}{v}\right)\right|^2 \right\}. \tag{6}$$

If we drop the factor ν from equation (6), we obtain just the probability that a single encounter with an ion of speed v, passing by at distance r, will result in a transition. The effect of other encounters, which occur at the average rate ν, is simply additive, because the encounters occur at random times.

Now it would not be proper to use equation (6) for encounters so close that the transition probability in a single encounter, computed by equation (6), is of the order of unity. Interactions as strong as that call for special treatment. The problem is greatly simplified by the fact that, for values of v and ω of interest here, the intereaction is strong in the sense just defined only for values of r so small that $\omega' r/v \ll 1$. In that limit equation (6) can be written to a very good approximation as

$$w' = \nu \frac{12 e^4 a_0^2}{\hbar^2 v^2 r^2}, \tag{7}$$

and our assertion is that we can find an impact radius r_0 such that

$$\frac{12 e^4 a_0^2}{\hbar^2 v^2 r_0^2} \ll 1 \qquad \text{and} \qquad \frac{\omega' r_0}{v} \ll 1. \tag{8}$$

Inserting numerical values, we find that the inequalities in expressions (8) are equivalent to the requirement $v^2 \gg 2.6 \times 10^{10}$ cm^2 sec^{-2}. As we shall be concerned with velocities of 10^6 cm/sec or greater, this requirement is easily fulfilled. For $r < r_0$ we can write, for the transition probability in a single encounter,

$$w' = \sin^2\left(\frac{b}{r}\right), \qquad \text{where} \qquad b^2 = \frac{12 e^4 a_0^2}{\hbar^2 v^2}. \tag{9}$$

This reduces to equation (7) before r becomes as large as r_0; and for small r it behaves like the usual solution of a time-dependent perturbation problem in which the perturbation is practically a δ-function.

[11] E. U. Condon and G. H. Shortley, *The Theory of Atomic Spectra* (Cambridge: At the University Press, 1935), chap. v.

We have now to integrate over the impact radius r and over the velocity distribution of the ions $f(v)$. If there are N_i ions of one sort per cubic centimeter, $2\pi N_i r v f(v) dr dv$ is the number of ions of this sort which pass a given atom, per second, at a distance between r and $r + dr$ and with a speed between v and $v + dv$. We make the simplifying assumption that the atom in question is at rest; we shall presently insert for $f(v)$ a Maxwellian distribution appropriate to the kinetic temperature of the ions. This approximation should have little effect on the result, which, as we shall see, is rather insensitive to the velocity assumed. Denoting by W_i' the total contribution of ions of a given type to the probability of the transition $2^2S_{1/2} \rightarrow 2^2P_{1/2}$, we have

$$W_i' = 2\pi N_i \int_0^\infty v f(v) \left[\int_0^{r_0} r \sin^2 \frac{b}{r} \, dr + \int_{r_0}^\infty \frac{\pi^2 b^2 \omega^2}{4 v^2} \left\{ \left| H_0^{(1)}\left(\frac{i\omega' r}{v}\right) \right|^2 + \left| H_1^{(1)}\left(\frac{i\omega' r}{v}\right) \right|^2 \right\} r \, dr \right] dv . \tag{10}$$

The first integral over r in equation (10) has been extended down to $r = 0$. This causes no significant error, since $r_0 \gg a_0$ and the main contribution to this integral comes from the neighborhood of the upper limit, r_0. The two definite integrals over r in equation (10) can be expressed in terms of the cosine integral and in terms of Hankel functions, respectively, and if $b < r_0 < v/\omega'$, as assumed, the quantity in brackets in equation (10) reduces to

$$b^2\left[\tfrac{3}{2} - C - \ln 2 - \ln\left(\frac{b}{r_0}\right)\right] + b^2\left[-C + \ln\left(\frac{\omega' r_0}{v}\right)\right] - b^2\left[\tfrac{3}{2} - 2C + \ln\left(\frac{v}{\omega' b}\right)\right],$$

where $C = 0.5772\ldots$. We then have

$$W_i' = 2\pi N_i b^2 \int_0^\infty \left[\tfrac{3}{2} - 2C + \ln\left(\frac{v}{\omega b}\right)\right] \frac{f(v)}{v} \, dv . \tag{11}$$

We put

$$f(v) = 4\pi \left(\frac{m_i}{2\pi kT}\right)^{3/2} v^2 e^{-mv^2/2kT},$$

where m_i is the mass of an ion and T the kinetic temperature of the ions. The resulting definite integral can be reduced to the form

$$\int_0^\infty \log x \, e^{-x} dx = -0.5772\ldots,$$

with the final result that

$$W_i' = N_i \frac{96\, e^4 a_0^2}{\hbar^2} \left(\frac{\pi m_i}{9kT}\right)^{1/2} \ln\left(\frac{0.46 kT\hbar}{e^2 a_0 m_i \omega'}\right). \tag{12}$$

For the transition $2^2S_{1/2} \rightarrow 2^2P_{3/2}$ the line strength is twice as great, and we must insert ω'' in place of ω'. The inequalities corresponding to equations (8) can still be satisfied for speeds of 10^6 cm/sec or greater, though with not so much room to spare as before. We then have

$$W_i'' = N_i \frac{192\, e^4 a_0^2}{\hbar^2} \left(\frac{\pi m_i}{9kT}\right)^{1/2} \ln\left(\frac{0.46 kT\hbar}{e^2 a_0 m_i \omega''}\right). \tag{13}$$

In Table 1 we give the transition probabilities computed from equations (12) and (13) for an atmosphere containing 1 proton and 1 electron per cubic centimeter, at various

kinetic temperatures. For any other ion density N, the transition probabilities are obtained by multiplying the tabulated values by N. For $T = 5000°$ K, the value of W''_{proton} is probably not very accurate, for the requirement that corresponds to equations (8) and permits the derivation of equation (13) is barely satisfied at that temperature.

The positive ions are roughly ten times as effective as the electrons. Note also that W', the $2^2S_{1/2} \rightarrow 2^2P_{1/2}$ transition probability, and W''', the $2^2S_{1/2} \rightarrow 2^2P_{3/2}$ transition probability, are about equal, although the line strength of the latter transition is twice that of the former. The total transition probability is a very slowly varying function of kinetic temperature, and our results can be summarized by saying that, for kinetic temperatures of the order of magnitude of 10^4 degrees, the lifetime of the $2^2S_{1/2}$ state is $(7 \times 10^{-4}\, N)^{-1}$ sec, where N is the number of protons per cubic centimeter.

Expressed in terms of a cross-section σ, defined by $W = N\bar{v}\sigma$, we have $\sigma \approx 7 \times 10^{-4}/\bar{v}$, or $\sigma \approx 5 \times 10^{-10}$ cm^2 for protons at 10^4 ° K. For this process, however, the concept of cross-section is peculiarly inappropriate. The main contribution to the transition probability comes from encounters in which the impact radius is so large that $12e^4a_0^2/\hbar^2v^2r^2 \ll 1$. That is to say, the cumulative effect of random remote encounters is greater

TABLE 1

	T (° K)				
	5000	10,000	15,000	20,000	25,000
W'_{proton}	4.03×10^{-4} sec^{-1}	3.46×10^{-4} sec^{-1}	3.12×10^{-4} sec^{-1}	2.90×10^{-4} sec^{-1}	2.72×10^{-4} sec^{-1}
W'_{electron}	0.31	0.24	0.20	0.17	0.16
W''_{proton}	2.47	2.98	3.02	2.99	2.92
W''_{electron}	0.49	0.38	0.32	0.29	0.27
W_{total}	7.30	7.06	6.66	6.35	6.07

than the effect of close encounters in which, individually, the transition probability is high.

The physical reasons for this unusual result are worth noting. One reason is the extraordinarily large value of the matrix elements connecting states of the same principal quantum number. But the main difference between the process here considered and the usual collision-excitation process is that the $2S \rightarrow 2P$ transition involves frequencies very much lower than $\bar{v}/a_0$. This enhances the contribution of remote encounters and is responsible for the unusual dependence on v.

It is interesting to speculate on the course our calculation would take if the $2S_{1/2}$ and $2P_{1/2}$ levels were really degenerate, as they were assumed to be before the Lamb-Retherford experiment. If ω' were zero, our result would diverge logarithmically. We should have to look for some grounds for limiting the integration over r. Now there is at least one effect that might impose such a limit. We have assumed that the encounters with the passing ion are statistically independent. But if we were to consider a very large volume around the atom, the motion of the ions within this volume would not be entirely uncorrelated, owing to the electrostatic forces between the charged particles. Presumably the effect of the correlation would be to smooth out fluctuations in the field at the atom and hence, in effect, to cut off the integral over r at some finite radius. To put it another way, the high conductivity of the medium will tend to limit large-scale fluctuations of the electric field. To confirm this, one would have to consider the nature of macroscopic fluctuations in a plasma. This question does not arise in the actual case because the integrand in equation (10) becomes negligible for $r \gg \bar{v}/\omega'$. Since $\bar{v}/\omega'$ is less than the average distance between ions when N is as large as 10^{11} cm^{-3}, and very much

less than an ionic mean free path, the motions of importance here must surely be uncorrelated.

Another, and more important, change would be needed in our treatment if the levels were degenerate. The natural width of the $2P_{1/2}$ level would have to be taken into account, and this alone would suffice, under most conditions, to limit the interaction to distances short enough to avoid any questions of correlation.[12]

We now consider the bearing of our result upon the estimates of the 2S state population in the chromosphere. Giovanelli's computations[3] cover a range of N from 10^8 to 10^{13} cm^{-3}. For $N > 2 \times 10^{11}$ cm^{-3}, according to equation (12), $W > 10^8$ sec^{-1}. Now the lifetime of the P states themselves is of the order of 10^{-8} sec. Hence, for ion densities greater than 2×10^{11} cm^{-3}, collision-induced transitions from S to P, and, of course, vice versa, mix up the S and P populations faster than the P states can decay. Under these conditions the metastability of the 2S level has little influence on its population, and the relative populations of the 2S and 2P levels will be nearly in the proportion of their statistical weights. The 2S population can be obtained, at least in order of magnitude, by simply taking one-third of the 2P population given by Giovanelli. This amounts to a reduction of his 2S estimates by a factor of the order of 100, in most cases.

For densities lower than 10^{11} cm^{-3}, we have to compare the rate of removal of atoms from the 2S state by the collision process with the other processes involved, mainly radiative excitation and ionization, according to Giovanelli. Accepting his estimates for the latter processes, we find that the collision-induced $2S \rightarrow 2P$ transition dominates down to an ion density of 10^9 cm^{-3}, if the photospheric radiation is not much diluted; and, of course, it always dominates if the photospheric radiation is neglected (dilution factor = 0). We have not attempted a detailed readjustment of Giovanelli's estimates, but very rough y the result is this: The population of the 2S level, where the density is low enough so that the 2S population substantially exceeds the 2P population, is in no case much greater than 100 cm^{-3}.

The consequences of this change, so far as the detection of the $2S_{1/2} \rightarrow 2P_{3/2}$ line is concerned, are quite severe. At high ion densities we still have a considerable population in the 2S state, something of the order of 10^6 cm^{-3} for the most extreme conditions. But now the 2S and 2P states are nearly in statistical equilibrium, and the absorption is nearly compensated by the stimulated emission.[13] Furthermore, the width of the line will now be determined by the rate of collision-induced $2S \rightarrow 2P$ transitions and will be greater than its normal width of 100 Mc/sec.

Apart from the line width, the important quantity, of course, is the *excess* of the $2S_{1/2}$ population over half the $2P_{3/2}$ population. It appears very doubtful that this excess ever exceeds 10^3 cm^{-3}; and in the part of the chromosphere accessible to 10,000 Mc/sec radiation, where T is 10^4° K or greater, it is probably not more than 10^2 cm^{-3}. This is one hundred times less than the minimum required for an observable line, according to Wild's computation. Nevertheless, in view of the importance of the question, a careful revision of Giovanelli's estimates, with particular attention to the *difference* between the $2S_{1/2}$ population and half the $2P_{3/2}$ population, would be desirable.

[12] I am indebted to Professor W. E. Lamb, Jr., for this observation and for a helpful discussion of several related points.

[13] In the limit, the populations of the 2S and 2P states (relative only to each other) will, by these collisions, be adjusted to equilibrium at the kinetic temperature of the ions. In this case the line would appear in *emission* rather than in absorption, for the presence of the 2S and 2P states would simply increase the opacity of the medium at the line frequency, thereby shifting the effective layer of emission outward to a region of higher temperature.

INHOMOGENEOUS STELLAR MODELS. II. MODELS WITH EXHAUSTED CORES IN GRAVITATIONAL CONTRACTION

A. R. SANDAGE* AND M. SCHWARZSCHILD†
Princeton University Observatory
Received June 28, 1952

ABSTRACT

Seven shell-source models with exhausted, gravitationally contracting cores have been computed in detail. The models form an evolutionary sequence starting from a configuration whose isothermal core contains the Schönberg-Chandrasekhar limitating mass. It is found that, as the cores contract, the envelopes greatly expand. Thus from the initial configuration, which is near the main sequence, the stars evolve rapidly to the right in the H-R diagram, amply covering the giant region. In this evolution the gravitational contraction contributes less than 4 per cent to the total luminosity.

A comparison of this theoretical evolution with the observed H-R diagram for globular clusters appears to explain the sudden turnoff from the main sequence to the giant region at about $M_{bol} = +3.5$.

I. INTRODUCTION

The identification in 1938 of the source of stellar energy with nuclear processes created the problem of finding equilibrium models for giant stars with the high central temperatures required for the nuclear reactions. In recent years a number of investigations[1] have indicated that the solution probably lies with chemically inhomogeneous models. These investigations have shown that certain types of inhomogeneities do lead to large radii with high central temperatures. The various models proposed have differed in the way the inhomogeneities were introduced, according to a variety of assumptions regarding the degrees of mixing and the evolutionary process involved (nuclear transmutations or accretion).

This paper considers a model whose inhomogeneity arises from the following evolutionary process. An initially homogeneous star with a convective core and radiative envelope (Cowling model) which experiences no mixing between the core and envelope starts exhausting its hydrogen supply in the core. The subsequent early stages of the evolution follow those computed by Schönberg and Chandrasekhar,[2] with the core finally exhausted of hydrogen and therefore isothermal. The nuclear-energy production is then confined to a shell between the exhausted core and the radiative envelope. The assumption of no mixing creates a chemical discontinuity between the core and the shell. When the shell has burned outward until it reaches the Schönberg-Chandrasekhar limit for an isothermal core, a new evolutionary process must take place, which is most likely a gravitational contraction of the core. This paper is concerned with the quasi-equilibrium states through which an unmixed model passes after reaching the Schönberg-Chandrasekhar limit.

The main feature differentiating the present models from earlier ones is the occurrence of an additional energy source by gravitational contraction. The distribution of this energy source throughout the exhausted core has here been treated only approximately (assumption 3 in Sec. II), in accordance with the general result that the details of the energy-source distribution have little effect on the model. However, the total amount of energy released by the contraction of the core has been accounted for explicitly (Sec. III).

* William Charles Peyton Advanced Fellow in Astronomy at Princeton University.

† This research was supported in part by funds of the Eugene Higgins Trust allocated to Princeton University.

[1] See Paper I of this series for references, Oke and Schwarzschild, *Ap. J.*, **116**, 317, 1952.

[2] *Ap. J.*, **96**, 161, 1942.

II. ASSUMPTIONS, DEFINITIONS, AND EQUATIONS

The models here considered consist of a hydrogen-rich envelope in radiative equilibrium and a contracting hydrogen-exhausted core, also in radiative equilibrium.

The following simplifying assumptions have been made in the computations: (1) All the sources for nuclear energy are confined to a shell idealized to an infinitely thin sheet located immediately outside the exhausted core. (2) The temperature at the shell, necessary for the carbon cycle, is 3×10^7 ° K throughout the evolutionary stages considered. (3) The distribution of the gravitational energy source in the core is assumed as $\epsilon =$ Constant, where ϵ is the energy liberated per gram. If L_g is the total flux due to the gravitational source in the core, the flux crossing a shell of radius r within the core is $L(r) = L_g M_r/M_1$, where M_1 is the total mass within the core. (4) The evolutionary changes are sufficiently slow that dynamical terms in the equilibrium equations are negligible. (5) The mean molecular weight is discontinuous across the interface between the envelope and the core, with an arbitrary jump of a factor of 2 consistent with the assumed abundances of $X_i = 0$, $Y_i = 0.98$, $Z_i = 0.02$ in the core, and $X_e = 0.596$, $Y_e = 0.384$, and $Z_e = 0.02$ in the envelope. (6) The switch from the Kramers opacity law to electron scattering in the envelope is abrupt and occurs at the same place for stars of different masses. (7) Radiation pressure and degeneracy are negligible.

The following definitions and equations were used for constructing the models. Subscripts: i = Region interior to the shell; e = envelope; c = center; 1 = interface between envelope and core at the shell; and s = point of switch from Kramers' opacity to electron scattering.

Nondimensional variables:

$$P = p\,\frac{GM^2}{4\pi R^4}, \qquad T = t\,\frac{\mu_e H}{k}\,\frac{GM}{R}, \qquad M_r = qM, \qquad r = xR. \tag{1}$$

Transformation for core equations:

$$p = p_c p^*, \qquad t = t_c t^*, \qquad q = \frac{t_c^2}{l_i^2\sqrt{p_c}}\,q^*, \qquad x = \frac{t_c}{\sqrt{p_c}\,l_i}\,x^*. \tag{2}$$

Absorption coefficient:

Kramers' region:

$$\kappa = \kappa_0\,\frac{\rho}{T^{3.5}} \qquad \text{with} \qquad \kappa_0 = \frac{4 \times 10^{25}}{(t/g)}\,Z(1+X). \tag{3}$$

Electron-scattering region:

$$\kappa = \kappa_0\,\frac{\rho_s}{T_s^{3.5}}. \tag{4}$$

Eigenvalue parameters:

Envelope:

$$C = \frac{3\kappa_0}{4ac}\left(\frac{k}{\mu_e HG}\right)^{7.5}\left(\frac{1}{4\pi}\right)^3\frac{LR^{0.5}}{M^{5.5}}; \tag{5}$$

Core:

$$C^* = \frac{C}{q_1}\,j_1\,\frac{L_g}{L}\,\frac{p_s}{t_s^{4.5}}\,\frac{p_c}{t_c^4}. \tag{6}$$

Composition parameters:

$$l_i = \frac{\mu_i}{\mu_e} = \frac{2X_e + \frac{3}{4}Y_e + \frac{1}{2}Z_e}{2X_i + \frac{3}{4}Y_i + \frac{1}{2}Z_i} = 2.0, \qquad j_i = \frac{Z_i(1+X_i)\,\mu_i}{Z_e(1+X_e)\,\mu_e} = 1.253. \tag{7}$$

Differential equations:

Radiative envelope:

$$\frac{dp}{dx} = -\frac{pq}{tx^2}; \qquad \frac{dq}{dx} = \frac{x^2 p}{t}; \tag{8}$$

$$\frac{dt}{dx} = -\frac{Cp^2}{t^{8.5}x^2} \text{ in Kramers' region;} \tag{9}$$

$$\frac{dt}{dx} = -C\frac{p_s}{t_s^{4.5}}\frac{p}{t^4 x^2} \text{ in electron-scattering region.} \tag{10}$$

Contracting core:

$$\frac{dp^*}{dx^*} = -\frac{p^* q^*}{t^* x^{*2}}; \qquad \frac{dq^*}{dx^*} = \frac{x^{*2} p^*}{t^*}; \qquad \frac{dt^*}{dx^*} = -\frac{C^* q^* p^*}{t^{*4} x^{*2}}. \tag{11}$$

Homology invariants:

$$U = \frac{lpx^3}{tq}, \qquad V = \frac{lq}{tx}, \qquad \text{where} \quad l_e = 1 \quad \text{and} \quad l_i = 2; \tag{12}$$

$$(n+1)_e = \frac{t_s^{4.5}}{p_s}\frac{qt^4}{Cp}; \qquad (n+1)_i = \frac{t^{*4}}{C^* p^*} = \frac{t_s^{4.5}}{p_s}\frac{q_1}{C j_i}\frac{L}{L_g}\frac{t^4}{p}. \tag{13}$$

Fitting conditions at the discontinuity:

$$\frac{U_{1i}}{U_{1e}} = \frac{V_{1i}}{V_{1e}} = l_i = 2.0, \tag{14}$$

$$\frac{(n+1)_{1i}}{(n+1)_{1e}} = \frac{1}{j_i}\frac{L}{L_g}. \tag{15}$$

Density in nondimensional variables:

$$\rho = \frac{\mu}{\mu_e}\frac{p}{t}\frac{M}{4\pi R^3}. \tag{16}$$

III. GRAVITATIONAL ENERGY RELEASE AND THE EVOLUTIONARY FITTING CONDITION

To follow the quasi-static equilibrium states during the evolution, it is necessary to know how much energy is released by the gravitational contraction, since we must be able to apply the fitting condition equation (15). The ratio of the total luminosity to the gravitational luminosity is derived in this section.

The energy released by the core contraction in each step of the evolution is composed of three parts: (1) the change in the gravitational energy of the core between the initial and final configuration; (2) the change in the internal heat content of the core; and (3) the work, PdV, done on the core. An additional apparent source of energy must also be considered. Since the amount of mass in the core is continuously increasing as the shell exhausts its hydrogen and burns outward, additional mass is present in the final contracted state which was not present in the initial state. The additional energy due to this increment of mass, δM_1, carried into the core through the expanding interface must be subtracted from the total energy difference between the initial and final states to give the

net contractional energy release. Accordingly, the net released energy as a result of contraction is

$$L_g\,\delta\tau = \delta\Big[-\int_0^{r_1}\Big(C_vT-\frac{GM_r}{r}\Big)4\pi r^2\rho\,dr\Big]-4\pi r_1^2P_1\Big(\delta r_1-\frac{dr}{dM_r}\Big|_{r_1}\delta M_{r_1}\Big) + \Big(C_vT_1-\frac{GM_{r_1}}{r_1}\Big)\delta M_1 . \tag{17}$$

The specific heat, C_v, is given by $C_v = k/(\gamma-1)\mu H$. The value of γ is assumed to be $\frac{5}{3}$. To apply equation (17), it is convenient to express it in the nondimensional variables of equation (1). After some reduction, the result is

$$L_g\,\delta\tau = \frac{MkT_1}{\mu_1 H}\Big\{\delta q_1\Big(\frac{3\gamma-4}{\gamma-1}B_1^*+\frac{\gamma}{\gamma-1}-U_1^*-V_1^*\Big) + q_1\Big(\frac{3\gamma-4}{\gamma-1}\,\delta B_1^*-\frac{1}{x_1^*}\,\delta[U_1^*x_1^*]\Big)\Big\}, \tag{18}$$

where

$$B_1^* = \frac{1}{l_1^*q_1^*}\int_0^{x_1^*}x^{*2}p^*\,dx^* . \tag{19}$$

The increment of mass δM_1 carried through the expanding interface is the mass which was burned as the shell moved outward. It then follows that the nuclear energy, released simultaneously with the gravitational energy, is

$$L_n\,\delta\tau = 0.007\,c^2X_eM\,\delta q_1 . \tag{20}$$

The ratio of equation (18) to equation (20) gives the quantity needed for the fitting condition on $n+1$ of equation (15). With $L = L_g + L_n$, one obtains

$$\frac{L}{L_g} = 1+\frac{0.007\,c^2X_e}{(kT_1/\mu_1H)\{1.5B_1^*+2.5-U_1^*-V_1^*+(q_1/\delta q_1)(1.5\,\delta[B_1^*]-[1/x_1^*]\,\delta[U_1^*x_1^*])\}} . \tag{21}$$

Hence, for any proposed evolutionary change from an initial stellar state with a known temperature, pressure, and mass distribution to a known final state, the value of the right side of equation (21) may be computed. The value of L/L_g thus obtained must agree with the mean value of L/L_g obtained from equation (15) for the initial and final states of the evolution step considered. This condition makes it possible—within the present approximations—to determine uniquely the transition states in the evolution from a given initial configuration. In the next section this evolutionary track is followed for a star whose initial configuration has an isothermal core which contains the Schönberg-Chandrasekhar limiting mass.

IV. THE CONSTRUCTION OF THE MODELS

To construct the models, a family of solutions of equations (8)–(10) for the envelope and a family of solutions of equations (11) for the core are needed. Both sets of solutions are one-parameter families in terms of the eigenvalues C and C^* as long as the appropriate absorption law is given.

The solutions to the envelope equations were obtained as follows. From Paper I of

this series[1] envelope solutions of equations (8) and (9), valid for Kramers' law of opacity, were available. On the basis of trial models it became apparent, however, that, for the circumstances of interest here, electron scattering provides the main source of opacity in the inner portions of the envelopes. Accordingly, with the help of the trial models, the point where electron scattering becomes dominant was estimated for each envelope solution, and the solutions were carried from these points inward with equations (8) and (10) by numerical integration.[3] The Kramers envelope with the electron-scattering extensions are shown as heavy solid curves in Figure 1 plotted with the homology invariants U and V as co-ordinates. The electron-scattering extensions converge to the point $U = 0$, $V = 4$, which is unlike the complete Kramers envelopes that curl about $U = 1/11$, $V = 42/11$.

The one-parameter family of solutions for equation (11) of the core was obtained by numerical integration.[3] A power-series solution of equations (11) valid near the center provided starting values for the integrations. The core solutions are shown as broken curves in Figure 1.

To find the evolutionary sequence here considered, it remains only to assemble the individual models by fitting each core solution to an appropriate envelope solution by equations (14), (15), and (21). To apply equation (21), the value of B_1^* must be known. This was found along each of the seven core solutions by an elementary quadrature of equation (19). Since equation (21) connects two neighboring models in the evolutionary sequence, the individual models cannot be determined separately but must be derived successively—in the same sequence in which the star evolves through them.

To start with, the initial state has to be chosen, which—in accordance with the discussion in Section I—was here taken to be the Schönberg-Chandrasekhar limiting case for a model with an isothermal core. This initial state, represented by model I, is shown in the U–V plane of Figure 1 by the straight line (marked by I) showing the jump from (U_{1e}, V_{1e}) to (U_{1i}, V_{1i}) at the envelope-core interface.

To derive in a definite manner the next state in the evolution (to be represented by model II), a time interval for the evolution from model I to model II has to be chosen, not too long so that the changes are not too radical for the difference equation (21) to hold. Instead of choosing explicitly the time interval, the condition was here chosen so that the core of model II should correspond to $C^* = 0.200$, a value for which the core solution (see Fig. 1) does not lie too far from the core solution of model I ($C^* = 0$). Correspondingly, the point (U_{1i}, V_{1i}) for model II must lie on the core solution for $C^* = 0.200$. Choosing an arbitrary point on this solution as a trial for (U_{1i}, V_{1i}), one can read from the numerical tabulation of this solution $(n + 1)_{1i}$ needed for equation (15) and all the asterisked quantities needed for equation (21). Similarly, the point (U_{1e}, V_{1e}) corresponding to the trial for (U_{1i}, V_{1i}) can be obtained from conditions (14), and, at this point, $(n + 1)_{1e}$ and q_1 can be found by interpolation between the envelope solutions. Now all the necessary quantities are known to test the compatibility of equations (15) and (21). From equation (15) L/L_g for model II is obtained; since this quantity is already known for model I, the mean (geometrical) can be formed. From equation (21) one gets $\bar{L}/\bar{L}_g$ by using for δq_1, δB_1^*, and $\delta(U_1^* x_1^*)$ the corresponding differences between models I and II and by using for T_1, X_e, and μ_i the values assumed in Section II. If the results from the two equations do not agree, the trial point (U_{1i}, V_{1i}) must be changed—along the definite core solution—until agreement is reached. Thus unique values for U_{1i} and V_{1i} (and, in consequence, for all the other nondimensional characteristics) are found for model II. The same procedure leads from model II to model III, and so on through the entire evolution considered.

The model sequence thus obtained is precisely defined by the assumptions made in Section II. It must be remembered, however, that some of these assumptions were quite

[3] To appear in a forthcoming *Contribution of the Princeton University Observatory*.

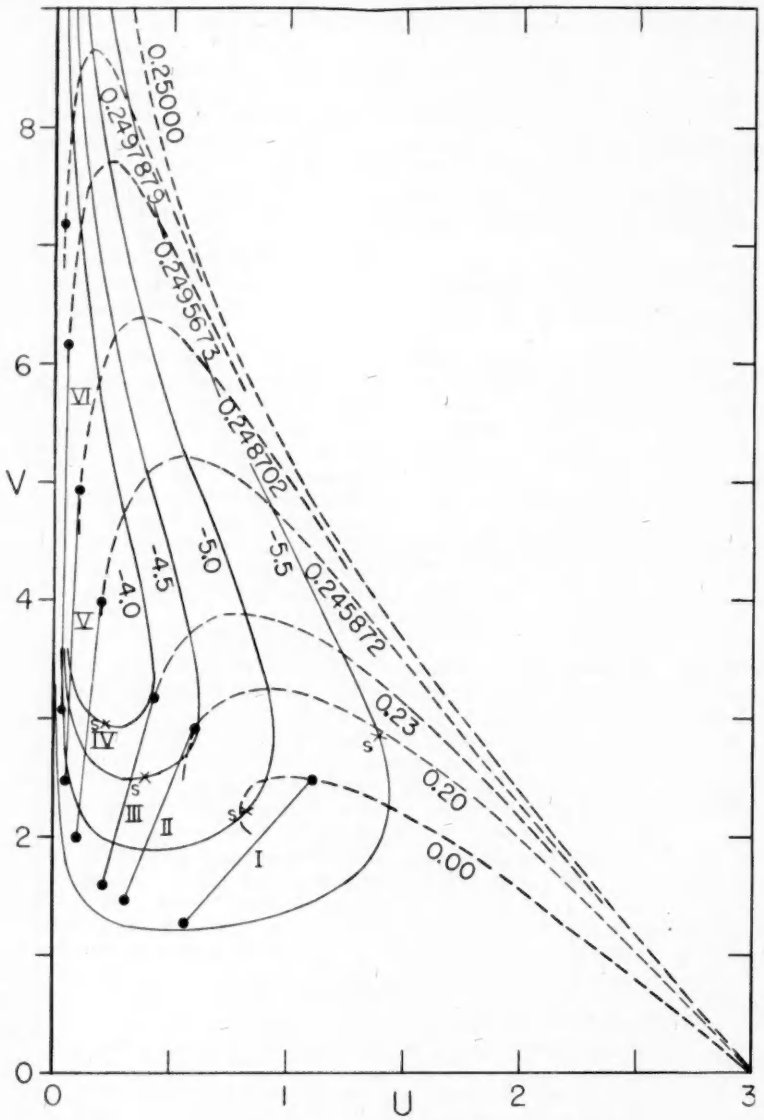

FIG. 1.—The core and envelope solutions in the U, V-plane. The heavy solid curves are envelope solutions, with their values of log C marked. Crosses marked S on the envelope solutions show the switch point from Kramers' opacity to electron scattering. The dashed curves are core solutions, with their C^* values marked. The fitting points between envelope and core for the assembled models are indicated by dots. Roman numerals on the straight connecting lines indicate the model number.

arbitrary, such as the value of 2.0 for the jump in the mean molecular weight, the assumption for the distribution of the gravitational energy sources, and the assumption of no mixing within the star.

The mathematical characteristics of the seven models shown in Figure 1 are exhibited in Table 1.

V. PHYSICAL PROPERTIES OF THE MODELS

Table 1 includes several quantities of physical interest which are independent of the mass or luminosity of the stars to which the models may be applied. The first of these quantities is log C. This parameter increases somewhat from model I to model VII but never differs greatly from its value for the corresponding Cowling model (log $C = -6.0$). Since C is, by its definition (5), the numerical coefficient of the mass-luminosity law, it follows that stars built according to the present models follow closely the mass-luminosity

TABLE 1

MATHEMATICAL CHARACTERISTICS OF MODELS

	I	II	III	IV	V	VI	VII
U_e	0.558	0.303	0.213	0.098	0.050	0.025	0.016
V_e	1.245	1.453	1.597	1.986	2.465	3.078	3.599
C^*	0.00	0.200	0.230	0.245872	0.248702	0.2495673	0.2497879
log C	−5.490	− 5.358	− 5.307	− 5.240	− 5.172	− 5.121	− 5.058
log p_1	2.590	2.960	3.182	3.705	4.370	5.460	7.332
log t_1	0.182	0.294	0.360	0.508	0.680	0.964	1.430
log t_c	0.182	0.466	0.630	0.949	1.246	1.646	2.184
log p_c	3.884	5.059	5.701	6.865	8.008	9.557	11.692
$(n+1)_e$	2.52	2.95	3.12	3.53	3.80	3.95	3.98
$(n+1)_i$	∞	148	118	101	95.1	93.4	88.0
B_1^*	1.000	1.119	1.256	1.676	2.181	2.824	3.329
L/L_g	∞	62.7	47.4	36.0	31.4	29.6	27.7
$X_1=r_1/R$	0.0643	0.0462	0.0341	0.0200	0.0109	0.0047	0.0014
$q_1=M_1/M$	0.1200	0.1232	0.1244	0.1260	0.1278	0.1298	0.1313
log $\rho_c/\bar{\rho}$	3.526	4.418	4.893	5.739	6.587	7.734	9.333

relation of main-sequence stars—contrary to previous red-giant models, which gave overluminous stars compared to main-sequence stars of the same mass.

Next, the values of $\rho_c/\bar{\rho}$ given in Table 1 show a very large increase from model I to model VII, which represents an exceedingly great change in the structure of the star. The same is shown by the steeply decreasing values of r_1/R, which gives the fraction of the radius occupied by the exhausted core.

Finally, the large values of L/L_g indicate that, throughout the evolution here considered, at most 4 per cent of the total luminosity is provided by gravitational-energy release. Hence, even a rather small gravitational-energy source, if situated in an exhausted core, may thoroughly alter the stellar structure.

To derive the other physical characteristics, such as the radius, bolometric magnitude, and effective temperatures, the models must be applied to stars with definite values of the mass and the guillotine factor. The seven models, together with the Cowling main-sequence model,[4] were applied to stars with 1, 2, and 4 solar masses. The guillotine factor was determined by fitting Morse's[5] opacity values with the Russell mixture to the run of temperature and density of model V for a mass of $2M_\odot$. The coefficient κ_0 in equation (3) was adopted as $\kappa_0 = 7 \times 10^{23}$ from this fit. This corresponds to a guillotine factor of $t/\bar{g} = 1.8$.

[4] T. G. Cowling, *M.N.*, **96**, 42, 1935.

[5] P. M. Morse, *Ap. J.*, **92**, 27, 1940.

With these values for the mass and opacity coefficient, the physical characteristics shown in Table 2 were computed in the following manner.

First, the radius of the star was obtained from the second of equations (1) by applying the equation at the shell with $T_1 = 3 \times 10^7$ ° K as assumed in Section II and t_1 given by the sixth row of Table 1. The absolute bolometric magnitude was next found by solving equation (5) for the luminosity L, using the value of log C of the fourth row in Table 1. The effective temperature follows from its definition in terms of the radius and luminosity.

TABLE 2

PHYSICAL CHARACTERISTICS OF THE MODELS

	Main Sequence	I	II	III	IV	V	VI	VII
	$M/M_\odot = 1.0$							
$R/R_\odot$	0.465	0.785	1.017	1.184	1.665	2.474	4.756	13.92
M_{bol}	5.22	4.27	4.09	4.04	4.06	4.10	4.33	4.75
T_e	7,350	7,060	6,460	6,050	5,090	4,130	2,830	1,500
$T_c \times 10^{-6}$	30	30	45	56	83	110	144	170
log ρ_c	2.699	3.991	4.545	4.825	5.226	5.556	5.854	6.051
log ρ_{14}	2.544	2.697	2.618	2.576	2.506	2.484	2.439	2.445
	$M/M_\odot = 2$							
$R/R_\odot$	0.931	1.570	2.035	2.368	3.330	4.949	9.512	27.84
M_{bol}	1.46	0.51	0.33	0.28	0.29	0.34	0.56	0.99
T_e ° K	12,300	11,900	10,900	10,200	8,570	6,950	4,760	2,520
$T_c \times 10^{-6}$ ° K	30	30	45	56	83	110	144	170
log ρ_c	2.097	3.389	3.942	4.223	4.624	4.953	5.252	5.449
log ρ_{14}	1.942	2.095	2.015	1.974	1.904	1.881	1.837	1.843
	$M/M_\odot = 4$							
$R/R_\odot$	1.861	3.140	4.070	4.736	6.660	9.898	19.02	55.67
M_{bol}	−2.30	−3.26	−3.44	−3.48	−3.47	−3.43	− 3.20	− 2.78
T_e	20,700	20,000	18,300	17,100	14,400	11,700	8,020	4,240
$T_c \times 10^{-6}$	30	30	45	56	83	110	144	170
log ρ_c	1.495	2.787	3.340	3.622	4.024	4.352	4.650	4.847
log ρ_{14}	1.340	1.493	1.413	1.373	1.304	1.280	1.235	1.241

The central temperature was next computed by noting from the second of equations (1) that $T_c = T_1(t_c/t_1)$. The sixth and seventh rows of Table 1 then give the central temperature. Log ρ_{14} and log ρ_c follow immediately from equation (16) and the values in the fifth, sixth, seventh, and eighth rows of Table 1.

The results are shown in Table 2. First, it is seen that large radii characteristic of giant stars are obtained simultaneously with internal temperatures high enough for the nuclear processes to exist. Indeed, if the evolution is followed beyond model VII on the present assumptions, excessively large radii are reached.

Second, it appears to be characteristic of stars evolving along this sequence that as the core contracts, the envelope greatly expands. The details of this core contraction and envelope expansion can indeed be computed, since for each model the integrations give the fractional mass and radius distribution. Figure 2 shows the results of this computa-

tion for a mass of $2M_{\odot}$. The abscissa is the radial distance for surfaces of constant mass, in units of the solar radius. The ordinate is a time scale, whose zero epoch is at model I, derived from the rate at which q_1 increases (fourteenth row, Table 1) by the burning of the shell. The numbers at the top in Figure 2 identify the fraction, in per cent, of the total mass interior to the shell considered. Figure 2 explicitly shows the contraction of the inner shells and the expansion of the envelope layers. The star must pump energy into the expansion of the outer layers so as to overcome the gravitational potential. This energy is supplied by the outgoing flux produced by the nuclear and gravitational sources closer in. The outgoing flux is then not strictly constant in the envelope, as is assumed in equations (9) and (10) but is a decreasing function of x. This has not been taken into account in the present approximation; but this refinement is virtually certain to change the models only slightly.

Third, Table 2 shows a sharp rise in the central temperature from 3×10^{7}° K in model I to 1.7×10^{8}° K in model VII as the core contracts. The reason, of course, is that only part of the contractional energy is released as radiation flux, while the re-

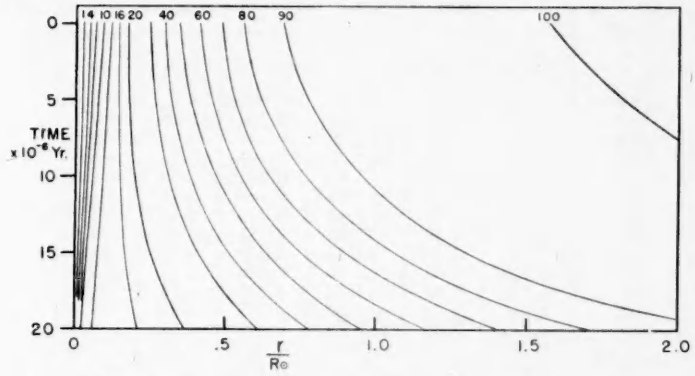

FIG. 2.—Motion of mass shells during the core contraction. Numbers at the top give the fraction of the mass, in per cent, interior to the shell considered. The abscissa is the radial distance from the center to the particular shell in units of the solar radius. The ordinate is the evolutionary time with the zero epoch at model I.

mainder goes to increase the internal energy. To illustrate the very great difference in the internal structure of models I and VII, Table 3 shows their distribution of mass, density, and temperature.

With the physical parameters for the models now known, it is possible to check certain of the assumptions of Section II. Model V with a mass of $2M_{\odot}$ was used for these checks; this is the same model to which the opacity coefficient was fitted.

The first check concerns the value of the shell temperature. If the assumed value of 30 million degrees is correct, an integration of the energy-generation equation[6] for this shell temperature must give the correct luminosity ($M_{bol} = 0.34$ model V, mass 2). Computation indicates that 28 million degrees at the shell would have given the exact required absolute magnitude and therefore that the 30-million-degree approximation is a very good one. This integration further indicated that the energy-producing shell is exceedingly narrow; the part producing 90 per cent of the energy occupies only 0.4 per cent of the radius. The idealization of representing the shell as an infinitely thin sheet therefore seems a valid one.

The second check concerns the opacity formulae (3) and (4) used in constructing the models. Equation (3) was found to represent satisfactorily the opacity in the part of the

[6] I. Epstein, *Ap. J.*, **112**, 207, 1950.

envelope outside the switching point. Equation (4), which is used to represent electron scattering in the inner parts of the models, gives a constant opacity, the value of which is chosen so as to make the absorption coefficient continuous across the switching point. This choice has the great practical advantage of making homology transformations applicable to the models. It has, however, the disadvantage that the value given by equation (4) depends strongly on the choice of the switching point, which, for best representation of the absorption coefficient, should be chosen differently for different masses (as has not been done here). Thus it is found for model V that equation (4) well represents electron scattering for stars of 4 solar masses but gives about three times too high an opacity for 2 solar masses. This malrepresentation for the lower masses appears, however,

TABLE 3

MARCH OF THE PHYSICAL VARIABLES IN MODELS I AND VII FOR $M/M_\odot=2$

r/R	Model I			Model VII		
	$M_{(r)}/M$	log T	log ρ	M_r/M	log T	log ρ
0.000	0.000	7.48	+3.39	0.000	8.23	+5.45
.005	0.001	7.48	+3.38	0.135	7.00	+0.15
.010	0.004	7.48	+3.30	0.140	6.77	−0.50
.015	0.009	7.48	+3.20	0.145	6.66	−0.82
.02	0.019	7.48	+3.09	0.150	6.59	−1.00
.03	0.040	7.48	+2.85	0.160	6.49	−1.22
.04	0.064	7.48	+2.61	0.172	6.42	−1.39
.05	0.084	7.48	+2.40	0.185	6.37	−1.50
.06	0.102	7.47	+2.14	0.200	6.32	−1.61
.07	0.120	7.45	+1.78	0.220	6.28	−1.70
.08	0.138	7.43	+1.72	0.240	6.25	−1.79
.09	0.156	7.41	+1.69	0.260	6.22	−1.84
.10	0.175	7.38	+1.63	0.290	6.18	−1.92
.15	0.285	7.27	+1.46	0.445	6.07	−2.30
.20	0.417	7 18	+1.25	0.580	5.97	−2.58
.25	0 555	7.08	+1.02	0.704	5.87	−2.88
.30	0.686	7.00	+0.80	0.800	5.78	−3.12
.40	0.849	6.83	+0.31	0.910	5.59	−3.60
.50	0.935	6.67	−0.19	0.975	5.42	−4.15
.60	0.975	6.49	−0.74	1.00	5.24	−4.75
.70	0.992	6.30	−1.40	1.00	5.07	−5.39
.80	0.998	6.06	−2.12	1.00	4.82	−6.12
0 90	1.00	5.70	−3.31	1.00	4.47	−7.30

to have very little effect on the models, as was shown by test models in which Kramers' absorption law was used throughout. Even though the opacity in the inner portions of these models was too small by a large factor, the test models differed little from the final ones. Hence it is not expected that the present models would be much changed by an improved representation of the absorption coefficient.

The third check concerns the neglect of radiation pressure. In the most unfavorable case, that of model VII with a mass of $4M_\odot$, the ratio of the total pressure to radiation pressure at the interface of the core and envelope is 20 to 1, while at the center this ratio becomes 490 to 1, indicating that for the range of masses here considered radiation pressure plays virtually no role.

The fourth and final check concerns the assumption for the neglect of degeneracy. The values in the fourth and fifth rows of Table 2 plotted in the degeneracy diagram of G. Wares[7] shows that models of mass $1M_\odot$ are all slightly degenerate at their centers.

[7] *Ap. J.*, **100**, 158, 1944.

The centers of mass $4M_\odot$ models are practically on the degeneracy criterion line. Since the degeneracy is very slight and is confined to the central region of the cores, the general features of the models based upon the assumption of no degeneracy should be quite generally valid.

One additional check on the assumptions is possible concerning the distribution of the gravitational-energy sources. Since the distribution of mass is known for the completed models, it is possible to compute the change of the gravitational potential from one contractional state to the next and check the assumption of ϵ = constant. This has not been

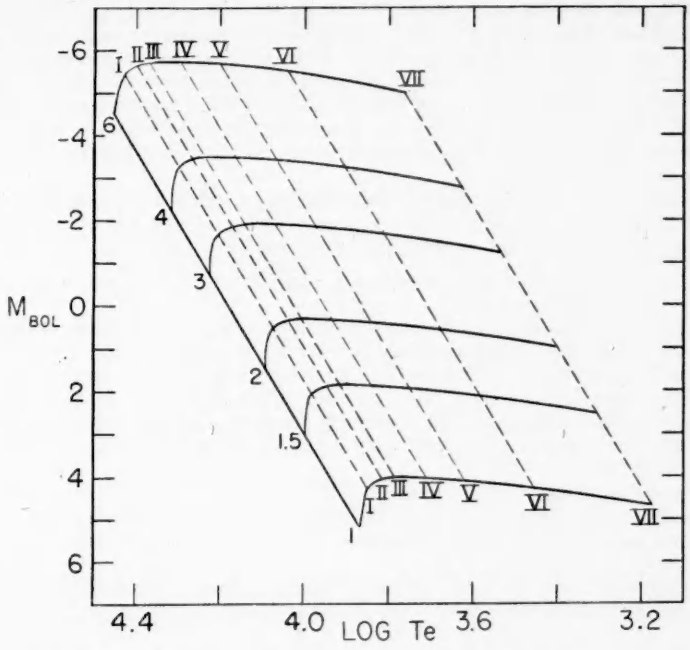

FIG. 3.—The evolutionary tracks in the H–R diagram. Each of the heavy curves gives the line of evolution for star of a given mass, the value of the mass being given at the left of the curve. The intersections of the dashed and solid lines are the positions of models I–VII for the various masses. The straight line to the left represents the main-sequence Cowling model.

done, but estimates indicate that the models are rather insensitive to the exact distribution of sources assumed.

All indications then seem to be that the models here presented are consistent with the assumptions used in deriving them.

VI. THE EVOLUTIONARY TRACK IN THE H-R DIAGRAM AND THE AGE OF GLOBULAR CLUSTERS

Figure 3 shows the evolutionary tracks in the H-R plane from the data of Table 2. This diagram summarizes the evolutionary path taken by stars of various masses during the time that their cores are contracting. No attempt has been made to fit the observational data for the main sequence.

As Schönberg and Chandrasekhar[2] first pointed out, the star increases slightly in luminosity in going from the main sequence to model I, becoming about 1 mag. brighter

when the 12 per cent limit for the exhausted mass is reached at model I. At this point $R = 1.7\ R_{\text{Cowling}}$, while the effective temperature has remained nearly constant. Thus, from the Cowling model to the limiting isothermal core model, the stars remain in the vicinity of the main sequence. The contraction of the core—with its consequent envelope expansion—begins with model I, and the stars rapidly move away from the main sequence into the giant region.

Figure 3 suggests the following phenomenon for the Hertzsprung-Russell diagram for old stellar systems—such as globular clusters—in which all stars are presumably of the same age. The fainter stars of such a system will not yet have burned up 12 per cent of their mass and will therefore be on or near the main sequence. The brighter stars will have burned up more than 12 per cent of their mass and will therefore—under the present assumptions—have moved to the right in the H-R diagram. According to Figure 3, the evolution to the right sets in rather sharply for any given star. Hence one should expect a fairly well-defined turnoff point in the H-R diagrams of these systems, as has indeed been observed.[8] The stars at the turnoff point should then be identified with those which have just reached the Schönberg-Chandrasekhar limit, i.e., have just burned out 12 per cent of their mass.

If this identification is correct, one may theoretically compute the absolute magnitude at which the turnoff point should occur in a system of an age of, say, $t = 3 \times 10^9$ years. For stars which have burned out q_1 per cent of their mass, one has

$$L\tau = 0.007\, c^2 X_e q_1 M\ . \tag{22}$$

Combining this with the appropriate mass-luminosity relation and using, as before, $X_e = 0.596$ and $q_1 = 12$ per cent, one gets a mass of 1.3 solar masses and a luminosity corresponding to $M_{\text{bol}} \approx +3.3$. (This result is fairly independent of the assumed hydrogen content, X_e, since, for varying X_e also, the jump of the molecular weight at the discontinuity varies. In consequence, the core-mass fraction q_1 of the Schönberg-Chandrasekhar limit varies[9] in such a way that the product $X_e\, q_1$ occurring in eq. [22] remains nearly constant.)

On the observational side, the turnoff point in M 92 and M 3 is found at $M_{\text{bol}} = +3.6$. The agreement between the computed and observed values appears so good that it may fairly be taken as a confirmation of the above interpretation of the observed turnoff point.

Inverting the argument, one may also take this agreement as indicating the correctness of the assumed age of the globular clusters, at least within a factor of 2.

VII. SPECULATION ON THE BRIGHTER STARS IN GLOBULAR CLUSTERS

In the previous section we have discussed the early evolutionary phases of unmixed stars, from the Cowling model through the Schönberg-Chandrasekhar limit to the beginning of the core contraction with simultaneous envelope expansion. It is tempting now to speculate on the subsequent evolutionary phases which presumably are represented by the brighter globular cluster stars which may have gone through the earlier phases at a relatively faster rate, owing to a somewhat larger mass. However, for these subsequent phases the present models are soon found quite inadequate, and only some qualitative estimates seem possible until further integrations are made.

The first difficulty arises when the rate is computed with which a star evolves from model I to model VII. By using equation (22) (but replacing L by L_n and q_1 by δq_1), one finds that a star evolves from model I to model VII in about a twentieth of the time it takes to evolve from the Cowling model to model I. Hence one should expect in the H-R

[8] Arp, Baum, and Sandage, *A.J.*, **57**, 4, 1952.

[9] Harrison, *Ap. J.*, **105**, 322, 1947.

diagram of a globular cluster a good deal fewer stars just beyond the Schönberg-Chandrasekhar limit (model I) than just below this limit contrary to observation. Preliminary tests, however, seem to indicate that the evolution rate during the core contraction may possibly be appreciably modified by moderate changes in the present assumptions, so that this difficulty, though not solved, does not seem too serious.

A second difficulty arises when the extent of the envelope expansion is considered. Under the present assumptions there is no reason why the envelope expansion should stop at or before model VII, while the observed H-R diagrams of globular clusters seem to indicate that the expansion should essentially stop about at model V, and then mainly a brightening (increase in C) and only little further expansion (little increase in t_1) should occur. One may speculate that around model V a physical process not included in the present computations should start to play an essential role.

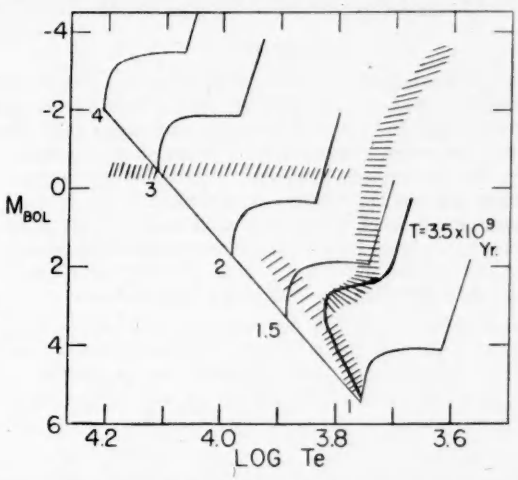

FIG. 4.—Speculative evolutionary tracks for stars of various masses with an assumed temperature of $1.1 \times 10^{8\,\circ}$K for the helium burning. The schematic globular cluster H–R diagram is shown for comparison. The heavy line is the theoretical appearance of the diagram 3.5×10^9 years after the formation of the stars.

As a first hypothesis for the needed process, one may think of the transmutation of helium into heavier elements. The central temperature reached in model V ($1.1 \times 10^{8\,\circ}$ K) is rather lower than the temperature needed for helium burning ($2 \times 10^{8\,\circ}$ K) as derived by Salpeter,[10] but still just within the limits of the uncertainty of this derivation. Following this hypothesis, preliminary estimates were made for the subsequent models which should consist of a hydrogen-rich envelope, a shell in which hydrogen burns, a helium-rich intermediate zone, a shell in which helium burns, and an inert core of heavy elements. The estimated evolution through these phases is indicated in Figure 4 in the vertical upper ends of the heavy lines, with the assumption of $1.1 \times 10^{8\,\circ}$ K for the temperature of the helium burning. (The main-sequence model and models I–V are not quite plotted at the same places in Figs. 3 and 4, since in the latter case shell temperatures ranging from $20 \times 10^{6\,\circ}$ K for the main sequence to $30 \times 10^{6\,\circ}$ K for model V were used instead of $30 \times 10^{6\,\circ}$ K throughout Fig. 3.) Whenever the evolution tracks for individual stars are given in the H-R diagram, one can derive a curve

[10] E. Salpeter, *Ap. J.*, **115**, 326, 1952.

crossing the tracks and connecting all points reached by stars of various masses at the same time. Such a curve, computed for a time of 3.5×10^9 years, is shown by the heavy line in Figure 4. This curve seems to fit well the main observed feature of the lower portions of the H-R diagram of globular clusters. Nevertheless, it seems far from certain whether this hypothesis regarding the early termination of the envelope expansion is correct, since the necessary temperature for the helium burning seems rather low.

As a second hypothesis for the process causing the termination of the expansion, one might think of moderate mixing of the layers near the shell caused by rotation. This would decrease the effect of the chemical inhomogeneity and thus reduce the expansion. The mixing by rotation should affect all evolutionary phases but possibly the later ones particularly strongly. It then seems plausible that the observed feature of the H-R diagram of globular clusters might be explained by changing the present models by introducing a moderate amount of mixing. To follow this, however, further integrations are necessary.

VIII. SUMMARY

The application of the evolutionary fitting condition of Section III has made it possible to follow from an initial state the evolution of stars built on a shell-source model with a chemical discontinuity between the envelope and a contracting core. The detailed computations show that as the core contracts, liberating gravitational energy, the envelope greatly expands (Fig. 3), giving giant stars with internal temperatures high enough for the nuclear processes to provide the required luminosities.

A theoretical Hertzsprung-Russell diagram based on the derived models was compared with the observed diagrams for globular clusters. Good agreement was found for the fainter stars, i.e., the earlier evolution phases. However, the present models were found inadequate to explain the brighter features of the diagram.

THE TRANSFER OF RADIATION BY AN EMITTING ATMOSPHERE

HENRY G. HORAK*
University of Kansas
Received July 24, 1952

ABSTRACT

The transfer of radiation by a plane-parallel atmosphere containing a uniform distribution of emission sources is considered for two cases: (*a*) isotropic scattering with an albedo ϖ_0, (*b*) scattering according to the asymmetric phase function $\varpi_0(1 + x \cos \Theta)$. The exact expressions for the emergent intensity are derived for both semi-infinite and finite atmospheres. It is also shown how the intensity at any optical depth may be obtained. The formulae are applied to the case of the galactic light.

I. INTRODUCTION

The problem of the transfer of radiation by an emitting atmosphere has arisen in several contexts, e.g., in the study of the diffuse radiation in the galaxy.[1] The object of this paper is to present the exact solutions of several of the theoretical problems. We shall restrict the discussion to a plane-parallel atmosphere (semi-infinite or finite) with a uniform distribution of energy sources. A variety of phase functions can be studied; however, we shall consider only two types, viz., (*a*) the spherical phase function ϖ_0 and (*b*) the asymmetric phase function $\varpi_0(1 + x \cos \Theta)$. The methods and notation we shall use are those developed by Chandrasekhar.[2]

II. SYMMETRIES AND INVARIANCES

Consider a plane-parallel atmosphere of finite optical thickness τ_1, which contains a uniform distribution of energy sources. It is apparent that the radiation field will exhibit axial symmetry about an axis perpendicular to the stratification; and, if we measure the optical depth normally from the top surface, we must have (Fig. 1):

$$I(\tau, +\mu) = I(\tau_1 - \tau, -\mu) \qquad (0 \leqq \mu \leqq 1), \tag{1}$$

where $I(\tau, +\mu)$ represents the specific intensity of radiation (including both the direct light from the emission and the diffuse light) at the level τ which is traveling in the direction $\mu = \cos \vartheta$ $(0 \leqq \vartheta \leqq 90°)$.

There are two principles of invariance which we shall use in the subsequent discussion. These may be formulated as follows:

1. The intensity $I(\tau, +\mu)$ in the upward direction at any level τ is the sum of the intensity $\mathfrak{J}_{\tau_1-\tau}(\tau, +\mu)$ which would be emitted at the level τ if there were no layer from 0 to τ, plus the intensity at the level τ which is due to the intensity $I(\tau, -\mu')$ being scattered upward by the layer below τ.

The mathematical formulation of this principle is (Fig. 2):

$$I(\tau, +\mu) = \mathfrak{J}_{\tau_1-\tau}(\tau, +\mu) + \frac{1}{2\mu}\int_0^1 S(\tau_1 - \tau; \mu, \mu')\, I(\tau, -\mu')\, d\mu', \tag{2}$$

where $S(\tau_1 - \tau; \mu, \mu')$ is the scattering function (*R.T.*, p. 20).

2. The emergent intensity $I(\tau_1, -\mu)$ in the downward direction is the sum of the intensity $\mathfrak{J}_{\tau_1-\tau}(\tau_1, -\mu)$ which would be emitted at τ_1 if there were no layer from 0 to τ,

* Visiting professor at the Yerkes Observatory during July and August, 1951.

[1] Henyey and Greenstein, *Ap. J.*, **93**, 70, 1941.

[2] *Radiative Transfer* (Oxford: Clarendon Press, 1950); hereafter referred to as "*R.T.*"

plus the intensity at τ_1 due to the intensity $I(\tau, -\mu')$ being transmitted by the layer below τ.

The mathematical formulation of this principle is (Fig. 3):

$$I(\tau_1, -\mu) = \mathfrak{J}_{\tau_1-\tau}(\tau_1, -\mu) + e^{-(\tau_1-\tau)/\mu} I(\tau, -\mu) + \frac{1}{2\mu}\int_0^1 T(\tau_1-\tau; \mu, \mu')\, I(\tau, -\mu')\, d\mu', \tag{3}$$

where $T(\tau_1 - \tau; \mu, \mu')$ is the transmission function (*R.T.*, p. 20).

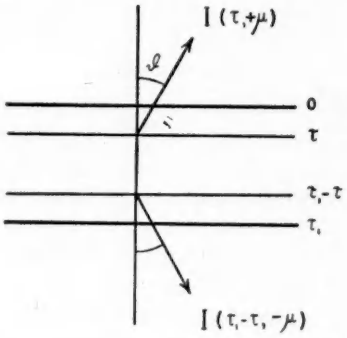

FIG. 1.—The finite, plane-parallel, emitting atmosphere

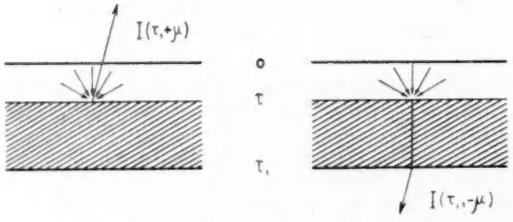

FIG. 2.—Invariance principle 1 FIG. 3.—Invariance principle 2

Owing to the symmetry of the problem, we have

$$\mathfrak{J}_{\tau_1-\tau}(\tau, +\mu) = \mathfrak{J}_{\tau_1-\tau}(\tau_1, -\mu), \tag{4}$$

and we can combine equations (2) and (3). Thus

$$I(\tau, +\mu) = I(\tau_1, -\mu) - e^{-(\tau_1-\tau)/\mu} I(\tau, -\mu) + \frac{1}{2\mu}\int_0^1 S(\tau_1-\tau; \mu, \mu') \times I(\tau, -\mu')\, d\mu' - \frac{1}{2\mu}\int_0^1 T(\tau_1-\tau; \mu, \mu')\, I(\tau, -\mu')\, d\mu'. \tag{5}$$

Differentiating with respect to τ and setting $\tau = 0$, we obtain

$$\left[\frac{dI(\tau, +\mu)}{d\tau}\right]_0 = -e^{-\tau_1/\mu}\left[\frac{dI(\tau, -\mu)}{d\tau}\right]_0 + \frac{1}{2\mu}\int_0^1 S(\tau_1; \mu, \mu') \times \left[\frac{dI(\tau, -\mu')}{d\tau}\right]_0 d\mu' - \frac{1}{2\mu}\int_0^1 T(\tau_1; \mu, \mu')\left[\frac{dI(\tau, -\mu')}{d\tau}\right]_0 d\mu'. \tag{6}$$

The equation of transfer may be written for the axially symmetric case as follows:

$$\mu\frac{dI(\tau, \mu)}{d\tau} = I(\tau, \mu) - \mathfrak{J}(\tau, \mu), \tag{7}$$

where $\mathfrak{J}(\tau, \mu)$ is the source function. The derivatives which appear in equation (6) may be obtained directly from equation (7), thus:

$$\left[\frac{dI(\tau, +\mu)}{d\tau}\right]_0 = \frac{1}{\mu}[I(0, +\mu) - \mathfrak{J}(0, +\mu)], \tag{8}$$

and

$$\left[\frac{dI(\tau, -\mu)}{d\tau}\right]_0 = \frac{1}{\mu}\mathfrak{J}(0, -\mu). \tag{9}$$

Substituting equations (8) and (9) in equation (6), we obtain the fundamental equation for the emergent intensity:

$$I(0, +\mu) = \mathfrak{J}(0, +\mu) - e^{-\tau_1/\mu}\mathfrak{J}(0, -\mu) + \frac{1}{2}\int_0^1 S(\tau_1; \mu, \mu')\,\mathfrak{J}(0, -\mu') \times \frac{d\mu'}{\mu'} - \frac{1}{2}\int_0^1 T(\tau_1; \mu, \mu')\,\mathfrak{J}(0, -\mu')\,\frac{d\mu'}{\mu'}. \tag{10}$$

For various types of phase functions the scattering and transmission functions have been determined by Chandrasekhar (e.g., *R.T.*, pp. 209, 227), and, of course, the source functions are known. The source function for the case of a finite (or semi-infinite) atmosphere with a uniform distribution of energy sources may be written as follows:

$$\mathfrak{J}(\tau, \mu) = \frac{1}{2}\int_{-1}^{+1} p^{(0)}(\mu, \mu')\, I(\tau, \mu')\, d\mu' + \epsilon, \tag{11}$$

where ϵ is the constant source function for the emission sources,

$$p^{(0)}(\mu, \mu') = \frac{1}{2\pi}\int_0^{2\pi} p(\mu, \phi; \mu', \phi')\, d\phi'$$

and $p(\mu, \phi; \mu', \phi')$ is the phase function.

The invariance principles can also be used to find the intensity at any optical depth τ. From equation (2) we have:

$$I(\tau, +\mu) = \mathfrak{I}_{\tau_1-\tau}(\tau, +\mu) + \frac{1}{2\mu}\int_0^1 S(\tau_1 - \tau; \mu, \mu')\, I(\tau, -\mu')\, d\mu',$$
$$I(\tau, -\mu) = \mathfrak{I}_{\tau}(\tau, -\mu) + \frac{1}{2\mu}\int_0^1 S(\tau; \mu, \mu')\, I(\tau, +\mu')\, d\mu', \tag{12}$$

where $\mathfrak{I}_{\tau_1-\tau}(\tau, +\mu)$, $\mathfrak{I}_{\tau}(\tau, -\mu)$, $S(\tau_1 - \tau)$, and $S(\tau)$ are all known. A method of successive approximation can be used to find $I(\tau, +\mu)$ and $I(\tau, -\mu)$. However, in order to start the solution, it is necessary to have approximate values for $I(\tau, +\mu)$ and $I(\tau, -\mu)$.

The latter can be obtained by solving the equation of transfer by an approximation method which will be described later.

When $\tau = \tau_1/2$, equations (12) reduce to the single equation:

$$I\left(\frac{\tau_1}{2}, +\mu\right) = I\left(\frac{\tau_1}{2}, -\mu\right) = \mathfrak{J}_{\tau_1/2}\left(\frac{\tau_1}{2}, +\mu\right) + \frac{1}{2\mu}\int_0^1 S\left(\frac{\tau_1}{2}; \mu, \mu'\right) I\left(\frac{\tau_1}{2}, +\mu'\right) d\mu' . \tag{13}$$

III. ISOTROPIC SCATTERING

In the case of isotropic scattering with an albedo $\varpi_0 \leqq 1$, we have the following relations (*R.T.*, p. 209):

$$\begin{aligned} p^{(0)}(\mu, \mu') &= \varpi_0 , \\ \mathfrak{J}(\tau, \mu) &= \frac{\varpi_0}{2}\int_{-1}^{+1} I(\tau, \mu')\, d\mu' + \epsilon , \\ S(\tau_1; \mu, \mu') &= \varpi_0 \frac{\mu\mu'}{\mu + \mu'}\left[X(\mu) X(\mu') - Y(\mu) Y(\mu')\right] , \\ T(\tau_1; \mu, \mu') &= \varpi_0 \frac{\mu\mu'}{\mu - \mu'}\left[Y(\mu) X(\mu') - X(\mu) Y(\mu')\right] , \end{aligned} \tag{14}$$

where the X- and Y-functions are defined with respect to the characteristic function $\Psi = \varpi_0/2$.

Using relations (14), it is possible to write equation (10) in the form

$$I(0, +\mu) = \{\varpi_0 J(0) + \epsilon\}\left\{\left[1 + \frac{1}{2}\int_0^1 S(\tau_1; \mu, \mu')\frac{d\mu'}{\mu'}\right] - \left[e^{-\tau_1/\mu} + \frac{1}{2}\int_0^1 T(\tau_1; \mu, \mu')\frac{d\mu'}{\mu'}\right]\right\} , \tag{15}$$

where

$$J(0) = \frac{1}{2}\int_0^1 I(0, \mu')\, d\mu' . \tag{16}$$

It follows that

$$I(0, +\mu) = \{\varpi_0 J(0) + \epsilon\}\left[X(\mu) - Y(\mu)\right] . \tag{17}$$

It remains to determine $J(0)$. Multiplying through equation (17) by $\frac{1}{2}$ and integrating over the range of μ gives

$$J(0) = \tfrac{1}{2}\{\varpi_0 J(0) + \epsilon\}\left[\alpha_0 - \beta_0\right] , \tag{18}$$

where α_0 and β_0 are, respectively, the zero moments of X and Y. Solving for $J(0)$, we obtain

$$J(0) = \frac{\epsilon(\alpha_0 - \beta_0)}{2 - \varpi_0(\alpha_0 - \beta_0)} . \tag{19}$$

Substituting this expression in equation (17) gives the final and exact solution for the emergent intensity:

$$I(0, +\mu) = \frac{2\epsilon}{2 - \varpi_0(\alpha_0 - \beta_0)}\left[X(\mu) - Y(\mu)\right] . \tag{20}$$

We have a relation between a_0 and β_0. (*R.T.*, theorem p. 189):

$$\beta_0^2 = a_0^2 - \frac{4}{\varpi_0} a_0 + \frac{4}{\varpi_0}. \tag{21}$$

When $\tau_1 \to \infty$, $Y(\mu) \to 0$, $X(\mu) \to H(\mu)$, and from theorem 1 (*R.T.*, p. 106) we have

$$\varpi_0 a_0 = 2 - 2\sqrt{(1-\varpi_0)}\ . \tag{22}$$

It follows that the emergent intensity in the semi-infinite case is given by

$$I(0, +\mu) = \epsilon (1-\varpi_0)^{-1/2} H(\mu)\ . \tag{23}$$

This result can be obtained directly from invariance 1 (eq. [2]), which, for a semi-infinite atmosphere, takes the form

$$I(\tau, +\mu) = I(0, +\mu) + \frac{1}{2\mu}\int_0^1 S(\infty; \mu, \mu')\, I(\tau, -\mu')\, d\mu'. \tag{24}$$

We shall next obtain the solution of the equation of transfer in the nth approximation. The equation of transfer appropriate to the problem has the form

$$\mu \frac{dI(\tau, \mu)}{d\tau} = I(\tau, \mu) - \frac{\varpi_0}{2}\int_{-1}^{+1} I(\tau, \mu')\, d\mu' - \epsilon. \tag{25}$$

Following the now standard practice, we shall replace the integral by a sum and the equation (25) by a simultaneous system of linear differential equations. Thus

$$\mu_i \frac{dI_i}{d\tau} = I_i - \frac{\varpi_0}{2}\sum_j a_j I_j - \epsilon \qquad (i, j = \pm 1, \ldots, \pm n), \tag{26}$$

where a_i and μ_i are, respectively, the Gaussian weights and divisions and I_j is the intensity $I(\tau, \mu_j)$.

The solution of the homogeneous system is known to be (*R.T.*, p. 195)

$$I_i = \sum_{\alpha=-n}^{+n} \frac{L_\alpha e^{-k_\alpha \tau}}{1+\mu_i k_\alpha} \qquad (i = \pm 1, \ldots, \pm n), \tag{27}$$

where the k_α's are the $2n$ roots of the characteristic equation

$$1 = \varpi_0 \sum_{j=1}^{n} \frac{a_j}{1-\mu_j^2 k^2}, \tag{28}$$

and the L_α's are $2n$ constants of integration determined from the boundary conditions.

The particular integral is

$$I_i = \frac{\epsilon}{1-\varpi_0} \qquad (\varpi_0 < 1), \tag{29}$$

so that the complete solution for the intensities at the points of the Gaussian division is given by

$$I_i = \sum_{\alpha=-n}^{+n} \frac{L_\alpha e^{-k_\alpha \tau}}{1+\mu_i k_\alpha} + \frac{\epsilon}{1-\varpi_0} \qquad (i = \pm 1, \ldots, \pm n). \tag{30}$$

The boundary conditions are

$$\text{and} \qquad \begin{aligned} I_{-i} &= 0 \quad \text{at} \quad \tau = 0 \\ I_{+i} &= 0 \quad \text{at} \quad \tau = \tau_1 \end{aligned} \qquad (i = 1, \ldots, n). \tag{31}$$

Let us define the function

$$T(\tau, \mu) = \sum_{a=-n}^{+n} \frac{L_a e^{-k_a \tau}}{1 + \mu k_a} + \frac{\epsilon}{1 - \varpi_0}. \tag{32}$$

The boundary conditions are then equivalent to

$$T(0, -\mu_i) = T(\tau_1, +\mu_i) = 0 \qquad (i = 1, \ldots, n). \tag{33}$$

The solution for the intensity at any depth is obtained from the formal solution of the equation of transfer, viz.,

$$I(\tau, +\mu) = \int_{\tau}^{\tau_1} e^{-(t-\tau)/\mu} \mathfrak{J}(t) \frac{dt}{\mu}. \tag{34}$$

The source function, $\mathfrak{J}(t)$, may be written

$$\mathfrak{J}(t) = \sum_{a=-n}^{+n} L_a e^{-k_a t} + \frac{\epsilon}{1 - \varpi_0}; \tag{35}$$

whence it follows that

$$I(\tau, +\mu) = I(\tau_1 - \tau, -\mu) = T(\tau, \mu) - e^{(\tau - \tau_1)/\mu} T(\tau_1, \mu) \tag{36}$$

and

$$I(\tau, -\mu) = T(\tau, -\mu) - e^{-\tau/\mu} T(0, -\mu). \tag{37}$$

These equations give us the solution in the nth approximation for the intensity at any optical depth τ.

It is possible to express the solution for the emergent intensity, $I(0, \mu)$, in a closed form which does not involve the constants L_a explicitly; however, this cannot be done for the intensity $I(\tau, \mu)$, because the solution involves other functions than those which express the boundary conditions.

IV. SCATTERING ACCORDING TO THE PHASE FUNCTION $\varpi_0(1 + x \cos \Theta)$

In the case of scattering according to the asymmetric phase function $\varpi_0(1 + x \cos \Theta)$ we have the following relations (*R.T.*, p. 227):

$$\begin{aligned} p^{(0)}(\mu, \mu') &= \varpi_0 (1 + x \mu \mu'), \\ \mathfrak{J}(\tau, \mu) &= \frac{\varpi_0}{2} \int_{-1}^{+1} I(\tau, \mu')\, d\mu' + \epsilon + \mu \frac{\varpi_0 x}{2} \int_{-1}^{+1} I(\tau, \mu')\, \mu' d\mu', \\ S(\tau_1; \mu, \mu') &= \varpi_0 \frac{\mu \mu'}{\mu + \mu'} \{\psi(\mu)\psi(\mu') - \chi(\mu)\chi(\mu') \\ &\qquad - x[\phi(\mu)\phi(\mu') - \zeta(\mu)\zeta(\mu')]\}, \\ T(\tau_1; \mu, \mu') &= \varpi_0 \frac{\mu \mu'}{\mu - \mu'} \{\chi(\mu)\psi(\mu') - \psi(\mu)\chi(\mu') \\ &\qquad + x[\zeta(\mu)\phi(\mu') - \phi(\mu)\zeta(\mu')]\}, \end{aligned} \tag{38}$$

where

$$\psi(\mu) = 1 + \frac{1}{2}\int_0^1 S(\tau_1; \mu, \mu')\frac{d\mu'}{\mu'},$$

$$\phi(\mu) = \mu - \frac{1}{2}\int_0^1 S(\tau_1; \mu, \mu')\, d\mu',$$

$$\chi(\mu) = e^{-\tau_1/\mu} + \frac{1}{2}\int_0^1 T(\tau_1; \mu, \mu')\frac{d\mu'}{\mu'}, \tag{39}$$

$$\zeta(\mu) = \mu e^{-\tau_1/\mu} + \frac{1}{2}\int_0^1 T(\tau_1; \mu, \mu')\, d\mu'.$$

Using equations (38), it is possible to write equation (10) in the form

$$I(0, +\mu) = \{\varpi_0 J(0) + \epsilon\}\left\{\left[1 + \frac{1}{2}\int_0^1 S(\tau_1; \mu, \mu')\frac{d\mu'}{\mu'}\right] - \left[e^{-\tau_1/\mu} + \frac{1}{2}\int_0^1 T(\tau_1; \mu, \mu')\frac{d\mu'}{\mu'}\right]\right\} + \left\{\frac{\varpi_0 x}{4}F(0)\right\}\left\{\left[\mu - \frac{1}{2}\int_0^1 S(\tau_1; \mu, \mu')\, d\mu'\right] + \left[\mu e^{-\tau_1/\mu} + \frac{1}{2}\int_0^1 T(\tau_1; \mu, \mu')\, d\mu'\right]\right\}, \tag{40}$$

where

$$J(0) = \frac{1}{2}\int_0^1 I(0, \mu')\, d\mu' \tag{41}$$

and

$$F(0) = 2\int_0^1 I(0, \mu')\, \mu' d\mu', \tag{42}$$

or

$$I(0, +\mu) = [\varpi_0 J(0) + \epsilon][\psi(\mu) - \chi(\mu)] + \left[\frac{\varpi_0 x}{4}F(0)\right][\phi(\mu) + \zeta(\mu)]. \tag{43}$$

Furthermore, it can be shown that (*R.T.*, p. 230)

$$\begin{aligned} \psi(\mu) &= (1 - c_1\mu)\, X(\mu) - c_2\mu\, Y(\mu), \\ \chi(\mu) &= (1 + c_1\mu)\, Y(\mu) + c_2\mu X(\mu), \\ \phi(\mu) &= \mu[q_1 X(\mu) + p_1 Y(\mu)], \\ \zeta(\mu) &= \mu[p_1 X(\mu) + q_1 Y(\mu)], \end{aligned} \tag{44}$$

where the X- and Y-functions are defined in terms of the characteristic function $\Psi(\mu) = \varpi_0/2[1 + x(1 - \varpi_0)\mu^2]$, and the constants c_1, c_2, p_1, and q_1 are given by

$$c_1 = x\varpi_0(1 - \varpi_0)\frac{(2 - \varpi_0\alpha_0)\,\alpha_1 - \varpi_0\beta_0\beta_1}{(2 - \varpi_0\alpha_0)^2 - \varpi_0^2\beta_0^2},$$

$$c_2 = x\varpi_0(1 - \varpi_0)\frac{-(2 - \varpi_0\alpha_0)\,\beta_1 + \varpi_0\beta_0\alpha_1}{(2 - \varpi_0\alpha_0)^2 - \varpi_0^2\beta_0^2}, \tag{45}$$

$$p_1 = \frac{2\varpi_0\beta_0(1 - \varpi_0)}{(2 - \varpi_0\alpha_0)^2 - \varpi_0^2\beta_0^2}, \qquad q_1 = \frac{2(2 - \varpi_0\alpha_0)(1 - \varpi_0)}{(2 - \varpi_0\alpha_0)^2 - \varpi_0^2\beta_0^2}.$$

It remains to evaluate $J(0)$ and $F(0)$. This can be done by multiplying through equation (43) by $\frac{1}{2}$ and 2μ, respectively, and integrating over the range of μ. We obtain two simultaneous linear equations for the unknowns $J(0)$ and $F(0)$, and when we perform the reductions, we find that the coefficient of μ in the final expression for $I(0, +\mu)$ vanishes. This means that we have

$$I(0, +\mu) = [\varpi_0 J(0) + \epsilon][X(\mu) - Y(\mu)], \tag{46}$$

or

$$I(0, +\mu) = \frac{2\epsilon}{2 - \varpi_0(\alpha_0 - \beta_0)}[X(\mu) - Y(\mu)], \tag{47}$$

which has exactly the same form as in the isotropic case (eq. [20]), and the X- and Y-functions are defined in terms of the characteristic function $\Psi(\mu) = \varpi_0/2[1 + x(1 - \varpi_0)\mu^2]$.

For the semi-infinite case it can be readily verified that the emergent intensity is given by

$$I(0, +\mu) = \frac{2\epsilon}{2 - \varpi_0\alpha_0} H(\mu), \tag{48}$$

where the H-function is defined in terms of the same characteristic function.

We shall next obtain the solution of the equation of transfer in the nth approximation. The equation of transfer appropriate to the problem may be written

$$\mu \frac{dI(\tau, \mu)}{d\tau} = I(\tau, \mu) - \frac{\varpi_0}{2}\int_{-1}^{+1} I(\tau, \mu')\, d\mu' - \mu\frac{\varpi_0 x}{2}\int_{-1}^{+1} I(\tau, \mu')\,\mu' d\mu' - \epsilon. \tag{49}$$

We shall replace this equation by a system of $2n$ equations, and replace the integrals by sums, thus:

$$\mu_i \frac{dI_i}{d\tau} = I_i - \frac{\varpi_0}{2}\sum_j a_j I_j - \mu_i\frac{\varpi_0 x}{2}\sum_j a_j\mu_j I_j - \epsilon \qquad (i, j = \pm 1, \ldots, \pm n), \tag{50}$$

where a_j and μ_j are, respectively, the Gaussian weights and divisions.

The solution of the homogeneous part is[3]

$$I_i = \sum_{a=-n}^{+n} \frac{L_a[1 - x(1 - \varpi_0)\mu_i/k_a]}{1 + \mu_i k_a} e^{-k_a\tau} \qquad (i = \pm 1, \ldots, \pm n), \tag{51}$$

where the k_a's are the $2n$ roots of the characteristic equation

$$1 = \varpi_0\sum_{j=1}^{n} \frac{a_j[1 + x(1 - \varpi_0)\mu_j^2]}{1 - \mu_j^2 k^2}, \tag{52}$$

and the L_a's are $2n$ constants of integration which can be determined from the boundary conditions.

The particular integral is

$$I_i = \frac{\epsilon}{1 - \varpi_0} \qquad (\varpi_0 < 1). \tag{53}$$

Hence the complete solution of equation (50) at the points of the Gaussian division is given by

$$I_i = \sum_{a=-n}^{+n} \frac{L_a[1 - x(1 - \varpi_0)\mu_i/k_a]}{1 + \mu_i k_a} e^{-k_a\tau} + \frac{\epsilon}{1 - \varpi_0} \qquad (i = \pm 1, \ldots, \pm n). \tag{54}$$

[3] Chandrasekhar, "Radiative Equilibrium. IX," *Ap. J.*, **103**, 169, eq. (32), 1946.

The $2n$ constants L_a can be found from the boundary conditions, viz., $I_{-i} = 0$ at $\tau = 0$ and $I_{+i} = 0$ at $\tau = \tau_1$ for $i = 1, \ldots, n$, or, equivalently,

$$T(0, -\mu_i) = T(\tau_1, +\mu_i) = 0 \qquad (i = 1, \ldots, n), \tag{55}$$

where

$$T(\tau, \mu) = \sum_{a=-n}^{+n} \frac{L_a [1 - x(1-\varpi_0)\mu/k_a]}{1 + \mu k_a} e^{-k_a \tau} + \frac{\epsilon}{1-\varpi_0}. \tag{56}$$

The radiation field can be found from the formal solution of the equation of transfer, viz.,

$$I(\tau, +\mu) = \int_{\tau}^{\tau_1} e^{-(t-\tau)/\mu} \mathfrak{J}(t, \mu) \frac{dt}{\mu}, \tag{57}$$

where the source function is given by

$$\begin{aligned} \mathfrak{J}(t, \mu) &= \frac{\varpi_0}{2} \sum_j a_j I_j + \mu \frac{\varpi_0 x}{2} \sum_j a_j \mu_j I_j + \epsilon, \\ &= \sum_{a=-n}^{+n} L_a \left[1 - x(1-\varpi_0)\frac{\mu}{k_a}\right] e^{-k_a \tau} + \frac{\epsilon}{1-\varpi_0}. \end{aligned} \tag{58}$$

It may be verified that the intensity at any optical depth τ is given by

$$I(\tau, +\mu) = I(\tau_1 - \tau, -\mu) = T(\tau, \mu) - e^{(\tau-\tau_1)/\mu} T(\tau_1, \mu), \tag{59}$$

and

$$I(\tau, -\mu) = T(\tau, -\mu) - e^{-\tau/\mu} T(0, -\mu). \tag{60}$$

V. CONSERVATIVE SCATTERING

In conservative scattering the albedo ϖ_0 is unity. The results obtained from the invariance principles in the preceding sections formally still apply, and the emergent field for an atmosphere of finite thickness is given by

$$I(0, +\mu) = \frac{2\epsilon}{2 - (a_0 - \beta_0)} [X(\mu) - Y(\mu)]. \tag{61}$$

However, in view of the nonuniqueness of the conservative case,[4] it is necessary to make use of the standard solutions; thus:

$$\begin{aligned} X(\mu) &= X_s(\mu) + Q\mu [X_s(\mu) + Y_s(\mu)], \\ Y(\mu) &= Y_s(\mu) - Q\mu [X_s(\mu) + Y_s(\mu)], \\ a_0 &= 2 + Q(a_1^s + \beta_1^s), \\ \beta_0 &= -Q(a_1^s + \beta_1^s). \end{aligned} \tag{62}$$

It can be shown that Q must be given by

$$Q = -\frac{a_1^s - \beta_1^s}{(a_1 + \beta_1)\tau_1 + 2(a_2 + \beta_2)}, \tag{63}$$

and the final solution has the form

$$I(0, +\mu) = \frac{\epsilon}{-Q(a_1 + \beta_1)} [X^*(\mu) - Y^*(\mu)], \tag{64}$$

[4] Cf. *R.T.*, pp. 190 ff.

where X^* and Y^* are the X- and Y-functions determined from equations (62) when Q has the value given by equation (63).

It is apparent that for a semi-infinite atmosphere the emergent field becomes infinitely large in the conservative case.

It may be added here that in the finite approximation solutions with $\varpi_0 = 1$ it is necessary to use new particular integrals, since equations (29) and (53) are valid only for $\varpi_0 < 1$. It may be verified that equation (29) must be replaced by $I_i = -3\epsilon\tau^2/2 - 3\epsilon\tau\mu_i - 3\epsilon\mu_i^2$, and equation (53) by $I_i = (-3+x)\epsilon\tau^2/2 - 3\epsilon\tau\mu_i - 3\epsilon\mu_i^2$.

VI. COMPUTATIONS

The radiation field produced by an emitting atmosphere can be calculated for any assigned values of τ_1, ϖ_0, and x. We shall not concern ourselves with ϵ but shall evaluate $I(\tau, \mu)/\epsilon$.

We can distinguish between the total radiation field, $I(\tau, \mu)/\epsilon$, already discussed; the direct field, $I_0(\tau, \mu)/\epsilon$; and the diffuse field, $I_1(\tau, \mu)/\epsilon$. The direct field is found by solving the equation of transfer in the form

$$\mu \frac{dI_0(\tau, \mu)}{d\tau} = I_0(\tau, \mu) - \epsilon, \tag{65}$$

the solution of which is

$$I_0(\tau, +\mu) = \epsilon(1 - e^{-(\tau_1 - \tau)/\mu}). \tag{66}$$

The diffuse field is then given by

$$\frac{I_1(\tau, \mu)}{\epsilon} = \frac{I(\tau, \mu)}{\epsilon} - \frac{I_0(\tau, \mu)}{\epsilon}. \tag{67}$$

Some computations have been made which are summarized in Tables 1–5. In Table 1

TABLE 1

SEMI-INFINITE ATMOSPHERE

$I(0, \mu)/\epsilon$

μ	$\varpi_0 = 0.5$	$\varpi_0 = 0.5$, $x = 1$	μ	$\varpi_0 = 0.5$	$\varpi_0 = 0.5$, $x = 1$	μ	$\varpi_0 = 0.5$	$\varpi_0 = 0.5$, $x = 1$
0.00	1.414	1.432	0.30	1.618	1.674	0.70	1.723	1.813
.05	1.477	1.502	.40	1.652	1.718	0.80	1.741	1.836
.10	1.517	1.549	.50	1.680	1.754	0.90	1.756	1.857
0.20	1.575	1.620	0.60	1.703	1.785	1.00	1.770	1.876

the emergent radiation field is tabulated for a semi-infinite emitting atmosphere. Two cases only are given, viz., isotropic scattering with $\varpi_0 = 0.5$ and scattering according to the phase function $0.5(1 + \cos\Theta)$. The calculations were made by means of equations (23) and (48) and the exact H-functions and moments.[5] Table 2 gives factors to assist the computer in computing the emergent field of a semi-infinite atmosphere for various values of ϖ_0.

Table 3 gives the radiation field at the surface and at other optical depths for a finite atmosphere of optical thickness $\tau_1 = 0.20$. Two cases are considered, viz., $\varpi_0 = 0.5$ and $\varpi_0 = 0.5$, $x = 1$. These are second-approximation solutions based on equations (33), (36), (55), and (59) with $n = 2$. The constants for these solutions are given in Table 4. It is interesting to notice the close agreement between the isotropic and asymmetric cases.

The exact intensities are given in Table 5 for an atmosphere of optical thickness

[5] Chandrasekhar and Breen, *Ap. J.*, **106**, 143, 1947, and **107**, 216, 1948.

$\tau_1 = 0.20$, which scatters light isotropically with albedo, respectively, $\varpi_0 = 0.5, 0.8, 0.9, 0.95$, and 1.00. The emergent fields are given as computed from equations (20), (64), (66), and (67). The exact X- and Y-functions and moments were used.[6] The exact solution for $I(\tau_1/2, \mu)/\epsilon$ under $\varpi_0 = 0.5$ was obtained by iteration, using equation (13). The iteration was started with the intensities determined in the second approximation. The quadratures were performed by the "repeated Weddle's" rule, using ten equal intervals.

TABLE 2

ϖ_0	$p(\cos\Theta)=\varpi_0$ $(1-\varpi_0)^{-1/2}$	$p(\cos\Theta)=\varpi_0(1+\cos\Theta)$ $2/2-\varpi_0a_0$	ϖ_0	$p(\cos\Theta)=\varpi_0$ $(1-\varpi_0)^{-1/2}$	$p(\cos\Theta)=\varpi_0(1+\cos\Theta)$ $2/2-\varpi_0a_0$	ϖ_0	$p(\cos\Theta)=\varpi_0$ $(1-\varpi_0)^{-1/2}$	$p(\cos\Theta)=\varpi_0(1+\cos\Theta)$ $2/2-\varpi_0a_0$
0.100...	1.05409	1.05445	0.500...	1.41421	1.43183	0.900...	3.16228	3.43078
.200...	1.11803	1.11967	.600...	1.58114	1.61344	.950...	4.47213	4.99139
.300...	1.19523	1.19955	.700...	1.82574	1.88494	0.975...	6.32455	7.22530
0.400...	1.29099	1.30018	0.800...	2.23607	2.35081			

TABLE 3

$\tau_1 = 0.20$; SECOND-APPROXIMATION SOLUTIONS

μ	$\varpi_0=0.5$				$\varpi_0=0.5$, $x=1$	
	$I(0,\mu)/\epsilon$	$I(\tau_1/4,\mu)/\epsilon$	$I(\tau_1/4,-\mu)/\epsilon$	$I(\tau_1/2,\mu)/\epsilon$	$I(0,\mu)/\epsilon$	$I(\tau_1/2,\mu)/\epsilon$
0.00....	1.100	1.110	1.110	1.113	1.100	1.112
0.02....	1.104	1.111	1.017	1.105	1.105	1.104
0.05....	1.087	1.056	0.700	0.961	1.088	0.959
0.10....	0.958	0.863	0.435	0.702	0.959	0.700
0.20....	0.701	0.586	0.245	0.437	0.702	0.435
0.30....	0.540	0.437	0.170	0.314	0.540	0.312
0.40....	0.436	0.347	0.130	0.245	0.437	0.243
0.60....	0.314	0.246	0.088	0.170	0.315	0.168
0.80....	0.245	0.190	0.067	0.130	0.246	0.128
1.00....	0.201	0.155	0.054	0.106	0.201	0.103

TABLE 4

CONSTANTS FOR THE SECOND APPROXIMATION

$\tau_1 = 0.20$

$\mu_{\pm 1} = \pm 0.339981$, $\mu_{\pm 2} = \pm 0.861136$

$a_1 = a_{-1} = 0.652145$, $a_2 = a_{-2} = 0.347855$

	$\varpi_0=0.5$	$\varpi_0=0.5$, $x=1$
k_1	+0.988751	+0.910385
k_2	+2.415233	+2.421830
L_1/ϵ	−0.30034	−0.30984
L_2/ϵ	−0.21866	−0.20509
L_{-2}/ϵ	−0.13415	−0.12635
L_{-1}/ϵ	−0.24645	−0.25827

[6] Chandrasekhar, Elbert, and Franklin, *Ap. J.*, **115**, 244, 1952.

TABLE 5

$\tau_1 = 0.20$; EXACT SOLUTIONS FOR ISOTROPIC SCATTERING

μ	DIRECT LIGHT		$\varpi_0 = 0.5$				$I(0, \mu)/\epsilon$			
	$I_0(0, \mu)/\epsilon$	$I_0(\tau_1/2, \mu)/\epsilon$	$I(0, \mu)/\epsilon$	$I_1(0, \mu)/\epsilon$	$I(\tau_1/2, \mu)/\epsilon$	$I_1(\tau_1/2, \mu)/\epsilon$	$\varpi_0 = 0.8$	$\varpi_0 = 0.9$	$\varpi_0 = 0.95$	$\varpi_0 = 1.00$
0.00	1.000	1.000	1.122	0.122	1.159	0.159	1.215	1.249	1.268	1.287
0.02	1.000	0.993	1.137	.137	1.155	.162	1.241	1.280	1.301	1.323
0.05	0.982	0.865	1.124	.142	0.997	.132	1.232	1.273	1.294	1.316
0.10	0.865	0.632	0.993	.128	0.728	.096	1.090	1.126	1.146	1.166
0.20	0.632	0.393	0.726	.094	0.453	.060	0.798	0.825	0.839	0.854
0.30	0.486	0.283	0.559	.073	0.326	.043	0.614	0.635	0.646	0.657
0.40	0.393	0.221	0.452	.059	0.254	.033	0.497	0.514	0.522	0.532
0.50	0.330	0.181	0.379	.049	0.208	.027	0.416	0.430	0.438	0.445
0.60	0.283	0.154	0.326	.043	0.177	.023	0.358	0.370	0.376	0.383
0.70	0.249	0.133	0.286	.037	0.153	.020	0.314	0.325	0.330	0.336
0.80	0.221	0.118	0.254	.033	0.135	.017	0.279	0.289	0.294	0.299
0.90	0.199	0.105	0.229	.030	0.121	.016	0.252	0.260	0.265	0.269
1.00	0.181	0.095	0.208	0.027	0.109	0.014	0.229	0.237	0.241	0.245

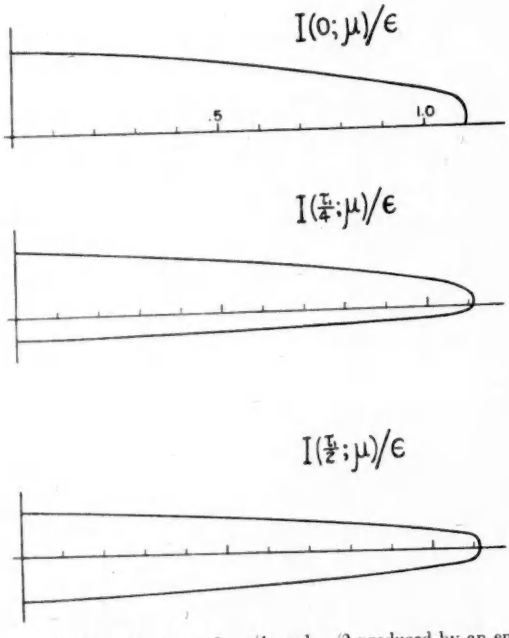

FIG. 4.—The total radiation field at $\tau = 0$, $\tau_1/4$, and $\tau_1/2$ produced by an emitting atmosphere of thickness $\tau_1 = 0.20$, which scatters light according to $p(\cos \Theta) = \varpi_0 = 0.5$. These are polar diagrams in which the intensity is plotted as a function of ϑ. The vertical lines indicate $\vartheta = 0^0$.

Some of the results are illustrated graphically in polar form. Figure 4 shows the total radiation field, as given by the second approximation, at optical depths $\tau = 0.00$, 0.25, and 0.50 for a finite atmosphere of thickness $\tau_1 = 0.20$ with $\varpi_0 = 0.50$. Figure 5 shows the corresponding diffuse field as given by the exact solutions. The curve for $\tau = 0.25$ was not directly calculated but was obtained by applying corrections to the second-approximation solution intermediate to those at $\tau = 0.0$ and $\tau = 0.5$.

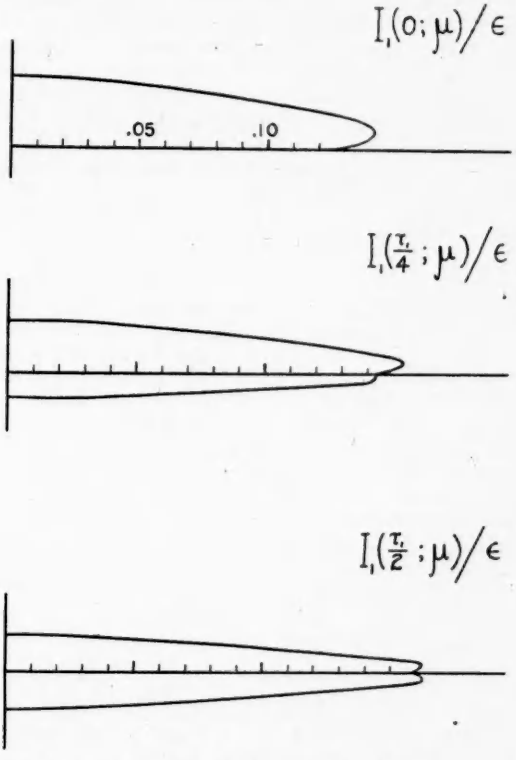

FIG. 5.—The diffuse-radiation field at $\tau = 0$, $\tau_1/4$, and $\tau_1/2$ produced by an emitting atmosphere of thickness $\tau_1 = 0.20$, which scatters light according to $p(\cos\Theta) = \varpi_0 = 0.5$. These are polar diagrams in which the intensity is plotted as a function of ϑ. The vertical lines indicate $\vartheta = 0°$.

VII. THE RADIATION FIELD IN THE GALAXY

The galaxy may be idealized as a plane-parallel "atmosphere," infinite in extent but of finite optical thickness τ_1. The radiation field has its origin in the stars which are assumed to be distributed uniformly throughout the atmosphere. Diffuse radiation is produced by the scattering of starlight by interstellar material. The sun is located approximately in the middle of the finite layer. We are particularly interested in the intensity distribution of the galactic radiation in the vicinity of the sun, i.e., $I(\tau_1/2, \mu)$. This model of the galaxy is undoubtedly oversimplified; nevertheless, the theoretical results should give a standard with which to compare actual observations.

Photometric observations of the galactic light were made by Henyey and Greenstein.[6] They measured the intensity of the diffuse light as a function of galactic latitude at galactic longitudes 40° (Cygnus) and 140° (Taurus-Auriga). They state: "In view of the uncertainties in the observational problem, it seems undesirable to make a detailed comparison between the observational and theoretical results." We shall therefore be content to make a few remarks about their observations based upon our theoretical calculations.

Let us assume that the galaxy can be represented by a plane-parallel atmosphere of finite optical thickness $\tau_1 = 0.20$. On the basis of Van Rhijn's star counts,[7] ϵ must then be of the order of 210 as the average for the Milky Way and for the Cygnus region and 125 for the Taurus-Auriga region (intensities are expressed in terms of the number of tenth-magnitude stars per square degree). We can also assume that the light is scattered isotropically, since the asymmetry of the phase function could be determined only from observations of very high accuracy. Now the average value over all longitudes of the diffuse galactic light in the Milky Way plane is about 60.[8] Thus it follows that $I_1(\tau_1/2, 0)/\epsilon \sim 60/210 = 0.29$. This indicates that the albedo $\varpi_0 \sim 0.95$. This also applies to the Cygnus region. In the Taurus-Auriga region $I_1(\tau_1/2, 0)/\epsilon \sim 35/125 = 0.28$, and this again indicates $\varpi_0 \sim 0.95$. The results of second-approximation calculations for this model of the galaxy is given in Table 6. Now the exact value of $I_1(\tau_1/2, 0)/\epsilon$ will be

TABLE 6

THE THEORETICAL RADIATION FIELD IN THE GALAXY (SECOND APPROXIMATION)

$\tau_1 = 0.20$, $\varpi_0 = 0.95$

μ	$I(\tau_1/2, \mu)/\epsilon$	$I_1(\tau_1/2, \mu)/\epsilon$	$I_1(\tau_1/2, \mu)$ $\epsilon = 210$
0.00	1.238	0.238	50.0
0.02	1.228	.235	49.3
0.05	1.066	.202	42.3
0.10	0.778	.146	30.7
0.20	0.484	.091	19.0
0.30	0.349	.065	13.7
0.40	0.272	.051	10.7
0.60	0.189	.035	7.4
0.80	0.144	.027	5.7
1.00	0.117	0.022	4.6

Constants for the second approximation:

$$k_1 = 0.379500, \qquad k_2 = 2.012568,$$

$$L_1/\epsilon = -9.37697, \qquad L_{-1}/\epsilon = -8.69423,$$

$$L_2/\epsilon = -0.43027, \qquad L_{-2}/\epsilon = -0.28746.$$

somewhat larger than the second-approximation value, say, 0.29, so that the estimate $\varpi_0 = 0.95$ is probably fairly reliable. It will be noticed that the concentration of the diffuse light to the plane of the galaxy is about the same as that of the direct light.

I wish to thank Dr. Chandrasekhar for suggesting this problem and for valuable discussion.

[7] *Ap. J.*, **93**, 72, Table 2, 1941.

[8] *Ibid.*, p. 75.

TRANSFER THEORY FOR PURELY PRESSURE-BROADENED BAND SPECTRA

JEAN I. KING*
Department of Physics, University of Utah, Salt Lake City, Utah
Received June 9, 1952

ABSTRACT

A complete analysis is given for the following model of atmospheric transmission: The atmosphere is in local thermodynamic equilibrium without scattering; the half-width of any line is proportional to the total pressure prevailing at any level. In view of the application to transfer in the far infrared bands of the earth's atmosphere, an idealized molecular band consisting of a series of equal and equidistant lines is assumed. It is possible to express the radiative cooling rates and the conditions of radiative equilibrium for this model in terms of integrals containing only elementary functions under the integral sign. For intense lines the formalism becomes greatly simplified.

I. INTRODUCTION

Some time ago Strong and Plass[1] gave a formula for the radiation of a single spectral line through an atmosphere, under the assumption that the line shape is of the standard dispersion type and that the half-width at any point of the atmosphere is proportional to the total pressure prevailing there. The paper quoted was limited in its treatment to the radiation escaping from an isothermal atmosphere, with a black body as the lower boundary. The formalism has been extended by the author[2] so as to furnish integrals of the transfer equations for isolated pressure-dependent spectral lines in atmospheres of quite general thermal structure. Implicit in all the formalism is the assumption of local thermodynamic equilibrium and zero scattering of the radiation. In actual planetary atmospheres, especially for the case of infrared radiation in the earth's atmosphere, the lines are not isolated but appear in rotation or rotation-vibration bands. It then becomes necessary to take into account overlapping of neighboring lines. For the purpose there is the Elsasser model[3] of a band of equally strong equidistant lines. It is possible to obtain simple analytical expressions for the integrals of Schwarzschild's radiative-transfer equations in the physically most significant case where the line spacing is appreciably larger than the line width. The present memoir is essentially limited to a development of the general theory in its analytical aspects, although occasional references to the actual condition in the far infrared band spectra of the earth's atmosphere are made. Detailed applications and numerical values pertaining thereto will be given in later publications.

II. THE TRANSFER FORMULAE

We begin with the heat-flow equation,

$$\frac{\partial T}{\partial t} = -\frac{1}{c_p \rho} \nabla \cdot F , \tag{1}$$

where c_p and ρ are the specific heat and density of the atmosphere and F is the radiant flux density, a complicated function of the spectrum, temperature, and concentration of the radiating gas.

* Research supported by the Geophysics Division of the Air Force Cambridge Research Center.

[1] *Ap. J.*, **112**, 365, 1950.

[2] Jean I. King, J. Meteorol. **9**, 311 (1952).

[3] Walter M. Elsasser, *Heat Transfer by Infrared Radiation in the Atmosphere* (Cambridge: Harvard University Press, 1942); and *Phys. Rev.*, **54**, 126, 1938.

The variation of the radiant intensity with path length is given by Schwarzschild's equation,

$$dI_\nu = -k \sec \theta \, (I_\nu - B_\nu) \, du \,, \tag{2}$$

where I_ν is the specific intensity of a parallel beam: energy per unit solid angle, per unit frequency interval, crossing unit area per unit time; $B_\nu = 2hc^2\nu^3/\exp(hc\nu/kT) - 1$, the Planck black-body specific intensity; θ is the angle of the radiation with the vertical (chosen $\leqq \pi/2$, i.e., *different for the two cases* [3] *and* [4]); and

$$u = \int_z^\infty w \rho \, dz \,,$$

the total mass per unit area of the radiating gas, measured vertically, counting from the top of the atmosphere down. Hence $u = u_0$ represents the bottom, $u = 0$ the top, of the atmosphere. It should be particularly emphasized that the mixing ratio, or concentration of the radiating gas, denoted by w, is assumed constant throughout the atmosphere in this paper.

In order to obtain the cooling rate, using Schwarzschild's equation, we must (*a*) integrate over the spectrum, (*b*) integrate the parallel intensity over all vertical angles to obtain the radiant flux, and (*c*) differentiate this flux with respect to a vertical variable to obtain the flux divergence. Since these three operations are linear and refer to as many independent variables, the particular sequence in which they are applied becomes one of convenience only. We will perform the operations in the order *a*, *c*, *b*.

Suitable solutions of Schwarzschild's equation for the downward and upward radiant intensities are

$$I_\nu^\downarrow (u) = I_\nu^\downarrow (0) \, \tau_\nu (0, u) + \int_0^u B_\nu (v) \frac{\partial \tau_\nu}{\partial v} (v, u) \, dv \,, \tag{3}$$

$$I_\nu^\uparrow (u) = I_\nu^\uparrow (u_0) \, \tau_\nu (u, u_0) - \int_u^{u_0} B_\nu (v) \frac{\partial \tau_\nu}{\partial v} (u, v) \, dv \,, \tag{4}$$

where $I_\nu^\downarrow (0)$ and $I_\nu^\uparrow (u_0)$ are the specific intensities incident downward on the top of the atmosphere and upward on the base, respectively, and τ_ν is the transmission function per unit frequency interval, defined as

$$\tau_\nu (v, u) = \exp \left(- \int_v^u k \sec \theta \, du \right). \tag{5}$$

The transmission function must lie within the range $0 \leqq \tau_\nu \leqq 1$. From equation (5) $\tau_\nu(u, u) = 1$. *With these definitions, the second variable of* τ_ν *must always be greater than, or equal to, the first*, since for $v > u$, $\tau_\nu(v, u) > 1$, which is physically impossible.

We now convert from the independent variable u to the dry-air pressure p,[4] by

$$du = \frac{w \, dp}{g} \,. \tag{6}$$

Equations (3) and (4) become

$$I_\nu^\downarrow (p) = I_\nu^\downarrow (0) \, \tau_\nu (0, p) + \int_0^p B_\nu (q) \frac{\partial \tau_\nu}{\partial q} (q, p) \, dq \,, \tag{7}$$

$$I_\nu^\uparrow (p) = I_\nu^\uparrow (p_0) \, \tau_\nu (p, p_0) - \int_p^{p_0} B_\nu (q) \frac{\partial \tau_\nu}{\partial q} (p, q) \, dq \,. \tag{8}$$

[4] Actually, barometers measure the total atmospheric pressure. The difference, however, between this moist-air pressure and the dry-air pressure, even for saturated air at 15° C, is less than 2 per cent.

In the integration over the spectrum we assume B_ν, $I_\nu^{\downarrow}(0)$, and $I_\nu^{\uparrow}(p_0)$ to be essentially constant over the frequency range in which k varies significantly from zero. We define the transmission function and radiant intensity averaged over a spectral interval $\Delta\nu$ by

$$\tau(q, p) = \int_{\Delta\nu} \tau_\nu(q, p) \frac{d\nu}{\Delta\nu}, \qquad I(p) = \int_{\Delta\nu} I_\nu(p) \frac{d\nu}{\Delta\nu}. \tag{9}$$

We now average equations (7) and (8) over $\Delta\nu$, where it is understood that $\Delta\nu$ is large compared to the line width but small enough so that the black-body intensity B_ν can be considered constant within each $\Delta\nu$. Then equations (7) and (8) become

$$I^{\downarrow}(p) = I_\nu^{\downarrow}(0)\, \tau(0, p) + \int_0^p B_\nu(q) \frac{\partial \tau}{\partial q}(q, p)\, dq, \tag{10}$$

$$I^{\uparrow}(p) = I_\nu^{\uparrow}(p_0)\, \tau(p, p_0) - \int_p^{p_0} B_\nu(q) \frac{\partial \tau}{\partial q}(p, q)\, dq. \tag{11}$$

Integrating the last terms by parts yields

$$I^{\downarrow}(p) = [I_\nu^{\downarrow}(0) - B_\nu(0)]\tau(0, p) + B_\nu(p) - \int_0^p B_\nu'(q)\, \tau(q, p)\, dq, \tag{12}$$

$$I^{\uparrow}(p) = [I_\nu^{\uparrow}(p_0) - B_\nu(p_0)]\tau(p, p_0) + B_\nu(p) + \int_p^{p_0} B_\nu'(q)\, \tau(p, q)\, dq. \tag{13}$$

Differentiating with respect to the pressure, we obtain

$$\frac{dI^{\downarrow}}{dp} = [I_\nu^{\downarrow}(0) - B_\nu(0)] \frac{\partial \tau}{\partial p}(0, p) - \int_0^p B_\nu'(q) \frac{\partial \tau}{\partial p}(q, p)\, dq, \tag{14}$$

$$\frac{dI^{\uparrow}}{dp} = [I_\nu^{\uparrow}(p_0) - B_\nu(p_0)] \frac{\partial \tau}{\partial p}(p, p_0) + \int_p^{p_0} B_\nu'(q) \frac{\partial \tau}{\partial p}(p, q)\, dq. \tag{15}$$

Finally, from equations (1) and (6) and the relation $du = -w\rho dz$, we see that the general cooling formula for an atmosphere, considering parallel radiation only, is

$$\frac{\partial T}{\partial t} = \frac{g\Delta\nu}{c_p} \left\{ [I_\nu^{\uparrow}(p_0) - B_\nu(p_0)] \frac{\partial \tau}{\partial p}(p, p_0) - [I_\nu^{\downarrow}(0) - B_\nu(0)] \frac{\partial \tau}{\partial p}(0, p) + \int_p^{p_0} B_\nu'(q) \frac{\partial \tau}{\partial p}(p, q)\, dq + \int_0^p B_\nu'(q) \frac{\partial \tau}{\partial p}(q, p)\, dq \right\}. \tag{16}$$

III. APPLICATION TO BAND SPECTRA

We proceed now to the calculation of $\partial\tau(p, q)/\partial p$ and $\partial\tau(q, p)/\partial p$ for the schematic band spectrum of Elsasser. The treatment of the diffuse nature of the radiation is deferred until the end of the paper. For such a model,[5]

$$k(\nu) = \sum_{-\infty}^{\infty} \frac{S}{\pi} \frac{a}{(\nu - nd)^2 + a^2} = \frac{S}{d} \frac{\sinh \beta}{\cosh \beta - \cos \sigma}, \tag{17}$$

where a and d are the line half-widths and distance between line centers in frequency units; $\sigma = 2\pi\nu/d$; and $\beta = 2\pi a/d$.

[5] Elsasser, *Phys. Rev.*, **54**, 126, 1938.

The band transmission function per unit frequency interval, using equations (5) and (17) and the half-width–pressure relationship ($a = bp$), becomes

$$\tau_\nu(p, q) = \exp\left(-\int_p^q kw \sec\theta \frac{dp}{g}\right) = \exp\left(-\frac{Sw \sec\theta}{2\pi b g}\int_\beta^\gamma \frac{\sinh\beta d\beta}{\cosh\beta - \cos\sigma}\right)$$
$$= \left[\frac{\cosh\beta - \cos\sigma}{\cosh\gamma - \cos\sigma}\right]^\eta, \tag{18}$$

where $\eta = Sw \sec\theta / 2\pi bg$ is a nondimensional parameter.

Differentiation with respect to the pressure yields

$$\frac{\partial\tau_\nu}{\partial p}(p, q) = \frac{d\beta}{dp}\frac{\partial\tau_\nu}{\partial\beta}(p, q) = \frac{2\pi\eta b}{d}\sinh\beta\frac{(\cosh\beta - \cos\sigma)^{\eta-1}}{(\cosh\gamma - \cos\sigma)^\eta}.$$

Since the band consists of evenly spaced equal lines of frequency width d, the averaging over the spectrum is given by

$$\frac{\partial\tau}{\partial p}(p, q) = \frac{1}{d}\int_{-d/2}^{d/2}\frac{\partial\tau_\nu}{\partial p}(p, q)\, d\nu = \frac{2\eta b}{d}\sinh\beta\int_0^\pi \frac{(\cosh\beta - \cos\sigma)^{\eta-1}}{(\cosh\gamma - \cos\sigma)^\eta}\, d\alpha. \tag{19}$$

This integral can be evaluated by the substitution $\cos\sigma = (1 - y^2)/(1 + y^2)$, giving

$$\frac{\partial\tau}{\partial p}(p, q) = \frac{4\eta b}{d}\sinh\beta\int_0^\infty \frac{[(\cosh\beta + 1)y^2 + (\cosh\beta - 1)]^{\eta-1}}{[(\cosh\gamma + 1)y^2 + (\cosh\gamma - 1)]^\eta}\, dy.$$

We can evaluate this for *integral* values of η. Expansion of the numerator then gives a finite series:

$$\frac{\partial\tau}{\partial p}(p, q) = \frac{4\eta b}{d}\sinh\beta\sum_{m=0}^{\eta-1}\frac{(\eta - 1)!\,(\cosh\beta + 1)^{\eta-m-1}(\cosh\beta - 1)^m}{(\eta - m - 1)!\,m!}$$
$$\times\int_0^\infty \frac{y^{2(\eta-m-1)}dy}{[(\cosh\gamma + 1)y^2 + (\cosh\gamma - 1)]^\eta}.$$

Now we have

$$\int_0^\infty \frac{y^{2(\eta-m-1)}dy}{[(\cosh\gamma + 1)y^2 + (\cosh\gamma - 1)]^\eta} = \frac{B(\eta - m - \frac{1}{2}, m + \frac{1}{2})}{2(\cosh\gamma + 1)^{\eta-m-1/2}(\cosh\gamma - 1)^{m+1/2}},$$

where $B(\lambda, \mu) = (\lambda - 1)!\,(\mu - 1)!/(\lambda + \mu - 1)!$ is the beta function, or Eulerian integral of the first kind,[6] so that, for integral values of η, we finally get

$$\frac{\partial\tau}{\partial p}(p, q) = \frac{2\eta b}{d}\frac{\sinh\beta}{\sinh\gamma}\sum_{m=0}^{\eta-1}\left[\frac{\cosh\beta + 1}{\cosh\gamma + 1}\right]^{\eta-m-1}\left[\frac{\cosh\beta - 1}{\cosh\gamma - 1}\right]^m \frac{(\eta - m - \frac{3}{2})!}{(\eta - m - 1)!}\frac{(m - \frac{1}{2})!}{m!}. \tag{20}$$

A similar procedure, which will be omitted here, yields, for the downward transmission,

$$\frac{\partial\tau}{\partial p}(q, p) = -\frac{2\eta b}{d}\sum_{m=0}^{\eta}\left[\frac{\cosh\gamma + 1}{\cosh\beta + 1}\right]^{\eta-m}\left[\frac{\cosh\gamma - 1}{\cosh\beta - 1}\right]^m \frac{(\eta - m - \frac{1}{2})!}{(\eta - m)!}\frac{(m + \frac{1}{2})!}{m!}. \tag{21}$$

[6] Whittaker and Watson, *Modern Analysis* (Cambridge: At the University Press, 1927), p. 253, and chap. xii.

We can find simplified expressions valid for small and large η. From equation (19) for small η,

$$\frac{\partial \tau}{\partial p}(p, q) \approx \frac{2\pi\eta b}{d}, \qquad \frac{\partial \tau}{\partial p}(q, p) \approx -\frac{2\pi\eta b}{d}, \qquad \text{for} \quad \eta \ll 1. \tag{22}$$

To obtain an expression valid for large η, we rearrange equation (20) and use the asymptotic approximation for large η:

$$\frac{(\eta - m - \frac{3}{2})!}{(\eta - m - \frac{1}{2})!} \approx \frac{1}{\eta^{1/2}},$$

obtaining

$$\frac{\partial \tau}{\partial p}(p, q) \approx \frac{2\eta^{1/2} b}{d} \frac{\sinh \beta}{\sinh \gamma} \left[\frac{\cosh \beta + 1}{\cosh \gamma + 1}\right]^{\eta-1} \sum_{m=0}^{\eta-1} \frac{(m - \frac{1}{2})!}{m!} \left[\frac{(\cosh \gamma + 1)(\cosh \beta - 1)}{(\cosh \beta + 1)(\cosh \gamma - 1)}\right]^{m}.$$

Also using the relationship, valid for large η,

$$\sum_{m=0}^{\eta-1} \frac{(m - \frac{1}{2})!}{m!} x^m \approx \frac{\pi^{1/2}}{(1 - x)^{1/2}},$$

we have

$$\frac{\partial \tau}{\partial p}(p, q) \approx \frac{(2\pi\eta)^{1/2} b}{d} \frac{\sinh \beta}{(\cosh \gamma - \cosh \beta)^{1/2}} \left[\frac{\cosh \beta + 1}{\cosh \gamma + 1}\right]^{\eta - 1/2}.$$

This expression can be further simplified in the practically most interesting case in which β is small or at least not numerically large. Physically, this implies that the line half-width α is small compared to (at least several times smaller than) the distance d between adjacent lines. In the case of the pressure-independent band absorption this led to the error integral formula for the absorption.[3] Actually, we know that the values of β for the P and R branches of CO_2 in the atmosphere do not exceed 0.7 and are smaller for the H_2O bands. We can then write

$$\begin{aligned}\left[\frac{\cosh \beta + 1}{\cosh \gamma + 1}\right]^{\eta - 1/2} &= \exp\left[(\eta - \tfrac{1}{2}) \log \frac{1 + \frac{1}{2}(\cosh \beta - 1)}{1 + \frac{1}{2}(\cosh \gamma - 1)}\right] \\ &\approx \exp\left[(\eta - \tfrac{1}{2})(\tfrac{1}{2}\cosh \beta - \tfrac{1}{2}\cosh \gamma)\right] \\ &\approx \exp \frac{\left[-(\eta - \frac{1}{2})(\gamma^2 - \beta^2)\right]}{4}.\end{aligned}$$

Here we have broken up the approximation into two steps. It so happens that the region in which the logarithm can be represented by the first term in its power series coincides just about with the region where $\cosh \beta \approx 1 + \beta^2/2$. Now we reintroduce p and q by $\beta = 2\pi b p/d$ and $\gamma = 2\pi b q/d$ and replace $\sinh \beta$ by β, to obtain, finally,

$$\frac{\partial \tau}{\partial p}(p, q) = \frac{2(\pi\eta)^{1/2} b}{d} \frac{p}{(q^2 - p^2)^{1/2}} e^{-(\eta - 1/2)\pi^2 b^2 (q^2 - p^2)/d^2} \qquad \text{for} \quad \eta \gg 1. \tag{23}$$

For the downward transmission we similarly find

$$\frac{\partial \tau}{\partial p}(q, p) = \frac{-2(\pi\eta)^{1/2} b}{d} \frac{p}{(p^2 - q^2)^{1/2}} e^{-(\eta + 1/2)\pi^2 b^2 (p^2 - q^2)/d^2} \qquad \text{for} \quad \eta \gg 1. \tag{24}$$

From the general cooling formula (16) and expressions (22), (23), and (24), we note that the cooling rate is a monotonic increasing function of η, and hence of the line intensity S. Thus for $\eta \ll 1, \partial T/\partial t \propto S$; for $\eta \gg 1, \partial T/\partial t \propto S^{1/2}$. Since the main contribution to the cooling will come from the strong lines, we are justified in using our large η approximations (eqs. [23] and [24]) in equation (16), particularly since, for CO_2 lines, for instance, $\eta \sim 10^2$. We then have, as the *band-cooling formula for parallel radiation*,

$$\frac{\partial T}{\partial t} = \frac{2N(\pi\eta)^{1/2} bg}{c_p} \left\{ [I_\nu^{\uparrow}(p_0) - B_\nu(p_0)] \frac{p}{(p_0^2 - p^2)^{1/2}} e^{-\eta\pi^2 b^2 (p_0^2 - p^2)/d^2} \right.$$
$$+ [I_\nu^{\downarrow}(0) - B_\nu(0)] e^{-\eta\pi^2 b^2 p^2/d^2} + p\int_p^{p_0} B_\nu'(q) \frac{e^{-\eta\pi^2 b^2 (q^2 - p^2)/d^2} dq}{(q^2 - p^2)^{1/2}} \quad (25)$$
$$\left. - p\int_0^p B_\nu'(q) \frac{e^{-\eta\pi^2 b^2 (p^2 - q^2)/d^2} dq}{(p^2 - q^2)^{1/2}} \right\},$$

where $N = \Delta\nu/d$ is the number of lines in the band.

Apart from the exponential factors, this band-cooling formula is identical with N times the cooling rate for a single isolated line.[1] As the distance between lines becomes large ($d \gg 1$), the above formula reduces to the line-cooling expression[2] for N widely spaced lines. It is clear, then, that the factors of the type $e^{-\eta\pi^2 b^2 p^2/d^2}$ represent the "quenching" effect of the mutual overlapping of the lines.

IV. OBLIQUITY

We now take into account the anisotropy of the radiation. The total flux per unit area emerging vertically from a given level is defined as

$$F = \int I \cos\theta d\omega = 2\pi \int_0^{\pi/2} I \cos\theta \sin\theta d\theta, \quad (26)$$

since we are dealing with a plane-parallel atmosphere having azimuthal symmetry. For the special case of isotropic radiation, we see from equation (26) that $F_0 = \pi I_0$, a well-known result.

In our equations the obliquity dependence is carried solely by the parameter $\eta = Sw \sec\theta / 2\pi bg$. Thus it suffices in the integration over the vertical angles to consider only those factors involving η.

The computation of the flux for the single-line case where the exponentials of equation (25) reduce to unity is particularly simple. Indeed, $\eta^{1/2}$ appears as a common factor in all four terms of equation (25). Hence by equation (26) the flux integration yields

$$F = 2\pi \int_0^{\pi/2} \cos^{1/2}\theta \sin\theta d\theta = \frac{4\pi}{3} I, \qquad \text{a flux factor of } \frac{4\pi}{3}. \quad (27)$$

In the band formula for $\eta \gg 1$, η appears both as a common square-root factor and in the exponents. In particular, for the second term of equation (25) the flux integration yields

$$F = 2\pi I \int_0^{\pi/2} e^{-\eta'\pi^2 b^2 p^2/d^2 \cos\theta} \cos^{1/2}\theta \sin\theta d\theta = 2\pi I Ei_{5/2}\left(\frac{\eta'\pi^2 b^2 p^2}{d^2}\right), \quad (28)$$

where $\eta' = \eta \cos\theta$, and $Ei_n(x)$ is the nth exponential integral of x, defined, as usual by,

$$Ei_n(x) = \int_1^\infty e^{-x\mu} \frac{d\mu}{\mu^n}.$$

One notes that $Ei_{5/2}(0) = \frac{2}{3}$, so that, for large d, the flux factor reduces again to the single-line case.

The clumsy nature of the exponential integral has led many authors to account for the diffuse radiation merely by multiplying the vertical path length by an appropriate correction factor. To determine this diffusivity factor, we equate the exact solution (28) to the vertical-beam case, in which the exponential term is multiplied by the factor λ, that is, we define λ by the condition

$$F = 2\pi I Ei_{5/2}(x) = \tfrac{4}{3}\pi I e^{-\lambda x}. \tag{29}$$

Equation (29) is identically fulfilled at $x = 0$. Taking logarithms, we find

$$\lambda x = \ln \frac{3Ei_{5/2}(x)}{2}. \tag{30}$$

A plot of λ versus x, the arguments of the overlapping factors of equation (25), is given in Figure 1. λ decreases monotonically from a value of 3 at $x = 0$ to $\lambda = 1$ as $x \to \infty$. Hence a reasonably satisfactory approximation is often obtained by setting $\lambda = 2$ in equation (25). If the atmosphere is divided into layers, the value of λ corresponding to each pair of p and q can be read off the graph.

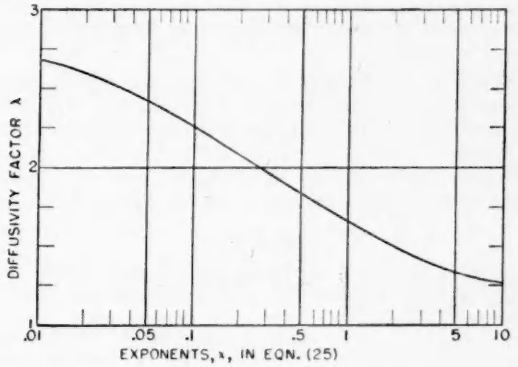

FIG. 1.—Conversion factor for diffuse radiation

V. CONCLUSION

This paper has been limited to a presentation of the analytical apparatus for radiative transfer owing to pressure-broadened lines or bands in an atmosphere where the conditions are such that pressure-broadening prevails. This is the case for the infrared spectra of water vapor, carbon dioxide, and probably ozone up to a height of about 40 km. At higher elevations Doppler broadening becomes appreciable, and the present theory no longer applies. The formulae should also have application to the band spectra in the atmosphere of Mars, a topic to which we hope to return.

In order to apply our formulas to radiative cooling and radiative equilibrium conditions in the earth's atmosphere, extensive numerical tabulations of the functions introduced above are required. Such work is now being undertaken at this university; a report about the results and their meteorological significance is to be given elsewhere at a later date.

The author wishes to thank Professor Walter M. Elsasser for his valuable suggestions and helpful criticism concerning this paper.

THE LOW-TEMPERATURE SPECTRUM OF HD 45910

PAUL W. MERRILL
MOUNT WILSON AND PALOMAR OBSERVATORIES
CARNEGIE INSTITUTION OF WASHINGTON
CALIFORNIA INSTITUTE OF TECHNOLOGY
Received June 9, 1952

ABSTRACT

A faint absorption spectrum of type gM2 is measurable in the red region of the spectrum of this peculiar Be shell star. The D lines of sodium in the M-type spectrum are abnormally weak. The varying displacements of the M-type lines correspond to motion in a circular orbit of period 232 days, semiamplitude 52 km/sec. J. S. Plaskett's measurements appear to show corresponding motion for the B-type component. This system has a curious similarity to that of T Coronae as observed by R. F. Sanford. The radial velocity derived from the interstellar lines corresponds to a stellar distance of 900 parsecs and an absolute magnitude of −3.1.

Previous observations of the peculiar Be shell star HD 45910,[1] although extensive, have been limited largely to the spectral region shortward from $H\beta$. For a description of this portion of the spectrum and for references to earlier observations see *Mount Wilson Contributions*, No. 751.[2]

In 1945 a spectrogram of the red region, 20 A/mm, showed a faint absorption-line spectrum resembling in many respects that of α Ceti, type gM2. All suitable spectrograms taken since that time (Table 1) have shown the M-type spectrum without much change except that the lines have shifted in position after the manner of a spectroscopic binary.

TABLE 1*

SPECTROGRAMS IN THE VISUAL REGION OF HD 45910

PLATE	DATE	JD 243	RADIAL VELOCITY (KM/SEC)	
			M-Type Lines	Interstellar *Na*
Ce 4036	1945 Oct. 24	1753	+60.2	+22.4
5323	1948 Sept. 13	2808	−40.1	+20.4
5353	Oct. 13	2838	−20.9	+21.8
5495	Dec. 12	2898	+51.9	+23.9
6033	1949 Nov. 13	3234	−26.2	(+14.1)
6090	1950 Jan. 5	3287	−39.7	(+15.6)
6154	Feb. 21	3334	+14.6	+23.4
6168	Feb. 23	3336	.....	+20.7
6695	Nov. 27	3613	+61.3	+20.4
Pc 247	1952 Jan. 8	4020	+ 1.4	(+11.5)
256	Feb. 1	4044	+35.0	+25.7

* Dispersion of the first six, 20 A/mm; of the last five, 15 A/mm.

A remarkable peculiarity of the low-temperature spectrum is the absence of the D lines of sodium. The interstellar D lines are strong and sharp, with a mean velocity of +22.3

[1] 1900 R.A., 6^h25^m2; Dec., +5°57′; mag., 6.7.

[2] *Ap. J.*, **108**, 481, 1948.

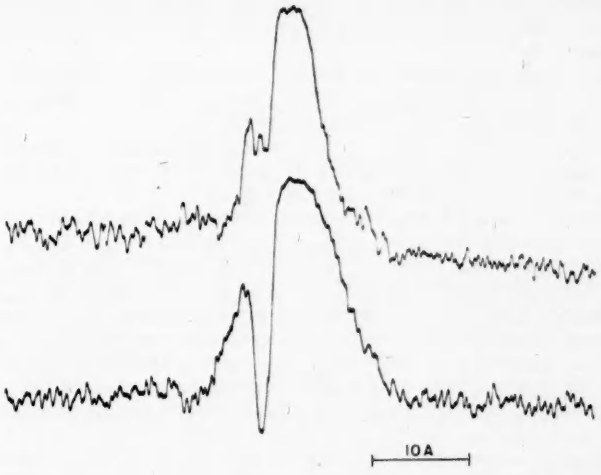

FIG. 1.—Tracings of the *Hα* line in the spectrum of HD 45910. Upper, Ce 6168, 1950 Feb. 23; lower, Pc 247, 1952 Jan. 8.

TABLE 2

ELEMENTS OF MOTION OF M-TYPE COMPONENT OF HD 45910

P = 232 days	K = 52 km/sec
T = Time of γ velocity on rising branch of velocity-curve = JD 2432865	e = 0
	γ = +10 km/sec
	$a \sin i = 166 \times 10^6$ km

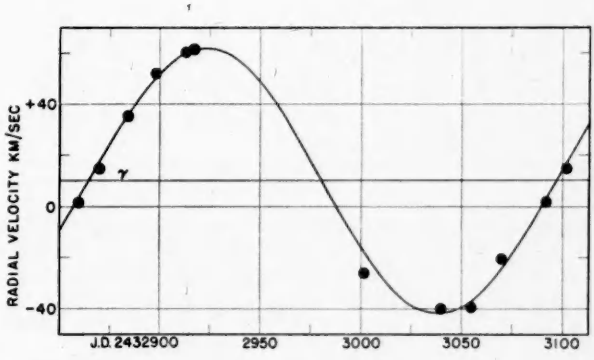

FIG. 2.—Velocity-curve derived from the M-type spectrum of HD 45910

km/sec. In addition, there seems to be a weak component of variable intensity whose position does not correspond to the velocity yielded by the M-type lines; this component may have some connection with the B-type star. Other lines in the visual region probably connected with the early-type spectrum are the dark lines *He* I λ 5876, *Si* II λ 6347 and λ 6371, and *Hα* λ 6563 (both bright and dark). The lines of *He* and *Si* appear to vary in intensity, and *Hα* certainly varies in structure (see Fig. 1).

The velocities of the M-type lines, with one exception, are well represented by the circular elements in Table 2. The residual of Plate Ce 6033 appears slightly large and may possibly indicate a small eccentricity (see Fig. 2).

If the elements in Table 2 represent an actual orbit of one component of a double star, the other component ought to exhibit a sine curve of opposite phase. The Be spectrum is so complex and variable that my plates do not afford a satisfactory confirmation. From an extensive series of observations between 1922 and 1926, however, J. S. Plaskett[3] found from the hydrogen lines "a fairly definite period of about 235 days and an amplitude of 120 km ± 30 km for both emission and absorption components." It appears possible to consider this motion as the gravitational counterpart of the circular motion deduced for the low-temperature star. If this hypothesis is correct, then the masses of the two components are nearly equal and each mass is about sixteen times that of the sun (if $i = 90°$).

In the system of T Coronae Borealis, R. F. Sanford[4] found that the velocities derived from a spectrum of type gM3 could be represented by a sine curve of period 230.5 days, with $K = 21$ km/sec. The coincidence appears remarkable if we recall that at one time T Coronae had a shell spectrum about like that of HD 45910.

The mean displacement of the interstellar lines of *Ca* II and *Na* I, +22.6 km/sec, corresponds to a stellar distance of 900 parsecs and, with no allowance for space absorption, to a combined absolute magnitude of −3.1.

[3] *Pub. Dom. Ap. Obs. Victoria*, **4**, 1, 1927.

[4] *Mt. W. Contr.*, No. 756; *Ap. J.*, **109**, 81, 1949.

MEASUREMENTS IN THE SPECTRA OF TEN SHELL STARS

PAUL W. MERRILL
MOUNT WILSON AND PALOMAR OBSERVATORIES
CARNEGIE INSTITUTION OF WASHINGTON
CALIFORNIA INSTITUTE OF TECHNOLOGY
Received June 9, 1952

ABSTRACT

This account of ten shell stars is based on 95 spectrograms, of which about 70 have a dispersion of 10 A/mm. The spectrum of each star is described briefly with notes on previous observations. Radial velocities derived from lines of hydrogen and of metals are recorded. Where the material is sufficient, detailed studies of the progression of velocities along the Balmer series are included. In most of the stars the velocities change slowly with time.

The phenomena of a gaseous "shell" far above the usual stellar reversing layer are complex and variable. The spectral lines of shell stars may undergo striking changes in intensity; the radial motions may be large and may exhibit cyclic alternations of sign. In certain stars the cycle of change covers many years. Hence very extensive observational data, preferably including numerous stars, will be required before we can hope to understand the interesting physical causes of the formation, the motions, and the disappearance of the shells.

TABLE 1

TEN SHELL STARS

STAR	MWC	1900		MAG.
		R.A.	Decl.	
HD 44351	803	6^h16^m3	+14° 21′	8.5
HD 45677	142	6 23.7	−13 0	7.5
β Mon A	143	6 24.0	− 6 58	4.7
HD 50138	158	6 46.7	− 6 51	6.6
HD 54858	838	7 5.4	− 9 11	8.4
BD+30°3526	985	19 17.4	+30 58	9.2
HD 183656	988	19 25.5	+ 3 14	6.3
HD 351123	372*	19 53.1	+17 6	9.0
BD+47°3487	374	21 32.2	+47 28	9.1
HD 220300	1081	23 17.6	+55 49	7.8

* Star No. 372 in "Additional Stars Whose Spectra Have a Bright *Hα* Line," *Mt. W. and P. Obs. Reprint*, No. 24; *Ap. J.*, **112**, 72, 1950.

Spectroscopic observations of a number of shell stars made over a term of years at the Mount Wilson and Palomar Observatories have been described in several recent articles. Data concerning ten additional stars (Table 1) are included in the present paper, which will complete the series, with the exception of studies of 48 Librae and HD 33232 to appear soon. I hope later to make a comparative study of all shell stars observed with high dispersion.

HD 44351, MWC 803.—A bright *Hα* line was discovered on an objective-prism photograph taken with the 10-inch telescope on Mount Wilson in February, 1939. Slit spectrograms obtained at Mount Wilson and at Palomar (Table 2) show a well-developed

shell spectrum with unusually strong dark lines. The hydrogen lines are extremely intense with an astonishing amount of continuous absorption near the limit of the Balmer series (see Fig. 1). A hint of the shell characteristics is contained in the remark in the *Henry Draper Catalogue:* "The lines are narrow. The spectrum may be of Class A2."

The three high-dispersion plates show that some of the lines are slightly asymmetrical and that their profiles are not quite identical on all plates. Various metallic lines differ somewhat in sharpness, those of *Ti* II being particularly sharp, while λ 3769

TABLE 2

SPECTROGRAMS OF HD 44351

PLATE	DATE	DISP. AT $H\gamma$ (A/MM)	OBSERVER	RADIAL VELOCITY (KM/SEC)		NO. *M* LINES
				H	*M*	
γ 27439.....	1946 Feb. 9	80	W. C. Miller	(+ 4)	(+22)	2
γ 28174.....	Oct. 18	35	W. C. Miller	+37	+37	10
γ 31257.....	1949 Nov. 13	35	W. C. Miller	+61	+59	43
γ 31907.....	1951 Feb. 16	35	W. C. Miller	+16	+13	36
Pc 219.....	Nov. 10	9	I. S. Bowen	−18.5	−11.8	59
Pc 249.....	1952 Jan. 9	9	I. S. Bowen	− 8.0	− 2.0	50
Pc 260.....	Feb. 3	9	I. S. Bowen	−24.0	−16.0	47

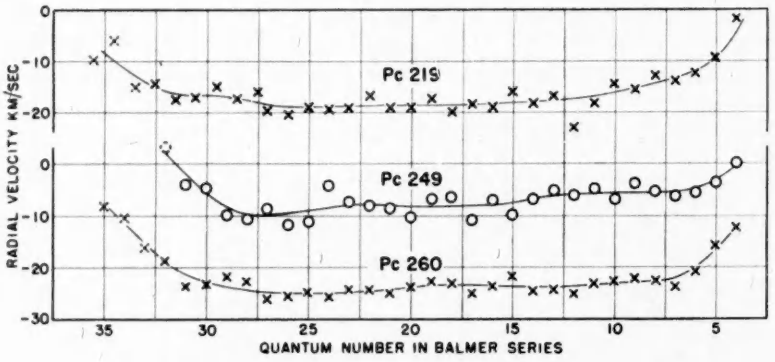

FIG. 2.—Progression in radial velocities from successive Balmer lines of HD 44351

Ni II is rather wide. The displacements of various metallic lines agree quite well; lines of *Ti* II, however, yield a mean displacement about 5 km/sec greater algebraically than that of lines of other metals.

The measured displacements of individual hydrogen lines are plotted in Figure 2. The progression curves are nearly flat except that both ends turn upward. At the long-wave-length end the effect is especially interesting. The dark core of $H\beta$ has weak, bright borders, that on the longward edge being the stronger. The measured position of the core, however, has a positive relative displacement, not a negative one as might have been expected. Thus the displacement is not due directly to the emission but probably arises from an asymmetry within the core itself, the longward edge of which becomes relatively stronger in the series lines toward $H\beta$. Unfortunately, $H\alpha$ is not available for comparison; it should be included in a future investigation.

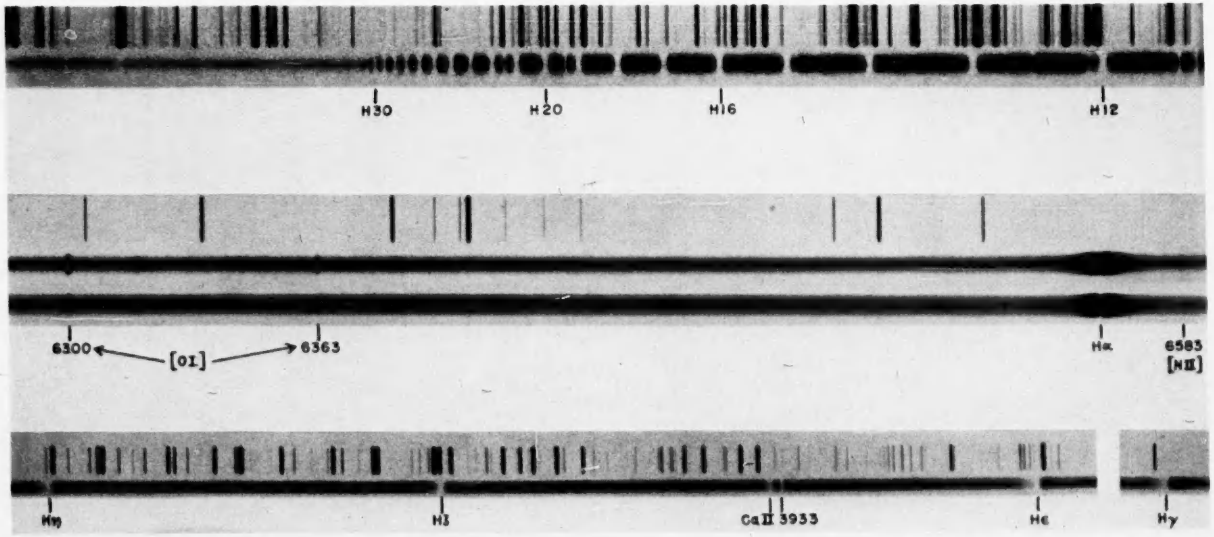

FIG. 1.—Spectrograms of shell stars. *Upper:* HD 44351, Pc 260. *Center:* Above, HD 45677, Ce 4043; below, HD 50138, Ce 4047. *Lower:* MWC 374, Ce 6428

The mean radial velocities from lines of hydrogen and of metals, mostly ionized, are in Table 2. For the high-dispersion plates the hydrogen velocities were read from the progression-curves near *H*20. The data suggest that the velocity-curve had a maximum in 1948, with a period of 8 years or longer. The second of the high-dispersion plates, Pc 249, shows a slight but interesting deviation from the curve defined by the other plates. Because of the extremely strong lines and the large velocity range, this star is an attractive subject for further spectroscopic observation.

HD 45677, MWC 142.—A bright *Hβ* line was discovered by Mrs. W. P. Fleming[1] on an objective-prism photograph taken at the Harvard College Observatory in 1898. The first slit spectrogram on record[2] was obtained at Mount Wilson in 1923, and others were taken in following years. In addition to the outstanding bright lines of hydrogen, these plates showed bright lines of ionized iron and numerous others of unknown origin, a few of which had previously been observed in gaseous nebulae. Nearly all the unknown

TABLE 3

SPECTROGRAMS OF HD 45677

Plate	Date	Disp. at *Hγ* (A/mm)	Radial Velocity (Km/Sec)						
			*H*6 Abs.	*H*15 Abs.	Forbidden Emission		*M* II		*Ca* II Abs.
					Vel.	No.	Vel.	No.	
G 530	1932 Feb. 28	66*	.....	.....	+24	2	+25	3e	.....
V 719	1934 Dec. 25	37	+16	.....	+18	6	+19	1e	.....
γ 21540	1938 Nov. 8	35	+ 4	.....	+22	4	.....	.....	+19.8
γ 22144	1939 Sept. 21	80	− 6	.....	.....	.....	.....	.....	+18.1
γ 22428	1940 Jan. 20	35	+ 4	.....	+22	4	.....	.....	+18.7
γ 24661	1942 Nov. 1	35	+16	.....	+21	8	+15	6e	+18.7
Ce 3291	1943 Nov. 14	10	+ 8	+20	+17.0	18	+20.4	23a	+18.9
Ce 4043	1945 Oct. 25	21*	+12*	.....	+20.4	3	+16	1e	+19.8†
Ce 4046	Oct. 26	10	+12	(+16)	+18.8	13	+21.9	5a	+19.7
Ce 4465	1946 Oct. 13	10	+18	+22	+19.4	12	+22.5	5a	+18.1
Ce 4927	1947 Oct. 23	10	+24	+26	+19.8	15	+24.7	7a	+20.7
Mean	.....	.....	.....	+22	+19.7	.....	+21.4	.....	+19.3

* *Hα*. † D lines.

lines were later identified with forbidden transitions in atoms of ionized iron,[3, 4] of ionized sulphur,[5] and of neutral oxygen.[6]

Spectrograms taken at Mount Wilson between 1923 and 1927 were described in a previous article.[4] Several minor variations in the intensity and structure of certain lines were noted. The spectrum had not changed appreciably in 1939, when it was observed by Swings and Struve[7] at the McDonald Observatory; but in 1943[8] changes in the structure of the hydrogen lines were apparent. Spectrograms taken at Mount Wilson since 1927 are listed in Table 3.

[1] *Harvard Circ.*, No. 32.

[2] P. W. Merrill, *Pub. A.S.P.*, **37**, 163, 1925.

[3] P. W. Merrill, *Mt. W. Contr.*, No. 354; *Ap. J.*, **67**, 391, 1928.

[4] P. W. Merrill, *Mt. W. Contr.*, No. 355; *Ap. J.*, **67**, 405, 1928.

[5] I. S. Bowen, *Nature*, **123**, 450, 1929.

[6] I. S. Bowen, *Phys. Rev.*, **36**, 600, 1930.

[7] *Ap. J.*, **91**, 546, 1940.

[8] *Ap. J.*, **98**, 91, 1943.

The hydrogen lines are complex, their structure variable. The emission at *Hα* is wide and extremely intense (see Fig. 1). At *Hβ* also the emission is outstanding (Fig. 3), with a relatively slow decrement down the series. In fact, on plate Ce 4927 tracings show a trace of emission on the longward edge of the core as far as *H*15 or *H*16 (Fig. 3). The dark cores are not so clean-cut as in many shell spectra but are frequently unsymmetrical or almost double. For this reason the behavior of the progression-curves is more complex than in most shell spectra. The lines *Hβ*–*Hε* show considerable variation in displacement from year to year, especially on the early low-dispersion plates, while on the coudé plates the lines *H*10–*H*20 yield consistent values on individual plates and show relatively small changes from year to year. This behavior may reflect the fact that differences in the intensities of close dark components and of the outer emission will be more apparent in the first few lines of the series. The values in Table 3 under the headings "*H*6" and "*H*15" are taken from smoothed progression-curves and hence are, in effect, means of several adjacent lines in the Balmer series.

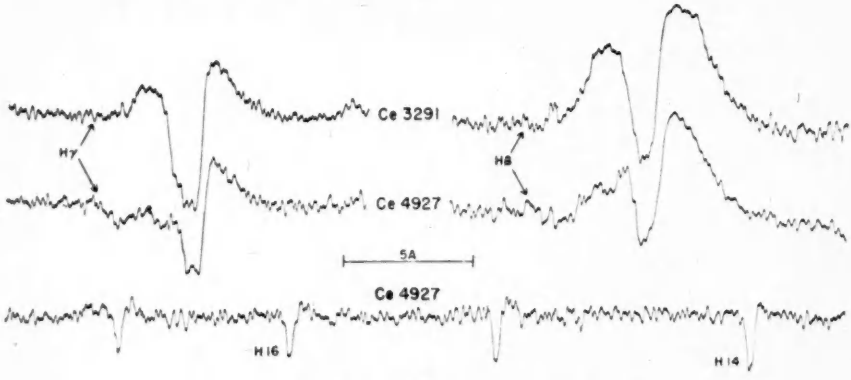

FIG. 3.—Tracings of lines in the spectrum of HD 45677

The dark metallic lines of *Ti* II, *Cr* II, *Mn* II, and *Ni* II are very narrow and much weaker than in typical shell spectra; only H and K of *Ca* II are outstanding. Many of them are centrally superposed on wider emission lines whose intensities may change from year to year. On the low-dispersion plates the weak dark cores are usually invisible, but settings on the narrow patches of emission yield velocities comparable with those from the cores. The velocity appears to have been constant from 1932 to 1947. The dark *Ca* II lines are strong and clean-cut, with traces of emission on both edges. They yield very nearly the same velocity as the other metallic lines and a practically zero velocity when corrected for solar motion. It seems probable that they are largely stellar or circumstellar, the contribution from interstellar space being minor. Diffuse dark lines of *He* I and λ 4481 of *Mg* II yield about the same velocities as do the sharp lines. Forbidden lines of [*Fe* II], [*S* II], [*O* I], and [*N* II] are well marked; they yield the same velocity as the permitted lines. Lines in the red are shown in Figure 1.

This star is not a typical shell star but rather an object intermediate between an ordinary Be star and a planetary nebula. Perhaps it can be thought of as a shell star whose outer atmosphere is extraordinarily extended and brilliant.

β Monocerotis A, MWC 143.—A bright *Hβ* line was discovered by Mrs. W. P. Fleming[9] in the spectrum of the brightest component of the well-known triple star β Mono-

[9] *Astr. and Ap.*, 11, 418, 1892.

cerotis on an objective-prism photograph taken at the Harvard Observatory on December 14, 1888. Mrs. Fleming's description of the changing relative positions of the bright and dark portions of $H\beta$ indicates that the dark core had a positive displacement in December, 1888, December, 1889, and January, 1890, and a negative displacement in February, 1892.

Since the early discovery of bright lines at Harvard the spectrum has been photographed at several observatories. During the last 27 years the radial velocities obtained from the dark cores of the hydrogen lines have shown a systematic variation in a cycle of

TABLE 4

SPECTROGRAMS OF β MONOCEROTIS A

Plate	Date	Disp. at $H\gamma$ (A/Mm)	Emul.	Radial Velocity (Km/Sec)			No. *M* II Lines
				*H*15	*H*32	*M* II	
V 657	1934 Oct. 27	37	I.E.S.	(+28)	.....	+24.5	2
G 1225	1935 Feb. 15	34*	III-F	.....	.....	.....	.....
Ce 1854	1938 Dec. 6	10	144-J	(+ 7)	.....	+10.7	4
1920	1939 Mar. 4	21*	III-E	+27.1*	.....	+18.0†	2
2927	1942 Dec. 21	3	103*a*-O	+37.2	.....	(+20.3)	2
4131	1946 Jan. 16	10	II*a*-O	+36.1	+41	+35.7	11
4134a	17	10	II*a*-O	+35.6	+35	+31.9	12
4134b	17	10	II*a*-O	+34.9	(+35)	+34.8	8
4134c	17	10	II*a*-O	+35.3	(+37)	+31.7	7
4171	Feb. 14	10	II*a*-O	+35.3	+33	+33.1	7
4201	Mar. 23	10	II*a*-O	+33.9	+35	+32.8	13
4205	24	10	II*a*-O	+31.7	+31	+30.7	16
4206	24	21*	103*a*-E	+22*	.....	.....	.....
4609	1947 Mar. 8	10	II*a*-O	+26.3	+25	+28.1	12
4923	Oct. 8	10	II*a*-O	+21.1	+21	+23.0	10
4924	8	10	II*a*-O	+20.5	+19	+21.0	8
5045	1948 Jan. 3	10	II*a*-O	+19.5	+18	+21.3	16
5131	Mar. 23	10	II*a*-O	+18.1	+17	+21.3	12
5354	Oct. 13	10	II*a*-O	+12.5	+12	+16.1	13
5488	Dec. 11	10	II*a*-O	+10.8	+ 6	+13.2	13
5524	1949 Feb. 5	10	II*a*-O	+10.2	+ 6	+15.9	11
5927	Sept. 10	10	II*a*-O	+ 5.8	+ 5	+11.6	7
6086	1950 Jan. 4	10	II*a*-O	+ 4.9	+ 5	+10.5	9
6087	4	10	II*a*-O	+ 5.8	+ 5	+11.4	8
6703	Nov. 28	10	III-O	+ 3.6	(+ 6)	+ 7.1	3
6959	1951 Mar. 27	10	III-O	+ 2.8	.....	.....	.....

* $H\alpha$. † D lines.

about 12.5 years. The changes noted by Mrs. Fleming may have arisen from similar variations about 1890; but, curiously enough, the velocity was constant from 1905 to 1914. Perhaps it is characteristic of shell stars to have periods of inactivity.

Because Dr. Dean B. McLaughlin is making a comprehensive study[10] of the spectroscopic history of this star, the present account will be confined to a presentation of data derived from spectrograms obtained at Mount Wilson (Table 4). I am indebted to R. F. Sanford, O. C. Wilson, and W. S. Adams for the first, third, and fifth plates, respectively.

Most of the hydrogen lines consist of narrow, well-defined dark cores with very weak wide wings (see Fig. 4). Emission edges are intense at $H\alpha$ but diminish so rapidly down the series that at $H\delta$ they are inconspicuous. Radial velocities measured from the dark cores of the Balmer series are listed in Table 4. Under the heading "*H*15" are the mean

[10] *A.J.*, **56**, 44, 1951.

values for all the lines $H5$–$H25$, inclusive; these are plotted against time in Figure 5. Under "$H32$" are values read from a smooth progression-curve drawn through the plotted displacements of all the Balmer lines measured; they are considerably less accurate than the $H15$ values.

The Balmer progression is never marked. Beginning in October, 1947, a slight negative progression appears in most of the plotted curves, but some of them are flat. A few of the earlier plates show a slight positive progression. Evidence for the reality of these minor changes is found in the fact that $H\beta$ behaves in a corresponding manner. On plates Ce 4205 (March 24, 1946) and 4609 (March 8, 1947) $H\beta$ yields very nearly the same velocity as the other H lines; on the earlier plates it has a negative residual, and on the later plates a positive one.

Figure 4 shows the changes in structure of $H\beta$ as the dark core shifts in position. The

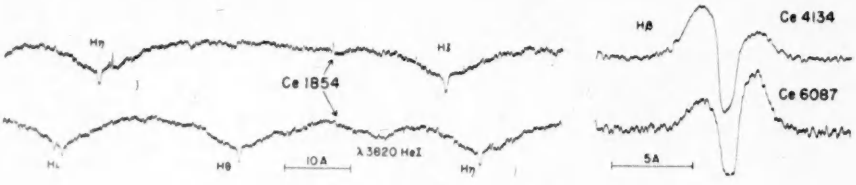

FIG 4.—Tracings of lines in the spectrum of β Monocerotis A

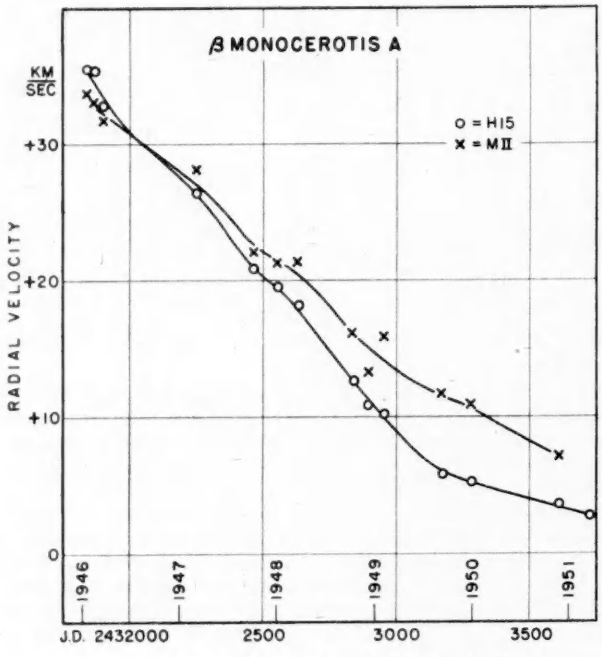

FIG. 5.—Radial velocities of β Monocerotis A

decrease in intensity of the emission on the side toward which the dark line shifts is characteristic of shell spectra. This behavior suggests at once that the emission moves less than the core, or might even be stationary. A comparison of the tracings of $H\beta$ in β Monocerotis and a few approximate measurements indicate that the emission as a whole shifts in the same direction as the core, but by a smaller amount. An accurate determination of the relative shifts of core and emission by a careful study of the profiles would be a valuable aid to the physical interpretation of stellar shells.

The metallic lines are narrow and so weak that only a very few are measurable. Lines of *Ni* II are relatively prominent. The mean velocities are shown in Table 4 and Figure 5. The amplitude of the velocity variation is somewhat less than that for the hydrogen lines, owing largely to the fact that since 1946 the *M* II velocities tend to be algebraically higher than those from *H* lines. This peculiarity should be borne in mind in intercomparing the behavior of various shell stars. The H and K lines shift with the other metallic lines and are therefore stellar.

The small velocity residuals of *H*14 and *H*28 show that the blending lines of *Ti* II and *Cr* II are weaker relative to the Balmer lines than in Pleione and certain other shell stars.

HD 50138, MWC 158.—A bright *Hα* line was discovered[11] on an objective-prism photograph taken by M. L. Humason with the 10-inch telescope on Mount Wilson on December 10, 1920. A large number of one-prism slit spectrograms obtained at Mount Wilson between 1920 and 1930 were reported upon in a previus article.[12] The appearance of the bright *Hα* line in 1930 is shown in an illustration accompanying a description[13] of a grating spectrograph for the visual region. Bright lines of *Fe* II were photographed by Struve and Swings[14] in 1940. A later article[8] by the same authors contains a description of a spectrogram taken in 1943.

Thirteen spectrograms (Table 5), dispersion 10 A/mm, obtained with the 100-inch telescope on Mount Wilson between 1943 and 1951, are described in the present article.

The hydrogen lines exhibit marked variations in structure, which are probably similar to those previously observed.[12] Details are now seen more clearly because of the higher dispersion; sample types of structure of $H\gamma$ are shown in Figure 6. Continuity of observation, unfortunately, is lacking, because intervals between plates are months or years, whereas the earlier series indicated changes measured by days or weeks. Radial velocities read at *H*5 and *H*15 from smoothed progression-curves are recorded in Table 5. Progression along the series is not marked except in the main component on plates Ce 4202 and 4930, on both of which a weaker component lies shortward. When two components are recorded in Table 5, the stronger one is given first, the weaker below. The position of the main component does not change greatly. The weaker component usually lies shortward, but plate Ce 4135 offers an exception.

Narrow dark lines of ionized metals vary greatly in intensity (Table 5). The *Ca* II lines H and K are usually outstanding, and a few *Ti* II lines, λλ 3685, 3759, 3761, are sometimes fairly strong; other lines are weak. To a first approximation the intensities of the metallic lines rise and fall as a group. The velocities behave in much the same way as do those from the hydrogen lines. Weak dark lines of *Mg* I, *Mg* II, and *He* I measured on a few plates yield about the same mean velocities as those recorded in Table 5. This is true also of the D lines of *Na* I, measured on Ce 4037. The *Ca* II lines H and K yield somewhat smaller velocities and may be somewhat affected by interstellar components. The red lines of [*O* I] yield a velocity of +36 km/sec on Ce 4037.

[11] Humason and Merrill, *Pub. A.S.P.*, **33**, 112, 1921.

[12] P. W. Merrill, *Mt. W. Contr.*, No. 423; *Ap. J.*, **73**, 348, 1931.

[13] P. W. Merrill, *Mt. W. Contr.*, No. 432; *Ap. J.*, **74**, 188, 1931.

[14] *Pub. A.S.P.*, **52**, 294, 1940.

An interesting feature of this spectrum is its partial resemblance to that of HD 45677. The glowing atmosphere of HD 50138 appears to be less extensive but more active. A series of spectrograms with dispersion of 10 A/mm, taken at intervals of a few days to bring out the sequence of quick changes in the atmospheric motions, would be valuable.

HD 54858, MWC 838.—A bright *Hα* line was discovered on an objective-prism photograph taken with the 10-inch telescope on Mount Wilson in December, 1939. A shell spectrum is shown by several slit spectrograms (Table 6). An underexposed one-

TABLE 5

SPECTROGRAMS OF HD 50138 WITH RADIAL VELOCITIES

Plate Ce	Date	*H*5 (Km/Sec)	*H*15 (Km/Sec)	Ionized Metals		
				Km/Sec	No.	Int.
3285	1943 Nov. 13	+28	+ 32	+32	20	10
3369	1944 Jan. 18	(+32)	+ 49	+46	32	8
3630	Oct. 30	+44	+ 42	+42	23	15
4037	1945 Oct. 24	+32*	.....	.....	.....	.....
4135	1946 Jan. 17	+30	+ 34	+32	6	4
		.....	+102	(+98)	2	1
4202	Mar. 23	+27	+ 18	+ 9†	2	3
		(−40)	− 30	−30†	1	.....
4551	1947 Jan. 11	+37	+ 27	+34	7	3
4610	Mar. 8	+39	+ 33	+35	7	5
4614	9	+37	+ 35	+36	6	5
4930	Oct. 25	+21	+ 4	+15†	2	2
		−46	− 42	−47†	1	.....
5046	1948 Jan. 3	+31	+ 18	+28	4	4
		−22	.....	.....	.....	.....
6702	1950 Nov. 28	+27	.....	+33	4	(7)
		−56	.....	.....	.....	.....
6966	1951 Apr. 14	+40	+ 42	+38	27	11
Mean	.....	+33	+ 30	+36	.....	.....

* *Hα*. † *Ca* II.

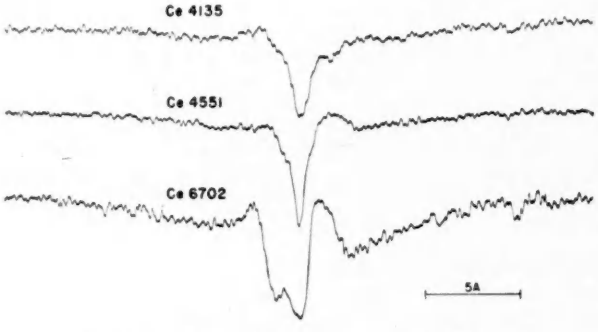

FIG. 6.—Tracings of *Hγ* in the spectrum of HD 50138

prism plate of the red region taken on February 9, 1946, shows a bright *Hα* line with two nearly equal components separated by 6.2 A. On the other spectrograms the dark core of *Hβ* has weak emission borders on either side. All lines both of hydrogen and of metals are narrow and of moderate intensity compared to lines in some of the more striking shell spectra, such as that of HD 44351. On the only plate with high dispersion, Pc 259, lines of *H*, *Ca* II, *Ti* II, *Cr* II, *Fe* II, and *Ni* II all yield the same velocity within errors of observation. The Balmer progression-curve appears perfectly flat. The velocities from the one-prism plates also are reasonably accordant (Table 6). Thus between the years 1945 and 1952 the shell of HD 54858 appears to have been stable.

MWC 985, BD+30°3526.—A bright *Hα* line was discovered on an objective-prism photograph taken with the 10-inch telescope on Mount Wilson in August, 1940. The star

TABLE 6

SPECTROGRAMS OF HD 54858

Plate	Date	Disp. at *Hγ* (A/Mm)	Observer	Radial Velocity (Km/Sec)		
				H	*M* II	No. *M* II Lines
γ 26397	1945 Jan. 13	35	W. C. Miller	+41	+38	6
γ 26421	27	35	W. C. Miller	+45	+38	3
γ 28341	1947 Feb. 7	35	A. G. Mowbray	+32	+33	3
Pc 259	1952 Feb. 2	9	I. S. Bowen	+37.6	+37.1	28

TABLE 7

SPECTROGRAMS OF MWC 985

Plate	Date	Disp. at *Hγ* (A/Mm)	Radial Velocity (Km/Sec)		
			H	*M*	No. *M* Lines
γ 26845	1945 July 28	80	+31	+34	11
Pc 122	1951 July 20	9	+28.0	+27.2	118

has a well-developed shell spectrum, first seen on a low-dispersion slit spectrogram taken by W. C. Miller with the 60-inch telescope on July 28, 1945 (Table 7). On another plate taken on April 9, 1948, *Hα* appears as a weak bright line. An excellent high-dispersion spectrogram was obtained by I. S. Bowen with the 200-inch telescope on July 20, 1951, with an exposure of only 115 minutes in fair seeing. This plate shows an unusually large number of metallic lines. The agreement of velocities measured from lines of various elements is shown in Table 8. The velocity is the same as in 1945, and the hydrogen series shows no progression; hence the spectrum is probably stable, at least for the time being. The H and K lines of *Ca* II are double, the stronger component being stellar, with a velocity displacement agreeing with that of other lines. The weaker component, if interstellar, indicates by its displacement a stellar distance of 2400 parsecs and an absolute magnitude (without correction for space absorption) of −2.7.

HD 183656, MWC 988.—A bright *Hα* line was discovered on an objective-prism photograph taken with the 10-inch telescope on Mount Wilson in July, 1929. Shell

characteristics were noticed by W. P. Bidelman[15] on slit spectrograms taken at Yerkes Observatory in April, 1949. Previously, W. E. Harper[16] had been struck with the peculiarities of the spectrum as observed on numerous plates taken at Victoria in the years 1927–1935. He wrote: "A most peculiar spectrum. Hydrogen is very intense and narrow. Then strong *Fe* II is present from 5018 down to violet. K sometimes sharp and all lines except the hydrogen seem to vary. No doubt of being a binary though the range is small. The mean of 24 plates is −42.1 [km/sec]."

On numerous coudé spectrograms (Table 9) the dark hydrogen lines are strong and

TABLE 8

MWC 985: RADIAL VELOCITIES OF VARIOUS LINES (PL. PC 122)

Element	Rad. Velocity (Km/Sec)	No. Lines	Element	Rad. Velocity (Km/Sec)	No. Lines
H	+28.0	27	*Ni* II	+31.1	3
Ti II	+27.3	40	*Mg* I	+29.9	3
Fe II	+26.4	34	*Si* II	+25.6	2
Fe I	+28.5	13	*Ca* II	+26.0	2
Cr II	+25.8	13	*M* I, II	+27.2	118
V II	+28.3	5	All	+27.4	145
Sc II	+29.4	3	Int. *Ca* II	− 4.3	2

TABLE 9

SPECTROGRAMS OF HD 183656
(Dispersion 10 A/Mm)

Plate	Date	Radial Velocity (Km/Sec)			No. *M* II Lines
		*H*30	*H*7	*M* II	
Ce 5679*	1949 June 11	.....	(−29.)*	(−42)*	4
5748	July 12	−48.5	−41.0	−45.8	27
5806	Aug. 3	−39.5	−35.5	−36.5	14
5917	Sept. 9	−30.5	−25.5	−26.4	21
5983	Oct. 9	−27.5	−25.0	−24.	6
6023	Nov. 12	−31.0	−28.5	−29.1	17
6427	1950 Aug. 4	−15.0	−17.5	−14.8	20
6443	7	−15.0	−17.5	−14.7	26
6690	Nov. 27	.....	+ 2.	+ 3.6	17
7016	1951 May 15	+ 8.5	+ 1.0	+ 5.1	26
7077	June 22	+19.5	+13.5	+16.9	31
7086	24	+18.0	+12.5	+18.6	21
7087†	24	.....	(− 6)†	+18.†	6
7215	July 31	+16.5	+11.0	+14.8	48
7222	Aug. 2	+16.0	+10.0	+14.6	44
7223	2	+16.5	+12.0	+16.2	40
Pc 197	Oct. 18	+ 6.0	0.0	− 0.1	15
Pc 303	1952 Apr. 5	−10.0	−10.5	− 9.1	23

* Red region; dispersion 20 A/mm.
† Red region; dispersion 15 A/mm.

[15] *Pub. A.S.P.*, **62**, 48, 1950.

[16] *Pub. Dom. Ap. Obs. Victoria*, **7**, 1, 1937.

well defined, but the metallic lines are rather weak. Very weak emission is seen on either side of the strong dark core of $H\beta$. Stronger emission, but still of moderate intensity, is present at $H\alpha$. At both these lines the longward portion of the emission was stronger than the shortward in 1949 but weaker in 1951.

The radial velocities derived from the dark H lines show considerable range (Table 9). The successive lines of the Balmer series had a negative progression in 1949, when the velocity was negative, and a positive progression in 1951, when the velocity was alge-

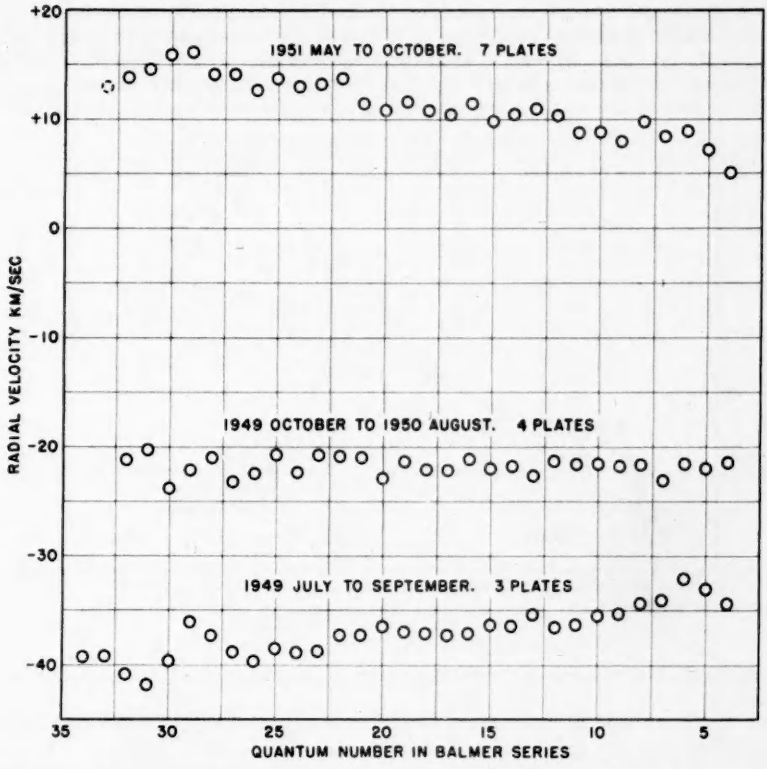

FIG. 7.—Mean progression-curves in radial velocities from successive Balmer lines of HD 183656

braically higher (see Fig. 7). Thus the dark $H\beta$ and $H\alpha$ lines have relatively small velocity ranges, and the wide emission portions of these two lines have even smaller ranges. The same general behavior has been noticed in several other shell spectra. These facts are of interest for a study of the velocities and accelerations in the extended atmospheres of shell stars. The velocities labeled "*H*30" and "*H*7" in Table 9 were read from the smoothed progression-curves for the individual plates.

The metallic lines, of moderate number and intensity, yield velocities which, on the whole, are intermediate between those for *H*30 and those for *H*7 (see Table 9 and Fig. 8). In 1951, when the velocities were positive, displacements of lines of *Ti* II had residuals of about +6 km/sec with respect to lines of other metals. The *Ca* II lines have

stellar and interstellar components which are of about the same intensity, being blended on most plates. When measurable separately, the stellar components yield a displacement agreeing with that derived from other metallic lines; the mean displacement of the interstellar components is −16.0 km/sec. Both the intensity and the displacement of the interstellar components point to a relatively faint absolute magnitude for the star.

The radial velocities derived from two points on the hydrogen progression-curve, *H*7 and *H*30, and from the metallic lines are plotted in Figure 8. Two velocities by Bidelman[15] at the McDonald Observatory agree with the Mount Wilson results. The curve shows a systematic trend with a maximum near JD 2433830. The whole cycle, if the curve is periodic, covers 4 years or more. Harper's velocities are bunched and do not define a velocity-curve. A period of about 6.5 years is not excluded. Figure 8 shows that velocities from *H*30 have a greater range than those from *H*7. Similar behavior has been noticed in other shell stars showing variable velocity. The velocity-curve shows certain

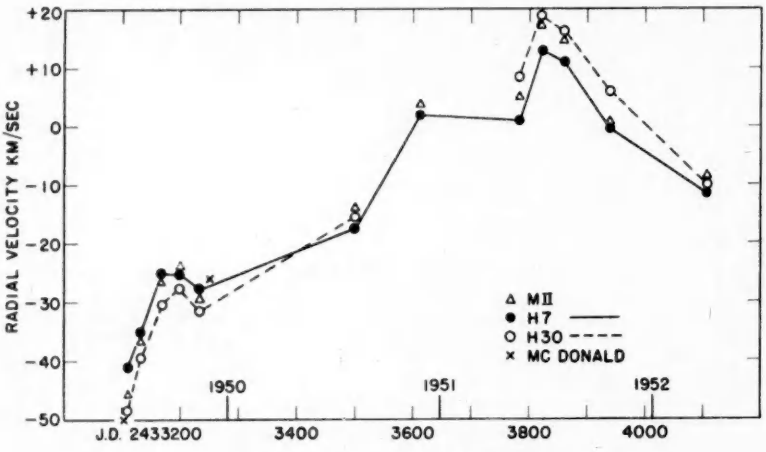

FIG. 8.—Radial velocities of HD 183656

irregularities which may be of considerable interest in the physical interpretation of the motions.

I am indebted to Miss Sylvia Burd for accurate measurements of more than half the spectrograms.

HD 351123, AS 372.—The *Hα* line is bright on objective-prism photographs taken with the 10-inch telescope on Mount Wilson on August 3, 1940, and August 30, 1946. Low-dispersion slit spectrograms taken by W. C. Miller in 1950 and 1951 (Table 10) show the hydrogen lines to have strong dark cores of the shell type. On the first plate *Hα* is a strong bright line. Metallic lines are weak, only H and K being seen with certainty.

Although the first plate is not very good, the difference in velocity between the two plates exceeds errors of measurement. The object may be a binary, but it is probably a star with an unstable shell. On the second plate the cores of the H lines from *Hβ* to *H*15 yield consistent velocities, but some of the ultraviolet lines in this range appear to have dark wings shortward. Lines *H*16–*H*18 are poor, and the cores cannot be distinguished from the wings; bisection of these lines yields velocities of approximately −80 km/sec. This behavior is somewhat like that of Pleione in 1951 toward the end of its shell episode.

MWC 374.—A bright *Hα* was discovered[17] in the spectrum of BD+47°3487 (now known as MWC 374) on an objective-prism photograph taken with the 10-inch telescope on Mount Wilson on August 16, 1928. A slit spectrogram taken with the 100-inch telescope on July 19, 1929, showed P Cygni characteristics, and later plates showed that numerous ultraviolet members of the Balmer series consisted of strong displaced dark cores without visible emission. Portions of the spectrum are illustrated in Figure 1. The star is strongly reddened, presumably by space scattering.

A number of spectrograms taken at the McDonald Observatory in September, 1939, were described by Swings and Struve.[7] Many data and an extended discussion of the line profiles have been given by C. S. Beals.[18, 19]

The Mount Wilson and Palomar spectrograms are listed in Table 11, with the radial

TABLE 10

SPECTROGRAMS OF HD 351123, AS 372

Plate	Date	Disp. at $H\gamma$ (A/Mm)	Radial Velocity (Km/Sec)	
			H	*Ca* II
γ 31578	1950 June 3	80	− 9	.....
E 2443	1951 June 16	65	−34	(−43)

TABLE 11

SPECTROGRAMS OF MWC 374

Plate	Date	Disp. at $H\gamma$ (A/Mm)	Radial Velocity (Km/Sec)				
			Hydrogen			*M* II Abs	*Ca* II Int.
			Em.	Abs.			
				*H*25	*H*5		
C 5248	1929 July 19	40	(+27)	.....	−116	.....	.....
C 7697	1941 Aug. 8	40	(+ 9)	.....	−128	−124	−10
γ 26770	1945 July 1	80	− 2	.....	−143	(−111)	−12
Ce 5752	1949 July 13	10	+30	− 80	− 94	− 72	−10.3
Ce 5924	Sept. 10	10	−13	.....	−113	−114	− 7.8
Ce 6428	1950 Aug. 4	10	−27	−130	−137	−125	− 8.5
Ce 6439	6	15*	.....	.....	.....	(−124)*	−10.6*
Ce 6691	Nov. 28	10	+14	− 92	−104	− 91	−10.0
Ce 7220	1951 Aug. 1	10	− 4	(−106)	−116	−120	− 9.1
Pc 216	Nov. 9	9	− 4	.....	−138	(−160)	− 5.7
Mean	.....	.....	.....	.....	.....	.....	− 9.1

* D lines.

[17] Merrill, Humason, and Burwell, *Mt. W. Contr.*, No. 456; *Ap. J.*, **76**, 156, 1932.

[18] *J. R.A.S. Canada*, **37**, 241, 1943. [19] *Pub. Dom. Ap. Obs. Victoria*, **9**, 88, 123, 1951.

velocities derived from various lines. The dark hydrogen lines vary through a considerable range, and the bright components probably shift with them. The plates with a large number of measurable hydrogen lines show a positive Balmer progression; this is indicated roughly by the values of *H*5 and *H*25 in Table 11.

Metallic lines observed in absorption are as follows: *Ca* II strong but of variable intensity (especially weak on plate Ce 7220); *Ni* II, moderate intensity; *Fe* II and *Na* I, weak. All these lines yield nearly the same velocities as the dark H lines. Additional plates will be needed to determine whether the changes in velocity are periodic. Interstellar lines of *Ca* II and *Na* I are strong and well separated from the stellar components.

The extreme redness of this star and of DM−27°11944, another P Cygni star with

TABLE 12

SPECTROGRAMS OF MWC 1081, HD 220300

Plate	Date	Disp. at $H\gamma$ (A/Mm)	Observer	Radial Velocity (Km/Sec)			
				*H*5	*H*20	*M* II	*Ca* II Int.
γ 26772	1945 July 1	80	W. C. Miller	−14	(− 18)	.....	.....
γ 26843	27	35	W. C. Miller	−26	.....	.....	.....
γ 26932	Aug. 26	35	W. C. Miller	−24	.....	.....	.....
Pc 143	1951 Aug. 20	9	I. S. Bowen	−50	− 68	−68	−14
Pc 218	Nov. 10	9	I. S. Bowen	−74	−102	(−95)	−17

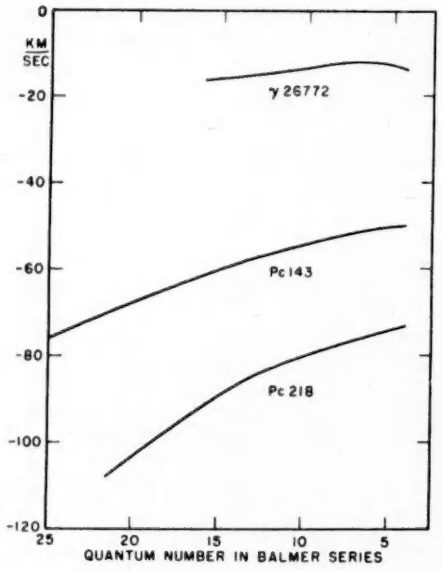

FIG. 9.—Radial velocities from Balmer lines of MWC 1081

greatly displaced lines,[20] together with the smaller color excess of P Cygni itself, leads one to wonder whether the color of these objects is due wholly to normal space reddening or whether a local cloud arising in the course of time from the rapid atmospheric outflow may have some effect. An alternative hypothesis is that the stars have extremely high absolute magnitudes and are thus unusually distant for their apparent magnitudes.

MWC 1081, HD 220300.—A strong bright $H\alpha$ line was discovered on an objective-prism photograph taken with the 10-inch telescope on Mount Wilson in September, 1944. Slit spectrograms (Table 12) show a shell spectrum with fairly strong hydrogen cores and a few weak, narrow, dark metallic lines. Emission of low intensity is seen on the longward edge of the dark $H\beta$ line.

The displacement of the lines varies through a considerable range (Table 12). On the last two plates with large negative velocities, the Balmer series shows marked negative progression (Fig. 9). As in certain other shell stars, the displacements of the metallic lines tend to agree with those of the shortward hydrogen lines. The data are not sufficient to indicate the period, but the rather quick change in 1951 suggests a possible cycle of a few years. The distance indicated by the displacement of the interstellar calcium lines corresponds to stellar absolute magnitude about 0.

My cordial thanks go to I. S. Bowen, W. C. Miller, and A. G. Mowbray for obtaining a number of spectrograms used in these studies; and to Miss Sylvia Burd and Miss Louise Lowen for skilful assistance in measuring and computing.

[20] P. W. Merrill, *Pub. A.S.P.*, **60**, 381, 1948.

OSCILLATIONS IN THE SHELL STAR HD 33232

PAUL W. MERRILL
MOUNT WILSON AND PALOMAR OBSERVATORIES
CARNEGIE INSTITUTION OF WASHINGTON
CALIFORNIA INSTITUTE OF TECHNOLOGY

Received July 28, 1952

ABSTRACT

A new series of spectrograms, dispersion 10 A/mm, obtained during the years 1943–1952 shows that the observed displacements are probably due to slow oscillations in the atmosphere of a shell star rather than to motion in a binary orbit, as previously supposed. As in other shell stars, the dark cores of the Balmer series exhibit progressively larger amplitudes of velocity variation from $H\beta$ shortward. Velocities from lines of ionized metals agree approximately with those of hydrogen lines toward the limit of the series. Comparison of velocity-curves from the first and second series of spectrograms shows that the cycle has lengthened from 3710 days to more than 4000 days and that the shape of the curve has changed. The atmospheric oscillations evidently do not repeat exactly.

The broad emission at $H\beta$ becomes weaker on the side toward which the dark core moves. A partial explanation may lie in the fact that, if radial motions are appreciable, the emission of the forward half of the atmosphere should be more strongly absorbed than the emission of the rear half.

In discussing an early series of spectrograms (1921–1933) of HD 33232,[1] the object was called a spectroscopic binary,[2] period 3710 days; but several puzzling features were noted, and it was recognized that the changes in the positions of the lines could not be due wholly to orbital motion.

A second series of spectrograms obtained with higher dispersion during the years 1943–1952 shows that the motions are probably due to oscillations in the upper atmosphere of a shell star. There is now little reason for using a binary orbit as a basis for discussing the changing displacements of various spectral lines.

The new spectrograms, listed in Table 1, have the advantage over the older ones not only in higher dispersion (10 A/mm against about 30) but in the greater range of wave lengths. Most of the new plates show the spectrum from $H\beta$ shortward past the limit of the Balmer series.

The narrow dark lines exhibit the shell characteristics, but the metallic lines are relatively weak. Emission borders are well marked at $H\beta$, weak at $H\gamma$. The various lines were subject to changes in intensity and structure during the period of observation. The appearance of a portion of the spectrum in 1945 and in 1948 is shown in Figure 1. With certain fluctuations, the changes have been in the direction of a decrease in the intensity and sharpness of the dark lines. The emission at $H\beta$ also decreased in intensity. The general course of the changes in the dark cores of the hydrogen lines is reflected by the curve in Figure 2, which shows the quantum number of the last Balmer line distinctly visible in the measuring microscope. One might expect the intensities and shapes of the lines to be related to motions in the stellar atmosphere. Hence data on radial velocities will be presented before further discussion of the line profiles.

The radial velocities derived from various dark lines are listed in Table 1. The velocity for $H\beta$ was directly measured from that line; the velocities for $H7$ and $H25$ are those read from smoothed progression-curves for the individual plates; the M II velocity is the mean of velocities from all available lines of ionized metals. As in several other shell stars, the displacements change from year to year. Moreover, at times various lines on the same plate yield different velocities. The behavior of the Balmer series is shown by the mean

[1] MWC 100. 1900 R.A. 5^h3^m7; Dec. $+40°53'$; mag. 8.1; spectrum (HD) B3.

[2] P. W. Merrill, *Mt. W. Contr.*, No. 491; *Ap. J.*, **79**, 343, 1934.

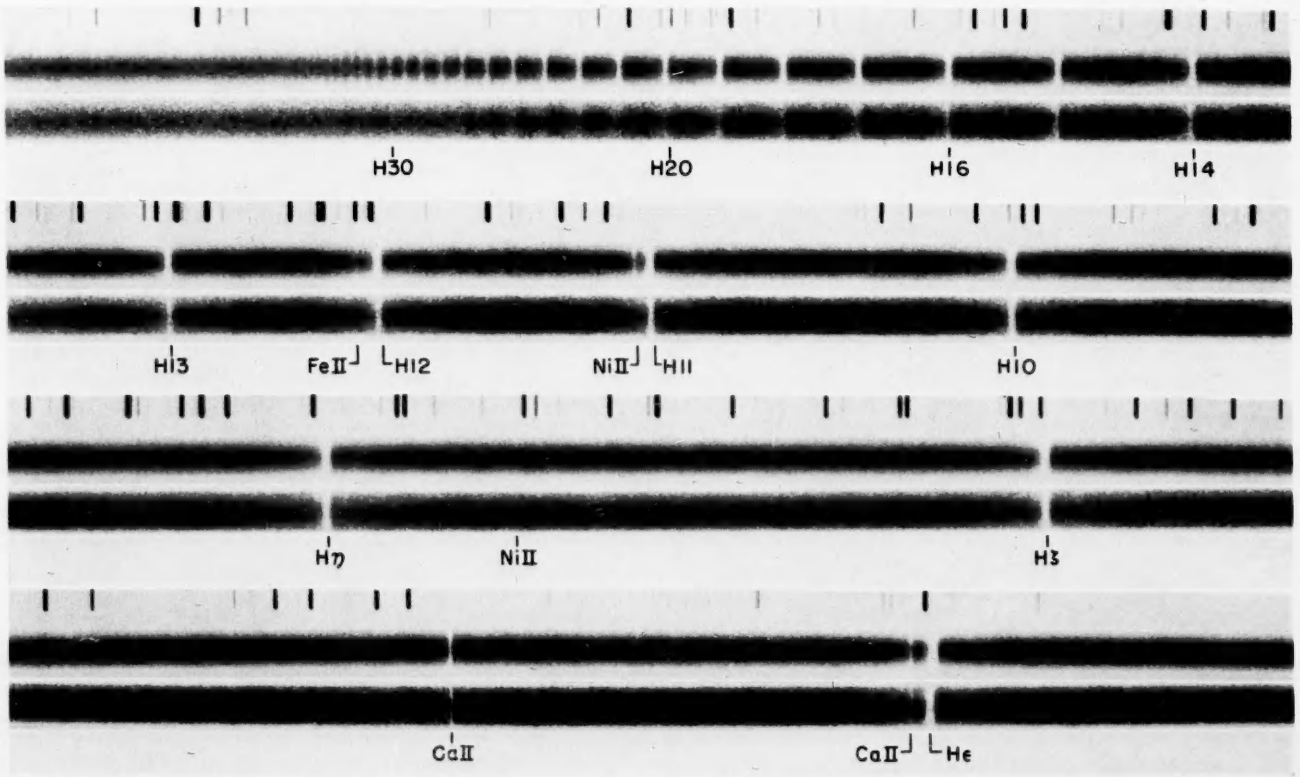

FIG. 1.—Portions of the spectrum of HD 33232. The upper spectrum of each pair is from plate Ce 3991, September 25, 1945; the lower is from Ce 5494, December 12, 1948.

progression-curves in Figures 3 and 4. As in other shell stars, the curves are nearly flat at times of mean velocity but develop a positive progression when the velocity is greater than the mean, a negative progression when the velocity is less than the mean. In other words, the shortward lines of the Balmer series have a larger amplitude of variation than do $H\beta$ and $H7$. This is shown also by the velocity-curves in Figure 5. From 1944 to 1946 the metallic lines gave about the same velocities as $H25$; thereafter, the lines were few and weak and the velocities not very accurate. In the fall of 1948, at the time of minimum velocity of $H25$, weak components of the H and K lines of *Ca* II yielded velocities

TABLE 1

JOURNAL OF OBSERVATIONS

Plate	Date	Radial Velocity (Km/Sec)				No. of *M* II Lines Measured
		Hβ	*H*7	*H*25	*M* II	
Ce 3290	1943 Nov. 14	+25	+44	+58	+58	9
3615	1944 Oct. 9	+25	+34	+39	+36	34
3687	1945 Jan. 1	+24	+30	+32	+30	28
3991	Sept. 25	+13	+14	+14	+14	34
4058	Nov. 20	+16	+10	+ 8	+10	25
4139	1946 Jan. 18	+10	+ 5	+ 4	+ 6	24
4461	Oct. 12	− 4	−10	−10	0	3
4550	1947 Jan. 11	− 4	−12	−16	− 4	2
4922	Oct. 8	− 2	−15	−23	.....	.....
4981	Nov. 29	+ 1	−15	−29	.....	.....
5320	1948 Sept. 12	+ 2	−10	−50	(−66)	1
5494	Dec. 12	+ 1	−10	−48	(−62)	2
5987	1949 Oct. 9	− 1	− 3	−20	.....	.....
6032	Nov. 13	+ 3	− 4	−16	.....	.....
6089	1950 Jan. 5	+ 6	− 2	−13	− 6	3
6155	Feb. 21	.....	− 3	−11	− 5	1
6167	23	0	− 4	− 9	− 8	1
6440	Aug. 6	+ 3	0	+ 8	− 4	1
6448	7	− 1	0	+ 5	− 3	1
6694	Nov. 27	− 1	+ 6	+15	+ 9	3
6700	28	+ 1	+ 5	+15	+ 9	1
6701	28	.....	+ 4	+14	+11	1
6963	1951 Mar. 29	.....	+ 9	.....	.....	.....
6964	Apr. 13	+ 6	+ 9	.....	.....	.....
7228	Aug. 2	+ 3	(+ 8)	.....	.....	.....
Pc 165	Sept. 22	+ 5	+20	+60	.....	.....
193	Oct. 16	+ 5	+12	(+57)	.....	.....
217	Nov. 9	.....	+14	.....	.....	.....
245	1952 Jan. 4	+ 4	+14	+66	.....	.....
258	Feb. 2	+13	+19	(+58)	.....	.....
261	3	+ 8	+19	(+68)	.....	.....
301	Apr. 5	+ 8	+28	(+84)	.....	.....

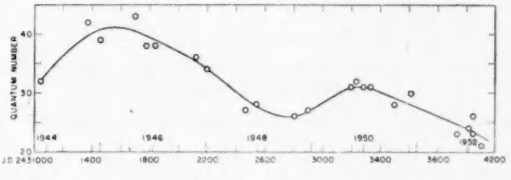

FIG. 2.—Quantum number of the last line measured in the Balmer series

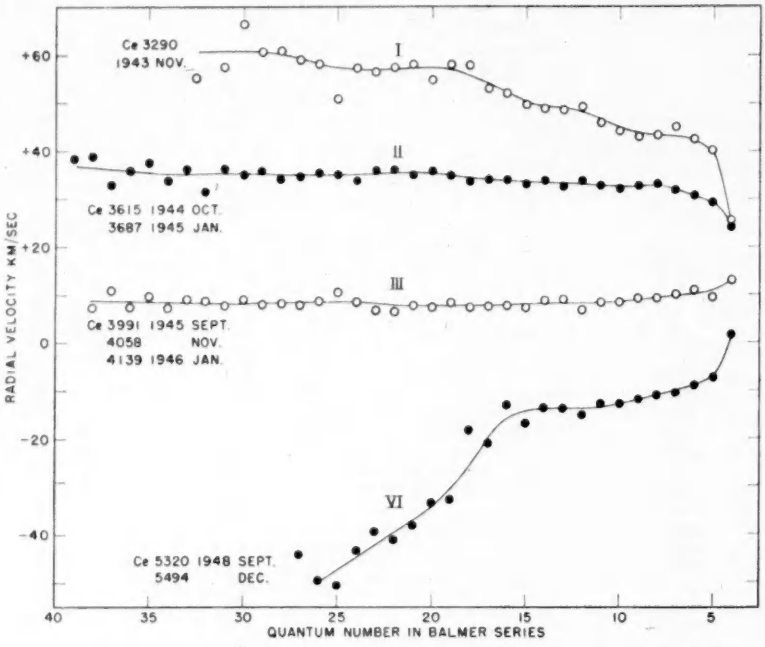

FIG. 3.—Progression-curves, showing displacements of individual hydrogen lines

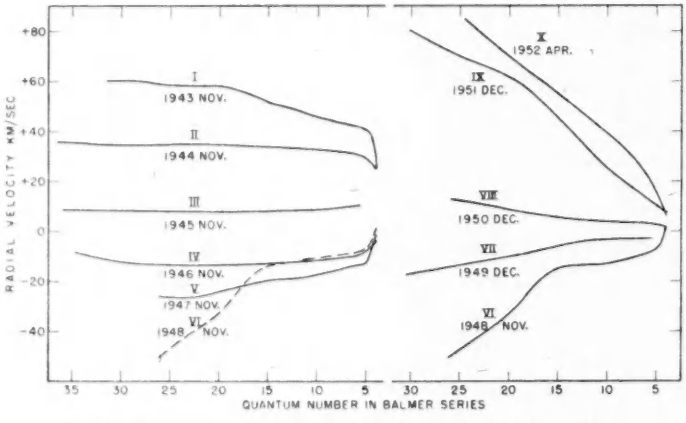

FIG. 4.—Mean progression-curves of displacements of hydrogen lines

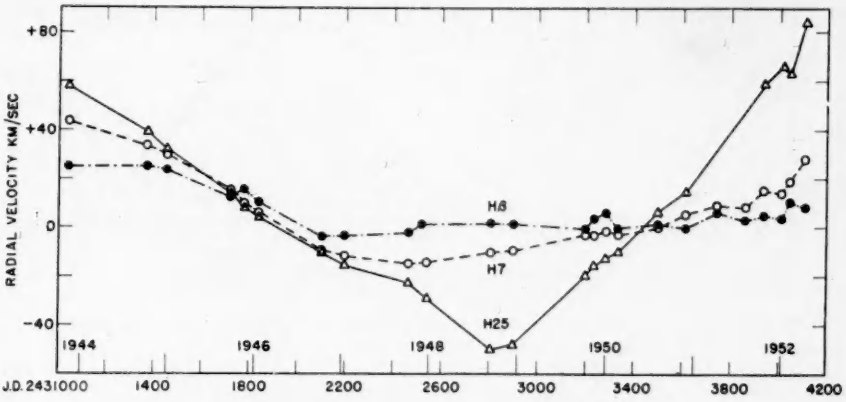

FIG. 5.—Velocity-curves from hydrogen lines

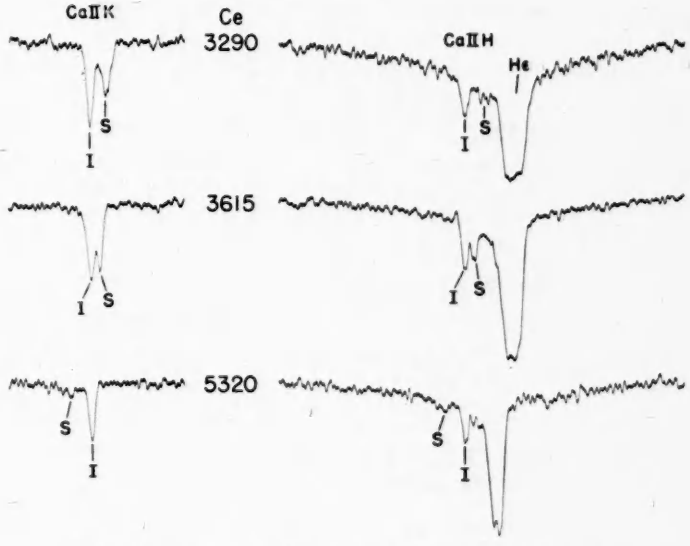

FIG. 6.—H and K lines of *Ca* II. Stellar components, *S;* interstellar, *I*

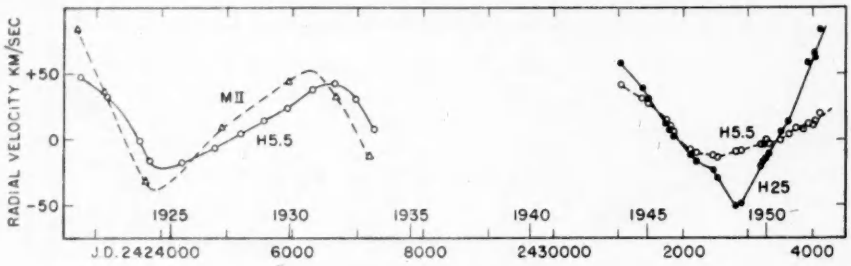

FIG. 7.—Velocity-curves from both series of spectrograms

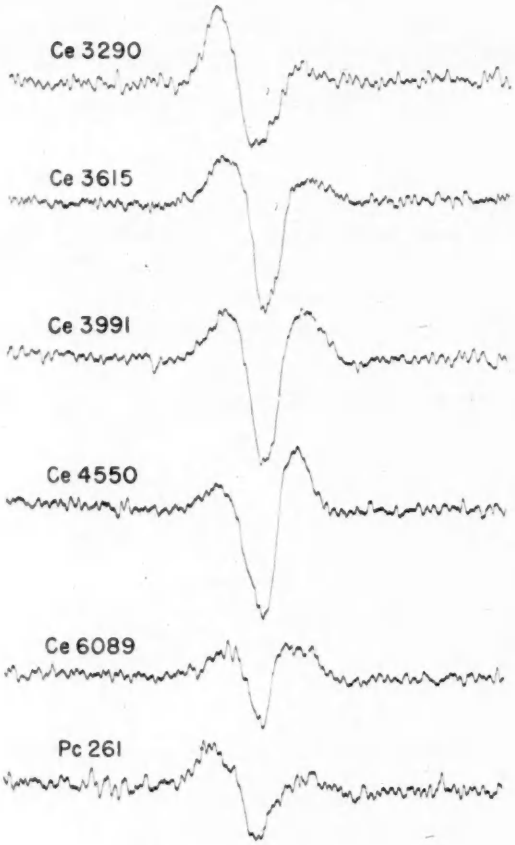

FIG. 8.—Tracings of $H\beta$

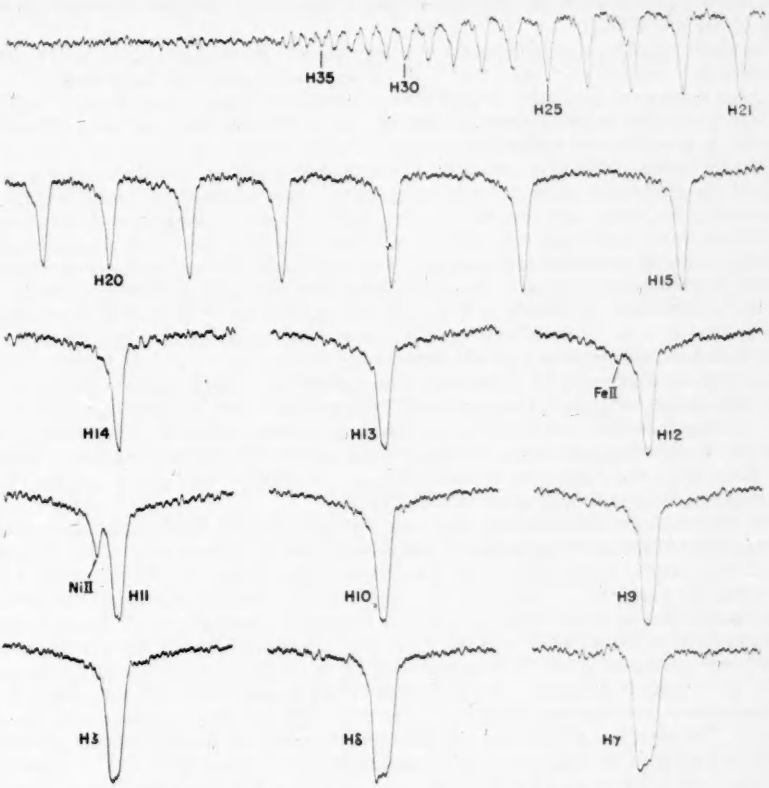

FIG. 9.—Tracings of hydrogen lines on plate Ce 3615

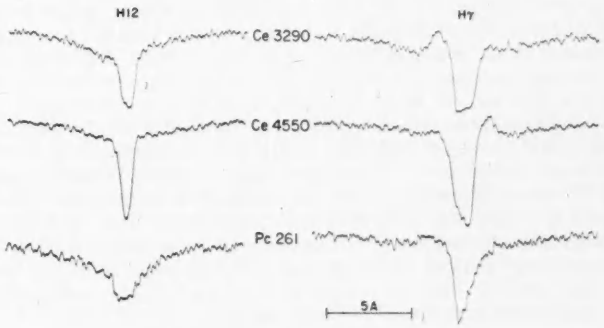

FIG. 10.—Tracings of $H12$ and $H\beta$

even below those of *H*25. In 1950 one or two lines of *Ni* II yielded velocities between those of *H*7 and *H*25.

The mean velocity derived from the interstellar lines H and K is +5.8 km/sec, which corresponds to a stellar distance of only 91 parsecs and an absolute magnitude of +3.3; but these values are unreliable because the residual velocity of the interstellar calcium (assumed to be due to galactic rotation) is only −0.3 km/sec. The luminosity of the star, however, is probably not very high.

The conclusion in *Mt. W. Contr.*, No. 491,[2] concerning the calcium lines was wrong because of the erroneous assumption that the stellar calcium lines had the same displacements as the hydrogen lines *Hβ*–*Hε*. The new series of spectrograms shows that the stellar calcium components, like lines of other ionized metals, have a much greater range of variation than do the longward hydrogen lines. Moreover the stellar *Ca* II lines clearly vary in intensity and sharpness. On most plates they are scarcely visible, but on a few they are conspicuous, as shown by Figure 6. On plate Ce 3615 they are as sharp and almost as strong as the interstellar lines. This shows that stellar and interstellar lines cannot always be distinguished by their appearance.

Velocity-curves from both the first and the second series of plates are plotted on the same time scale in Figure 7. Comparison shows that the cycle has lengthened from 3710 days to more than 4000 days and that the shapes of the curves have greatly altered. Residuals from any single compromise solution would be far greater than errors of observation. Evidently, the atmospheric oscillations in this star do not repeat exactly. Their future behavior should be of considerable interest.

The asymmetry of the emission components of *Hβ*, Figure 8, is related to the velocity-curve in the same way as that shown in Figure 1 of *Mt. W. Contr.*, No. 491.[2] That is to say, at the times of mean velocity the two bright components are approximately equal, but when the dark core moves longward, the longward emission becomes weaker, and when the core moves shortward, the shortward emission becomes weaker. This phenomenon is probably characteristic of shell stars, if not, indeed, of all Be stars with variable atmospheric motions; it would have a formal explanation if the dark core moved back and forth across a fixed emission line. But the emission is probably not stationary; it appears to move in the same direction as the dark core, although perhaps by a smaller amount. The structure of the emission line probably depends partly on Stark effect and partly on motions throughout the stellar atmosphere. The absorption which modifies the emission profile, however, probably originates largely in the outermost layers. Thus the position of the relatively narrow dark core depends on the motion of that portion of the upper atmosphere that lies between the observer and the rest of the star. More generally, if atmospheric motions perpendicular to the surface of the star are appreciable, emission from the hemisphere of the atmosphere toward us will, in general, be somewhat more strongly absorbed than the emission from the rear hemisphere. This hypothesis may explain at least partially the observed effects. A test might be had from a close study of the profiles of the *Hα*, *Hβ*, and *Hγ* lines at various times in the velocity cycle.

On most of the plates, various dark lines are nearly symmetrical. In 1946, however, the hydrogen lines from *Hβ* to about *H*15 were sharper on their longward edges, while in 1952 the same lines were sharper on their shortward edges. These asymmetries (see examples in Figs. 9 and 10) do not present a simple correlation with the asymmetries of the emission components of *Hβ* or with the radial velocity derived from the dark cores. They may be connected with systematic accelerations in the stellar atmosphere. Similar asymmetries were previously noticed in the spectrum of 48 Librae[3] and may be present at times in other shell spectra. Their proper interpretation might shed considerable light on the behavior of extended atmospheres in early-type stars.

[3] P. W. Merrill and R. F. Sanford, *Mt. W. Contr.*, No. 690; *Ap. J.*, **100**, 14, 1944.

SPECTROGRAMS OF TEN HIGH-VELOCITY Me VARIABLE STARS

PAUL W. MERRILL
MOUNT WILSON AND PALOMAR OBSERVATORIES
CARNEGIE INSTITUTION OF WASHINGTON
CALIFORNIA INSTITUTE OF TECHNOLOGY

Received June 13, 1952

ABSTRACT

Sample spectrograms, dispersion 9 A/mm, of ten long-period variables having high velocities show that the absorption spectra do not differ markedly from the spectra of ordinary giant stars. The bright lines appear to behave in about the same way as do those of other Me variables of similar types and periods.

When numerous high-velocity stars were found among the Me variables many years ago,[1,2] it was noticed that most of them had spectra earlier than M6e and periods between 150 and 250 days. These stars might appear to have a relationship to typical Me variables of periods exceeding 300 days paralleling that of RR Lyrae variables to "classical" cepheids and thus would now be assigned to population II. But no marked differences in

TABLE 1

DATA CONCERNING TEN HIGH-VELOCITY VARIABLES

STAR	DESIG.	PERIOD (DAYS)	MAG. AT MAX.	PREVIOUSLY OBSERVED			ADOPTED TYPE AT MAX.
				Spect.	Radial Vel. (Km/Sec)		
					Em.	Abs.	
X Mon	065208	156	7.3	M3e	+153	+160	M1e
S Gem	073723	293	8.8	M5e	+101	(+111)	M5e
S Lib	151520	193	8.5	M2e	+285	(+294)	M2e
RW Lib	151723	203	8.6	Se	+128	(+140)	?
X CrB	154536	240	9.0	M6e	−113	(−104)	M5e
RZ Sco	155823	160	8.8	M4e	−182	(−174)	M4e
W Lyr	181136	196	7 7	M4e	−183	−174	M3e
RT Cyg	194048	190	7.3	M2e	−126	−116	M2e
Z Cyg	195849	262	8.8	M5e	−173	(−166)	M5e
SV And	235939	316	8.6	M7e	− 99	(− 87)	M6e

spectroscopic behavior were found between these objects and variables of the same types and periods with smaller velocities. As far as could be determined, the absorption spectra were like those of ordinary giant stars. On these early low-dispersion spectrograms, the bright hydrogen lines and the dark *TiO* bands from λ 4500 to *Hβ* were well shown, but on most of them the continuous spectrum was too weak for satisfactory study of the dark atomic lines. In RT Cygni, however, well-exposed spectrograms showed an absorption-line spectrum[2,3] much like that of α Orionis, type cM2; but this behavior was probably an extreme example.

Recently, during the period of adjusting the coudé spectrograph of the 200-inch tele-

[1] P. W. Merrill, *Mt. W. Contr.*, No. 264; *Ap. J.*, **58**, 215, 1923.
[2] P. W. Merrill, *Mt. W. Contr.*, No. 649; *Ap. J.*, **99**, 171, 1941.
[3] Marjorie S. Pettit, *Pub. A.S.P.*, **56**, 107, 1944.

scope, I. S. Bowen has most generously obtained one or two spectrograms, dispersion 9 A/mm, for further study of each of the high-velocity stars listed in Tables 1 and 2. I am indebted to Mrs. Margaret W. Mayall, of the Harvard College Observatory, for photometric data.

Inspection of the recent spectrograms shows that the absorption spectra resemble those of ordinary giant stars, with possibly a tendency toward enhancement of those features which in normal stars indicate high absolute magnitude. The bright lines appear to behave in about the same way as do those of other Me variables of the same types and periods. Data on spectral types and measured velocities are in Table 2. The velocities

TABLE 2*

SPECTROGRAMS OF TEN HIGH-VELOCITY VARIABLES
(Dispersion 9 A/Mm)

Star	Plate Pc	Date 1951	Mag.	Days from Max.	Spect.	Radial Velocity (Km/Sec) and Numbers of Lines				$A-E$
						Em.		Abs.		
X Mon	77	Mar. 28	7.4	− 6	M1e	+156.3	23	+165.9	63	+ 9.6
S Gem	190†	Oct. 15	9.8	−11	M4e	+101.8	3	+107.4	8	+ 5.6
	199	Oct. 18	9.6	− 8	M4e	+ 99.6	3	+108.4	51	+ 8.8
S Lib	102	May 23	9.5	−24	.....	+292.8	3	.....		.....
RW Lib	120	July 20	(9)	.....	.....	+125.1	3	.....		.....
	123	July 21	(9)	.....	(M4)e	+126.2	7	.....		.....
X CrB	114	June 26	9.6	+14	M5e	(−114.2)	20	(−105.5)	30	+ 8.7
RZ Sco	69	Mar. 23	10.8	−49	M5e	−175.3	3	−171.4	48	+ 3.9
W Lyr	119	July 19	8.4	− 5	M3e	.....		.....		.....
	121	July 20	8.3	− 4	M3e	−182.7	6	−176.8	40	+ 5.9
RT Cyg	76	Mar. 27	7.7	−17	M3e	−127.7	2	−115.3	76	+12.4
	103	May 23	8.5	+40	M3e	−127.4	15	−117.2	35	+10.2
Z Cyg	99‡	May 21	10.4	−42	M6e	−172.7	2	−166.5	16	+ 6.2
SV And	244	Jan. 4§	9.2	− 6	M6e	− 99.6	6	− 90.2	42	+ 9.4

* The absorption spectrum of X Mon resembles that of β And gM0 more closely than it does that of α Cet gM2. It does not differ greatly from that of α Ori cM2, but the lines are not quite so strong and clear-cut. The bright hydrogen lines are very strong from $H\beta$ to the ultraviolet. The He line is about as strong as $H\zeta$. This circumstance is quite unusual at or before maximum light; it may be partly explained by the fact that the H absorption line of *Ca* II is unusually narrow. Emission of *Ca* II displaced shortward is visible at H and in lower intensity at K. In several respects the spectrum seems to correspond to a phase later than that indicated by the light-curve.

For the other stars the appearance of the spectrum is not unusual for the spectral type, and for the phase in the light-cycle when the spectrogram was taken.

† Negative by O. C. Wilson.

‡ Plate Pd 99; dispersion 18 A/mm.

§ 1952.

show no significant deviations from those previously determined. The shortward displacement of the bright lines with respect to the dark lines, $A - E$, has about the same range as that previously observed for other comparable Me variables.[4]

There can be no doubt that Me variables with high velocities have a strong statistical preference for the shorter periods and the earlier spectral types. It is not known whether this preference is correlated with chemical composition. For a fair comparison between high-velocity and low-velocity variables, stars of comparable types and periods should be studied. But the spectra of Me variables change with phase and may differ from cycle to cycle. Hence a satisfactory comparison would be a formidable task. It would be interesting to find real chemical differences between the two groups of stars; but the present material seems to indicate that such differences, if any, are relatively minor.

[4] P. W. Merrill, *Mt. W. Contr.*, No. 644; *Ap. J.*, **93**, 380, 1941.

INTENSITIES OF ATOMIC ABSORPTION LINES IN THE SPECTRA OF LONG-PERIOD VARIABLE STARS

WILLIAM BUSCOMBE* AND PAUL W. MERRILL

MOUNT WILSON AND PALOMAR OBSERVATORIES
CARNEGIE INSTITUTION OF WASHINGTON
CALIFORNIA INSTITUTE OF TECHNOLOGY

Received June 9, 1952

ABSTRACT

Photometric measurements in the spectra of o Ceti (M6e), R Leonis (M8e), and R Andromedae (Se) were made from coudé spectrograms, 10 A/mm, taken at various phases of the light-curves. Central depths were derived for more than 200 absorption lines in the region from λ 3700 to λ 4100, which is nearly free of absorption by molecular bands. Equivalent widths were measured for 40 unblended atomic lines on each tracing.

As an aid in establishing a "fiducial continuum" from which to measure the line absorption, gradient temperatures were estimated by comparing the general intensity in each spectrum near λ 3750 and λ 4050 with Planck's formula. The calculated temperatures vary with the star's brightness in a range similar to that found by other methods.

In the spectrum of Mira Ceti, the strong resonance lines of *Al* I and *K* I weaken at maximum light to one-third their intensities at a phase 3 mag. fainter, owing to ionization, while the H and K lines of *Ca* II strengthen. An electron pressure of 10^{-10} atm. would be consistent with this behavior. The neutral lines of elements of higher ionization potential generally appear considerably stronger near maximum. Since this effect is especially marked among the subordinate lines, an increase in excitation temperature appears to occur, along with a great decrease in opacity at the brightest phases.

Although actual relative abundances are as yet very uncertain, the indications are strong that for each atom of *Fe* there are several times as many atoms of the heavier elements *Y*, *Zr*, and *Nb* in the reversing layer of the S-type star R And as in that of R Leo. Mira Ceti shows an intermediate distribution of these elements, as suggested previously by Merrill from visual comparisons.

I. INTRODUCTION

Several authors have described the spectra of individual long-period variables very minutely, with emphasis on precise measures of wave length for the absorption and emission lines, leading to an analysis of the motions of gases in the atmospheres of these stars. But spectrophotometric data, which would yield definite information on the differences in physical and chemical conditions prevailing among these cool giants, are extremely meager. A few measurements in the spectrum of Mira Ceti with low dispersion were made by Roderic M. Scott.[1]

In the introduction to a general spectrographic study of Mira, Alfred H. Joy[2] has written:

> The mean period is 330 days, but the interval from maximum to maximum may vary by as much as 30 days. The magnitude at maximum is normally about 3.5, with extremes of 1.5 and 5.6. The minimum is also uncertain, varying from 8.0 to 10.0, but most frequently is about 9.2. At maximum the star is of spectral type M5–M6, with strong bands of titanium oxide and sharp hydrogen emission lines. The bright lines of hydrogen have their maximum intensity at or soon after the maximum of light. They are accompanied by faint emission lines of ionized iron. The appearance of most of the other bright lines is delayed for three or four months until the star has reached fainter magnitudes. When the star is fainter than the eighth magnitude, the bright lines of the companion are well seen, and its continuous spectrum shows sufficient strength to give the combined spectrum a curious distorted effect which is especially noticeable in the region of the bands.

* Present address: Commonwealth Observatory, Canberra, Australia.

[1] *Ap. J.*, **101**, 71, 1945.

[2] *Mt. W. Contr.*, No. 311; *Ap. J.*, **63**, 281, 1926.

To compare the spectra of different long-period variables in detail, one must first investigate how certain features vary in a typical star. Since it is practicable to obtain fairly high-dispersion spectrograms of stars as faint as the 9th photographic magnitude, the spectrum of Mira can be studied at various phases of the light-curve until the presence of its companion becomes noticeable. No other long-period variable has been studied in this way over such a large range of photographic brightness.

Among the brighter northern long-period variables, R Andromedae shows most conspicuously the *ZrO* absorption bands, characteristic of S-type stars. R Leonis, on the other hand, is an advanced Me variable with very strong *TiO* bands. The spectra of these two stars are compared in this paper, after a detailed study of the variations in the spectrum of *o* Ceti at different phases. In several respects the spectrum of *o* Ceti is intermediate between that of R Leonis and that of R Andromedae.

II. OBSERVATIONS

From a large collection of spectrograms taken by P. W. Merrill with the coudé spectrograph of the 100-inch telescope, the plates listed in Table 1 were selected, chiefly

TABLE 1

JOURNAL OF OBSERVATIONS

Star	Plate	Date G.C.T.	Phase (Days)	m_v	Exposure (Min.)	T°_{grad} K
o Ceti	Ce 4047	1945 Nov. 14	− 50	7.4	470	1700
	4103	1945 Dec. 12	− 9	4.3	50	1900
	5925	1949 Sept. 11	+ 14	3.0	34	2700
	5981	1949 Oct. 9	+ 42	4.2	122	3100
	6028	1949 Nov. 14	+ 78	5.7	62	2800
	6088	1950 Jan. 6	+131	7.7	134	2100
R Leo	3366	1944 Jan. 17	+ 17	6.1	120	2600
	3689	1945 Jan. 2	+ 65	6.5	150	3200
R And	3522	1944 Aug. 2	+ 10	6.9	304	2600
	3560	1944 Sept. 6	+ 45	7.3	452	3000

on the basis of density suitable for photometry in the near ultraviolet. Among the plates of *o* Ceti listed in Table 1, one of which was kindly contributed by A. H. Joy, the first two represent the ascending branch of the light-curve at a rather faint maximum, and the other four the decline from a very bright maximum. R Leo and R And are each represented by a plate near maximum and another about 2 months after maximum.

The dispersion is 10.2 A/mm, and the Eastman II*a*-O emulsion was used throughout. All plates exposed for longer than 1 hour had been pre-sensitized by baking at 50° C for 3 days. The slit-width corresponds to about 15 μ on the plate. Most of the plates are second-order spectra from a grating ruled by R. W. Wood with 600 lines per millimeter, filled by a collimator mirror 4 inches in aperture and 114 inches in focal length. The last three plates of *o* Ceti were taken with the third order of a 400-line grating ruled by H. W. Babcock on a larger area, filled by a 6-inch collimator 184 inches in focal length. This arrangement permits more efficient use of starlight in average seeing, as the slit can be opened 60 per cent wider than formerly without loss of resolving power. The spectra were widened by trailing to secure uniform density over a width of 1.0 mm on the plate.

For calibrating the intensity scale of the stellar spectrograms, on each plate is recorded a series of sixteen spectra of an incandescent lamp, whose light passes through a set of rectangular apertures in the plane of the slit, adjacent to the stellar image. The

areas of successive step slits are in the ratio 1:1.26. From measures of the blackness of the spectrogram plate exposed to the lamp for about one-fifth the duration of the exposure to starlight, a characteristic curve is prepared from which the relative intensity corresponding to any degree of blackening on the plate can be interpolated.

III. PHOTOMETRY

The region from λ 3700 to λ 4100, which is nearly free of absorption by molecular bands, was selected for detailed comparison. Even this region is somewhat restricted at the ends, where the atomic lines are blended with band lines of *ZrO* near λ 3682, and of *SiH* near λ 4126, respectively. The six spectrograms were traced in this region with the microdensitometer on a scale of 1.0 A/cm. As an aid in establishing a "fiducial continuum" from which to measure the line absorption, additional tracings were made on a smaller scale, which permitted the recording of the entire spectral region on a single sheet of photographic paper. By adjustment between the two tracings for each plate, a straight line was finally adopted which passes slightly above the highest points on the tracings near λ 3750 and λ 4050.

The intensity of a cool source in a region of wave length far shortward from that of maximum energy rises rapidly with wave length, with a slope which is very sensitive to the temperature. The gradient temperatures indicated in Table 1 have not been corrected for atmospheric extinction, finite slit-width, efficiency of the grating, or plate sensitivity. Over such a short wave-length interval the effect of these items is relatively unimportant. The light of a star at a large zenith distance is dispersed by the earth's atmosphere, so that the image in the focal plane of a large telescope appears as a short spectrum. The greatest photographic efficiency is obtained by keeping the ultraviolet radiation (especially of a red star) on the slit of the spectrograph. Because of differences in seeing and in zenith distance, however, there may be slight differences in the effective guiding from one exposure to another. In spite of these uncertainties, the range of gradient temperatures agrees well with the radiometric determinations[3] during earlier cycles of Mira's light-variation. The plates used in the present investigation were not taken specifically for determining gradient temperatures, and they suffer from one obvious discontinuity. On the day following the exposure of Ce 5925, the second-order grating and small collimator were replaced by the third-order grating and large collimator. The relative efficiency of the spectrograph at different wave lengths depends critically on the contour of the rulings. R. M. Scott[1] has found a similar range of temperatures from Harvard objective-prism spectrograms of lower dispersion, which are better adapted to the study of intensity gradients. The fact that reasonable temperatures have been found shows that the fiducial continuum is probably drawn almost parallel to the correct position on each tracing, from which differential comparisons at least can be made.

The atomic lines were identified principally by reference to measured wave lengths[4] in the spectra of R Leo and R And and to the *Revised Multiplet Table*.[5] For the majority of lines in these complex blended spectra, only the central depth in percentage absorption can be measured. The entire profile of about one line in five can be sketched with some confidence. The equivalent widths of these lines, measured by averaging the widths in steps of 10 per cent absorption, were used to calibrate the results from the central depths of the other lines. The average equivalent widths in angstrom units for small groups of lines, arising from the same lower-energy state of the same atom, are listed in Table 2, in order of increasing atomic number and excitation potential. The individual values for a few typical lines, in Table 3, show the uncertainties of measurement.

[3] Pettit and Nicholson, *Mt. W. Contr.*, No. 478; *Ap. J.*, **78**, 320, 1933.

[4] Paul W. Merrill, *Mt. W. Contr.*, No. 743; *Ap. J.*, **107**, 303, 1948.

[5] Charlotte E. Moore, *Contr. Princeton U. Obs.*, No. 20, 1945.

TABLE 2

MEAN EQUIVALENT WIDTHS IN ANGSTROMS

			o CETI						R LEONIS		R ANDROMEDAE		
Plate			4047	4103	5925	5981	6028	6088	3366	3689	3522	3560	
Phase			−50	−9	+14	+42	+78	+131	+17	+65	+10	+45	NOTES
Mag.			7.4	4.3	3.0	4.2	5.7	7.7	6.1	6.5	6.9	7.3	
Atom	E.P.	n											
Mg	2 7	3	0 16	0 22	0 21	0 16	0 14	.....	0 18	0 27	0 18	0 22	2
Al	0 0	2	2 1	1 1	0 8	0 9	1 4	2 3	1 5	2 2	4 0	5 3	1
K	0 0	1	0 38	0 27	0 16	0 13	0 22	0 18	0 49	0 52	0 20	0 32	
Ca II	0 0	2	13	14	15	14	11	10	13	12	18	14	1, 2
Sc	0 0	7	0 20	0 26	0 34	0 25	0 21	0 16	0 37	0 41	0 34	0 45	
Ti	0 0	2	0 19	0 26	0 28	0 22	0 16	0 17	0 43	0 47	.....	.....	
Ti	0 0	5	0 27	0 36	0 39	0 31	0 24	0 22	0 54	0 54	0 38	0 57	3
Ti	0 0	6	0 15	0 22	0 26	0 21	0 17	0 14	0 35	0 36	0 30	0 40	3
Ti	0 0	5	.....	0 30	0 32	0 27	0 25	0 30	0 47	0 53	0 59	0 64	1
Ti	1 0	6	0 13	0 22	0 29	0 20	0 18	0 14	0 28	0 31	0 26	0 35	
Ti	1 4	2	0 12	0 18	0 22	0 18	0 16	0 11	.....	.....	.....	.....	
Ti	2 0	4	0 11	0 13	0 16	0 14	0 11	0 10	0 23	0 30	0 20	0 24	
Ti	2 1	6	0 12	0 14	0 16	0 12	0 09	0 08	.....	.....	.....	.....	
V	0 0	7	0 19	0 26	0 28	0 26	0 26	0 28	0 54	0 59	0 37	0 43	
V	0 0	7	0 18	0 30	0 33	0 26	0 29	0 31	0 56	0 65	0 36	0 40	
V	0 0	3	0 17	0 26	0 32	0 24	0 20	0 25	0 48	0 52	0 38	0 39	
V	0 3	6	0 16	0 24	0 28	0 18	0 17	0 20	0 37	0 34	0 23	0 19	
V	1 0	5	0 17	0 23	0 20	0 14	0 12	0 11	0 24	0 26	0 20	0 19	
V	1 8	3	0 12	0 14	0 16	0 12	0 08	0 08	.....	.....	.....	.....	
Cr	1 0	8	0 16	0 23	0 28	0 19	0 16	0 14	0 48	0 47	0 24	0 32	
Cr	2 6	4	0 13	0 15	0 17	0 12	0 10	0 09	0 20	0 31	0 20	0 18	
Cr	3 0	2	0 09	0 12	0 16	0 13	0 11	0 09	0 30	0 23	0 16	0 14	
Mn	2 2	7	0 15	0 20	0 22	0 17	0 14	0 12	0 29	0 37	0 17	0 17	
Fe	0 1	9	0 37	0 69	0 64	0 49	0 44	0 30	1 9	1 3	1 2	1 1	1, 2, 3
Fe	0 1	6	.....	0 75	0 69	0 62	0 50	.....	2 8	1 2	1 1	1 4	1, 2
Fe	1 0	6	0 19	0 27	0 41	0 27	0 28	0 22	0 66	0 54	0 30	0 46	2
Fe	1 0	5	0 26	0 28	0 33	0 21	0 20	0 14	0 67	0 52	0 24	0 31	2
Fe	1 0	6	.....	0 36	0 43	0 33	0 26	0 22	0 73	0 55	0 45	0 48	2
Fe	1 0	6	0 15	0 28	0 28	0 22	0 19	0 17	0 52	0 47	0 27	0 18	2
Fe	1 6	7	0 26	0 32	0 36	0 22	0 20	0 18	0 53	0 42	0 22	0 28	2
Fe	2 2	3	0 13	0 14	0 16	0 13	0 09	0 09	.....	.....	.....	.....	2
Fe	2 7	4	0 12	0 16	0 14	0 12	0 08	0 09	0 13	.....	0 13	0 16	
Fe	3 3	3	0 18	0 20	0 16	0 12	0 11	0 10	0 24	0 21	0 20	0 22	
Co	0 1	6	0 22	0 26	0 27	0 18	0 16	0 14	0 41	0 40	0 20	0 26	
Co	0 5	6	0 17	0 20	0 21	0 16	0 12	0 10	0 32	0 24	0 14	0 21	
Co	0 5	6	0 18	0 24	0 26	0 19	0 18	0 15	0 42	0 40	0 25	0 29	
Co	1 0	6	0 18	0 19	0 21	0 14	0 11	0 11	0 31	0 26	0 14	0 17	2
Ni	0 1	5	0 17	0 29	0 28	0 20	0 16	0 13	0 44	0 46	0 32	0 23	
Ni	0 1	4	0 14	0 24	0 24	0 19	0 18	0 18	0 39	0 46	0 28	0 26	
Ni	0 4	5	0 17	0 26	0 26	0 18	0 19	0 16	0 51	0 37	0 25	0 21	2
Sr II	0 0	1	0 55	0 91	0 79	0 52	0 35	0 24	0 44	0 42	1 0	1 2	
Y	0 0	1	0 11	0 13	0 22	0 14	0 11	0 09	0 11	.....	0 26	0 37	
Y II	0 1	3	.....	0 21	0 21	0 15	0 12	0 14	0 40	0 39	0 30	0 24	
Zr	0 1	6	0 12	0 16	0 19	0 14	0 12	0 11	0 19	0 29	0 28	0 33	
Zr	0 1	5	0 12	0 16	0 20	0 14	0 11	0 10	0 24	0 26	0 29	0 30	
Zr	0 5	4	0 11	0 14	0 17	0 12	0 08	0 08	0 09	.....	0 18	0 26	
Zr	0 7	6	0 15	0 19	0 20	0 13	0 10	0 09	0 17	.....	0 25	0 27	
Zr II	0 4	3	0 14	0 19	0 18	0 14	0 11	0 11	0 17	.....	0 28	0 28	
Nb	0 1	6	.....	0 17	0 21	0 14	0 11	0 14	0 17	0 32	0 24	0 20	
Ru	0 2	3	.....	0 28	0 27	0 22	0 17	0 14	0 28	0 38	0 28	0 24	
Ru	1 0	2	0 12	.....	0 17	0 12	0 10	0 09	0 15	0 20	0 14	0 20	
Yb	0 0	1	0 13	.....	0 15	0 16	0 15	0 16	0 36	0 46	0 36	0 36	

NOTES TO TABLE 2

1. Broad wings.
2. Emission edges on some plates.
3. Individual measures given in Table 3.

The complexity of these spectra is shown in the tracings of representative spectral regions for each of the three stars, including o Ceti at various phases. Figure 1 reproduces a section including the very broad H and K lines of *Ca* II, expanded tenfold in linear dispersion from the original spectrograms. Although the fiducial continuum appears rather high in this region, it was found necessary to draw the base line this far above the general level of the spectrum to permit the sketching of reasonable damping profiles for the wings of the strongest lines. The twenty-five fold enlargement of the adjacent long-

TABLE 3

EQUIVALENT WIDTHS FOR TYPICAL LINES

Element	E.P.	(Mult. No.)	λ	o Ceti						R Leonis		R Andromedae	
				4047	4103	5925	5981	6028	6088	3366	3689	3522	3560
Ti	0.0	(12)	3981.76	0.32	0.40	0.32	0.32	0.28	.....	0.59	0.32	.....	.....
			3989.76	.33	.43	.45	.39	.27	0.24	.65	.65	.....	.....
			3998.64	.29	.37	.49	.30	.25	.25	.59	.65	0.55	0.67
			4008.93	.22	.29	.32	.24	.20	.20	.49	.59	.30	.53
			4024.57	0.18	0.30	0.38	0.28	0.21	0.20	0.38	0.48	0.29	0.50
			Mean	0.27	0.36	0.39	0.31	0.24	0.22	0.54	0.54	0.38	0.57
Ti	0.0	(13)	3898.49	0.17	0.22	0.32	0.24	0.20	0.20	0.44	.....	0.35	0.46
		(14)	3914.74	.15	.....	.27	.19	.15	.10	.30	0.30	.30	.40
		(15)	3881.40	.14	.....	.20	.19	.17	.17	.33	.39	.30	.38
			3900.96	.14	0.23	.28	.26	.20	.....	.38	.46	.30	.46
			3914.33	.13	.....	.23	.20	.16	.11	.30	0.31	.28	.35
			3915.88	0.15	.....	0.27	0.18	0.16	0.13	0.34	.....	0.25	0.38
			Mean	0.15	0.22	0.26	0.21	0.17	0.14	0.35	0.36	0.30	0.40
Fe	0.1	(4)	3824.44	.....	0.65	0.83	0.52	0.46	.....	1.0	1.5	0.91	0.93
			3856.37	0.27	0.72	0.55	0.52	.63	0.29	1.9	1.2	1.1	2.1
			3859.91	.30	1.1	1.0	1.1	.72	.....	4.0	3.4	2.1	2.3
			3878.58	.32	0.69	0.52	0.30	.39	.31	1.6	0.83	1.4	0.52
			3886.28	.....	.....	0.47	0.19	.19	0.31	2.2	0.63	.....	0.48
			3895.66	.46	0.66	0.66	0.43	.....	.....	1.5	0.62	0.47	1.3
			3899.71	.38	0.62	0.62	0.52	.38	.....	.....	.....	.....	.....
			3906.48	.33	0.55	0.62	0.48	.38	.....	1.0	0.72	.....	0.40
			3920.26	0.50	0.59	0.47	0.41	0.38	.....	.....	.....	.....	.....
			Mean	0.37	0.69	0.64	0.49	0.44	0.30	1.9	1.3	1.2	1.1

ward region (Fig. 2) represents a more convenient scale for measuring the fainter absorption lines. These are reduced facsimiles of the 100-power tracings actually used. To show the differences in density of the several plates, the microphotometer records for the clear photographic negative and for no light falling on the photocell are shown at the ends of each tracing. The marginal scales represent fractions of the intensity at the fiducial continuum, as interpolated from the characteristic curve of the density of the step spectra on each plate.

Several conspicuous emission lines, as well as weaker emission edges on certain absorption lines, may be noted on the tracings. The mutilation of the Balmer series of hydrogen emission lines in the spectrum of o Ceti has been discussed by A. H. Joy.[6]

[6] *Mt. W. Contr.*, No. 737; *Ap. J.*, **106**, 288, 1947.

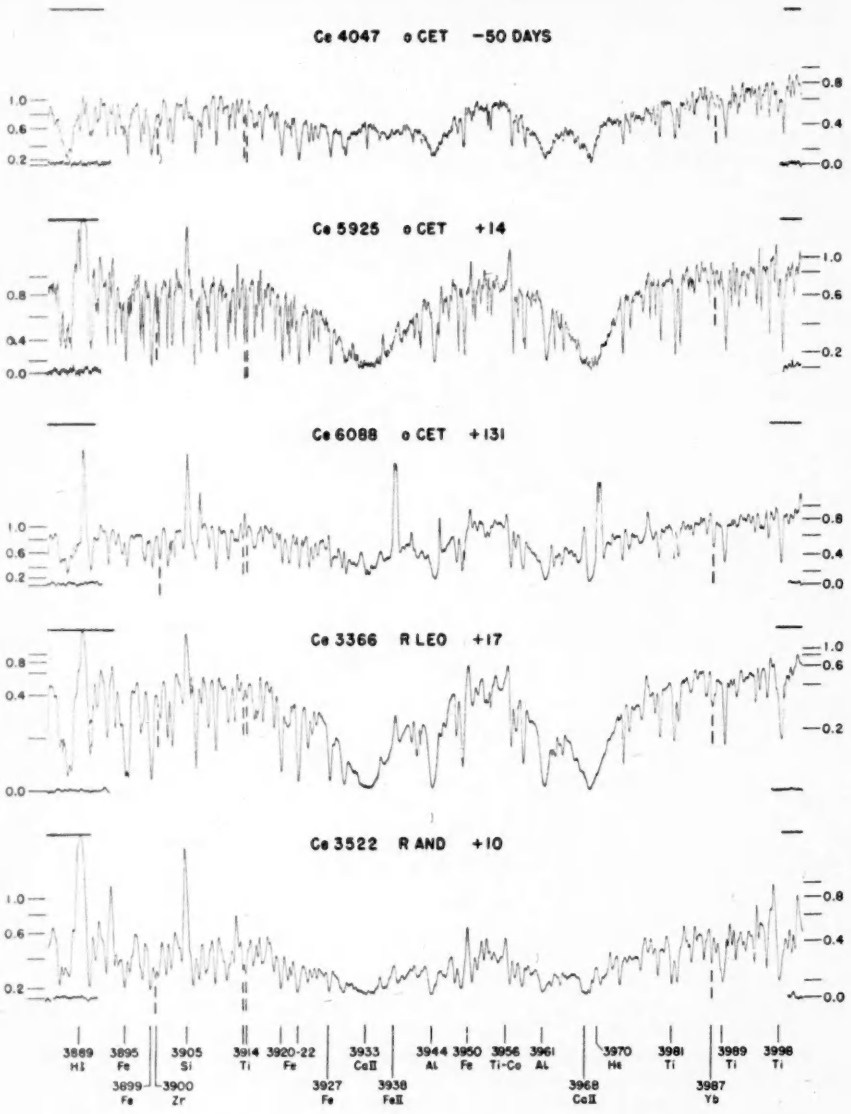

FIG. 1.—Microphotometer tracings of spectra of long-period variable stars, λλ 3887–4000. Marginal scales show fractions of intensity in continuum. Vertical leaders indicate weak lines which are sensitive to temperature and abundance.

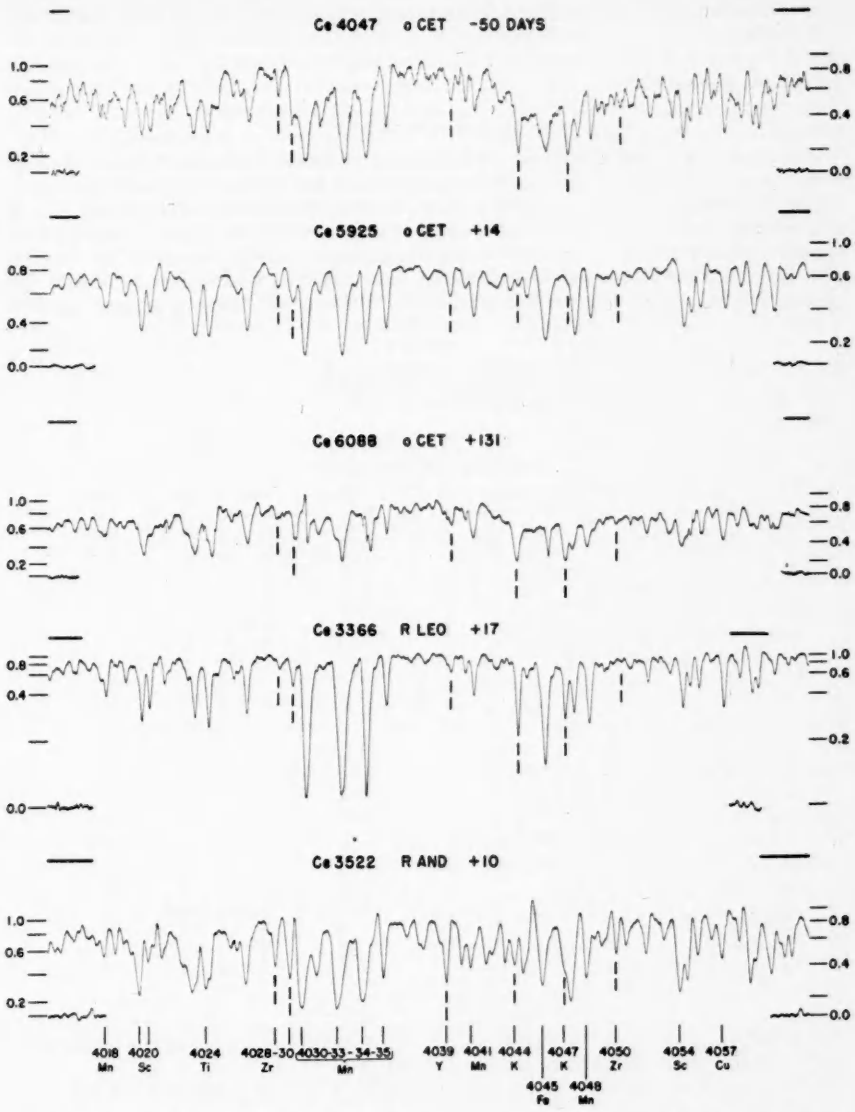

FIG. 2.—Microphotometer tracings of spectra of long-period variable stars, λλ 4015–4060. Marginal scales show fractions of intensity in continuum. Vertical leaders indicate weak lines which are sensitive to temperature and abundance.

Other emission effects are described in considerable detail by P. W. Merrill with reference to χ Cygni,[7] R Andromedae,[8] R Leonis,[9,10] and R Hydrae.[11,12] The emission in the core of the K line in the top tracing of *o* Ceti is thought to be partly due to the variable B-type companion star.

IV. PHASE CHANGES OF *o* CETI

The most striking changes are in the intensities of resonance lines of the easily ionized atoms *Al* and *K*, as shown in Figures 1 and 2. Table 2 shows that their mean equivalent widths decrease near maximum light to less than one-third the corresponding values at minimum light. The H and K lines of *Ca* II, as well as λ 4077 *Sr* II, on the other hand, become stronger at maximum light, when larger proportions of *Ca* and *Sr* are ionized. The ionization equilibria for several elements of astrophysical interest, obtained by solving the Saha equation, are summarized by Table 4. An electron pressure of 10^{-4}

TABLE 4

PERCENTAGE IONIZATION

Group	Element	I.P.	b_1/b_0	*Pe* (Dynes/Cm²)	*T*° (K)			
					1700	2000	2250	2500
1	*K, Rb, Cs*	4.2	½	10^{-4}	50	90	99.5	99.95
2	*Ba*	5.2	2		0.04	20	98	99.4
3	*Na, Li*	5.2	½		0	6	70	98
4	*Sr, La, Sm, Eu*	5.7	2		0	1	30	95
5	*Ca, Yb, Gd*	6.1	2		0	0.1	6	70
6	*Al, Ga, In, Tl*	6.0	⅛		0	0.01	0.8	20
7	*Sc, Ti, V, Nb, Cr, Y, Zr*	6.7	1		0	0	0.1	7
1				10^{-3}	9	40	94	99.5
2					0	2	40	94
3					0	0.6	20	80
4					0	0.1	5	70
5					0	0.01	0.6	20
6					0	0	0.08	3
7					0	0	0.01	1
1				10^{-2}	1	6	60	95
2					0	0.2	6	60
3					0	0.06	2	30
4					0	0.01	0.5	20
5					0	0	0.06	2
6					0	0	0.01	0.3
7					0	0	0	0.1

dynes/cm² appears to be the largest at which the ionization level varies as sensitively with temperature as is observed in the atmosphere of *o* Ceti.

Owing to the great scarcity of weak unblended lines, it is not possible to delineate with

[7] *Mt. W. Contr.*, No. 735; *Ap. J.*, **106**, 274, 1947.
[8] *Mt. W. Contr.*, No. 730; *Ap. J.*, **105**, 360, 1947.
[9] *Mt. W. Contr.*, No. 720; *Ap. J.*, **103**, 275, 1946.
[10] *Mt. W. and P. Reprint*, No. 72; *Ap. J.*, **116**, 337, 1952.
[11] *Mt. W. Contr.*, No. 717; *Ap. J.*, **103**, 6, 1946.
[12] *Mt. W. and P. Reprint*, No. 68; *Ap. J.*, **116**, 18, 1952.

confidence a curve of growth for the lines of any element in the atmosphere of Mira. Plots of equivalent width against experimentally determined oscillator strength for *Ti* I, *V* I, *Cr* I, and *Fe* I (such as those used in forming a curve of growth) showed that near maximum light an excitation temperature of 2500° K is not inconsistent with the observations. Those few lines whose equivalent widths are less than 0.1 A are subject to great uncertainty, especially as it is quite likely that unidentified blends contribute appreciably to their intensities. This renders any inference about opacity, turbulence, or relative abundances very hazardous, but a statistical approach reveals a few facts. Ratios of the intensities between plates were averaged for groups of from 5 to 8 lines each, arising from the same lower-energy state for the same atom. When these average differences were grouped to include all lines of different atoms but of the same excitation potential, it was found that the method is barely sensitive enough to detect from the measured intensities any significant change in excitation temperature with phase. The values indicated in Table 5 are based on the assumption of a temperature of 2500° K for *o* Ceti at maximum.

The fractional uncertainty in the equivalent width of a single line is of the order of 30 per cent, mainly because of blending and of difficulty in locating the continuous back-

TABLE 5

PHYSICAL PARAMETERS

Star	Phase	Relative Opacity	Excitation Temperature (° K)	Star	Phase	Relative Opacity	Excitation Temperature (° K)
o Ceti.....	− 50	8	(2600)	R Leo.....	+ 17	0.1	2300
	− 9	1.7	2450		+ 65	0.1	2300
	+ 14	1	2500				
	+ 42	4	2500	R And.....	+ 10	1	2300
	+ 78	10	2400		+ 45	0.3	2300
	+131	16	2350				

ground. Accordingly, a departure of more than 20 per cent, between the average of a group of lines and the general average of all lines seems rather significant. The *V* I lines of less than 0.5 volts excitation potential appear abnormally strong on plate Ce 6088, long after maximum light, especially when compared with plate Ce 4047, taken at the same brightness before maximum. All the *Co* I lines appear conspicuously strengthened on Ce 4047.

For lines on the transitional portion of the curve of growth,

$$\frac{W}{\lambda}\frac{c}{v} \propto \left(\frac{Nf}{v\kappa_\nu}\right)^{1/2}, \tag{1}$$

gives the approximate dependence of equivalent width on the number of absorbing atoms, turbulent velocity, and continuous opacity coefficient. The variation of the mean equivalent widths may be expressed reciprocally by relative opacity coefficients, as in Table 5. This indicates that the star's atmosphere becomes most transparent to continuous radiation in the near ultraviolet at maximum light, unless the turbulent velocity also changes considerably with phase.

While the majority of absorption lines of all elements are much stronger at maximum light, not all elements show exactly the same variations with phase. When the observed equivalent widths have been adjusted for opacity and temperature differences, it appears that the lines of *Co* I, *Zr* I, and ultimate lines of *Fe* I show relatively strongest absorption

before *o* Ceti reaches maximum light; those of *Sc* I, *Cr* I, and *Ni* I close to maximum; and those of *Ti* I, *V* I, and *Mn* I on the declining branch of the light-curve. While the incidence of emission components may narrow the shortward wings of ultimate *Fe* I lines and thus weaken these lines, no emission features attributed to either *Ti* I or *V* I have been recognized in the spectrum of *o* Ceti. Owing to the combination of these effects, the ratio of equivalent widths of lines of similar strength of zirconium and vanadium decreases steadily from 0.67 to 0.38 through the observed range of phases of *o* Ceti. The corresponding ratio of titanium to vanadium lines decreases from 1.11 to 0.81. As outlined in Section V, the atomic lines of *Zr* and, to a smaller extent, those of *Ti* show greater strength in absorption in the spectra of S-type stars, while little difference is seen in the lines of *V* and other elements. On this basis, one might say that the atomic absorption lines in the spectrum of *o* Ceti show somewhat more resemblance to those of the S stars before and during the phase of maximum light than during the latter part of the star's decline in brightness. From the present measures the transition appears to be continuous. Part of the change may be due to oxidation at the lower temperatures near minimum light. It would be of special interest to follow such changes in the spectrum of a star which can be observed throughout its light-cycle.

V. DIFFERENCES AMONG THE THREE STARS

Visual comparisons on a spectrocomparator of the plates used in this investigation indicate that, apart from the ionization and emission effects previously described, the most conspicuous differences between these stars occur in the zirconium lines. A large part of the absorption in these stellar atmospheres is in the overlapping wings of many lines of moderate intensity. Consequently, it is rarely possible to resolve the profiles of the faint lines whose equivalent widths are required to establish the Doppler portion of the curve of growth. Instead of the usual graphical treatment, a numerical statistical analysis of the measured intensities will be given, from which we derive inferences of the relative abundances of the elements and other physical parameters. In applying equation (1), we make the simplifying assumption that the turbulent velocities of absorbing atoms in the atmospheres of the three stars are the same.

An estimate of the excitation temperature of R Leo at maximum, obtained from an empirical curve of growth, using laboratory *f*-values[13] for the *Cr* I lines, is 2300° K. A temperature of 2500° K is reasonably consistent with the observed strengths of the *Ti* I and *Fe* I lines in the spectrum of *o* Ceti at maximum brightness. The lines of those elements for which ionization is negligible show in their variation a small dependence on excitation potential, which would suggest the changes in excitation temperature indicated in Table 5. Provided that the over-all abundances and the turbulent velocity are unchanged, the intensities of the ground-level lines lead to relative values of the continuous absorption coefficient, which are listed in Table 5 as ratios of the corresponding value for the plate Ce 5925 of *o* Ceti, taken just after maximum light. It appears that the opacity increases with temperature faster than predicted by Chandrasekhar and Breen[14] for pure H^- absorption, and other sources of opacity may also be active.

The complexity of the observational data is further reduced in Table 6, by forming mean equivalent widths for all the lines of certain elements, averaged over all the plates taken near the maximum brightness of each star. The two plates of each were included for R Leo and R And, while for *o* Ceti the means were extended over four plates, omitting only those taken at the fainter phases. The enhancement of the *Zr* I lines in the spectrum of R And appears quite significant, with a smaller increase in the *Ti* I lines. It is also noteworthy that the stronger ultimate lines of practically all elements have broader wings in the spectrum of R Leo than in the other stars.

[13] A. J. Hill and R. B. King, *J. Opt. Soc. America*, **41**, 315, 1951.

[14] *Ap. J.*, **104**, 430, 1945.

By applying equation (1) to the observed mean intensities of each group of lines, one can remove the effects of temperature and opacity to form an estimate of the relative abundances of the elements in each of the three stars. This procedure leads to the conclusion that, for every atom of zirconium present in the reversing layer of R Leo, there are 10 in *o* Ceti and nearly 60 in R And. The other differences are less spectacular and are numerically closer to the statistical limit of significance. The absorption lines of the elements *Mg* and *Ru* appear relatively strongest in the spectrum of *o* Ceti, whereas *Sc*, *Ti*, and *Nb*, like *Zr*, show strongest absorption in the spectrum of R And. Little change is noted in the relative strengths of *V*, *Cr*, *Mn*, *Fe*, *Co*, and *Ni*, adjacent elements in the periodic table, between these three stars, while the evidence concerning *Y* and other elements, represented by fewer lines in the observed spectral region, is inconclusive. The enhancement of *Sr* II λ 4077 in R And may be due to higher ionization temperature as well as greater abundance. The strengthening of the atomic lines of *Zr* in the spectra of stars which also show the *ZrO* bands more conspicuously adds confidence to the idea that zirconium is actually more abundant in the atmospheres of these stars. Several writers have previously proposed arguments favoring oxidation of zirconium rather than titanium in these stars, without definite evidence concerning the relative abundances of the various elements. The increase in strength of the *Ti* absorption lines may be due to less complete oxidation of the titanium atoms under the temperature and pressure conditions prevailing in the S-star atmospheres. The total abundance of *Ti* may be the same as in the M stars.

TABLE 6

MEAN EQUIVALENT WIDTHS FOR PLATES NEAR MAXIMUM LIGHT

ELEMENT	*n*	MEASURED			REDUCED TO CONSTANT $\kappa\rho^{-4}$		
		o Ceti	R Leo	R And	*o* Ceti	R Leo	R And
Ti	28	0.24	0.39	0.40	0.29	0.25	0.38
V	32	.22	.41	.28	.27	.26	.26
Cr	14	.16	.33	.23	.20	.21	.22
Fe	52	.32	.75	.48	.39	.47	.45
Co	24	.19	.34	.22	.23	.21	.21
Ni	14	.22	.44	.26	.27	.28	.24
Zr	21	0.15	0.18	0.27	0.18	0.11	0.25

The authors are grateful to Jesse Greenstein, Philip Keenan, and Martin Schwarzschild for helpful suggestions, and to Mrs. Charlotte Moore Sitterly for providing information concerning several lines not listed in her *Revised Multiplet Table*.

A NEW SPECTRUM VARIABLE OF SHORT PERIOD, HD 124224

ARMIN J. DEUTSCH
MOUNT WILSON AND PALOMAR OBSERVATORIES
CARNEGIE INSTITUTION OF WASHINGTON
CALIFORNIA INSTITUTE OF TECHNOLOGY*

Received July 24, 1952

ABSTRACT

The "silicon star" HD 124224 shows absorption lines of *He* I that vary in strength with a period of 0.5 day. The lines of *Si* II and a group of unidentified lines vary in opposite phase. Within the large errors of measurement, the radial velocity is constant except for the lines of *He* I, which before maximum strength are displaced about 5 A to the violet of their position after maximum. The contour of *Mg* II 4481 is compatible with the hypothesis that the star rotates with a period of 0.5 day, with its axis perpendicular to the line of sight. Suppression of convection by a magnetic field may be responsible for the simultaneous strengthening of *He* I and weakening of *Si* II.

In the spectrum of the fifth-magnitude A0p star HD 124224,[1] there appear abnormally strong absorption lines of *Si* II at λλ 4128–4131, and an abnormally weak K line. These peculiarities were first noted in the *Henry Draper Catalogue* and are typical of perhaps 5 per cent of the stars in the range B9–A3.[2] Prototype of these "silicon stars" is θ Aurigae, in which W. W. Morgan has reported spectrum variation.[3] The stars 56 Arietis and HD 34452 are other spectrum variables in the group; both show lines of *He* I that vary in strength with a period of about 2.5 days.[4]

Variable lines of *He* I in HD 124224 were found on spectrograms made in 1949 at the Agassiz Station of the Harvard College Observatory. The Harvard spectrograph works at the Newtonian focus of the Wyeth reflector; a two-prism instrument, it has an 8-inch camera and gives a dispersion of 63 A/mm at K. Subsequent observations at Mount Wilson, at 50 and 24 A/mm, have now led to the period of 0.52 day, the shortest period among the known spectrum variables. The elements of variation are:

$$He \text{ I max.} = \text{JD } 2434144.05 + 0.52067E.$$

Table 1 lists the spectrograms on which these elements are based. For each plate, the table gives the mean of two estimates of the strength of the line *He* I 4026. The estimates, on an arbitrary scale, are plotted against phase in Figure 1. At maximum, λ 4026 has an equivalent width of 0.8 A, a strength appropriate to a B5 dwarf. At minimum the line is evanescent, its equivalent width being certainly less than 0.3 A. This line and every other except the Balmer lines are shallow and broad throughout the cycle.

At *He* I maximum, λ 4472 and λ 4922 of *He* I are strong; the weaker helium lines are so shallow that they can be seen only with difficulty. The helium lines from metastable levels, at λ 3964 and λ 3889, are inconspicuous, and *Mg* II 4481 is normal for the type. Therefore, dilution effects must be negligible. The Balmer lines are invariable; they are much more heavily winged than in θ Aurigae or HD 34452. *Hγ* has an equivalent width of 12 A, corresponding to an absolute magnitude of +1.1.[5] Unlike most of the other spec-

* The part of this research conducted while the author was on the staff of the Harvard College Observatory was aided by an Office of Naval Research contract.

[1] BD+3°2867; R.A., 14^{h}09^m.7; Dec., +2°38′ (1950); mag., 4.9.

[2] M. E. Walther, *Ap. J.*, **110**, 67, 1949.

[3] *Ap. J.*, **77**, 330, 1933.

[4] A. J. Deutsch, *Ap. J.*, **105**, 283, 503, 1947.

[5] R. M. Petrie and C. D. Maunsell, *Pub. Dom. Ap. Obs. Victoria*, **8**, 253, 1950.

trum variables, this one appears not to lie above the main sequence. *Fe* II 4233 appears with normal strength. The *Si* II lines are nearly twice as strong at *He* I minimum as at the opposite phase. The ones in the near ultraviolet and in the visual region are all extraordinarily intense; at its maximum, the blend at λ 4129 is more than seven times as strong as in a normal B9 star. Since these lines lie on the damping part of the curve of growth, their observed strength implies an effective abundance of Si^{+} about fifty times normal. The excess cannot be produced by ionization abnormalities alone, for, in a normal B9 reversing layer, about 95 per cent of all the *Si* atoms are already in the singly ionized state.

Unidentified lines of considerable strength (>0.2 A equivalent width) appear at λλ 3954, 3991, and 4201. These lines have already been noted[6] in the other silicon stars.

TABLE 1

OBSERVATIONS OF HD 124224

	Plate	JD 243	Strength of *He* I 4026	Phase* (*P*)		Plate	JD 243	Strength of *He* I 4026	Phase* (*P*)
Sp	137	2966.83	3	0.04	γ	32472	4133.70	2	0.13
	143	2990.78	3	.04		32482	4134.68	3	.01
	156	2995.86	2	.80		32490	4134.96	1	.55
	164	3014.72	3	.02		32494	4135.67	2½	.91
	167	3016.85	2	.11		32502	4135.95	1	.45
	177	3028.80	3	.06		32507	4136.67	2	.83
	183	3035.62	1	.16		32517	4136.95	1	.37
	194	3040.71	3	.93		32521	4137.73	2	.87
	201	3045.68	1	.48		32529	4137.96	1	.31
	204	3050.61	3	.95		32533	4138.67	1	.68
	205	3050.77	1	.25		32539	4138.85	3	.02
	212	3058.74	1	.56		32544	4139.71	1	.67
γ	31965	3719.85	1	.29		32547	4140.70	1	.57
	31968	3720.02	1	.62		32552	4140.93	2	.02
	31975	3720.96	1	.42		32553	4140.95	3	.05
	32001	3729.04	3	.94		32568	4142.66	1	.34
	32034	3752.94	3	0.84		32587	4143.93	2	0.78

* Phase = 0 at JD 2434144.05 + 0.52067*E*.

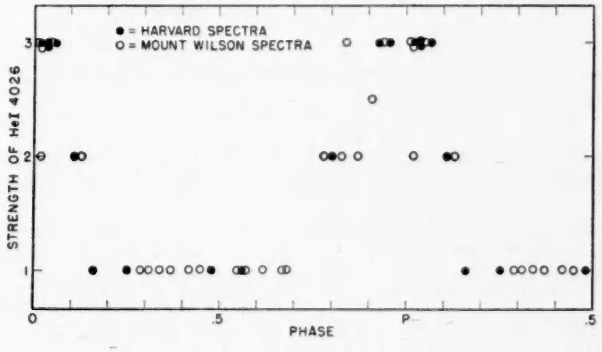

FIG. 1.—Intensity variation of *He* I 4026 in Hd 124224. The observations span 2260 cycles.

[6] Deutsch, *op. cit.*

Other strong lines that cannot be identified are listed in Table 2. All these lines vary in phase with *Si* II. Because the lines are so poor, the wave lengths are not precisely determined. Measurement of four plates yields a mean radial velocity compatible with the catalogue[7] value of +3 km/sec. The measurements give no evidence for variation of radial velocity, but they do not exclude the possibility of changes amounting to, say, 40 km/sec. R. H. Baker[8] found a total range of 134 km/sec from measures of seven spectrograms, but observers at Lick, Yerkes, and Victoria agree on a much smaller observed range, consistent with constant velocity. However, inspection at the Hartmann com-

TABLE 2

UNIDENTIFIED LINES IN THE SPECTRUM OF HD 124224

λ (A)	λ (A)	λ (A)	λ (A)
3904.2	4056.2	4295	4490
3954.4	4189.0	4377.1	4621.1
3991.3	4201.2	4405.5	4673.2

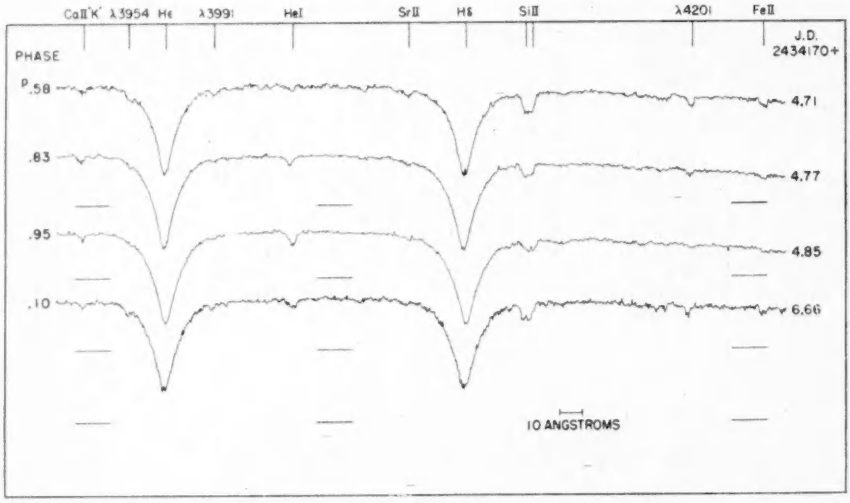

FIG. 2.—Direct-intensity tracings in the spectrum of HD 124224

parator of two pairs of plates on which the *He* I lines are weak indicates that, before maximum strength, they are shifted 4 or 5 A to the violet of their positions after maximum.

The wide and shallow lines of this spectrum seem to indicate rapid rotation. Is it possible that the period of spectrum variation is just the period of rotation? In order to examine this question, I have made a series of widened coudé spectrograms on Eastman III-O plates at 10 A/mm. Figure 2 shows direct-intensity tracings of the violet region in four of these spectrograms. From five of the spectra, a mean observed profile of *Mg* II

[7] R. E. Wilson, *New General Catalogue of Radial Velocities* (Washington, D.C.: Carnegie Institution of Washington, 1953).

[8] *Pub. Allegheny Obs.*, 1, 121, 1909.

4481 has been derived, and this has been compared with the contour of an equally strong line disturbed by rotation with a period equal to 0.5 day. For the undisturbed contour of the line (broadened by the spectrograph and microphotometer, but not by rotation) I have taken a Voigt profile[9] with damping parameter one-fourth the Doppler parameter and with central absorption of 70 per cent. This is the profile shown by the dashed line in Figure 3; it is typical of λ 4481 in sharp-line objects, as delineated by the same instrumental combination.

A B9 star with $M = +1.1$ will have a radius about 1.9 $R \odot$. If the period of rotation is 0.5 day, the equatorial velocity V is 190 km/sec. Since it is improbable that we observe the star from a point exactly in its equatorial plane, we choose a slightly smaller value for the maximum component of V in the line of sight, $V \sin i = 170$ km/sec. Tak-

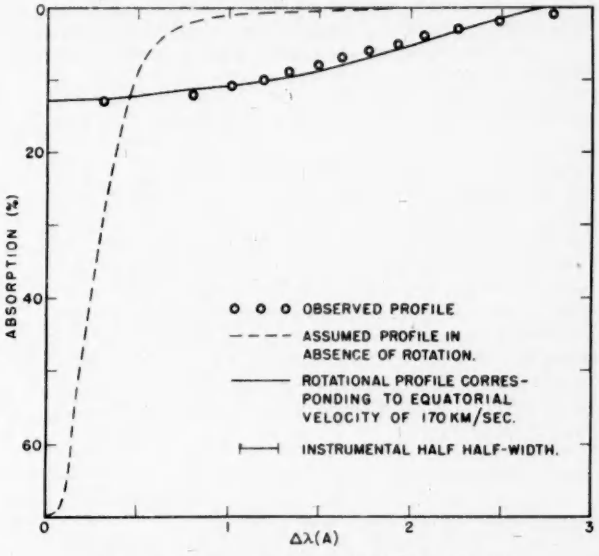

FIG. 3.—The profile of *Mg* II 4481 in HD 124224

ing into account the appropriate limb darkening, we find by numerical integration that the original Voigt contour becomes the broad profile shown by the full line in Figure 3. The agreement with the observed profile is seen to be very satisfactory.

If the period of this spectrum variable is, in fact, just its period of rotation, then the *He* I lines are formed preferentially over a large part of one hemisphere, and the *Si* II lines over a large part of the other. The question arises whether there is a mechanism that would permit us to look so deep into the atmosphere of a B9 star that we should encounter temperatures near the 16,000° typical of the reversing layer of a B5 star. If so, we could then understand the reciprocal behavior of the *Si* II lines relative to *He* I as the result of second ionization. In a normal B5 star, second ionization has suppressed the *Si* II lines without yet bringing to prominence the highly excited lines of *Si* III.

Normally, the atmosphere of a main-sequence star near A0 becomes unstable against convection at a level above the photosphere. For example, it is readily calculated from

[9] H. C. van de Hulst and J. J. M. Reesinck, *Ap. J.*, **106**, 121, 1947.

the work of Unsöld[10] and his collaborators[11] that, at the level where $T = T_e$ and with an electron pressure of about 10^4 bar, the radiative gradient $d \log T / d \log P$ is more than ten times as large as the adiabatic gradient, which is its limit for stability! However, the recent work of Chandrasekhar[12] indicates that a sufficiently strong magnetic field may inhibit the onset of convection and support the radiative gradient to optical depths beyond those where convection normally begins. This mechanism has been adduced[13] to provide a qualitative explanation of the relative darkness of sunspots: where the temperature falls more steeply than elsewhere, the effective temperature will be lower. In the case of HD 124224, however, there is probably no appreciable difference in effective temperature between the two hemispheres; for the star, though of magnitude 4.9, is not known to be of variable brightness. Therefore, we should inquire what effect would be produced by the inhibition of convection, under the condition of constant effective temperature.

Calculations of the relevant model atmospheres would seem to be required for a definitive answer. Qualitatively, however, it can be said that if the effective temperature is to be the same either with or without a magnetic field, then the respective curves giving $T(\tau)$ must intersect at some point τ^* in the neighborhood of $\tau = 1$, the curve for the radiative case lying below the other for $\tau < \tau^*$, and above it for $\tau > \tau^*$. If τ^* is small enough, the magnetic field may act to increase $T(\tau)$ significantly at the level where the helium and silicon lines are formed.

This speculative proposal would require that the helium lines be formed over an area of, say, one-half the hemisphere, within which a magnetic field supports the radiative gradient to depths at least of order $\tau = 1$. The magnetic flux issuing from this large "spot" re-enters the star through the rest of the reversing layer, over which the field strength will be less by a factor of 3. The stellar rotation gives the "spot" radial velocities varying between about ± 150 km/sec. On the two pairs of plates with weak helium lines, the displacements found at the comparator are of appropriate order and sign.

The lines in this star are far too wide to show the Zeeman splitting studied by H. W. Babcock in other peculiar A stars. The hypothesis of a magnetic field can therefore not be put to this direct test. It may be significant, however, that some of the stars in which he finds magnetic fields—e.g., α^2 Canum Venaticorum—are spectrum variables with abnormally strong lines of *Si* II.

[10] *Zs. f. Ap.*, **25**, 11, 1948.

[11] A. Rosa, *Zs. f. Ap.*, **25**, 1, 20, 1948; E. Vitense, *Zs. f. Ap.*, **28**, 81, 1951.

[12] *Phil. Mag.*, **43**, 501, 1952; see also *Pub. A.S.P.*, **64**, 98, 1952.

[13] L. Biermann, *Vierteljahrsschr. Astr. Gesellsch.*, **76**, 194, 1941; C. Walén, *On the Vibratory Rotation of the Sun* (Stockholm: Henrik Lindståhls Bokhandel, 1949).

NOTES ON THE SPECTRUM OF GAMMA URSAE MINORIS

HAROLD F. WEAVER
Berkeley Astronomical Department, University of California
Received July 7, 1952

ABSTRACT

Spectrographic observations made at the Lick Observatory have shown that at certain stages the absorption lines of γ Ursae Minoris display profiles which are more nearly V-shaped than is consistent with a rotational origin of the line broadening. This effect does not appear in *Mg* II 4481, and it is imperceptible in the case of the weaker metallic lines, but it is conspicuous in such strong lines as λ 4549.5, 4534.1, etc. It is suggested that this difference in the line profiles might be due to the temporary existence of a tenuous shell whose influence upon the rotational-line profiles from the underlying reversing layer resembles, on a smaller scale, the effect of the shell of 14 Comae Berenices.

1. The variable radial velocity of γ UMi was first suspected by Barrett and Lee. Struve's[1] discussion of 200 spectrograms obtained at the Yerkes Observatory during February–August, 1922, led to the following conclusions:

a) The radial-velocity variation was essentially periodic, with $P \sim 2.5$ hours. However, the shape and amplitude of the velocity-curve varied considerably over a time interval of a few days, and even from one cycle to the next.

b) Different spectral lines gave different results for the radial-velocity variation. In particular, *Mg* II, λ 4481, gave a velocity-curve of appreciably different amplitude and systemic velocity than the other (principally *Ti* II and *Fe* II) lines.

On the basis of a much later examination of these early plates and some subsequent ones, Struve[2] confirmed the reality of the short-period velocity changes. "The velocity curves on different dates," Struve remarks,[2] "are not the same: there are large changes in the amplitude and shape of the curve: there are occasionally long interruptions with no perceptible variation in velocity. When the velocity does change there is an apparent periodicity with $P = 2\frac{1}{2}$ hours."

Henroteau[3] lists γ UMi among the β CMa stars; this listing is repeated by Payne-Gaposchkin and Gaposchkin.[4] However, on the basis of the spectral characteristics of γ UMi, this assignment seems incorrect.

2. Photometric observations of γ UMi show that it undergoes irregular brightness fluctuations of the same general character as the fluctuations found for the velocity-curve. Guthnick,[5] in the years 1914–1915, found the star to vary in brightness, but the amplitude of the variation was irregular, being sometimes as great as 0.05 mag. and at other times as small as 0.01–0.02 mag. Bottlinger,[6] in May, 1922, found small brightness fluctuations occurring in short time intervals (2–3 hours), but no definite period was discovered. Struve's spectroscopic period did not permit the combination of photometric observations of different dates. It is not known now whether this combination was impossible because of the lack of a definite period or because of changes in the shape and amplitude of the light-curve.

R. H. Baker[7] photoelectrically compared γ UMi with ζ UMi in 1925 and found a light-variation of approximately 0.10 mag. in a period[8] of 2.5 or 3.5 hours. Baker was re-

[1] *Pop. Astr.*, **31**, 90, 1923. [2] *Ibid.*, **58**, 7, 1950. [3] *Handbuch d. Ap.*, **6**, 436, 1928.

[4] *Variable Stars* ("Harvard Observatory Monographs," No. 5 [1938]), p. 188.

[5] *Festschrift für Hugo von Seeliger* (Berlin: Julius Springer, 1924), p. 391.

[6] Quoted by Struve, *Pop. Astr.*, **31**, 90, 1923. [7] *Pub. A.S.P.*, **38**, 86, 1926.

[8] There appears to be possibly some confusion in regard to the period in Baker's article. In his Table 1 he states that $P = 0^d14335 = 3.44$ hours, which is not in agreement with Struve's spectroscopic period. However, his plot of the observations (his Fig. 2) seems to indicate a period of 2.5 hours.

luctant to assign this variation to γ UMi alone because of the larger amplitude than had been found by the Berlin observers. In view of the erratic behavior of γ UMi, such a change in amplitude would not seem unreasonable. The variation of the light-amplitude of γ UMi is, however, a quantity that definitely needs further observational checks.

3. γ UMi is a standard star in the Morgan, Keenan, and Kellman *Atlas*,[9] where it is classified A3 II–III. In the spectral-type range B9 through A5 there are 40 stars tabulated in the *Atlas* or in the more recent list of stars classified on the Yerkes system by Keenan and Morgan.[10] These 40 stars are distributed among the various luminosity

Lum. Class	No. of Stars	Lum. Class	No. of Stars
V	22	II–III	1
IV	5	*Ib*	1
III	5	*Ia*	6

classes as in the accompanying tabulation. γ UMi is the only standard star in the absolute-magnitude range between the "ordinary" giants (class III) and the supergiants (class I) and is thus an object of some importance in the classification scheme.

4. If the luminosity class II–III is accepted, the visual absolute magnitude[10] of γ UMi is approximately -1.4. It is thus considerably brighter than the regularly varying cluster-type variables; its spectral type puts it outside the range of the classical cepheids.

5. The spectrum of γ UMi taken with low dispersion is shown on Plate 25 of the *Atlas*. The hydrogen lines are broad; they appear to show appreciable Stark effect and hence arise in an atmosphere of moderate pressure. The general weakness of the *Fe* I lines in γ UMi compared with an ordinary dwarf is quite marked. On the other hand, *Fe* II and *Ti* II are quite strong in γ UMi. The luminosity class of γ UMi is, in fact, assigned on the basis of the ratio of the greater-than-dwarf strength of a *Ti* II, *Fe* II blend, λ 4417, to *Mg* II, λ 4481.

Higher-dispersion spectra (10 A/mm) taken with the Mills spectrograph of the Lick Observatory show several noteworthy features.

a) The underlying lines of the spectrum are broad and shallow and appear to arise from a very rapidly rotating star. Measurements of the width of λ 4481 show that $v \sin i$ has a value of at least 200 km/sec. Such a large rotational velocity would appear to indicate that γ UMi is more closely related to the dwarfs and ordinary giants than to the supergiants. Large rotational velocities are not characteristic of the supergiants. If we use Miss Westgate's[11] data on the rotational velocities of the 40 stars classified on the Yerkes system and mentioned previously, we find the average values given in the accompanying tabulation. No star on the list has a rotational velocity exceeding that of

Luminosity Class	Average Spectral Type	Average $v \sin i$ (Km/Sec)	No. of Stars	Luminosity Class	Average Spectral Type	Average $v \sin i$ (Km/Sec)	No. of Stars
V	A2	93	22	II–III	A3	200	1
IV	A2	44	4	*Ib*	A0	0	1
III	A1	135	5	*Ia*	A1	19	4

[9] *An Atlas of Stellar Spectra with an Outline of Spectral Classification* ("Astrophysical Monographs" [Chicago: University of Chicago Press, 1943]).

[10] *Astrophysics*, ed. J. A. Hynek (New York: McGraw-Hill Book Co., Inc., 1951), p. 12.

[11] *Ap. J.*, **78**, 46, 1933.

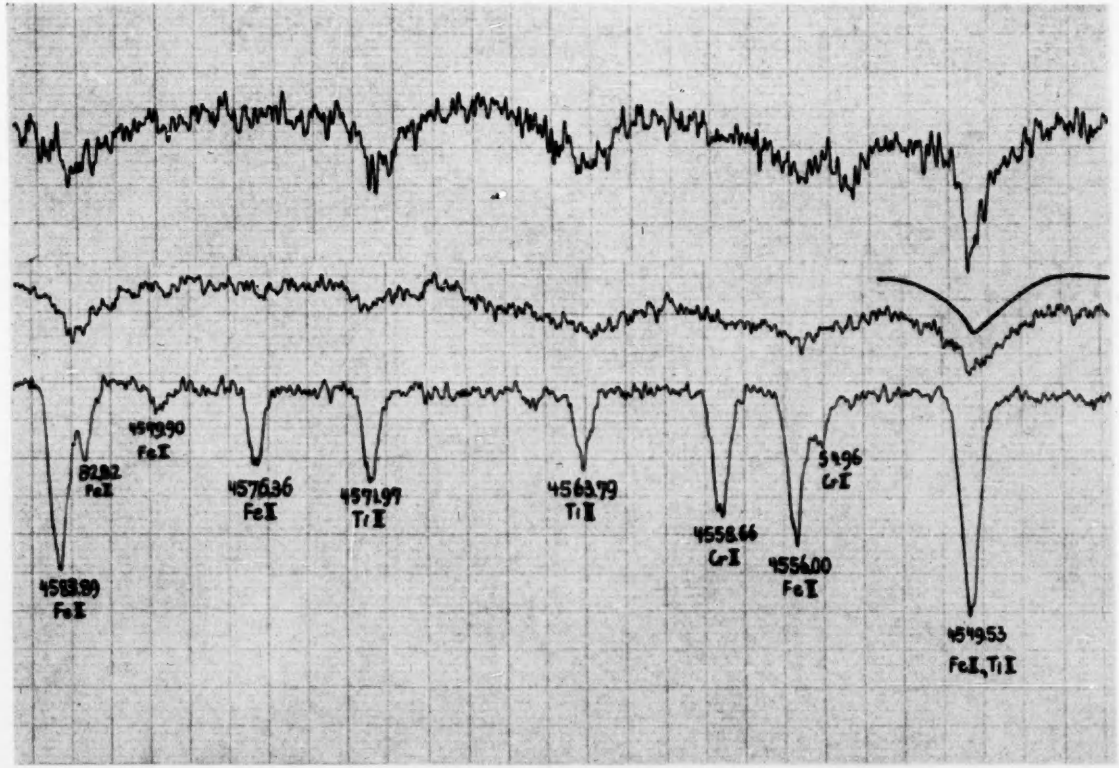

FIG. 1.—Microphotometer tracings of 14 Comae, April 10, 1913 (*upper*); γ UMi, February 2, 1912 (*middle*); and α Cyg, July 18, 1931 (*lower*). The wave lengths listed are those measured for α Cyg by A. B. Wyse (*Lick Obs. Bull.*, **18**, 129, 1938). Contours, drawn from the tracing, are shown above the tracing of γ UMi. The different forms of the contours of λ 4481 and strong *Ti* II and *Fe* II lines (such as λ 4550) are very marked.

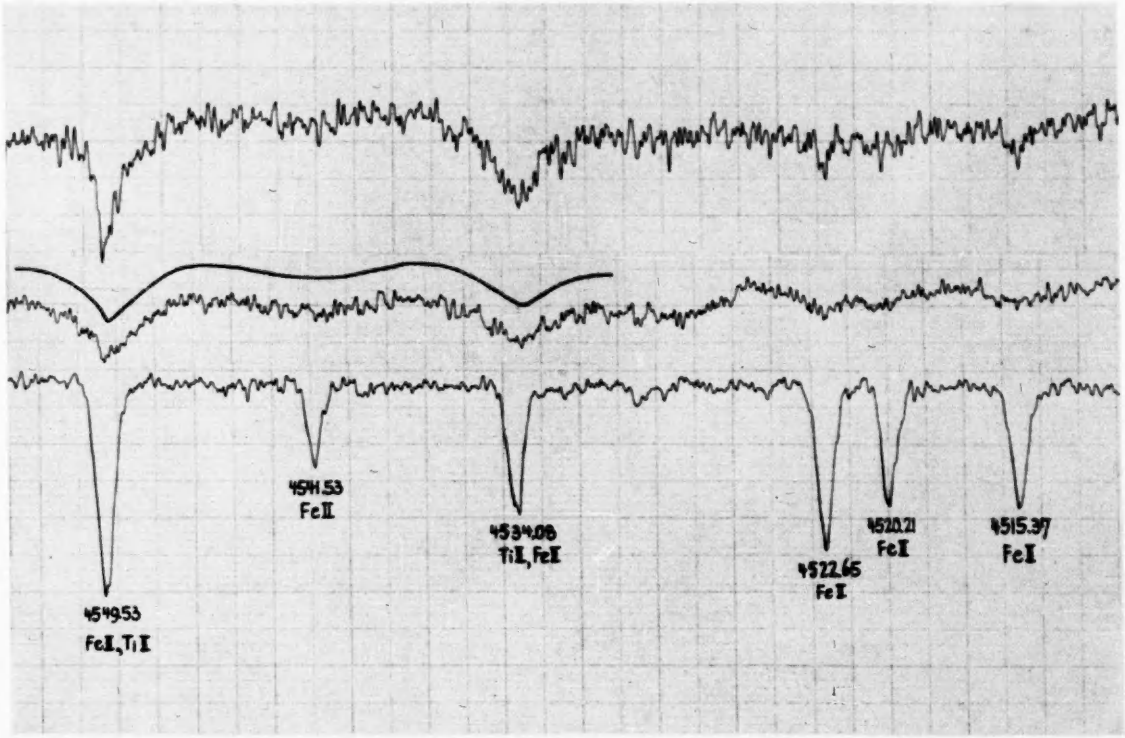

FIG. 2.—Microphotometer tracings of 14 Comae, April 10, 1913 (*upper*); γ UMi, February 2, 1912 (*middle*); and α Cyg, July 18, 1931 (*lower*). The wave lengths listed are those measured for α Cyg by A. B. Wyse (*Lick Obs. Bull.*, **18**, 129, 1938). Contours, drawn from the tracing, are shown above the tracing of γ UMi. The different forms of the contours of λ 4481 and strong *Ti* II and *Fe* II lines (such as λ 4550) are very marked.

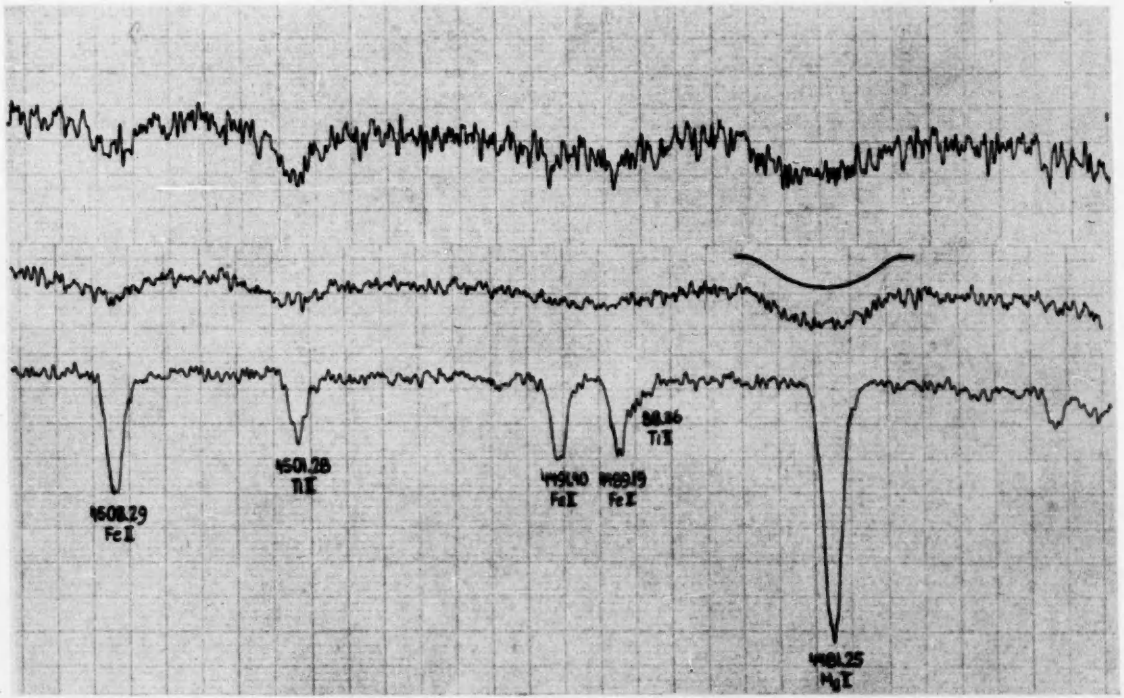

FIG. 3.—Microphotometer tracings of 14 Comae, April 10, 1913 (*upper*); γ UMi, February 2, 1912 (*middle*); and α Cyg, July 18, 1931 (*lower*). The wave lengths listed are those measured for α Cyg by A. B. Wyse (*Lick Obs. Bull.*, **18**, 129, 1938). Contours, drawn from the tracing, are shown above the tracing of γ UMi. The different forms of the Contours of λ 4481 and strong *Ti* II and *Fe* II lines (such as λ 4550) are very marked.

γ UMi. While the stars of luminosity types V–III appear to have large rotational velocities (93 km/sec on the average), the supergiants appear, on the basis of this small sample, to have essentially no rotational velocities. It is doubtful if even the small rotation of 19 km/sec is real or whether it is caused by the interpretation of turbulent line width as rotational width.

b) The spectrum of γ UMi varies in character. Over extended periods of time, shell lines have been visible, while at other times the spectrum shows no such lines and consists of broad, shallow lines characteristic of rotation. At present only broad, shallow lines appear in the spectrum. On Mills plates taken between June, 1911, and February, 1912, shell lines are clearly evident. They are only slightly less strong than the shell lines in the well-known shell star 14 Comae studied by Swings and Struve.[12] In Figures 1–3 microphotometer tracings of the spectra of 14 Comae, γ UMi in shell stage, and α Cyg are shown. The shell phenomenon can be identified most readily by comparing the profile of λ 4481, *Mg* II, which is shallow and broad in both 14 Comae and γ UMi, with the profiles of strong lines of *Ti* II (λ 4534 or λ 4549, for example), which arise from

TABLE 1

INTENSITIES OF LINES IN THE $b^4F-z^4D^\circ$ MULTIPLET OF *Fe* II IN γ UMi AND 14 COMAE

λ	Lab. Int.	Low E.P.	High E.P.	J	γ UMi	14 Comae
4583.83	11	2.79	5.49	$4\frac{1}{2}$–$3\frac{1}{2}$	Strong	Strong
4549.47	10	2.82	5.53	$3\frac{1}{2}$–$2\frac{1}{2}$	Strong	Strong
4522.63	9	2.83	5.56	$2\frac{1}{2}$–$1\frac{1}{2}$	Mod. strong	Moderate
4508.28	8	2.84	5.58	$1\frac{1}{2}$– $\frac{1}{2}$	Mod. strong	Moderate
4620.51	3	2.82	5.49	$3\frac{1}{2}$–$3\frac{1}{2}$	Invis	Invis.
4576.33	4	2.83	5.53	$2\frac{1}{2}$–$2\frac{1}{2}$	Invis.	Invis.
4541.52	4	2.84	5.56	$1\frac{1}{2}$–$1\frac{1}{2}$	Invis.	Invis.
4648.23	.....	2.83	5.49	$2\frac{1}{2}$–$3\frac{1}{2}$	.....	.....
4595.68	.....	2.84	5.53	$1\frac{1}{2}$–$2\frac{1}{2}$	.....	.....

metastable levels. Profiles of these strong *Ti* II lines are composite and are formed by the absorption in the stellar atmosphere proper, which produces a contour similar to λ 4481, and a very much narrower line of turbulent profile arising from the shell. The extreme weakness of *Cr* II λ 4959, which arises from a nonmetastable level is particularly striking in the shell stars. The lines of *Fe* II compared to those of *Ti* II are weak in γ UMi. This anomaly also exists in 14 Comae, as well as other stars, and has been commented upon by Swings and Struve.[12] No explanation of it exists.

The large amount of turbulence present in the shells of both γ UMi and 14 Comae is shown by the intensity gradient within multiplets. An example of the effect is shown in Table 1.

The rough intensity estimates in Table 1 refer only to the shell lines. The intensities of the underlying broad shallow lines arising from the rotating atmosphere are quite different. A comparison of intensities of the shell lines and lines of the atmosphere proper is instructive.

(i) λ 4483.83: lab. int. 11. In both γ UMi and 14 Comae the shell line is strong. On the basis of the profile of this line, one might reasonably conclude that the intensities of the shell line and the atmospheric line are roughly equal.

(ii) λ 4541.53: lab. int. 4. The case of this weak line is quite different from that of the strong line λ 4483.83. In the microphotometer tracings of both γ UMi and 14 Comae,

[12] *Ap. J.*, **94**, 291, 1941; *Contr. McDonald Obs.*, No. 37.

there are clear indications of a very broad, shallow line at λ 4541.53 arising from the underlying star. There is no trace of a shell line of this wave length in either star. If the λ 4541.53 shell line were proportionately as strong as in the case of the strong line, it would be readily visible. This difference in the behavior of strong lines and weak lines in the shell and in the underlying atmosphere is a curve-of-growth phenomenon directly traceable to turbulence in the shell. Clearly, $NH_{\text{shell}} \ll NH_{\text{star}}$; yet, for strong lines in the star, $\text{E.W.}_{\text{shell}} \sim \text{E.W.}_{\text{star}}$, while, for weak lines in the star, $\text{E.W.}_{\text{shell}} \ll \text{E.W.}_{\text{star}}$. This can occur only if the steep portion of the curve of growth for the shell extends far upward, that is, if the shell possesses very much larger turbulence than the star. If this is the case, small NHf_{shell} values will produce strong lines. However, *very* small NHf_{shell} values will produce lines that are very weak; the intensity gradient within the multiplet will thus be very steep, just as we observe to be the case for the shell lines in γ UMi and 14 Comae.

Unfortunately, no multiplets of *Ti* II with lines of the proper intensities are present in the spectral range visible on the Mills plates; hence a similar test cannot be made for that element.

6. Two quite different types of physical model for γ UMi can be suggested: the first is a rotating star on which some spot or spots appear, the second is a pulsating star.

a) We find $v \sin i = 200$ km/sec, $P = 2.5$ hours. If we accept the luminosity class II–III as indicating the true luminosity of γ UMi, $Mv = -1.4$, we find from Kuiper's[13] empirical mass-luminosity and mass-radius relations $\mathfrak{M}_{\gamma\ \text{UMi}} \sim 4.8\mathfrak{M}_\odot$, $R_{\gamma\ \text{UMi}} \sim 4R_\odot$. If the period of the velocity variation represents the true rotational period of the star, as would be the case if the velocity variation were caused by a single large disturbed area (perhaps even a hemisphere) of the surface, then the equatorial velocity of the star must be 2000 km/sec. This is an impossibly high value. For a star of the mass and radius assigned to γ UMi, breakup begins at an equatorial velocity of 490 km/sec.

If we assume that the luminosity classification of γ UMi is incorrect and that it is a main-sequence dwarf, we find $\mathfrak{M} \sim 2\mathfrak{M}_\odot$, $R \sim 2R_\odot$. For a star of $R = 2R_\odot$ the equatorial rotational velocity is still large, 1000 km/sec; breakup begins at 440 km/sec; hence the model is still not physically reasonable.

A "two-spot rotational model" in which disturbances or spots are assumed to exist at either end of a diameter of a dwarf star would have an equatorial rotational velocity of 500 km/sec and would just begin to fall within the range of compatibility of the mass-luminosity, mass-radius laws and stability, though the star would be just on the verge of breakup.

There is, of course, no compelling reason to assume that γ UMi obeys the mass-luminosity and mass-radius laws and therefore that a stable rotational model cannot be built up with a smaller star. But the fact that the rotational model requires many *ad hoc* assumptions plus the condition of an incorrect luminosity class forces one to look further for a more satisfactory model.

b) A physical model of γ UMi may also be constructed on the basis of an atmospheric pulsation. We assume that γ UMi is not a particularly stable object; its luminosity class may or may not be II–III. Some disturbances occur at some interior point; the star pulsates in a roughly periodic fashion. The violence of the disturbance varies from time to time; the amplitude of pulsation is not constant over a long period or even over a short period. Such irregular pulsation in a short period of time is not an uncommon phenomenon. The well-known irregular radial-velocity variation of α Cyg discussed by Paddock[14] is an analogous case. The velocity variations are smaller in amplitude than those in γ UMi but take place in a roughly comparable period. In addition, α Cyg shows a

[13] *Ap. J.*, **88**, 472, 1938.

[14] *Lick. Obs. Bull.*, **17**, 99, No. 472, 1935.

longer irregular velocity variation of greater amplitude, as well as changes of line profile[15] and color.[16]

As a result of its rotation and instability, γ UMi sometimes develops a shell, as shown by the observations of 1911–1912, when the shell lines were readily visible, though they were not quite so strong or quite so conspicuous as those of 14 Comae. It is not likely that they would have been noted as unusual on plates of small or moderate dispersion, though they would undoubtedly play an important role in the shape of the line profile and would strongly influence any radial-velocity measurements.

At present γ UMi shows no shell lines; it is not known when the shell vanished. Since shells appear to be moderately stable phenomena, lasting over years or decades in many instances, it is not unreasonable to assume that the shell visible in 1911–1912 was still to some extent present in 1922 when Struve's velocity measurements were made, and influenced the results for different elements.

(i) The *Mg* II line at λ 4481 was formed in the lower layers of the atmosphere; it was not influenced by shell components. It showed the full influence of atmospheric pulsation and would be expected to exhibit a large velocity amplitude.

(ii) The strong *Ti* II and *Fe* II lines in the spectrum of γ UMi were composite, being composed of the underlying broad rotational contour and the sharper turbulent shell line arising from the high atmosphere. The shell,[17] because of its effective distance from the photosphere of the star, might be expected to undergo a smaller amplitude of pulsation than the stellar atmosphere proper. The resultant effective amplitude of pulsation shown by the *Ti* II and *Fe* II lines was thus less than that shown by the line *Mg* II, λ 4481, which was not affected by the shell.

Such a difference in the amplitude of radial-velocity variation of the *Mg* II line and the strong lines of *Ti* II and *Fe* II, predicted on the basis of the pulsation model with shell, is in agreement with Struve's[1] 1922 observations of γ UMi.

[15] Payne-Gaposchkin and Gaposchkin, *op. cit.*, p. 177.

[16] Greaves, Davidson, and Martin, *Observations of Colour Temperatures of Stars* (Greenwich: Royal Observatory, 1932), p. 54.

[17] For 14 Comae, which is similar to γ UMi in dilution, $R_{\text{shell}} \sim 1.6 R_{\text{star}}$.

RADIAL VELOCITIES OF 31 CYGNI DURING ATMOSPHERIC ECLIPSE

DEAN B. MCLAUGHLIN
Observatory, University of Michigan

Received June 23, 1951

ABSTRACT

Near the eclipse contacts in 1951, radial velocities of 31 Cygni varied in a complicated manner impossible to explain in terms of rotation of the limb of the giant star. Before second contact, most elements departed from the orbital velocity about 5 km/sec negatively. After third contact, they also deviated −5 km/sec for the first 4–5 days, then changed to +5 to +10 km/sec for several days, before finally returning to the orbital velocity.

Lines of *Ca* II showed similar trends, but with greater amplitude and slower change. From 6 to 2 weeks before second contact, residuals were about −12 km/sec, but fell close to zero for several days before immersion. During egress, *Ca* II deviated −10 to −15 km/sec for 6 days, then changed to +10 to +15 km/sec a few days after most other elements had changed. After several days more, the lines returned approximately to the orbital velocity. Again, from 5 to 9 weeks after emersion, *Ca* II departed as much as +20 km/sec. These fluctuations were due in part to variation of the relative intensities of two components of a blend.

The behavior of *Ca* II is tentatively assigned to large-scale prominence activity. No interpretation is suggested, at this time, for the fluctuations of the lines formed in lower atmospheric layers.

The spectrum of 31 Cygni[1] has long been known as an excellent example of a composite spectrum. The primary star is a supergiant of class K1, and the secondary, whose lines are clearly seen only in the ultraviolet, is a main-sequence star of about class B8. The spectroscopic orbit of the primary was calculated by Miss Vinter Hansen,[2] who determined the period as 3803 days. She also obtained some measures of the secondary spectrum and an estimate of the mass ratio.

Michigan spectrograms taken in 1941 near the time of superior conjunction of the early-type star showed conspicuous sharp lines of *Ca* II, characteristic of an atmospheric eclipse.[3] In expectation of a deeper eclipse, even if no actual occultation occurred, observations were begun early in the season in 1951 at Michigan and Victoria. During the author's absence, Mr. Edwin B. Weston supervised the observing of the star at Ann Arbor. A good series of spectrograms was obtained during ingress, and the eclipse became total on August 13. The star was followed even more closely during egress, which began October 13.

The spectrograms were obtained with the two-prism spectrograph and the 37-inch reflector. Cameras with focal lengths of 12 and 24 inches were employed, giving dispersion at $H\gamma$ of 38 and 19 A/mm, respectively. The plates during ingress were of the lower dispersion, with the exception of two taken with the 24-inch camera on August 9 and 11. All the plates taken during egress were obtained with the higher dispersion.

A general description of the changing appearance of the spectrum has been given elsewhere.[4] The plates were measured for radial velocity in the expectation that, among other things, the rotation of the giant star might be determined. Effects probably due to

[1] HD 192577–8; $\alpha(1900) = 20^h10^m5$; $\delta(1900) = +46°26'$.

[2] *Ap. J.*, **100**, 8, 1944.

[3] *Pub. A.S.P.*, **62**, 13, 1950.

[4] *Pub. A.S.P.*, **64**, 109, 1952.

TABLE 1

RADIAL VELOCITIES OF SELECTED LINES OF 31 CYGNI

DATE (U.T.) 1951	*Fe* I	*Ca* II	*H*	*Ti* II		*Sr* II	*Mg* I	*Al* I	*Mn* I	*Cr* I	*Ca* I
				3759, 3761	3900, 3913						
May 20.31	− 7.0	−17.8				−10.2			−15.4	−14.8	
June 26.13	−15.5	−17.5							−20.3		
July 8.28	− 8.8	−23.3	−13.1		−10.9	− 5.0			−18.8	−12.4	+ 7.7
14.16*	−13.0	−23.5			− 1.0	− 6.6	−15.8		−14.6	−18.8	− 3.0
21.19	− 6.4	−22.5				−11.5	−17.2		−20.4	−16.8	− 0.7
24.20*	−14.5	−21.6	−18.2	−12.2	− 5.9	− 8.4	−17.1		−18.0	−13.0	+ 4.8
30.37	− 9.5	− 8.6	−14.3	− 7.9	−12.4	− 5.6	− 9.3		− 9.8	−16.8	−11.5
Aug. 1.10	−10.0	− 7.5	−11.0	−10.2	−11.2	−10.5	− 8.5		−12.9	− 9.1	− 7.8
4.24*	−11.6	−13.2	−12.4	−10.4	−13.2	− 9.2	−12.6	−14.4	−17.4	−11.4	−11.8
8.30†	−14.0	−12.8	−13.0	− 7.9	−13.1	−10.8	−14.4	−14.6	−15.6	−12.5	−10.9
9.21†	−13.4		− 8.8	−12.4	−12.4	−10.7	−14.5	−13.4	−15.7	−13.0	−13.4
9.32‡	−15.0		− 4.8	− 0.1	−13.1	−15.0	− 8.8	−13.8	−14.2	−13.0	−10.4
10.27†	−13.3		−14.0	− 9.9	−13.0	− 7.4	−12.2	− 9.7	−15.6	−11.1	− 8.2
11.18†	−10.2		− 7.4	− 3.1	−13.0	− 7.8	− 7.5	−13.5	−19.1	−14.5	− 9.8
11.29‡	−12.2		− 5.7		− 8.2	−13.5	+ 3.1	−14.9	−17.0	−10.8	− 5.9
12.13	−11.7				−10.6	− 8.9		−14.5	−16.4	−13.7	− 5.3
13.21	− 9.6					− 7.2			−16.0	−16.1	+ 0.6
17.10	−11.7					− 9.0		− 9.8	−16.8	−11.0	− 2.7
Sept. 4.12	−11.6				− 4.8	− 9.3	−16.0	−13.3	−17.0	−14.1	− 3.0
8.07	− 8.8			− 8.5	− 4.5	− 8.5	−11.2	−11.2	−17.5	−13.6	− 7.5
11.22	− 8.8				−11.8	− 7.7	−11.5	−14.1	−15.9	− 8.5	− 3.4
Oct. 5.08‡	− 9.7				− 1.9	−13.2		− 8.8	−17.0	− 9.8	− 8.6
9.17	− 8.6				− 3.8	− 5.3	− 6.3	−13.0	−14.6	− 8.5	− 4.9
11.07‡	− 1.6				+ 7.0	− 3.8		+ 2.2	− 8.0	+ 0.3	+ 2.7
14.11‡	−13.5	−15.0	−10.1	+ 1.6	− 7.4	−11.0	−12.2	−15.0	−16.0	−10.4	− 4.2
15.08‡	−11.6	−16.2	− 5.9	− 0.2	− 7.8	−11.0	− 8.0	−12.1	−12.8	−10.5	−10.6
16.06‡	−12.3	−15.8	−10.8	− 7.3	− 9.8	−14.4	−11.8	−12.2	−14.7	− 9.8	− 9.4
17.04‡	−13.2	−26.6	−17.3	− 6.6	−13.0	−12.6	−14.0	−12.6	−16.7	−13.2	−10.2
18.03‡	− 3.5	−22.3	− 5.5	+ 0.8	− 3.4	− 9.6	− 5.1	− 0.4	− 9.6	− 4.6	− 0.2
19.03‡	− 6.9	−23.8	−14.1	− 1.6	− 6.4	−11.8	− 7.5	− 8.8	−13.3	− 6.2	0.2
20.04‡	+ 1.2	−10.6	+ 3.7	+ 0.8	− 0.7	− 4.6	+ 3.8	+ 1.4	− 6.2	− 4.1	+ 4.0
21.06‡	− 2.5	− 9.0	− 4.6	− 0.4	+ 1.1	− 3.6	− 1.4	− 6.8	−13.7	− 4.4	+ 0.2
22.03‡	+ 3.6	+ 4.6	+ 6.0	+ 7.8	+ 3.8	− 0.6	+ 5.1		− 7.1	− 0.6	+ 8.6
22.15‡	− 0.1	+ 1.4	+ 2.2		+ 4.2	− 0.1	− 2.8	−11.9	− 8.1	+ 0.3	+ 7.7
25.21‡	− 7.9	+ 7.1	−10.6	− 0.2	+ 5.0	− 5.6	− 5.2	−11.4	−18.3	− 9.9	+11.6
26.03‡	− 6.2	+ 3.7	− 2.9	− 2.4	− 3.2	− 8.7	+ 1.4	−11.3	−12.0	− 6.8	+ 6.9
26.15‡	− 9.3	+ 1.1	− 6.8			− 7.2		−19.0	− 8.9	− 8.4	− 4.3
28.07‡	− 8.3	−10.1	− 8.5	− 5.8	+ 1.4	− 5.8	− 7.0	−19.6	−14.5	− 8.9	− 0.7
30.03‡	− 6.8	− 1.5	− 3.3			− 4.0			−13.9	− 7.1	+ 2.3
31.04‡	− 7.3	− 8.3	+ 1.7			−10.7		+ 2.6	−12.9	− 7.9	+ 8.8
Nov. 5.10‡	− 6.9	+ 1.4	− 1.6		+ 6.2	−10.4			− 9.3		
6.04‡	− 5.7	− 9.4	− 5.4		+ 6.1	− 8.3			−10.9		
10.06‡	− 5.5	−10.4	− 3.4		+ 0.5	+ 0.1		− 5.7	−14.6		
11.02‡		−11.4									
12.04‡	− 0.1	− 6.8	− 6.8			− 3.0			− 6.0		
Dec. 1.01‡	− 2.2	+11.4	− 0.7		+ 2.8	− 6.3		−14.1	− 5.6		
2.08‡	(− 6.2)	+14.2	+ 1.0			−10.6			−13.1		
8.00‡	− 8.6	+ 8.0	− 3.0		+ 9.9	−11.3		− 6.7	−12.0		

* Mean of two plates, dispersion 38 A/mm at H_γ.

† Mean of four plates, dispersion 38 A/mm at H_γ.

‡ One plate, dispersion 19 A/mm at H_γ.

direct rotation of the primary in the ζ Aurigae system were measured by Christie and Wilson.[5] I measured the following lines in 31 Cygni:

Hydrogen:	$H\gamma$, $H\delta$, $H\epsilon$, $H\eta$, $H\theta$, $H\iota$	*Cr* I:	4254, 4275, 4290
Mg I:	3829, 3832, 3838	*Mn* I:	4031, 4033, 4034
Al I:	3944, 3962	*Fe* I:	3764, 3767, 3795, 3800, 3816, 3820, 3824, 3826, 3838, 3856, 3860, 3896, 3900, 3903, 3920, 3923, 3928, 3930, 4046, 4064, 4072
Ca I:	4227		
Ca II:	3934, 3968	*Sr* II:	4078, 4216
Ti II:	3759, 3761, 3901, 3913		

The velocities are tabulated separately for the several elements in Table 1. Plates on which only the lines of *Ca* II were measured are omitted. These will be found in Table 3. The two pairs of lines of *Ti* II have been kept separate because of a systematic difference. Owing to a close blend, 4216 *Sr* II differed systematically from 4078, and an empirical correction has been applied to the former to bring the means of all measures of the two lines into agreement. The numbers of lines entering the mean for *Fe* I vary considerably. In general, fewer lines were measured far from eclipse, because of partial obliteration by

TABLE 2

COMPARISON OF MEASURED *Fe* I VELOCITIES WITH ORBITAL VELOCITY

Inclusive Dates 1951	Mean Date	No. of Plates	Weight	Mean Velocity (Km/Sec)	Tentative Orbital Velocity	Observed *minus* Orbital Velocity
May 20–July 8	June 18	3	1	−10.4	−10.8	+0.4
July 14–Aug. 1	July 23	7	3	−11.2	− 9.7	−1.5
Aug. 17–Sept. 11	Sept. 2	4	2	−10.2	− 8.7	−1.5
Oct. 5–11	Oct. 8	3	2	− 7.4	− 7.8	+0.4
Oct. 25–31	Oct. 28	6	5	− 7.6	− 7.4	−0.2
Nov. 5–Dec. 8	Nov. 17	6	4	− 4.8	− 6.8	+2.0
						+0.04

the continuum of the secondary star, especially in the ultraviolet. There were no clear indications of systematic differences between the several lines of *Fe* I, except on October 22, when the atmospheric eclipse for that element was just ending. On that date, the group λλ 3920, 3923, 3928, and 3930 had fallen into line with the orbital velocity of the K-type star, while the rest of the lines still showed residuals characteristic of the atmospheric eclipse. The higher hydrogen lines were measurable on relatively few plates, because of serious blending with metallic lines.

The measures of all lines except those of *Ca* II and the higher members of the Balmer series represent a blend of the absorption features in the normal spectrum of the K-type star with the lines superimposed on the early-type continuum by interposition of the atmosphere at the limb of the giant primary. During the deeper stages of atmospheric eclipse, the lines formed at the limb were undoubtedly of overwhelming strength, but farther from the contacts the normal lines of the giant star become completely dominant.

Comparison of the measures with the orbital velocity of the primary is complicated by the fact that the eclipse occurred 78 days earlier than the date predicted from the orbital elements.[6] As a basis for such comparison, we first examine the velocities measured during totality and those obtained so far from eclipse that lines formed at the limb were

[5] *Ap. J.*, **81**, 426, 1935.

[6] *Pub. A.S.P.*, **64**, 116, 1952.

surely of negligible strength. We shall depend entirely upon the lines of *Fe* I, which form the most numerous and most homogeneous group.

Table 2 lists six means formed from the velocities of *Fe* I in Table 1. Inclusive dates are given in the first column, the mean date in the second, the number of plates in the third, the weight in the fourth, and the mean velocity in the fifth. The tentative orbital velocity in the sixth column was obtained by a procedure described in the next paragraph.

As a basis of comparison, it was assumed (*a*) that the mean velocity, $\gamma' = \gamma + Ke \cos \omega = -8.44$ km/sec, given by the orbital elements should be the velocity at mid-

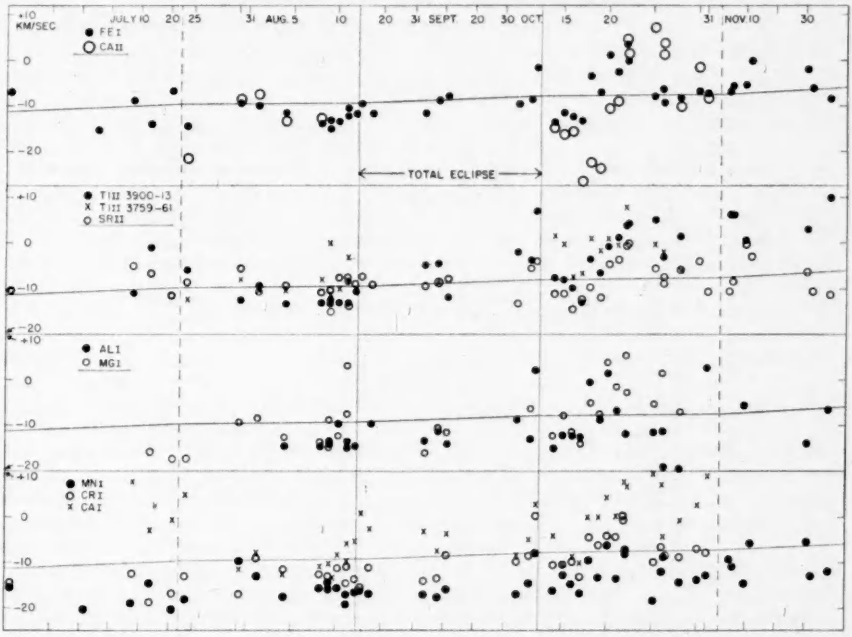

FIG. 1.—Velocities of lines of several elements during and near atmospheric eclipse of 31 Cygni. See legend at left for each strip of the figure. Vertical full lines bound the region of totality, shown on a compressed time scale. Vertical dashed lines at 20 days before and after eclipse bound the regions plotted to a compressed time scale far from eclipse. Orbital velocity is shown by a gently sloping line in each of four strips of the figure.

eclipse; (*b*) that the slope of the velocity-curve during the observed interval about eclipse should be the same as that computed from the elements. This amounts to postulating that the discrepancy of 78 days was due to some local effect upon the rising branch of the curve, without specifying whether it was caused chiefly by an error in the period or by systematic errors in some of the velocities. With these assumptions, the tentative orbital velocities in the sixth column of Table 2 were computed. The differences between these and the observed velocities are given in the seventh column. The weighted mean of all differences is +0.04 km/sec. It is concluded that no further adjustment is necessary, and henceforth the system of velocities defined by the sixth column of Table 2 will be referred to simply as "the orbital velocity."

The velocities of all except the hydrogen lines are plotted in Figure 1. A large time

scale is used for intervals of 20 days before second contact and 20 days after third contact. A compressed time scale is used for the period of total eclipse and for the observations more than 20 days from the contacts. The orbital velocity is shown by a gently sloping line in each section of the plot. The *Ca* II velocities have been omitted for times more than 20 days from eclipse.

Certain lines have appreciable systematic deviations. Thus *Mn* I is conspicuously negative both during totality and far outside atmospheric eclipse. *Ca* I and *Ti* II appear to be positive. On the other hand, all are in fair agreement in the direction of the fluctua-

TABLE 3

RADIAL VELOCITIES OF *Ca* II (H) AND (K) IN 31 CYGNI

DATE (U.T.)	JD 2433000+	VELOCITIES (KM/SEC)	
		K	H
Oct. 14.11	933.61	−15.0	.....
15.08	934.58	−16.0	−16.4
16.06	935.56	−18.4	−13.2
17.04	936.54	−22.5	−30.8
18.03	937.53	−18.4	−27.2
19.03	938.53	−20.8	−26.8
20.04	939.54	−10.2	−11.0
21.06	940.56	− 9.2	− 8.8
22.03	941.53	+ 5.2	+ 3.9
22.15	941.65	+ 2.0	+ 0.8
25.21	944.71	+ 5.6	+ 8.6
26.03	945.53	+ 5.6	+ 1.8
26.15*	945.65	+ 3.4	− 1.2
28.07	947.57	− 9.0	−11.2
30.03†	949.53	+ 2.2	− 5.2
31.04‡	950.54	− 5.9	−10.7
Nov. 5.10§	955.60	− 4.8	+ 7.6
6.04	956.54	− 3.9	−15.0
10.06	960.56	−12.4	− 8.5
11.02	961.52	−15.7	− 7.1
12.04	962.54	− 3.2	−10.5
16.00	966.50	− 1.4	.....
19.10	969.60	− 7.6	−11.7
21.01	971.51	+ 0.4	+ 0.9
22.07	972.57	+15.2 (−25.6)‖	.....
25.01	975.51	+ 7.8	+ 3.8
28.03	978.53	+15.8 (−32.0)	+16.9
Dec. 1.01#	981.51	+13.6	+ 9.3
2.08**	982.58	+11.3	+17.0
8.00	988.50	+12.5 (−20.3)	+ 3.4
14.02	994.52	+13.1 (−31.9)	.....
17.00††	997.50	+ 4.9	.....
23.01‡‡	003.51§§	+12.7 (−26.3)	.....

* Both K and H suspected double, with components about equal, as follows: K + 26.6, −19.8; H + 21.4, −23.9.

† Weak component of K at +137.2.

‡ Weak component of K at +117.3.

§ Weak component of K at +51.8.

‖ Parentheses indicate weaker blended components.

Weak component of K at −93.1.

** Weak component of K at − 91.8.

†† Weak component of K at −85.5.

‡‡ Weak component of K at −104.9.

§§ JD 2434003.51.

tions that occurred during the atmospheric eclipse, particularly during egress, when the plates were taken with the higher dispersion.

The lines of *Fe* I scattered about the orbital velocity until August 1. Thereafter, until totality, they were systematically negative. A similar negative displacement affects most other sets of lines during the ingress. However, all others are entitled to less weight than *Fe* I, because of the smaller numbers of lines. The velocities of *Fe* I on August 8, 9, 10, and 11 have particularly great weight, since four of the low-dispersion plates enter into each mean. In addition, there are high-dispersion plates for August 9 and 11.

The course of the changes is better defined during the egress. For several days all lines showed negative residuals, and this effect was particularly striking for *Ca* II. Subsequently, positive deviations were observed for all lines except those of *Mn* I, which fell into their normal position with systematically negative velocities.

The cross-over from negative to positive residuals was not simultaneous for all lines. Those of *Fe* I and *Al* I apparently changed first, on October 18. Lines of *Sr* II and perhaps *Mg* I lagged a day, and *Ca* II fully three days. *Ti* II is somewhat uncertain because of a tendency toward positive residuals, but, if its systematic difference is taken into account, it can be estimated that it crossed over with *Sr* II.

For most elements a short interval of positive residuals was followed by a return to the orbital velocity. The date of this change coincides, in almost every case, with the independent estimate of the end of atmospheric eclipse, as judged from the disappearance of sharp cores and decrease of total intensities of lines. Of the elements measured, *Al* I was the first, on October 21. Most of the lines of *Fe* I still had positive residuals on October 22 but had returned to the orbital velocity by October 25. However, the group λλ 3920, 3923, 3928, and 3930 had already assumed the orbital velocity on October 22. *Sr* II accompanied the more persistent lines of *Fe* I. The lines of *Mg* I were still positively displaced on October 26. *Ti* II λ 3900 and λ 3913 continued positive until October 28, when they had become too weak to be considered reliable.

The H and K lines of *Ca* II behaved differently from all others that were measured. By October 15 the wings had decreased somewhat, and by October 16 the lines, though wide, were without wings and had very well-defined edges that could be measured accurately. In order to show the degree of accordance between these lines, Table 3 gives separately the velocities for H and K during the egress. Means for *Ca* II and for hydrogen are plotted in Figure 2, in which the entire interval outside totality is represented on the same time scale. The period of totality is compressed.

Prior to July 30, during ingress, *Ca* II lines were strongly displaced negatively. Thereafter, so far as the measures go, they agree approximately with *Fe* I. In the deepest stages of ingress the lines were too broadly winged to be measured with any confidence. During egress, as already noted, the velocities were negative for several days and then crossed over to strongly positive residuals, which continued until October 30. Unlike the behavior of the other elements, the close agreement with the orbital velocity early in November does not indicate an end of atmospheric eclipse. The lines of *Ca* II were still strong and rather wide. Victoria plates show that each line was actually a close double.[7] During the next several weeks the two components of the double fluctuated in relative intensity. The duplicity is perceptible on some of the Michigan plates, as indicated by measures of two components of K in Table 3. The negative velocities on November 10 and 11 are due to the complete disappearance of the longward member of the pair, as shown by Victoria plates. The strong positive residuals, reaching 20 km/sec early in December, are related to the reappearance and final dominance of the longward component.

Besides these main components, fainter lines of briefer life and larger displacements were measured near the K line on several dates. These are appended in the notes to Table 3.

[7] McKellar, Odgers, Aller, and McLaughlin, *Nature*, **169**, 990, 1952.

The hydrogen lines showed fluctuations similar to those of *Ca* II during the first month of egress, but with smaller amplitude. However, the few measures that were obtained later fail to show the large positive residuals that characterized the lines of *Ca* II.

DISCUSSION

The picture that emerges from these measures is certainly not that of a reversing layer and chromosphere simply rotating with the giant star; nor can we even represent the observations by a model in which rotation controls the main trend of the velocities, with systematic changes with height above the photosphere. The negative velocities of the lines of *Fe* I close to the contacts at both limbs indicate that some other effect is dominant and that whatever rotation the star may have is thoroughly overshadowed.

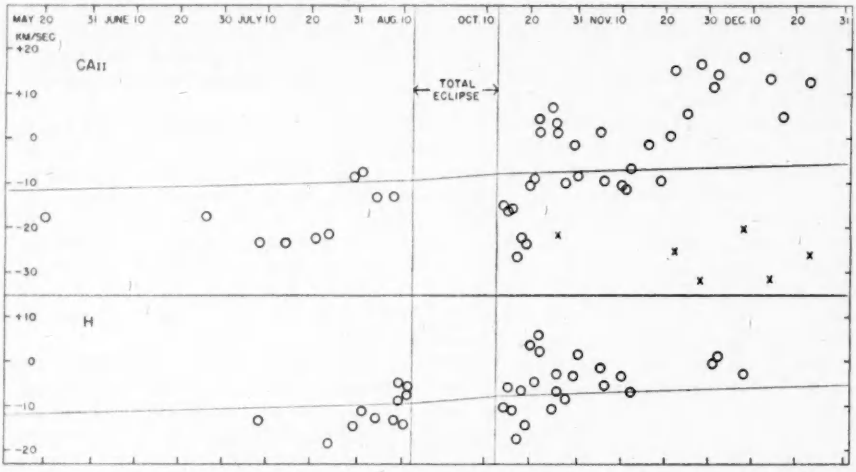

FIG. 2.—Velocities of *Ca* II and hydrogen during atmospheric eclipse of 31 Cygni. Period of totality is drawn to a compressed time scale. Orbital velocity is shown by a gently sloping line in each strip of figure. *Upper strip*, *Ca* II; circles for main component; crosses for weaker component of close pair. *Lower section*, hydrogen.

If the giant star, with a radius of approximately 150 ⊙, rotated in the orbital period, the velocity at the limb would be approximately 2 km/sec. Direct rotation would produce residuals from orbital motion, positive during ingress and negative during egress. Instead, we have negative residuals on *both* sides for the inner atmospheric layers, while somewhat higher layers give consistently positive residuals during egress. Finally, the outermost chromosphere, which shows only in *Ca* II, has large residuals just opposite to those required by direct rotation.

The behavior of *Ca* II appears to be such as to be interpreted most readily in terms of prominence activity on a grand scale. The changes of relative intensity of the two long-lived components of the close double lines seem to demand two fairly independent detached clouds of considerable thickness, and much higher dispersion might have revealed a more complex structure. The short-lived and thinner components of larger displacement appear to indicate less extensive and thinner clouds which were projected against the disk of the secondary star for only a few days at a time. The systematic character of the residuals of the strong lines, negative before eclipse and positive afterward, suggests that the ejection, or at least the subsequent trajectories, are not entirely random.

An attempt was made to account for these residuals in the following manner. Prominences erupted forward from the advancing side of the star would have excess angular momentum and would move outward, accounting for negative residuals before eclipse. Material ejected backward from the following side of the star would have its angular momentum largely canceled, and it would be accelerated toward the secondary star, producing positive residuals after eclipse. However, this hypothesis failed to meet the test of calculation. The duration of flight of a prominence to the heights concerned was 1–2 months, and no residuals in excess of 2 km/sec could be so explained. The hypothesis of a ring of material rotating in the retrograde direction fares no better. The observed velocities are very much less than the circular orbital speed of material moving at such distances under the gravitational attraction of the star.

The peculiar effects in the inner atmosphere, especially the reversal of sign of the residuals, are even more puzzling. At present it appears advisable to reserve judgment regarding the interpretation of any of these deviations. Possibly the study of eclipses of ζ Aurigae with high dispersion would shed some light on the problem. It is also possible that ϵ Aurigae, and perhaps VV Cephei, present similar features. In the case of ϵ Aurigae the departures of individual lines from the mean velocity-curves could be explained only in their broad features as a combination of radial motion and rotation of the infrared star.[8]

[8] Kuiper, Struve, and Strömgren, *Ap. J.*, **86**, 579 ff., 1937.

THE SOLAR SPECTRUM FROM 7 μ TO 13 μ*

J. H. SHAW, M. L. OXHOLM,† AND H. H. CLAASSEN‡
Department of Physics and Astronomy, Ohio State University

Received June 6, 1952

ABSTRACT

The infrared solar spectrum from 7 μ to 13 μ has been reinvestigated at the Ohio State University with a high-resolution grating spectrometer. A map of the spectrum is presented, together with a table of line frequencies, and line identifications are given where possible. Absorption bands of atmospheric H_2O, CO_2, O_3, N_2O, and CH_4 are described, and the existence of other possible atmospheric constituents is discussed briefly.

I. INTRODUCTION

The portion of the solar spectrum described here has been investigated previously by Adel and Lampland[1] with a prism spectrometer and also by Adel[2] with a grating instrument. Adel's grating studies were made at the Lowell Observatory, Flagstaff, Arizona, where the intensities of many atmospheric bands were much reduced compared with our data, which were obtained nearer sea-level. Although bands of H_2O and HDO, CO_2, O_3, and N_2O were identified in these early spectra, the resolution available was not sufficient to reveal the full detail of this region.

The present solar spectrum obtained at the Ohio State University, Columbus, Ohio (latitude 40° N., 800 feet above M.S.L.), shows a structure similar to that observed previously, but many more lines have now been identified. A description of the spectrometer and other apparatus has already been given.[3] For the present work a 3600 line/inch replica grating (dimensions 5.5 inches long, 3.5 inches high) was used as the dispersing element. The detecting system consisted of a Perkin-Elmer thermocouple together with a 13 cycles per second chopping system and amplifier. The spectra were obtained during the period May, 1950—May, 1951, and most regions of the spectrum were investigated at different solar altitudes and seasons of the year.

II. RESULTS

A. THE PRISMATIC SOLAR SPECTRUM FROM 7.5 μ TO 13 μ

The spectrum shown in Figure 1 was taken at the Observatories, Cambridge, England, during 1948 with a rock salt prism spectrometer by one of us (J. H. S.). This spectrum shows the positions and relative intensities of the atmospheric bands which are present in the grating spectrum (Figs. 2–7). There is complete absorption beyond 13.5 μ, caused by intense bands of atmospheric CO_2; and the ν_2 fundamental of H_2O absorbs all solar energy from 5.2 μ to 7.4 μ at the short-wave-length end of this spectrum.

Other prominent features are the band of O_3 at 9.6 μ and a strong absorption at 7.8 μ on the side of the H_2O band. This is caused by H_2O, N_2O, and probably CH_4, although the existence of this gas in the atmosphere over England has not yet been confirmed.

* Supported in part by a contract between the Geophysics Research Division of the Air Force Cambridge Research Center and the Ohio State University Research Foundation.

† Now at Purdue University, Lafayette, Indiana.

‡ Now at University of Oklahoma, Norman, Oklahoma.

[1] *Ap. J.*, **87**, 198, 1938; see also other papers in *Ap. J.*

[2] *Ap. J.*, **94**, 451, 1941.

[3] J. H. Shaw, R. M. Chapman, J. N. Howard, and M. L. Oxholm, *Ap. J.*, **113**, 268, 1951.

N_2O also has a weak band at 8.6 μ, which is partly obscured by H_2O lines. Two CO_2 bands at 9.4 μ and 10.4 μ lie on either side of the O_3 absorption, and the P branch of the 9.4 μ band is hidden by this band. The Q branch of a CO_2 band at 12.6 μ is also visible on this spectrum.

In addition to these absorptions, which have previously been identified by Adel,[2] there is a large number of "lines" of irregular intensity and frequency distribution throughout the region. In the grating map these absorptions have been further resolved, and it has been shown that they are due to atmospheric H_2O.

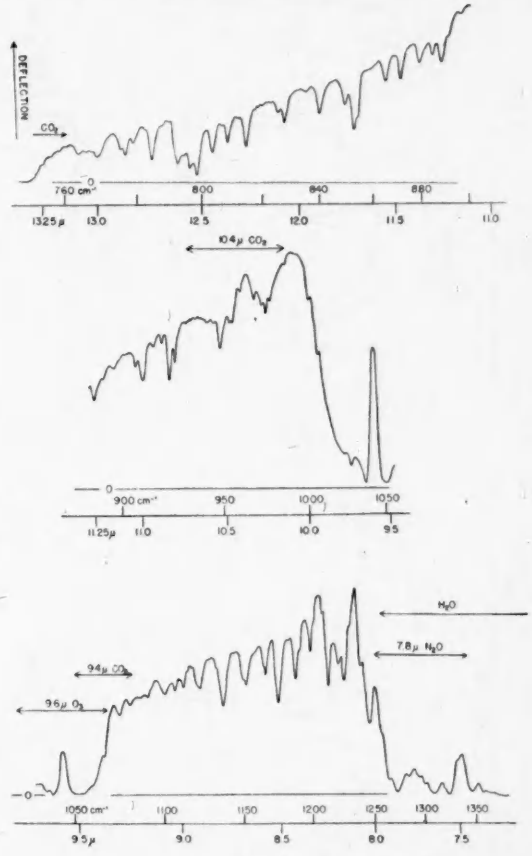

FIG. 1

B. THE GRATING SOLAR SPECTRUM FROM 7.0 μ TO 13 μ

The grating map shown in Figures 2–7 covers the same region as the prismatic spectrum shown in Figure 1. In the figures the date on which each portion of the spectrum was obtained is shown and also the mean solar altitude at the time of recording. As the appearance of the spectrum varies markedly with season of year and solar altitude, the records chosen to illustrate the figures were those showing the greatest possible detail.

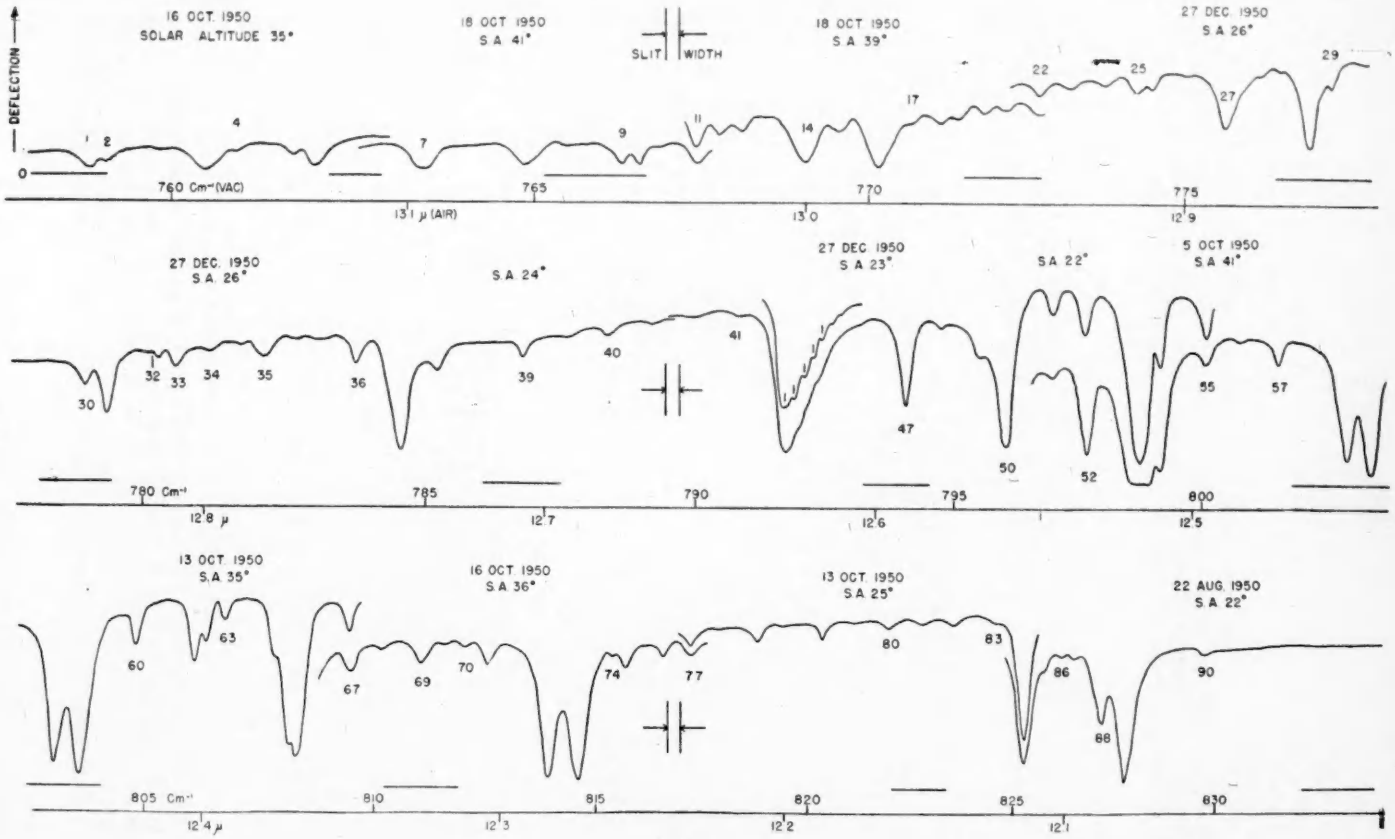
16 OCT. 1950
SOLAR ALTITUDE 35°
18 OCT. 1950
S.A. 41°
SLIT WIDTH
18 OCT. 1950
S.A. 39°
27 DEC. 1950
S.A. 26°
DEFLECTION
0
1
2
4
7
9
11
14
17
22
25
27
29
760 Cm⁻¹(VAC)
765
770
775
13·1 μ (AIR)
13·0
12·9
27 DEC. 1950
S.A. 26°
S.A. 24°
27 DEC. 1950
S.A. 23°
S.A. 22°
5 OCT. 1950
S.A. 41°
30
32
33
34
35
36
39
40
41
47
50
52
55
57
780 Cm⁻¹
785
790
795
800
12·8 μ
12·7
12·6
12·5
13 OCT. 1950
S.A. 35°
16 OCT. 1950
S.A. 36°
13 OCT. 1950
S.A. 25°
22 AUG. 1950
S.A. 22°
60
63
67
69
70
74
77
80
83
86
88
90
805 Cm⁻¹
810
815
820
825
830
12·4 μ
12·3
12·2
12·1

FIG. 2

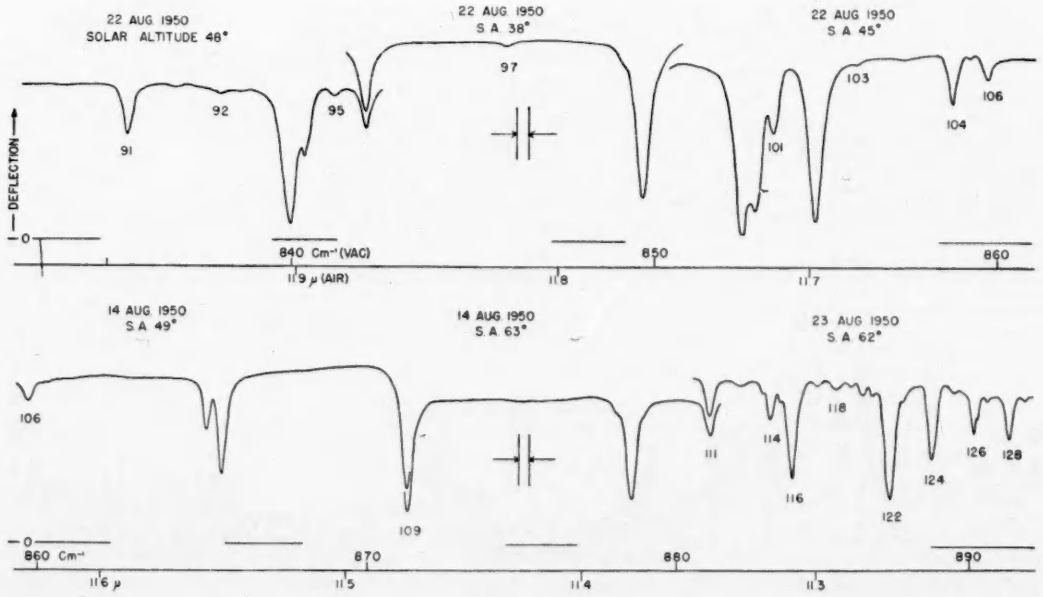
22 AUG. 1950
SOLAR ALTITUDE 48°
22 AUG. 1950
S.A. 38°
22 AUG. 1950
S.A. 45°
DEFLECTION
0
91
92
95
97
101
103
104
106
840 Cm⁻¹ (VAC)
850
860
11.9 μ (AIR)
11.8
11.7
14 AUG. 1950
S.A. 49°
14 AUG. 1950
S.A. 63°
23 AUG. 1950
S.A. 62°
106
109
111
114
116
118
122
124
126
128
0
860 Cm⁻¹
870
880
890
11.6 μ
11.5
11.4
11.3

FIG. 3

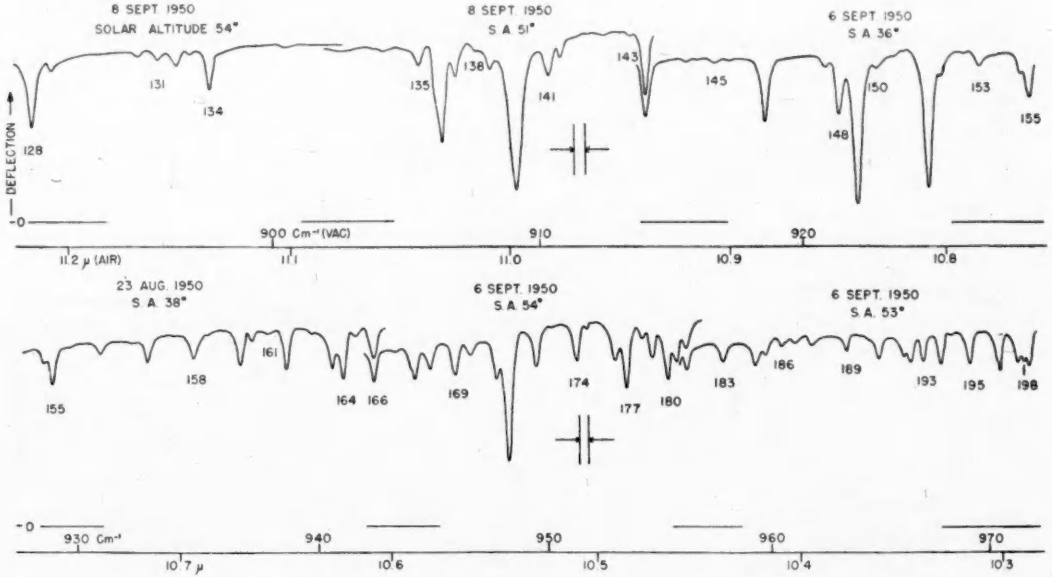
8 SEPT. 1950
SOLAR ALTITUDE 54°
8 SEPT. 1950
S.A. 51°
6 SEPT. 1950
S.A. 36°
DEFLECTION
0
128
131
134
135
138
141
143
145
148
150
153
155
900 Cm⁻¹ (VAC)
910
920
11.2 μ (AIR)
11.1
11.0
10.9
10.8
23 AUG. 1950
S.A. 38°
6 SEPT. 1950
S.A. 54°
6 SEPT. 1950
S.A. 53°
155
158
161
164
166
169
174
177
180
183
186
189
193
195
198
0
930 Cm⁻¹
940
950
960
970
10.7 μ
10.6
10.5
10.4
10.3

FIG. 4

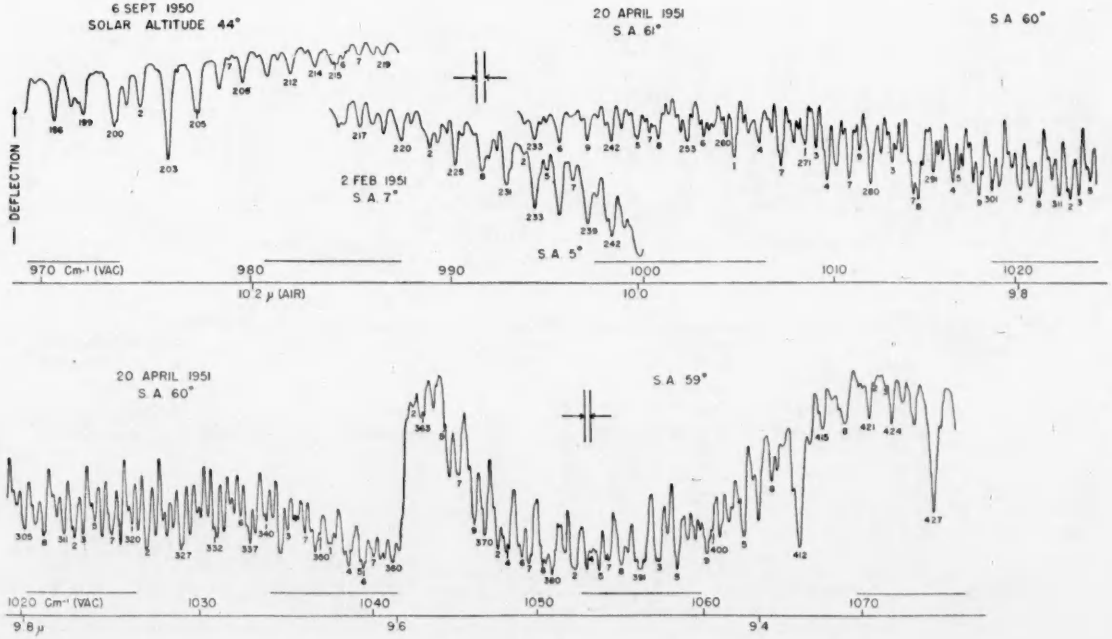
6 SEPT 1950
SOLAR ALTITUDE 44°
20 APRIL 1951
S.A. 61°
S.A. 60°
2 FEB 1951
S.A. 7°
S.A. 5°
DEFLECTION
970 Cm⁻¹ (VAC)
980
990
1000
1010
1020
10·2 μ (AIR)
10·0
9·8
20 APRIL 1951
S.A. 60°
S.A. 59°
1020 Cm⁻¹ (VAC)
1030
1040
1050
1060
1070
9·8 μ
9·6
9·4

FIG. 5

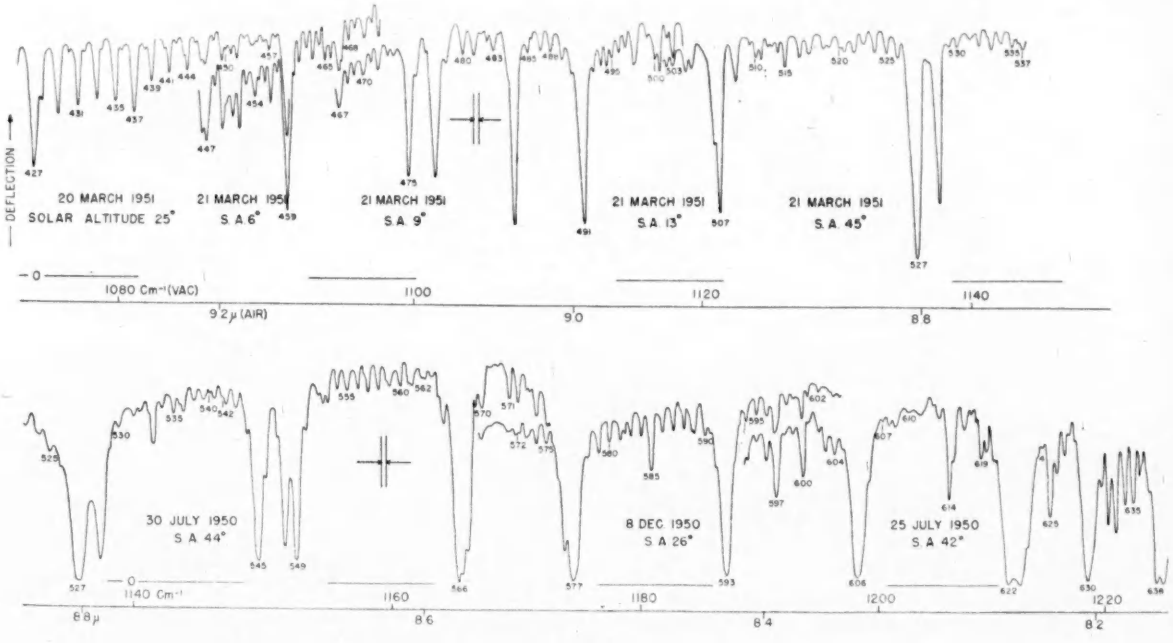
DEFLECTION
20 MARCH 1951
SOLAR ALTITUDE 25°
21 MARCH 1951
S.A. 6°
21 MARCH 1951
S.A. 9°
21 MARCH 1951
S.A. 13°
21 MARCH 1951
S.A. 45°
1080 Cm⁻¹(VAC)
1100
1120
1140
9·2μ (AIR)
9·0
8·8
30 JULY 1950
S.A. 44°
8 DEC 1950
S.A. 26°
25 JULY 1950
S.A. 42°
1140 Cm⁻¹
1160
1180
1200
1220
8·8μ
8·6
8·4
8·2

FIG. 6

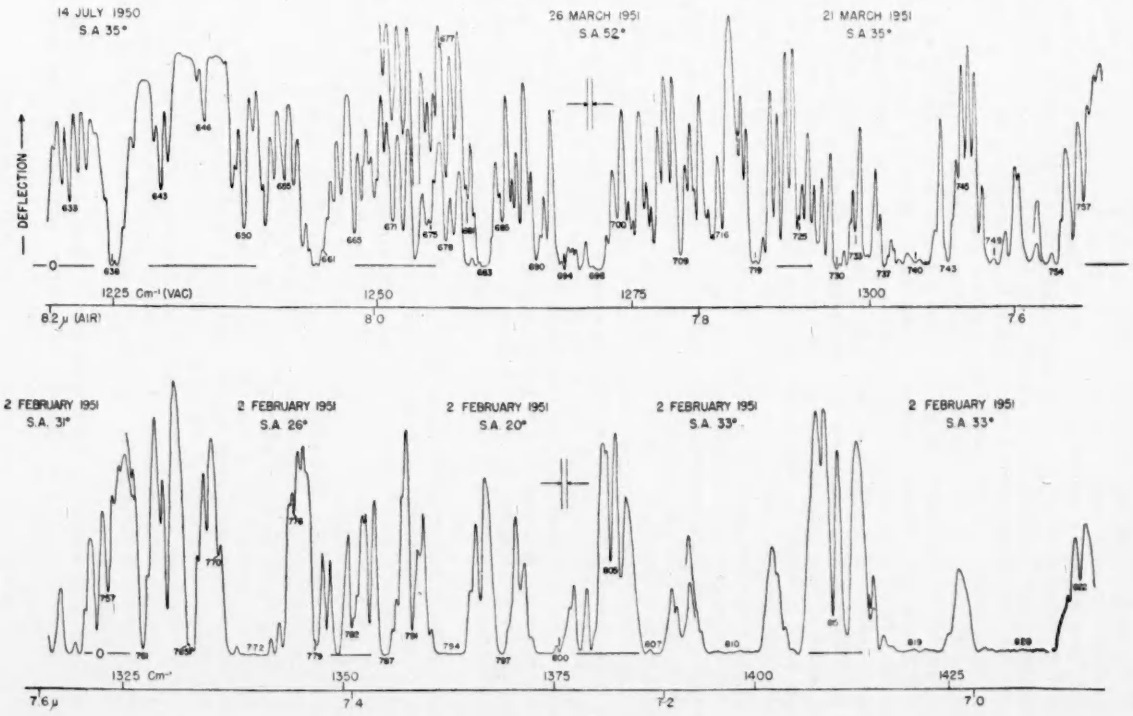
14 JULY 1950
S.A. 35°
26 MARCH 1951
S.A. 52°
21 MARCH 1951
S.A. 35°
— DEFLECTION —
1225 Cm⁻¹ (VAC)
1250
1275
1300
8·2 μ (AIR)
8·0
7·8
7·6
2 FEBRUARY 1951
S.A. 31°
2 FEBRUARY 1951
S.A. 26°
2 FEBRUARY 1951
S.A. 20°
2 FEBRUARY 1951
S.A. 33°
2 FEBRUARY 1951
S.A. 33°
1325 Cm⁻¹
1350
1375
1400
1425
7·6 μ
7·4
7·2
7·0

FIG. 7

All records of each portion of the spectrum were compared, to verify the appearance of some of the weaker lines, which may be visible on only a few records. In a few instances the original records used to illustrate the spectrum in Figures 2–7 did not show all the weak lines considered real. These lines were included by slightly redrawing the portions of the spectrum affected. Spectra taken during the winter months are usually given for regions where H_2O is absorbing strongly, and, where H_2O lines are weak, spectra obtained on hot, humid days have been included. In some regions traces obtained at very low solar altitudes are shown, in order to enhance weak lines.

The individual lines have been numbered consecutively, beginning at the lowest frequency covered by the map, and descriptions of the lines are given in Table 1. The first column in this table gives the line number, the second its frequency (cm^{-1}) corrected to vacuum, and the third its wave length (Angstroms) in air. The fourth column gives the number of records from which the line frequency was determined, and the last two columns give the molecular assignment and the frequency observed for the line in our laboratory spectra. Line frequencies (cm^{-1} air) were measured from the individual records and were corrected to vacuum by assuming that the laboratory air had an average refractive index of 1.0002565, corresponding to a barometric pressure of about 740 mm Hg and a temperature of 25° C. The wave lengths of the lines in Table 1 are the reciprocals of the frequencies in air multiplied by 10^4.

The accuracy of the measurements varied with the frequency range; below 900 cm^{-1} the angular dispersion of the grating increased rapidly, and measurements on well-defined lines could be repeated to ± 0.02 cm^{-1}. Between 900 and 1100 cm^{-1}, individual measurements showed a scatter of ± 0.05 cm^{-1}, and at higher frequencies a scatter of ± 0.10 cm^{-1} was found. Above 1200 cm^{-1} there are overlapping bands of H_2O, N_2O, and CH_4. Many of the numbered absorptions in this region are due to more than one component, and, as the individual lines in such "blends" vary in relative intensity, variations among frequency measurements of such blends were sometimes found. Over the rest of the spectrum the agreement in the frequency values for a given line was very satisfactory among records taken at different seasons of the year and at different solar altitudes.

In Table 1 some frequencies are listed to the nearest 0.1 cm^{-1} only. These include (*a*) weak lines, which appeared only when long atmospheric paths could be used; (*b*) very intense, wide absorptions, which gave complete absorption over several tenths of a wave number; and (*c*) absorptions due to more than one line. On some records the components of such blends may show signs of being resolved, but frequency measurements of the separate lines were unreliable. Such absorptions are marked ‡ in Table 1, and the frequency listed is near the center of the two lines. Many other absorptions are also due to more than one component, but the individual lines lie so close together that they appear as sharp lines on our spectra. Where it is known that more than one line is present in a given absorption, the strongest components have been marked * where possible.

Many H_2O lines occur throughout the spectrum which have not been resolved because of other overlapping lines. Their presence has been verified by observing variations in absorption in the region with the amount of atmospheric H_2O. In such cases no line number has been assigned, but the symbol H_2O has been included in the identification column of Table 1 and marked §.

No attempt has been made to give the intensities of the observed lines in Table 1 because of the large changes with solar altitude and possible variations from day to day. In particular, H_2O lines show very large intensity fluctuations, depending on the atmospheric temperature and humidity. Estimates of relative intensities of lines can be obtained from Figures 2–7.

The frequency differences observed in comparing lines in the solar spectrum with our laboratory data give an indication of the experimental accuracy of the measurements. Large deviations of individual line frequencies in the solar spectrum from the laboratory

TABLE 1

LINE FREQUENCIES AND IDENTIFICATIONS BETWEEN 7.0 μ AND 13.0 μ IN THE SOLAR SPECTRUM (FIGS. 2–7)

Line Number	Frequency (Cm^{-1} [Vac])	Wave Length (μ [Air])	No. of Measures	Identification	Lab. Value (Cm^{-1} [Vac])	Line Number	Frequency (Cm^{-1} [Vac])	Wave Length (μ [Air])	No. of Measures	Identification	Lab. Value (Cm^{-1} [Vac])
1	758.87	13.1740	9	CO_2	758.82	50	795.97	12.5600	14	H_2O	796.01
2	759.11	13.1698	8			51	796.96	12.5444	9	CO_2	796.97
3	760.42	13.1472	9	CO_2	760.37	52	797.61	12.5342	11	H_2O	797.65
4	760.83	13.1401	7			53	798.66	12.5177	8	CO_2	798.57
5	761.59	13.1270	8							H_2O*	798.75
6	761.87	13.1222	9	CO_2	761.86	54	799.08	12.5111	8	H_2O	799.11
7	763.37	13.0964	13	CO_2	763.40	55	800.08	12.4955	12	CO_2	800.09
8	764.87	13.0707	9	CO_2	764.86	56	800.8	12.483			
9	766.26	13.0470	8	CO_2	766.25	57	801.65	12.4710	12	CO_2	801.67
10	766.51	13.0427	8	CO_2	766.55	58	803.09	12.4486	11	H_2O	803.07
11	767.36	13.0283	12	H_2O	767.37	59	803.60	12.4408	11	H_2O	803.60
12	767.68	13.0229	6	CO_2	767.70	60	804.75	12.4230	13	CO_2	804.77
13	768.04	13.0168	10	CO_2	768.02	61	806.06	12.4028	15	H_2O	806.06
14	769.03	13.0000	9	H_2O*	769.1	62	806.33	12.3986	10	CO_2	806.33
				CO_2	769.08	63	806.75	12.3922	11	H_2O	806.75
15	769.53	12.9916	7	CO_2	769.58	64	807.9	12.375		CO_2	807.89
16	770.17	12.9808	7	H_2O*	770.17	65	808.17	12.3704	10	H_2O	808.14
				CO_2	770.38	66	808.33	12.3680	10	H_2O	808.29†
17	770.7	12.972		CO_2	770.70	67	809.44	12.3510	16	CO_2	809.46
18	771.14	12.9644	10	CO_2	771.12	68	810.2	12.340			
19	771.3	12.962		CO_2	771.34	69	810.99	12.3274	9	CO_2	811.01
20	771.76	12.9540	7	CO_2	771.74	70	812.0	12.312			
21	772.11	12.9482	5	CO_2	772.20	71	812.53	12.3040	9	CO_2	812.58
22	772.68	12.9386	10	CO_2	772.7	72	813.93	12.2829	9	H_2O	813.97
23	773.11	12.9314	7	CO_2	773.09	73	814.57	12.2732	9	H_2O	814.61
24	773.70	12.9216	6	CO_2	773.66	74	815.31	12.2621	6		
25	774.2	12.913		CO_2	774.3	75	815.64	12.2572	10	CO_2	815.69
26	774.4	12.910				76	816.53	12.2438	10	H_2O	816.55
27	775.65	12.8891	9	H_2O*	775.63	77	817.21	12.2336	10	CO_2	817.27
				CO_2	775.8	78	818.78	12.2102	7	CO_2	818.81
						79	820.35	12.1868	7	CO_2	820.35
28	777.08	12.8654	8	H_2O*	777.07	80	821.89	12.1640	6	CO_2	821.93
				CO_2	777.14	81	822.70	12.1520	5		
29	777.45	12.8592	7	CO_2	777.44	82	823.45	12.1409	7	CO_2	823.49
30	779.04	12.8330	8	CO_2	779.00	83	824.6	12.124			
31	779.36	12.8277	9	H_2O	779.40	84	825.24	12.1144	13	H_2O	825.24
32	780.2	12.814		CO_2	780.17	85	825.7	12.108			
33	780.58	12.8077	9	CO_2	780.58	86	826.2	12.100			
34	781.1	12.798		CO_2	781.06	87	826.56	12.0951	9	CO_2	826.62
35	782.13	12.7823	9	CO_2	782.18	88	827.20	12.0858	10	H_2O	827.21
36	783.79	12.7553	8	CO_2	783.72	89	827.76	12.0776	9	H_2O	827.80
37	784.52	12.7434	11	H_2O*	784.54	90	829.8	12.049		CO_2	829.75
				CO_2	784.68	91	835.60	11.9643	10	H_2O	835.64
38	785.20	12.7324	9	CO_2	785.32	92	838.1	11.928			
39	786.81	12.7062	11	CO_2	786.86	93	839.97	11.9021	10	H_2O	840.01
40	788.37	12.6810	10	CO_2	788.37	94	840.36	11.8965	10	H_2O	840.44
41	790.8	12.641				95	841.15	11.8854	8	H_2O	841.16
42	791.7	12.628		CO_2 (Q)		96	841.97	11.8738	15	H_2O?	
43	791.8	12.626		CO_2		97	845.8	11.820		H_2O	845.83
44	792.03	12.6224	6	CO_2		98	849.65	11.7665	9	H_2O	849.69
45	792.21	12.6196	6	CO_2		99	852.50	11.7272	9	H_2O	852.62
46	792.37	12.6170	9	CO_2		100	852.91	11.7215	9	H_2O	852.91
47	793.99	12.5913	10	CO_2	793.89	101	853.44	11.7143	10	H_2O	853.41
				H_2O*	794.01	102	854.66	11.6975	9	H_2O	854.66
48	794.7	12.580				103	855.9	11.681			
49	795.45	12.5682	6	CO_2	795.43	104	858.63	11.6435	14	H_2O	858.65

* Strongest component of doublet.

† Intensity and frequency of this line predicted from known energy levels of the H_2O molecule.

TABLE 1—*Continued*

Line Number	Frequency (Cm^{-1} [Vac])	Wave Length (μ [Air])	No. of Measures	Identification	Lab. Value (Cm^{-1} [Vac])
105	859.2	11.636			
106	859.75	11.6283	14	H_2O	859.78
107	865.02	11.5574	9	H_2O	865.07
108	865.51	11.5508	9	H_2O	865.54
109	871.32	11.4738	12	H_2O	871.36
110	878.61	11.3786	11	H_2O	878.65
111	881.15	11.3458	12	H_2O	881.08
112	882.2	11.333			
113	882.89	11.3235	6		
114	883.14	11.3203	10	H_2O	883.18
115	883.56	11.3149	7		
116	883.89	11.3107	9	H_2O	883.89
117	884.8	11.299			
118	885.44	11.2909	7		
119	885.8	11.287			
120	886.37	11.2790	6		
121	886.79	11.2737	6		
122	887.27	11.2676	9	H_2O	887.33
123	887.8	11.261			
124	888.69	11.2496	10	H_2O	888.71
125	889.5	11.240			
126	890.2‡	11.231		H_2O*	890.14
127	890.60	11.2255	5		
128	891.37	11.2158	15	H_2O	891.33
129	892.1	11.207		H_2O	892.1
130	895.2	11.167			
131	895.9	11.158			
132	896.57	11.1508	8	H_2O	896.56
133	897.1	11.144			
134	897.77	11.1358	10	H_2O	897.85
135	905.50	11.0407	9	H_2O	905.34†
136	906.32	11.0307	10	H_2O	906.32
137	906.81	11.0248	10	H_2O	906.8
138	907.5	11.017			
139	908.09	11.0092	8	H_2O	(908.24)
140	909.01	10.9981	10	H_2O	909.02
141	910.30	10.9825	8	H_2O	910.17
142	910.77	10.9768	9	H_2O	910.77
143	913.4	10.945			
144	914.03	10.9377	11	H_2O	914.06
145	916.6	10.907		CO_2?	
146	918.53	10.8841	11	H_2O	918.52
147	920.90	10.8561	8	CO_2?	
148	921.48	10.8493	10	H_2O	921.48
149	922.19	10.8409	9	H_2O	922.20
150	922.98	10.8316	7	CO_2	922.97
151	925.05	10.8074	11	CO_2 H_2O	924.98 925.11
152	925.50	10.8022	7		
153	927.06	10.7840	10	CO_2	927.04
154	928.71	10.7648	12		
155	929.04	10.7610	18	H_2O* CO_2	929.00 929.08
156	931.05	10.7378	11	CO_2	931.04
157	933.01	10.7152	12	CO_2	933.02
158	934.93	10.6932	11	CO_2	934.95
159	936.85	10.6713	11	CO_2	936.87
160	937.37	10.6654	8	H_2O	937.40
161	938.16	10.6564	4	H_2O	938.2
162	938.76	10.6496	12	CO_2	938.79
163	940.61	10.6286	16	CO_2	940.59
164	941.08	10.6233	17	H_2O	941.12
165	941.62	10.6172	6		
166	942.43	10.6080	14	CO_2	942.41
167	944.24	10.5877	10	CO_2	944.21
168	944.91	10.5802	10	H_2O	944.95
169	946.02	10.5678	11	CO_2	945.99
170	946.73	10.5599	10	H_2O	946.73†
171	947.83	10.5476	11	CO_2	947.79
172	948.30	10.5424	11	H_2O	948.35
173	949.53	10.5288	11	CO_2	949.51
174	951.25	10.5097	12	CO_2	951.24
175	951.71	10.5046	6		
176	952.95	10.4910	10	CO_2	952.94
177	953.41	10.4859	11	H_2O	953.49
178	954.17	10.4776	7	H_2O	954.19
179	954.61	10.4727	14	CO_2	954.57
180	955.33	10.4648	15	H_2O	955.50†
181	955.73	10.4605	16	H_2O	955.71
182	956.22	10.4551	15	CO_2	956.23
183	957.85	10.4373	10	CO_2	957.85
184	959.29	10.4217	11	H_2O* CO_2	959.33 959.42
185	959.78	10.4163	11		
186	960.5	10.408			
187	961.1	10.402		H_2O	960.77
188	961.88	10.3936	9	CO_2	962.07
189	963.28	10.3785	9	CO_2	963.31
190	964.81	10.3620	9	CO_2	964.85
191	965.98	10.3495	8	H_2O	966.01
192	966.28	10.3463	7	CO_2	966.32
193	966.95	10.3391	9	H_2O	967.00
194	967.76	10.3305	13	CO_2	967.75
195	969.20	10.3151	12	CO_2	969.19
196	970.6	10.300	15	CO_2 H_2O	970.57 970.66
197	971.43	10.2914	12	H_2O	971.53†
198	971.71	10.2885	8	H_2O	971.75
199	971.95	10.2859	11	CO_2	971.95
200	973.4‡	10.270		CO_2 H_2O*	973.28 973.59
201	974.04	10.2639	10	H_2O	974.08
202	974.66	10.2574	10	CO_2	974.60
203	976.0	10.244		CO_2 H_2O*	975.93 976.07
204	976.39	10.2392	6		
205	977.4‡	10.229		CO_2 H_2O*	977.23 977.54
206	978.52	10.2168	11	CO_2	978.48
207	978.96	10.2122	7		
208	979.74	10.2041	9	CO_2	979.71
209	980.4	10.198			
210	980.98	10.1912	8	CO_2	980.90
211	981.50	10.1858	6	H_2O?	
212	982.10	10.1796	8	CO_2	982.11
213	982.8	10.172			
214	983.32	10.1669	13	CO_2	983.29
215	984.2‡	10.157		CO_2	984.38

‡ On some records these lines are partially resolved.

TABLE 1—*Continued*

Line Number	Frequency (Cm^{-1} [Vac])	Wave Length (μ [Air])	No. of Measures	Identification	Lab. Value (Cm^{-1} [Vac])	Line Number	Frequency (Cm^{-1} [Vac])	Wave Length (μ [Air])	No. of Measures	Identification	Lab. Value (Cm^{-1} [Vac])
216	984.68	10.1529	7	.....	.....	274	1009.67	9.9017	11	O_3	.....
217	985.52	10.1443	13	CO_2	985.52	275	1010.1‡	9.897	.....	O_3 H_2O*	1010.12
218	986.14	10.1379	12	.....	.....	276	1010.5	9.893	.....	.....	.....
219	986.66	10.1325	13	CO_2	986.60	277	1010.8	9.890	.....	O_3 H_2O*	..... 1010.86
220	987.57	10.1232	14	CO_2	987.61						
221	988.10	10.1178	10	O_3	.....	278	1011.1	9.887	.....	.....	.....
222	988.93	10.1093	9	.....	.....	279	1011.41	9.8846	13	O_3	.....
223	989.38	10.1047	7	O_3	.....	280	1012.01	9.8788	12	O_3	.....
224	989.84	10.1000	8	.....	.....	281	1012.54	9.8736	12	O_3	.....
225	990.26	10.0957	13	H_2O	990.3	282	1012.94	9.8697	7	.....	.....
226	990.64	10.0918	12	O_3	.....	283	1013.18	9.8674	12	O_3	.....
227	991.32	10.0849	8	.....	.....	284	1013.36	9.8656	12	.....	.....
228	991.71	10.0810	13	O_3	.....	285	1013.69	9.8624	13	O_3	.....
229	992.02	10.0778	9	.....	.....	286	1014.0	9.859	.....	.....	.....
230	992.51	10.0728	11	.....	.....	287	1014.32	9.8563	6	O_3	.....
231	993.00	10.0678	14	O_3	.....	288	1014.54	9.8542	13	H_2O	1014.56
232	993.86	10.0591	10	.....	.....	289	1014.8	9.851	.....	O_3	.....
233	994.4	10.053	.....	O_3 H_2O	..... 994.4	290	1015.1	9.848	.....	.....	.....
234	994.82	10.0494	8	.....	.....	291	1015.44	9.8454	11	O_3	.....
235	995.08	10.0468	10	O_3	.....	292	1015.72	9.8427	7	O_3	.....
236	995.68	10.0408	13	O_3	.....	293	1015.92	9.8407	10	O_3	.....
237	996.38	10.0337	13	.....	.....	294	1016.49	9.8352	13	O_3	.....
238	996.80	10.0295	8	.....	.....	295	1016.85	9.8317	6	O_3	.....
239	997.08	10.0267	13	O_3	.....	296	1017.03	9.8299	6	O_3	.....
240	997.55	10.0219	13	.....	.....	297	1017.35	9.8268	7	O_3	.....
241	998.03	10.0171	11	.....	.....	.....	.....	.....	.....	H_2O§	1017.6
242	998.30	10.0144	14	O_3	.....	298	1017.67	9.8238	12	O_3	.....
243	998.89	10.0085	15	H_2O	998.87	.....	.....	.....	.....	H_2O§	1017.9
244	999.33	10.0041	6	.....	.....	299	1017.97	9.8209	14	O_3	.....
245	996.6‡	10.001	.....	O_3	.....	300	1018.48	9.8160	6	O_3	.....
246	1000.14	9.9960	9	.....	.....	301	1018.72	9.8136	18	O_3	.....
247	1000.42	9.9932	16	H_2O	1000.35	302	1019.11	9.8099	18	O_3	.....
248	1000.80	9.9894	16	O_3	.....	303	1019.65	9.8047	8	O_3	.....
249	1001.1	9.986	.....	.....	.....	304	1019.81	9.8032	15	O_3	.....
250	1001.30	9.9844	15	.....	.....	305	1020.21	9.7993	15	O_3	.....
251	1001.74	9.9800	16	.....	.....	306	1020.62	9.7954	8	O_3	.....
252	1002.00	9.9774	16	O_3	.....	307	1020.86	9.7931	15	O_3	.....
253	1002.28	9.9747	17	O_3	.....	308	1021.30	9.7888	16	O_3	.....
254	1002.5	9.972	.....	.....	.....	309	1021.73	9.7847	7	O_3	.....
255	1002.96	9.9679	10	.....	.....	310	1021.9	9.783	.....	O_3	.....
256	1003.22	9.9653	10	O_3	.....	311	1022.35	9.7788	12	O_3	.....
257	1003.5	9.962	.....	O_3	.....	312	1022.9‡	9.773	.....	O_3	.....
258	1003.7	9.960	.....	H_2O	1003.8	313	1023.40	9.7688	13	O_3	.....
259	1004.16	9.9560	7	.....	.....	314	1023.88	9.7642	9	O_3	.....
260	1004.37	9.9539	13	O_3	.....	315	1024.07	9.7624	12	O_3	.....
261	1004.79	9.9498	13	O_3	.....	316	1024.48	9.7585	13	O_3	.....
262	1005.33	9.9444	12	.....	.....	317	1025.0‡	9.754	.....	O_3	.....
263	1005.56	9.9421	12	O_3	.....	318	1025.49	9.7489	13	O_3	.....
264	1006.05	9.9373	11	O_3	.....	319	1025.96	9.7444	8	O_3	.....
265	1006.51	9.9326	8	.....	.....	320	1026.16	9.7425	9	O_3	.....
266	1006.71	9.9308	12	O_3	.....	321	1026.53	9.7390	11	O_3	.....
267	1007.2‡	9.926	.....	O_3	.....	322	1027.0‡	9.734	.....	O_3	.....
268	1007.7	9.921	.....	.....	.....	323	1027.53	9.7295	11	O_3	.....
269	1007.91	9.9190	10	O_3	.....	324	1027.98	9.7253	7	O_3	.....
270	1008.16	9.9165	7	.....	.....	325	1028.24	9.7228	8	O_3	.....
271	1008.48	9.9134	12	O_3	.....	.....	.....	.....	.....	H_2O§	1028.47
272	1008.85	9.9097	7	.....	.....	326	1028.56	9.7198	9	O_3	.....
273	1009.11	9.9072	11	O_3	.....	327	1029.0‡	9.715	.....	O_3	.....

§ Absorption due to this line observed, although the line itself has not been resolved.

TABLE 1—*Continued*

Line Number	Frequency (Cm^{-1} [Vac])	Wave Length (μ [Air])	No. of Measures	Identification	Lab. Value (Cm^{-1} [Vac])	Line Number	Frequency (Cm^{-1} [Vac])	Wave Length (μ [Air])	No. of Measures	Identification	Lab. Value (Cm^{-1} [Vac])
328	1029.54	9.7105	11	O_3	.....	381	1051.61	9.5068	9	O_3	.....
329	1029.9	9.707	.....	O_3	.....	382	1052.2‡	9.501	.....	O_3*	.....
330	1030.11	9.7052	11	O_3	.....					CO_2	1052.20
331	1030.55	9.7010	11	O_3	.....	383	1052.97	9.4945	10	O_3	.....
.....	.....	.....	.....	H_2O§	1030.58	384	1053.1	9.493	.....	.....	.....
332	1031.0‡	9.696	.....	O_3	.....	385	1053.63	9.4886	10	O_3	.....
333	1031.46	9.6924	11	O_3	.....	386	1054.11	9.4842	6	CO_2?	10.5396
334	1031.85	9.6888	8	O_3	.....	387	1054.29	9.4826	7	O_3	.....
335	1032.06	9.6868	10	O_3	.....	388	1055.00	9.4762	10	O_3	.....
336	1032.44	9.6833	11	O_3	.....	389	1055.38	9.4727	9	O_3	.....
337	1032.9‡	9.680	.....	O_3	.....	390	1055.8	9.469	.....	.....	.....
338	1033.29	9.6753	12	O_3	.....	391	1056.2‡	9.466	.....	O_3	.....
339	1033.8	9.670	.....	O_3	.....	392	1056.4	9.463	.....	O_3	.....
340	1034.0	9.668	.....	O_3	.....	393	1057.2‡	9.456	.....	O_3*	.....
341	1034.34	9.6655	11	O_3	.....					CO_2	1057.31
342	1034.82	9.6610	12	O_3	.....	394	1057.77	9.4513	13	O_3	.....
343	1035.21	9.6574	11	O_3	.....	395	1058.38	9.4459	13	O_3	.....
344	1035.6	9.654	.....	CO_2?	1035.51	396	1059.0	9.440	.....	O_3*	.....
345	1035.7	9.653	.....	O_3	.....					CO_2	1058.95
346	1035.8	9.652	.....	O_3	.....	397	1059.46	9.4363	11	O_3	.....
347	1036.18	9.6483	12	O_3	.....	398	1059.80	9.4332	7	O_3	.....
348	1036.5	9.645	.....	O_3	.....	.....	.....	.....	.....	H_2O§	1060.14
349	1036.75	9.6430	11	O_3	.....	399	1060.21	9.4296	11	O_3	.....
350	1037.0	9.640	.....	.....	.....	400	1060.6	9.427	.....	CO_2	1060.53
.....	.....	.....	.....	.....	.....	401	1061.08	9.4219	12	O_3	.....
351	1037.6‡	9.636	.....	O_3*	.....	402	1061.62	9.4171	10	O_3	.....
				CO_2	1037.46						
352	1037.85	9.6328	10	O_3	.....	403	1061.8	9.415	.....	.....	.....
353	1038.4	9.628	.....	.....	.....	404	1062.22	9.4118	10	.....	.....
354	1038.58	9.6260	12	O_3	.....	405	1062.54	9.4089	12	O_3	.....
355	1039.33	9.6191	9	CO_2?	1039.38	406	1063.19	9.4032	11	O_3	.....
				O_3	.....	407	1063.54	9.4001	12	O_3	.....
356	1039.5‡	9.617	.....	H_2O	1039.53	408	1064.38	9.3927	13	O_3	.....
357	1040.07	9.6122	10	O_3	.....	409	1064.74	9.3895	12	O_3	.....
358	1040.51	9.6082	8	O_3	.....	410	1065.1	9.386	.....	O_3	.....
359	1040.71	9.6063	8	O_3	.....	411	1065.84	9.3798	7	O_3	.....
				CO_2	1041.27	412	1066.15	9.3771	14	H_2O	1066.20
360	1041.2	9.602	.....	O_3	.....	413	1066.80	9.3714	11	O_3	.....
361	1041.6	9.599	.....	.....	.....	414	1067.3	9.367	.....	.....	.....
362	1042.57	9.5892	9	H_2O	1042.57	415	1067.57	9.3646	12	CO_2	1067.56
				CO_2	1043.17	416	1068.20	9.3591	10	.....	.....
363	1043.1‡	9.584	.....	O_3	.....	417	1068.64	9.3552	6	.....	.....
364	1043.68	9.5790	11	O_3	.....	418	1068.9‡	9.353	.....	CO_2	1069.02
365	1044.3	9.573	.....	.....	.....	419	1069.7	9.346	.....	.....	.....
366	1044.63	9.5703	13	O_3	.....	420	1069.96	9.3437	9	.....	.....
				CO_2	1045.03	421	1070.50	9.3390	12	CO_2	1070.48
367	1045.1‡	9.5657	.....	O_3*	.....	422	1070.8	9.336	.....	.....	.....
368	1045.79	9.5597	9	.....	.....	423	1071.6	9.330	.....	.....	.....
369	1046.1	9.556	.....	O_3	.....	424	1071.91	9.3267	10	CO_2	1071.92
370	1046.75	9.5509	12	O_3	.....	425	1072.61	9.3206	11	H_2O	1072.69
371	1047.33	9.5456	9	.....	.....	426	1073.32	9.3144	11	CO_2	1073.30
372	1047.61	9.5431	12	O_3	.....	427	1074.48	9.3044	16	H_2O	1074.46
373	1047.9	9.540	.....	.....	.....	428	1074.99	9.3000	9	.....	.....
374	1048.1‡	9.538	.....	O_3	.....	429	1076.04	9.2909	17	CO_2	1075.98
375	1048.79	9.5323	9	CO_2?	1048.69	430	1076.77	9.2846	7	.....	.....
376	1049.05	9.5300	9	O_3	.....	431	1077.33	9.2798	18	CO_2	1077.29
377	1049.5‡	9.526	.....	O_3	.....	432	1077.83	9.2755	7	.....	.....
378	1050.35	9.5182	10	O_3	.....	433	1078.61	9.2688	17	CO_2	1078.59
379	1050.53	9.5166	6	CO_2?	1050.47	434	1079.0	9.265	.....	.....	.....
380	1050.91	9.5131	10	O_3	.....	435	1079.85	9.2581	12	CO_2	1079.82
.....	.....	.....	.....	H_2O§	1051.28	436	1080.31	9.2542	11	.....	.....

TABLE 1—*Continued*

Line Number	Frequency (Cm^{-1} [Vac])	Wave Length (μ [Air])	No. of Measures	Identification	Lab. Value (Cm^{-1} [Vac])
437	1081.14	9.2471	12	CO_2	1081.05
438	1081.8	9.241	.....	.....	.....
439	1082.32	9.2370	13	CO_2	1082.29
440	1083.1	9.230	.....	.....	.....
441	1083.49	9.2270	12	CO_2	1083.45
442	1083.9	9.223	.....	.....	.....
443	1084.4	9.219	.....	.....	.....
444	1084.64	9.2173	16	CO_2	1084.61
445	1085.18	9.2127	10	.....	.....
446	1085.53	9.2097	17	H_2O	1085.4
447	1085.82	9.2073	15	CO_2	1085.77
448	1086.45	9.2019	8	.....	.....
449	1086.90	9.1981	17	CO_2	1086.86
450	1087.1	9.196	.....	.....	.....
451	1087.61	9.1921	12	.....	.....
452	1088.0	9.189	.....	CO_2 H_2O	1087.96 1088.1
453	1088.46	9.1849	9	.....	.....
454	1089.03	9.1801	15	CO_2	1088.98
455	1089.3	9.178	.....	.....	.....
456	1089.70	9.1745	11	.....	.....
457	1090.07	9.1714	13	CO_2	1090.02
458	1090.48	9.1679	9	.....	.....
459	1091.23	9.1616	19	H_2O	1091.24
460	1091.70	9.1577	7	.....	.....
461	1092.11	9.1542	9	CO_2	1092.11
462	1092.65	9.1497	8	.....	.....
463	1093.08	9.1460	10	CO_2	1093.03
464	1093.4	9.143	.....	.....	.....
465	1093.9	9.139	.....	CO_2	1093.79
466	1094.3	9.136	.....	.....	.....
467	1094.9‡	9.131	.....	CO_2	1094.72
468	1095.51	9.1258	13	CO_2	1095.64
469	1095.95	9.1221	10	.....	.....
470	1096.63	9.1164	12	.....	.....
471	1097.1	9.112	.....	.....	.....
472	1097.63	9.1081	11	.....	.....
473	1098.3	9.102	.....	.....	.....
474	1098.6	9.100	.....	.....	.....
475	1199.69	9.0911	13	H_2O	1099.74
476	1100.2	9.087	.....	.....	.....
477	1100.8	0.082	.....	.....	.....
478	1101.45	9.0766	14	H_2O	1101.47
479	1102.16	9.0707	7	.....	.....
480	1103.33	9.0611	11	.....	.....
481	1104.03	9.0553	12	.....	.....
482	1104.94	9.0479	6	.....	.....
483	1105.39	9.0442	11	.....	.....
484	1106.74	9.0332	12	H_2O	1106.76
485	1107.72	9.0252	11	.....	.....
486	1108.1	9.022	.....	.....	.....
487	1108.55	9.0184	14	.....	.....
488	1109.31	9.0123	11	.....	.....
489	1110.01	9.0066	8	.....	.....
490	1110.7	9.001	.....	.....	.....
491	1111.53	8.9943	15	H_2O	1111.59
492	1112.30	8.9880	7	.....	.....
493	1112.85	8.9836	9	.....	.....
494	1113.28	8.9801	8	.....	.....
495	1113.62	8.9774	8	.....	.....
496	1114.14	8.9732	10	.....	.....
497	1114.65	8.9691	11	.....	.....
498	1115.4‡	8.963	.....	.....	.....
499	1116.21	8.9566	8	.....	.....
500	1116.79	8.9519	8	.....	.....
501	1117.09	8.9495	10	.....	.....
502	1117.68	8.9448	16	H_2O	1117.71
503	1118.08	8.9416	14	.....	.....
504	1118.96	8.9346	13	.....	.....
505	1119.44	8.9307	12	.....	.....
506	1120.95	8.9187	13	H_2O	1120.9
507	1121.25	8.9163	13	H_2O	1121.24
508	1122.46	8.9067	15	.....	.....
509	1123.5	8.898	.....	.....	.....
510	1123.91	8.8952	13	.....	.....
511	1124.33	8.8919	13	.....	.....
512	1124.80	8.8882	6	.....	.....
513	1125.2	8.885	.....	.....	.....
514	1125.56	8.8822	9	.....	.....
515	1126.03	8.8785	15	.....	.....
516	1127.15	8.8696	18	.....	.....
517	1127.88	8.8639	15	.....	.....
518	1128.9	8.856	.....	.....	.....
519	1129.37	8.8522	8	.....	.....
520	1130.00	8.8473	8	.....	.....
521	1130.45	8.8438	9	.....	.....
522	1131.22	8.8377	11	.....	.....
523	1131.9	8.832	.....	.....	.....
524	1132.74	8.8258	14	.....	.....
525	1133.70	8.8183	12	N_2O	1133.68
526	1134.57	8.8116	10	N_2O	1134.41
527	1135.72	8.8017	12	H_2O	1135.80
528	1137.45	8.7893	16	H_2O	1137.46
529	1138.33	8.7825	9	N_2O	1138.32
530	1138.95	8.7777	9	N_2O	1139.10
531	1139.93	8.7702	10	N_2O	1139.87
532	1140.61	8.7649	13	N_2O	1140.66
533	1141.5‡	8.758	.....	N_2O H_2O	1141.45 1141.64
534	1142.17	8.7530	11	N_2O	1142.24
535	1143.03	8.7464	7	N_2O	1143.00
536	1143.4	8.744	.....	.....	.....
537	1143.78	8.7406	15	N_2O	1143.80
538	1144.59	8.7345	12	N_2O	1144.58
539	1145.38	8.7284	11	N_2O	1145.38
540	1145.9	8.724	.....	.....	.....
541	1146.2	8.722	.....	N_2O	1146.18
542	1147.0‡	8.716	.....	N_2O	1146.96
543	1147.77	8.7103	11	N_2O	1147.78
544	1148.61	8.7039	10	N_2O	1148.56
545	1149.46	8.6975	12	H_2O	1149.48
546	1150.1	8.693	.....	N_2O	1150.15
547	1151.00	8.6858	8	N_2O	1150.96
548	1151.59	8.6814	11	H_2O	1151.59
549	1152.46	8.6748	10	H_2O	1152.44
550	1153.25	8.6689	10	N_2O	1153.36
551	1154.19	8.6618	12	N_2O	1154.18
552	1154.6	8.659	.....	.....	.....
553	1155.0	8.656	.....	N_2O	1154.98
554	1155.74	8.6502	11	N_2O	1155.80

TABLE 1—*Continued*

Line Number	Frequency (Cm^{-1} [Vac])	Wave Length (μ [Air])	No. of Measures	Identification	Lab. Value (Cm^{-1} [Vac])
555	1156.58	8.6439	12	N_2O	1156.60
556	1157.39	8.6379	14	N_2O	1157.40
557	1158.22	8.6317	13	N_2O	1158.23
558	1159.04	8.6256	15	N_2O	1159.06
559	1159.8‡	8.620	.....	N_2O	1159.90
560	1160.68	8.6134	9	N_2O	1160.70
561	1161.6‡	8.607	.....	N_2O	1161.52
562	1162.4‡	8.601	.....	N_2O	1162.34
563	1163.1	8.595	.....	N_2O	1163.15
564	1163.7	8.591	.....	.....	.....
565	1164.0	8.589	.....	N_2O H_2O?*	1163.98
566	1165.27	8.5795	10	H_2O	1165.31
567	1165.4	8.578	.....	H_2O	1165.40†
568	1165.93	8.5746	11	H_2O	1165.9
569	1166.6	8.570	.....	.....	.....
570	1167.02	8.5666	13	H_2O	1167.04
571	1169.3	8.550	.....	H_2O	1169.4
572	1170.1‡	8.544	.....	N_2O H_2O?*	1169.71
573	1170.9‡	8.538	.....	N_2O	1170.56
574	1171.5	8.534	.....	H_2O* N_2O	1171.4 1171.46
575	1172.4	8.527	.....	N_2O	1172.31
576	1173.8	8.517	.....	H_2O	1173.76
577	1174.5	8.512	.....	H_2O	1174.54
578	1175.7	8.503	.....	N_2O H_2O?§	1175.74 .....
579	1176.6	8.497	.....	N_2O	1176.59
580	1177.41	8.4910	8	N_2O	1177.45
581	1178.4	8.484	.....	N_2O	1178.31
582	1178.68	8.4818	9	H_2O	1178.55
583	1179.19	8.4782	9	N_2O	1179.19
584	1180.11	8.4716	8	N_2O	1180.05
585	1180.8	8.467	.....	H_2O* N_2O	1180.75 1180.96
586	1181.82	8.4593	9	N_2O	1181.81
587	1182.67	8.4532	8	N_2O	1182.69
588	1183.60	8.4466	8	N_2O	1183.55
589	1184.2‡	8.442	.....	H_2O* N_2O	1184.14 1184.41
590	1185.4	8.434	.....	N_2O	1185.28
591	1185.8	8.431	.....	H_2O?	.....
592	1186.2	8.428	.....	N_2O	1186.15
593	1187.00	8.4224	9	H_2O	1187.00
594	1188.81	8.4096	8	N_2O	1188.79
595	1189.66	8.4036	8	N_2O	1189.65
596	1190.5	8.398	.....	N_2O H_2O?	1190.56 .....
597	1191.3	8.392	.....	H_2O* N_2O	1191.16 1191.44
598	1192.16	8.3860	7	N_2O	1192.30
599	1192.77	8.3817	9	CH_4	1192.90
600	1193.57	8.3760	9	H_2O	1193.67
601	1194.09	8.3724	8	N_2O	1194.09
602	1195.03	8.3658	8	N_2O CH_4	1194.97 1195.05
603	1195.42	8.3631	14	H_2O	1195.41
604	1196.3	8.357	.....	H_2O?* CH_4	..... 1196.41
605	1196.9	8.353	.....	.....	.....
606	1199.9	8.3438	15	H_2O	1198.22
607	1200.3	8.329	.....	.....	.....
608	1200.97	8.3244	8	H_2O	1200.80
609	1201.51	8.3207	11	H_2O	1201.55
610	1202.60	8.3132	7	CH_4	1202.54
611	1203.6	8.306	.....	.....	.....
612	1204.6	8.299	.....	.....	.....
613	1205.10	8.2959	11	H_2O?	.....
614	1206.07	8.2893	12	H_2O	1206.17
615	1206.37	8.2872	7	H_2O?	.....
616	1207.30	8.2808	10	H_2O	1207.35
617	1207.88	8.2768	10	CH_4	1207.91
618	1208.3	8.274	.....	.....	.....
619	1208.77	8.2707	10	H_2O?	.....
620	1209.26	8.2673	10	H_2O?	.....
621	1210.1‡	8.262	.....	H_2O CH_4	1209.79 1210.03
622	1211.32	8.2533	8	H_2O	1211.29
623	1212.23	8.2471	8	H_2O	1212.28
624	1214.3	8.233	.....	.....	.....
625	1214.97	8.2285	11	H_2O	1214.91
626	1215.52	8.2248	10	H_2O?	.....
627	1216.24	8.2199	10	CH_4	1216.37
628	1216.67	8.2170	6	CH_4	1216.7
629	1217.5	8.211	.....	.....	.....
630	1218.51	8.2046	11	H_2O	1218.63
631	1219.68	8.1967	11	CH_4	1219.78
632	1220.4	8.192	.....	CH_4 H_2O	1220.30 1220.43
633	1221.05	8.1875	12	CH_4	1220.97
634	1221.90	8.1818	12	CH_4	1221.99
635	1222.69	8.1765	12	CH_4	1222.79
636	1223.4‡	8.172	.....	CH_4	1223.38
637	1224.1	8.167	.....	CH_4	1224.08
638	1224.95	8.1615	7	H_2O	1225.08
639	1225.5	8.158	.....	H_2O	1225.5
640	1226.0	8.154	.....	H_2O	1226.1
641	1226.87	8.1487	12	.....	.....
642	1228.83	8.1357	11	CH_4	1228.82
643	1229.36	8.1322	9	CH_4 H_2O*	1229.38 1229.43
644	1230.09	8.1274	8	CH_4	1230.09
645	1232.76	8.1098	9	.....	.....
646	1233.43	8.1054	9	H_2O* CH_4	1233.31 1233.44
647	1235.2	8.094	.....	H_2O	1235.23
648	1236.03	8.0883	8	CH_4	1235.98
649	1236.31	8.0865	8	CH_4	1236.5
650	1237.11	8.0813	10	H_2O	1237.20
651	1237.98	8.0756	10	CH_4	1238.02
652	1238.76	8.0705	8	CH_4	1238.70
653	1239.20	8.0676	10	H_2O	1239.25
654	1239.97	8.0626	10	.....	.....
655	1240.94	8.0563	10	CH_4	1241.01
656	1241.91	8.0500	9	CH_4	1241.92
657	1242.79	8.0443	8	H_2O	1242.90
658	1243.41	8.0403	8	CH_4	1243.34
659	1243.92	8.0370	8	H_2O	1244.18
660	1244.28	8.0347	8		
661	1244.7	8.032	.....	H_2O	1244.77

TABLE 1—*Continued*

Line Number	Frequency (Cm^{-1} [Vac])	Wave Length (μ [Air])	No. of Measures	Identification	Lab. Value (Cm^{-1} [Vac])
662	1245.2	8.029	.....	CH_4	1245.26
663	1245.75	8.0252	10	CH_4	1245.79
664	1246.51	8.0203	10	CH_4	1246.47
665	1247.80	8.0120	9	CH_4	1247.79
666	1248.51	8.0074	10	H_2O	1248.52
667	1249.24	8.0028	7	.....	.....
668	1249.69	7.9999	9	CH_4	1249.64
669	1250.0	7.998	.....	CH_4	1249.95
670	1250.69	7.9935	10	N_2O	1250.57
671	1251.4	7.989	.....	H_2O*	1251.43
				N_2O	1251.57
672	1252.4	7.982	.....	H_2O*	1252.44
				N_2O	1252.53
673	1253.7	7.974	.....	H_2O*	1253.67
				CH_4	1253.77
674	1254.54	7.9690	13	N_2O	1254.47
				H_2O§ ?	.....
675	1254.95	7.9664	11	CH_4	1255.05
676	1255.44	7.9632	16	N_2O	1255.44
677	1256.0	7.959	.....	H_2O	1255.95
678	1256.53	7.9563	15	N_2O	1256.39
				CH_4	1256.60
679	1257.23	7.9519	15	H_2O	1257.07
				N_2O	1257.33
680	1258.4	7.945	.....	N_2O	1258.27
681	1258.6	7.943	.....	H_2O	1258.63
682	1259.4	7.938	.....	N_2O	1259.19
683	.....	.....	.....	CH_4	1259.74
				H_2O*	1260.38
				CH_4	1260.8
684	1261.7	7.924	.....	CH_4	1261.69
685	1262.0	7.922	.....	N_2O	1261.96
				CH_4	1262.19
686	1262.97	7.9158	13	N_2O	1262.91
687	1263.35	7.9134	14	CH_4	1263.33
688	1263.9	7.910	.....	N_2O*	1263.82
				H_2O	1264.04
689	1264.8	7.904	.....	N_2O	1264.74
690	1265.54	7.8997	10	H_2O*	1265.42
				CH_4	1265.50
691	1266.03	7.8966	4	H_2O	1266.11
692	1266.5	7.894	.....	N_2O	1266.59
				H_2O	1266.63
693	1267.9	7.885	.....	CH_4	1267.84
694	1268.2	7.883	.....	H_2O	1268.40
695	1269.0	7.878	.....	CH_4	1268.95
696	1269.4	7.876	.....	N_2O	1269.33
697	1270.1	7.872	.....	H_2O	1269.97
698	.....	.....	.....	CH_4	1270.83
				H_2O	1271.80
				H_2O	1272.37
699	1272.9	7.854	.....	N_2O	1272.88
				H_2O	1273.1
700	1273.56	7.8500	10	N_2O	1273.75
701	1274.67	7.8431	11	N_2O	1274.61
702	1275.09	7.8406	10	CH_4	1275.09
703	1275.4	7.839	.....	CH_4	1275.4
				N_2O	1275.47
704	1276.45	7.8322	9	N_2O	1276.35
705	1276.86	7.8297	10	CH_4	1276.85
706	1277.32	7.8269	13	CH_4	1277.47
707	1278.08	7.8222	13	N_2O	1278.02
708	1279.00	7.8166	13	N_2O	1278.91
709	1280.0	7.810	.....	H_2O	1280.09
710	1280.56	7.8071	8	N_2O	1280.55
711	1281.3	7.803	.....	H_2O	1281.22
712	1281.57	7.8009	8	CH_4	1281.61
713	1282.69	7.7941	8	CH_4	1282.7
714	1283.12	7.7915	7	CH_4	1283.1
715	1283.46	7.7894	7		
716	1284.30	7.7843	12	H_2O	1284.37
717	1286.06	7.7736	12	.....	.....
718	1286.63	7.7702	6	N_2O	1286.54
				CH_4	1286.62
719	.....	.....	.....	H_2O	1287.38
				H_2O	1288.28
720	1288.9	7.756	.....	H_2O	1288.92
721	1289.88	7.7506	10	CH_4	1289.74
				N_2O	1289.86
722	1290.51	7.7468	10	H_2O	1290.59
723	1291.40	7.7415	9	N_2O	1291.42
724	1292.5	7.735	.....	H_2O	1292.40
725	1292.8	7.733	.....	CH_4	1292.64
726	1293.1	7.732	.....	N_2O	1293.08
727	1293.92	7.7264	8	N_2O	1293.86
728	1294.7‡	7.722	.....	CH_4	1294.46
				N_2O	1294.66
729	1295.4	7.718	.....	CH_4	1295.25
				N_2O	1295.48
730	1296.7	7.710	.....	H_2O	1296.67
731	1297.1	7.705	.....	.....	.....
732	1297.56	7.7048	7	CH_4	1297.62
733	1298.5	7.699	.....	N_2O	1298.62
734	1299.6	7.693	.....	CH_4	1299.75
735	1300.0	7.690	.....	N_2O	1300.15
				CH_4	1300.28
736	1300.98	7.6845	6	N_2O	1300.92
737	1301.7	7.680	.....	CH_4	1301.6
738	1303.0	7.673	.....	CH_4	1302.89
739	1303.6	7.669	.....	CH_4	1303.55
740	1304.8	7.662	.....	CH_4?	.....
741	.....	.....	.....	H_2O	1305.60
				CH_4	1305.8
742	1306.9	7.650	.....	N_2O	1306.85
743	1308.1‡	7.643	.....	H_2O	1308.25
744	1308.5	7.640	.....	.....	.....
745	1309.2	7.636	.....	N_2O*	1309.11
				CH_4	1309.3
746	1309.77	7.6329	6	N_2O	1309.88
747	1310.60	7.6281	7	N_2O	1310.61
748	1311.5	7.623	.....	CH_4	1311.48
749	.....	.....	.....	H_2O	1312.61
				H_2O	1313.64

TABLE 1—*Continued*

Line Number	Frequency (Cm^{-1} [Vac])	Wave Length (μ [Air])	No. of Measures	Identification	Lab. Value (Cm^{-1} [Vac])
750	1314.9	7.603	....	H_2O	1314.82
751	1315.7	7.599	....	N_2O?	
752	1317.1	7.591	....	H_2O	1317.04
753			....	H_2O	1318.97
754	1320.1	7.574	....	H_2O	1320.09
755	1320.9	7.569	....	H_2O	1320.90
756	1322.15	7.5615	5	CH_4	1322.18
757	1323.38	7.5544	7	H_2O	1323.31
758	1324.2	7.550	....	H_2O	1324.30
759	1324.8	7.546	....	N_2O?	
760	1326.09	7.5390	9	H_2O	1326.14
761	1327.2	7.532	....	CH_4	1327.17
762	1327.9	7.528	....	H_2O	1327.72
763	1329.6	7.519	....		
764	1329.89	7.5174	6	H_2O	1329.90
765	1332.2	7.505	....	CH_4	1332.3
766	1332.4	7.504	....	CH_4	1332.5
767	1332.6	7.502	....	H_2O	1332.70
768	1333.45	7.4974	5		
769	1334.27	7.4928	6		
770	1335.56	7.4855	5	H_2O	1335.55
771	1336.6	7.479	....	H_2O	1336.64
				CH_4	1337.71
				H_2O	1338.56
772			....	H_2O	1339.23
				H_2O	1339.55
				H_2O	1340.35
773	1341.7	7.451	....	CH_4	1341.75
774	1342.7	7.445	....	CH_4	1342.77
775	1343.6	7.440	....		
776	1344.1	7.438	....	H_2O*	1344.04
777	1344.8	7.434	....	H_2O	1344.60
778	1345.6	7.429	....	H_2O	1345.59
779	1346.9	7.422	....	CH_4	1346.67
780	1348.0	7.416	....	CH_4	1347.99
781	1349.4	7.409	....	H_2O	1349.0
				H_2O	1349.39
782	1351.0	7.400	....	CH_4	1351.13
783	1351.4	7.398	....	CH_4	1351.6
784	1351.8	7.395	....	H_2O	1351.67
785	1352.41	7.3923	9	H_2O	1352.41
786	1353.20	7.3880	9	CH_4	1353.17
787			....	H_2O*	1354.87
				CH_4	1355.47
788	1356.0	7.373	....	H_2O	1356.0
789	1356.6	7.369	....	CH_4	1356.5
790	1357.1	7.367	....	H_2O	1357.21
791	1358.2	7.361	....	H_2O	1358.06
792	1359.0	7.356	....		
793	1360.0	7.351	....	CH_4	1360.02
794			....		
795	1365.1	7.324	....	CH_4	1365.08
796	1366.1	7.318	....	CH_4	1366.04
797			....	H_2O	1368.60
				H_2O	1369.78
798	1371.0	7.292	....	H_2O	1370.95
799			....	H_2O	1372.28
				H_2O	1373.76
				H_2O	1375.09
800	1375.7	7.267	....		
801	1377.0	7.260	....	CH_4	1377.1
802	1378.2	7.254	....	H_2O	1378.04
803	1379.7‡	7.246	....	H_2O	1379.63
804	1381.5	7.236	....	CH_4	1381.28
805	1382.15	7.2332	5	H_2O	1382.11
806	1383.40	7.2267	5	H_2O	1383.40
807			....	H_2O	1386.51
				H_2O	1387.55
808	1390.0	7.192	....	H_2O	1390.0
809	1390.8	7.188	....	H_2O	1390.95
				H_2O	1394.50
810			....	H_2O	1395.81
				H_2O	1397.74
				H_2O	1399.16
811	1402.9	7.126	....		
812	1403.7	7.122	....	H_2O	1403.54
813			....	H_2O	1404.98
814	1408.53	7.0977	4	H_2O	1408.51
815	1410.00	7.0903	4	H_2O	1409.94
816	1411.8	7.081	....	H_2O	1411.52
				H_2O	1411.91
817	1414.97	7.0654	5	H_2O	1414.99
818	1416.09	7.0598	5	H_2O	1416.11
				H_2O	1417.39
819			....	H_2O	1419.3
				H_2O	1423.90
				H_2O	1425.83
				H_2O	1428.31
				H_2O	1429.97
				H_2O	1432.06
820			....	H_2O	1433.31
				H_2O	1435.77
				H_2O	1436.72
				H_2O	1440.64
821	1441.3	6.936	....	H_2O	1441.42
822	1442.8	6.929	....	H_2O	1442.80

values are usually caused by overlapping lines in the solar spectrum which disturb the center of the measured line. Lines lying on the sides of strong lines generally have their frequencies shifted in the direction of the more intense absorption.

III. ABSORPTION BANDS OF INDIVIDUAL GASES

A. WATER VAPOR

The large number of absorption lines of H_2O between 4.5 μ and 13 μ accounts for a considerable fraction of the total atmospheric absorption observed in this region of the solar spectrum. The most intense H_2O lines lie close to the center of the ν_2 band at 1595 cm^{-1}, but, because of the large amount of H_2O in the atmosphere, many other weaker lines have also been observed in the solar spectrum throughout the entire region from 7 μ to 13 μ. Most of the lines in this region were also observed in the laboratory by using an 8-meter path of steam at 110° C and near atmospheric pressure.[4] Because the largest amount of H_2O used in the laboratory was less than that usually present in the atmosphere and since it was at a higher temperature (110° C, compared with about 10° C) the relative intensities of neighboring lines in the laboratory spectrum are sometimes very different from corresponding lines in the solar spectrum. In a few instances lines are completely absent from one set of spectra (i.e., have maximum absorptions of less than 2–3 per cent).

In the description of the H_2O spectrum, transitions were assigned to nearly all the lines, and line intensities were calculated. It was found that the intensity variations between the solar and the laboratory spectra could be well accounted for on the basis of path length and temperature differences. It was also possible to predict the appearance of several lines in the solar spectrum which did not appear in the laboratory spectrum. Lines identified in this manner are marked † in Table 1. A few atmospheric lines, not observed in the laboratory spectrum of H_2O, also vary in intensity with the amount of atmospheric H_2O and have been assigned to H_2O but are marked "(?)."

At Columbus no solar radiation has been detected in the region between 5.5 μ and 7.0 μ, which contains the most intense lines of the ν_2 fundamental. Between 7 μ and 8 μ the solar radiation reaching ground level is strongly dependent on the atmospheric H_2O content. During the summer months very little radiation can be detected, and most of the spectrum shown in Figure 7 was observed on one very cold day in February, 1951. In the region from 7.8 μ to 8.2 μ there are, in addition, strong bands of N_2O and CH_4, which further reduce the radiation reaching ground level. The resolving power of the instrument was not adequate to permit a complete interpretation of the structure in this region.

At wave lengths longer than 8 μ the lines of the ν_2 band become less numerous, although some are still very intense and obscure portions of the 8.6 μ N_2O and the 9.4 μ CO_2 bands. Between 9.5 μ and 10.5 μ absorption by water vapor is at a minimum. The strong ozone band lies in this region of minimum absorption, and the few H_2O lines which are present are not resolved from the fine structure of this band. They were identified by noting variations in absorption in the band in spectra taken in summer and winter. At longer wave lengths the intensity and number of lines increase, the majority being due to transitions between pure rotational levels of the H_2O molecule. Apart from the two weak CO_2 bands at 10.4 μ and 12.6 μ, almost all the structure observed in the solar spectrum from 10.5 μ to 13 μ has been identified with H_2O. Many of these lines are visible on Adel's spectrum[2] and also the prismatic spectrum in Figure 1.

Isotopic molecules.—The relative proportions of the most abundant isotopes of water vapor relative to H_2O^{16} are given in Table 2.

The other isotopic molecules are relatively rare, and their absorption lines are cor-

[4] W. S. Benedict, H. H. Claassen, and J. H. Shaw, *J. Res. Nat. Bur. Stand., Washington* (in press).

respondingly weaker than similar lines of H_2O^{16}. As absorptions less than 2–3 per cent are not visible in our spectra, only the most intense lines of isotopic molecules are expected to be observed. This conclusion agrees with the laboratory data,[4] where almost all the observed lines of water vapor between 4.5 μ and 13 μ which show more than 50 per cent maximum absorption were assigned to the H_2O^{16} molecule.

H_2O^{17} and H_2O^{18}.—Between 4.5 μ and 13 μ the most intense lines of water vapor are those of low J value in the ν_2 fundamental which lie near the center of the band. These lines of the H_2O^{16} molecule give complete absorption in the solar spectrum between 5.0 μ and 7.5 μ during most of the year in Columbus. Since the lines of the molecules H_2O^{17} and H_2O^{18} are displaced only a few wave numbers below the corresponding lines of H_2O^{16}, the strongest lines of these molecules are usually hidden by neighboring lines of H_2O^{16} and are not visible in the solar spectrum. A few lines of H_2O^{18} have been tentatively identified in the laboratory spectrum, where smaller amounts of water vapor could be used.

Most of the lines of these molecules which lie farther away from the center of the band are too weak to be observed, although some of the weak water-vapor lines in the solar spectrum may be due to these molecules.

HDO.—There is sufficient *HDO* in the atmosphere for strong bands of this molecule to appear in solar spectra. The ν_1 fundamental at 3.7 μ has already been observed in atmospheric spectra.[5,6] The ν_2 fundamental is considerably shifted from the ν_2 band of

TABLE 2

Isotope	Relative Abundance	Isotope	Relative Abundance
H_2O^{16}	2,500	H_2O^{18}	5
H_2O^{17}	1	HDO^{16}	1

H_2O^{16} and lies at 6.8 μ. Adel[7] has already identified an absorption in this region of his solar spectrum with this band. During most of the year, no radiation in the 6.8 μ region can be detected at Columbus, but on cold winter days some radiation can be detected down to 7 μ. Most of the lines observed have been identified with lines in the ν_2 fundamental of H_2O^{16}, and it has been shown[4] that the strongest lines in the *HDO* band are expected to be several times weaker than neighboring H_2O lines. Although some of the weak lines in this region may be due to *HDO*, most of the structure must be due to H_2O^{16}.

It must be concluded that H_2O^{16} is the only species of water molecule that plays a significant role in the absorption of solar radiation in the region from 4 μ to 13 μ.

B. CARBON DIOXIDE

Several weak CO_2 bands appear between 7 μ and 13 μ in the solar spectrum, and a series of bands, including the strong ν_2 fundamental at 15 μ, give complete absorption beyond 13.5 μ in the solar spectrum observed at ground level. Laboratory spectra of an 8-meter path length of CO_2 at atmospheric pressure were used to identify the CO_2 lines in the solar spectrum.

9.4 μ (001-02^{0}0) and 10.4 μ (001-10^{0}0) bands.—These bands have previously been observed in the laboratory by Barker and Adel[8] and in the solar spectrum by Adel.[9] Many of the rotational lines have been identified in the present solar spectrum, although most of the P branch of the 9.4 μ band is hidden by the much more intense O_3 absorption. The rest of this band and the 10.4 μ band lie in comparatively transparent regions, where only a few H_2O lines are present.

[5] H. A. Gebbie, W. R. Harding, C. Hilsum, and V. Roberts, *Phys. Rev.*, **76**, 1534, 1949.

[6] R. M. Chapman and J. H. Shaw, *Phys. Rev.*, **78**, 71, 1950.

[7] *Ap. J.*, **93**, 506, 1941. [8] *Phys. Rev.*, **44**, 185, 1933. [9] *Ap. J.*, **94**, 379, 1941.

CO_2 bands near 13 μ.—A weak band of CO_2 (11^10–02^00) occurs near 12.6 μ in the solar spectrum. The *Q* branch appears to be partially resolved in Figure 2 (lines *42–46*), and many weak lines of the *P* and *R* branches are also visible, although several are hidden by H_2O lines. In addition, a few lines of CO_2 are present at the beginning of the map in Figure 2, which Adel[10] has identified with the (11^10–02^20) band centered at 13.9 μ.

The CO_2 bands between 7 μ and 13 μ belong to the molecule $C^{12}O_2^{16}$. No bands of other isotopic molecules have been observed.

C. METHANE

Methane was first shown to be a constituent of the atmosphere by Migeotte,[11] who identified lines of the ν_3 fundamental at 3.3 μ in the solar spectrum. Goldberg[12] has shown that there are approximately 1.2 atmo-cm of gas in a vertical column through the atmosphere. The laboratory spectrum of 15 atmo-cm of CH_4 revealed only one band between 7 μ and 13 μ, the strong ν_4 fundamental at 7.8 μ. Although this band is overlapped by bands of N_2O and H_2O in the solar spectrum, a considerable fraction of the total absorption in this region is caused by atmospheric CH_4. Because of the intense absorption of H_2O at the short-wave-length side of the band, only a few lines in the *R* branch have been observed; however, the intense *Q* branch is clearly visible in Figure 7 at 1306 cm^{-1} (lines *737–741*) and many of the other lines in this figure have been identified with CH_4.

Isotopes.—The next most abundant isotope to $C^{12}H_4$ is $C^{13}H_4$ (1:100), but the ν_4 fundamental of this molecule is shifted only a few wave numbers from that of $C^{12}H_4$. It has not been observed in the laboratory, and, as it lies in a region of strong absorption in the solar spectrum, it has not been identified.

The ν_4 fundamental of CH_3D has been observed at 1156.0 cm^{-1}.[13] Since this molecule is expected to be 1200 times less abundant than CH_4, its bands are extremely weak. Although there is an unidentified line at 1154.6 cm^{-1} in our solar spectrum, it seems improbable that this line could be identified with the *Q* branch of this band.

D. NITROUS OXIDE

Estimates of the abundance of atmospheric N_2O suggest that there is about 0.4 atmo-cm present.[14] This is sufficient for the ν_1 fundamental at 7.8 μ to appear strongly in the solar spectrum and the overtone band $2\nu_2$ at 8.6 μ to be observed as a weak absorption. Although the ν_1 fundamental is the more intense band, it is obscured in the solar spectrum by overlapping bands of CH_4 and H_2O, and only a few lines have been identified. The much weaker $2\nu_2$ band lies in a comparatively transparent atmospheric window, and many more lines of this band have been observed. However, several intense H_2O lines in this region obscure many of the N_2O lines, especially during the summer months.

Adel[15] first suggested that the absorption at 7.8 μ in his solar spectra was due to atmospheric N_2O, and since then many other bands of this gas have been observed. In particular, Migeotte[16] has identified lines of the 8.6 μ band by comparison with the laboratory spectrum obtained by Plyler and Barker.[17] We have identified further lines of this band with the aid of our own laboratory spectrum.

[10] *Ap. J.*, **94**, 375, 1941.

[11] *Phys. Rev.*, **73**, 519, 1948; *Ap. J.*, **107**, 400, 1948.

[12] *Ap. J.*, **113**, 567, 1951.

[13] G. Herzberg, *Molecular Spectra and Molecular Structure*, Vol. **2**: *Infrared and Raman Spectra of Polyatomic Molecules* (New York: D. Van Nostrand Co., Inc., 1945), p. 274.

[14] R. R. McMath and L. Goldberg, *Proc. Amer. Phil. Soc.*, **93**, 362, 1949.

[15] *Ap. J.*, **88**, 186, 1938; **90**, 627, 1939.

[16] *Ap. J.*, **112**, 136, 1950.

[17] *Phys. Rev.*, **38**, 1827, 1931.

E. OZONE

The intense absorption of O_3 at 9.6 μ is clearly visible in both the prismatic and the grating solar spectra (Figs. 1 and 5). Most of the structure between 9.4 μ and 10.1 μ is believed to be due to O_3, with the exception of some lines of the P branch of the 9.4 μ CO_2 band and some H_2O lines. The CO_2 lines in this region are weak, and very few have been positively identified. The interfering lines of H_2O are also weak and appear to be considerably wider than the O_3 lines. This is probably due to pressure broadening, since the atmospheric H_2O occurs at much lower altitudes than the O_3. The interfering H_2O lines have not been fully resolved, although they do enhance the absorption of neighboring O_3 lines. By comparing solar spectra taken in winter and summer, differences in absorption can be observed, which show the presence of H_2O lines. Where such identifications have been made, the H_2O lines have been included in Table 1, marked §.

The remaining structure is believed to be entirely due to O_3. This identification was made with the aid of a laboratory spectrum of the 9.6 μ band of O_3 obtained by Dr. E. E. Bell, of the Department of Physics and Astronomy, Ohio State University, using the present apparatus. Although the laboratory spectrum did not show the same resolution as the solar spectrum, the main details are very similar, so that most of the stronger lines in the solar spectrum are positively identified with O_3.

Solar spectra taken during March, 1951, give indications of a weak atmospheric band at 9 μ. These lines were more intense than at other seasons of the year, but their origin is not yet known. It is possible that the lines may also be due to O_3 since a weak O_3 band at 1110 cm^{-1} has been observed by Wilson and Badger.[18]

F. UNIDENTIFIED LINES BETWEEN 7 μ AND 13 μ

Inspection of Figures 2–7 and Table 1 shows that very few of the observed lines remain to be identified. With the exception of the series of lines near 9μ, most of the remaining unidentified lines are weak and do not appear to be part of any band system. The unidentified lines near 9 μ may be due to a hitherto unsuspected atmospheric gas, but this appears improbable, since none of the suggested polyatomic constituents of the atmosphere have intense bands in this region of the spectrum.

G. OTHER POLYATOMIC ATMOSPHERIC CONSTITUENTS

The present work has included investigations of laboratory spectra of several gases which have been suggested as possible atmospheric constituents. These studies included ethane, C_2H_6 (11.9 μ band); ethylene, C_2H_4 (10.5 μ); ammonia, NH_3 (10.7 μ); cyanogen, C_2N_2 (4.6 μ); sulphur dioxide, SO_2 (8.6 μ); nitric oxide, NO (5.3 μ) and nitrogen dioxide, NO_2 (3.4μ). When these spectra were compared with the solar spectrum, no indication of any absorption due to these gases could be found in the latter. These results indicate that the abundances of these gases, if they are present in the atmosphere, must be considerably smaller than those of the other minor constituents, such as CH_4 or N_2O.

[18] *J. Chem. Phys.*, **16**, 741, 1948.

STATISTICS OF STELLAR COLOR EXCESSES. I

GUIDO MÜNCH
MOUNT WILSON AND PALOMAR OBSERVATORIES
CARNEGIE INSTITUTION OF WASHINGTON
CALIFORNIA INSTITUTE OF TECHNOLOGY
Received August 1, 1952

ABSTRACT

In this paper the color excesses of stars are analyzed statistically with a view to deriving information regarding the main characteristics of the distribution of interstellar reddening dust. The problem of describing a given collection of color excesses in terms of the discrete cloud of Ambarzumian is considered in detail. It is shown how any frequency-curve of observed color excesses of stars in a fixed distance range can be uniquely interpreted in terms of a probability density for the color excesses that individual clouds may produce. On the basis of the color observations of Stebbins, Huffer, and Whitford, an attempt has been made to evaluate the mean value, the standard deviation, and the skewness of the optical thicknesses of the hypothetical interstellar clouds.

1. *Introduction.*—The color excess $E(\mathbf{r})$ of a star with position vector $\mathbf{r}$, with respect to the observer, and referred to a certain wave-length interval (λ_1, λ_2), is defined in terms of the density $\rho(\mathbf{r})$ of the interstellar reddening dust along the line of sight by

$$E(\mathbf{r}) = c\int_0^r \rho(\mathbf{r})\,[\kappa(\lambda_1, \mathbf{r}) - \kappa(\lambda_2, \mathbf{r})]\,d\mathbf{r}\,, \tag{1}$$

where $c = \log_{10}e^{5/2}$, $r = |\mathbf{r}|$, and $\kappa(\lambda, \mathbf{r})$ is the mass-absorption coefficient of the interstellar dust at the point $\mathbf{r}$ for light of wave length λ. The relation expressed by equation (1) may be considered as an integral equation,

$$E(\mathbf{r}) = \int_0^r \eta(\mathbf{r})\,d\mathbf{r}\,, \tag{2}$$

for the determination of the differential volume-absorption coefficient,

$$\eta(\mathbf{r}) = c\,\rho(\mathbf{r})\,[\kappa(\lambda_1, \mathbf{r}) - \kappa(\lambda_2, \mathbf{r})]\,, \tag{3}$$

as a function of position and in terms of observational values of $E(\mathbf{r})$.

It is well known that the observed values of $E(\mathbf{r})$ do not show a "smooth" dependence on position; rather, they vary from point to point in an irregular fashion. For this reason the observed properties of $E(\mathbf{r})$ are usually described by means of its average dependence on distance, $\bar{E}_{l,b}(r)$, for directions with galactic co-ordinates l and b confined to a certain region. The most recent numerical determinations of $\bar{E}(r)$ have been carried out by P. J. Van Rhijn[1] and N. F. Florja.[2] It is clear, however, that the description of $E(\mathbf{r})$ by means of average values can be made more complete if the whole distribution of individual color excesses around their mean is also given as a function of distance. The problem then arises as to what can be said regarding the variations in space of $\eta(\mathbf{r})$, when an observed distribution of $E(\mathbf{r})$ is given.

A very simple interpretation for the mean, $\bar{E}(r)$, and the variance, $\delta^2(r)$, of $E(\mathbf{r})$ in the galactic plane can be given in terms of the discrete cloud model first advanced by

[1] *Pub. Kapteyn Astr. Lab.*, No. 53, 1949.

[2] *Pub. Sternberg Astr. Inst.*, Vol. **16**, Part 1, 1949.

Ambarzumian[3] for the structure of the interstellar medium. In this model the distribution of interstellar absorbing matter is idealized by a set of cloudlike units distributed homogeneously at random in the galactic plane. The number $n(r)$ of clouds intercepted by the line of sight out to a distance r is then considered as a random variable, with probability p_n given by

$$p_n = e^{-\nu r} \frac{(\nu r)^n}{n!} \qquad (n = 0, 1, 2, \ldots), \quad (4)$$

where ν is the expected number of clouds per unit distance. If it is supposed that every cloud produces the same color excess e_0, we may write, for r in the galactic plane,

$$E(r) = e_0 n(r); \quad (5)$$

and, accordingly,

$$\bar{E}(r) = e_0 \bar{n}(r) = e_0 \nu r, \quad (6)$$

$$\delta^2(r) = \overline{E^2}(r) - \bar{E}^2(r) = e_0^2 \nu r.$$

On the basis of equations (6), Van Rhijn[4] and also E. Schatzman[5] have shown that the values of $\bar{E}(r)$ and $\delta(r^2)$ as derived from the observations can be interpreted consistently in terms of the parameters e_0 and ν, as evaluated from the study of other observables of interstellar matter (e.g., diffuse nebulae, brightness fluctuations of the Milky Way, variations in the surface density of extragalactic nebulae at intermediate latitudes). The consistency with which Ambarzumian's model accounts for certain features of the observed color-excess distribution obviously does not prove that interstellar matter is actually concentrated in isolated clouds. One would expect, however, that further study of equation (2), considered as a relation between two random variables, will eventually enable us to derive a reliable representation for $\eta(r)$. The first step toward this aim is to show that not only the mean and the variance but also any observed distribution of $E(r)$ can be interpreted on the basis of Ambarzumian's model. This is essentially the object of the present paper.

2. *The probability distribution of color excesses of stars at a fixed distance.*—Consider a star in the galactic plane at a distance r from the observer in a certain direction. Let C_j, $(j = 1, 2, \ldots, n)$, denote any of n points distributed at random and independently of one another in the interval $(0, r)$. The points C_j will be called clouds and their number $n = n(r)$ will be considered, then, as a random variable with probability p_n given by equation (4). Let us suppose, now, that the function $\eta(r)$ appearing in equation (2) vanishes in the interval $(0, r)$, except at the points C_j, where it takes values such that

$$E(r) = \int_0^r \eta(r)\, dr = \sum_{j=1}^{n(r)} E_j. \quad (7)$$

The quantities E_j will be identified with the color excess produced by the cloud C_j and will be measured in terms of a certain unit ϵ. Let us now consider the E_j's as independent random variables which take discrete[6] values $m\epsilon$ $(m = 0, 1, 2, \ldots)$ with probability

[3] A summary of the work which led to the discrete-cloud hypothesis has been given recently by V. A. Ambarzumian in *Trans. Internat. Astr. Union*, **7**, 452, 1950, where references to early literature may be found. In connection with the theory of the fluctuations in brightness of the Milky Way, the discrete-cloud model has been the basis of a series of papers by S. Chandrasekhar and G. Münch: *Ap. J.*, **112**, 380 and 393, 1950; **113**, 150, 1951; **114**, 110, 1951; and **115**, 94, 1952.

[4] *Op. cit.*, § 6. [5] *Ann. d'ap.*, **13**, 367, 1950.

[6] The problem is formulated in terms of discrete random variables, in order to avoid the use of advanced mathematical concepts needed to treat probabilities in a continuum. In any event, since the observational data to be analyzed are always given in discrete form, the refinements required to deal with the continuous case are hardly necessary.

q_m, where, for convenience, we define $q_0 = 0$. Under these conditions, our problem is to establish a relation between the probability distribution of $E(r)$,

$$\text{prob}\{E(r) = k\epsilon\} = l_k \qquad (k = 0, 1, 2, \ldots), \tag{8}$$

and the sequences $\{p_n\}$ and $\{q_m\}$.

Formulated in this manner, the problem is readily identified with the composition of a random number of independent events in elementary probability theory. The solution follows immediately from the definition of conditional probabilities and may be written in the form

$$l_k = \sum_{n=0}^{\infty} p_n \,\text{prob}\{E_1 + E_2 + \ldots + E_n = k\epsilon\}. \tag{9}$$

This relation is most conveniently expressed in terms of the probability-generating functions

$$P(s) = \sum_{n=0}^{\infty} p_n s^n = e^{-\nu r(1-s)}, \tag{10}$$

$$T(s) = \sum_{k=0}^{\infty} l_k s^k, \qquad \text{and} \qquad Q(s) = \sum_{m=0}^{\infty} q_m s^m,$$

in the form[7]

$$T(s) = P[Q(s)] = \exp\{-\nu r[1 - Q(s)]\}. \tag{11}$$

Hence

$$Q(s) = 1 + \frac{1}{\nu r} \ln T(s). \tag{12}$$

This last equation establishes the required relation, since the generating functions uniquely represent the corresponding probability densities through the equations

$$q_m = \frac{1}{m!} \left| \frac{d^m}{ds^m} Q(s) \right|_{s=0} = \frac{1}{m!} \left| Q^{(m)}(s) \right|_{s=0} \tag{13}$$

and

$$l_k = \frac{1}{k!} \left| \frac{d^k}{ds^k} T(s) \right|_{s=0} = \frac{1}{k!} \left| T^{(k)}(s) \right|_{s=0}. \tag{14}$$

Taking successive derivatives of equation (12), we find, in general,[8]

$$Q^{(m)}(s) = \frac{m!}{\nu r} \sum_{k=1}^{m} \sum_{(\lambda)} \frac{(-1)^{k-1}(k-1)!}{\lambda_1!\lambda_2! \ldots \lambda_i!} \left(\frac{T'}{1!T}\right)^{\lambda_1} \left(\frac{T''}{2!T}\right)^{\lambda_2} \cdots \left(\frac{T^{(i)}}{i!T}\right)^{\lambda_i} \tag{15}$$

$$(m = 1, 2, 3, \ldots),$$

where the second summation is carried over all different sets (λ) of integers $0, 1, 2, \ldots, k$, which satisfy the conditions

$$\lambda_1 + \lambda_2 + \ldots + \lambda_i = k, \qquad \lambda_1 + 2\lambda_2 + \ldots + i\lambda_i = m. \tag{16}$$

[7] Cf. W. Feller, *An Introduction to the Theory of Probability and Its Applications* (New York: John Wiley & Sons, 1950), § 11.5, pp. 221–223.

[8] Cf. *Encykl. der math. Wiss.* (Leipzig: Teubner, 1915), Vol. 2, Part I, Sec. I, pp. 87–88.

According to equations (13) and (14), we thus have

$$q_m = \frac{1}{\nu r} \sum_{k=1}^{m} \sum_{(\lambda)} \frac{(-1)^{k-1}(k-1)!}{\lambda_1!\lambda_2!\ldots\lambda_i!} \left(\frac{l_1}{l_0}\right)^{\lambda_1} \left(\frac{l_2}{l_0}\right)^{\lambda_2} \ldots \left(\frac{l_i}{l_0}\right)^{\lambda_i} \quad (m = 1, 2, 3, \ldots). \tag{17}$$

In regard to the formal solution to our problem, as given by equation (17), it is of interest to notice that it is unique. This property is not quite obvious on "physical grounds" and does not seem to have been mentioned before in astronomical literature. It means that, if we could establish from the observations a statistically reliable frequency function of the color excesses, the probability densities of the absorbing powers of the clouds would be uniquely determined. As will be seen below, the available color data are not so extensive and complete as would be required for an unbiased determination of $\{q_m\}$ according to equation (17). It is of importance, therefore, to establish the general relation between the moments

$$\mu_j = \sum_{m=0}^{\infty} m^j q_m \qquad \text{and} \qquad m_j = \sum_{k=0}^{\infty} k^j l_k \tag{18}$$

of the sequences $\{q_m\}$ and $\{l_k\}$.

In the definitions (15) it is readily seen that $Q(e^s)$ and $T(e^s)$ generate the sequences $\{\mu_j/j!\}$and $\{m_j/j!\}$, respectively. We thus have

$$\mu_j = \left| \frac{d^j}{ds^j} Q(e^s) \right|_{s=0} \qquad \text{and} \qquad m_j = \left| \frac{d^j}{ds^j} T(e^s) \right|_{s=0}. \tag{19}$$

Now equation (15) holds as it stands when we replace s by e^s, and we keep the pseudo-exponents indicating derivatives with respect to s. Accordingly, in view of equations (19), we have, in general,

$$\mu_j = \frac{j!}{\nu r} \sum_{k=1}^{j} \sum_{(\lambda)} \frac{(-1)^{k-1}(k-1)!}{\lambda_1!\lambda_2!\ldots\lambda_i!} \left(\frac{m_1}{1!}\right)^{\lambda_1} \left(\frac{m_2}{2!}\right)^{\lambda_2} \ldots \left(\frac{m_i}{i!}\right)^{\lambda_i}, \tag{20}$$

with the integers λ_i as defined by equations (16). In particular, we have

$$\mu_1 = \frac{1}{\nu r} m_1, \qquad \mu_2 = \frac{1}{\nu r}(m_2 - m_1^2),$$

and

$$\mu_3 = \frac{1}{\nu r}(m_3 - 3m_2m_1 + 2m_1^3). \tag{21}$$

The general moment relation (20) can also be established directly from equation (12), where it may be noticed that, by definition, the moments of $\{q_m\}$ are the semi-invariants of $\{l_k\}$, except for the proportionality factor $1/\nu r$.

3. Probability distribution of color excesses of stars in a fixed distance range.—We have established the relation between the probability density of the color excesses of stars at a fixed distance and the probability distribution of the absorbing powers of the interstellar clouds. In practice, the number of stars with measured color excess that can be selected at a given distance is quite small. It is therefore a matter of importance to generalize the developments of the preceding section, in order to make proper allowance for a spread in the distances of the stars forming the sample. Let us suppose, then, that the stars under consideration are uniformly distributed in the distance interval $(r - \frac{1}{2}\Delta r, r + \frac{1}{2}\Delta r)$. The probability-generating function of the color excesses of all stars in this

interval, which we shall denote by $\mathfrak{T}(s)$, clearly should be obtained by integrating equation (11) over the relevant distance range:

$$\mathfrak{T}(s) = \frac{1}{\Delta r}\int_{r-(1/2)\Delta r}^{r+(1/2)\Delta r} T(s)\,dr = \exp\{-\nu r[1-Q(s)]\} \times \frac{\exp\{\tfrac{1}{2}\nu\Delta r[1-Q(s)]\} - \exp\{-\tfrac{1}{2}\nu\Delta r[1-Q(s)]\}}{\nu\Delta r[1-Q(s)]}. \tag{22}$$

The fraction appearing on the right side of this equation can always be expanded in a series of powers in $\nu\Delta r[1-Q(s)]$, and we may write

$$\mathfrak{T}(s) = \exp\{-\nu r[1-Q(s)]\}\left\{1+\frac{1}{24}\left(\frac{\Delta r}{r}\right)^2(\nu r)^2[1-Q(s)]+o(\nu\Delta r)^2\right\}. \tag{23}$$

Now taking logarithms of both sides of this equation and expanding in series the logarithm of the factor within braces, we obtain

$$Q(s) = 1+\frac{\ln \mathfrak{T}(s)}{\nu r}\left[1-\frac{1}{24}\left(\frac{\Delta r}{r}\right)^2 \ln \mathfrak{T}(s)\right], \tag{24}$$

where terms $o(\Delta r/r)^2$ have been neglected. Equation (24) now holds in place of (12), and formally solves the problem. For we have

$$\nu r\, q_m = \frac{1}{m!}\left|\frac{d^m}{ds^m}\ln \mathfrak{T}(s) - \frac{1}{24}\left(\frac{\Delta r}{r}\right)^2\frac{d^m}{ds^m}\ln^2 \mathfrak{T}(s)\right|_{s=0}; \tag{25}$$

and, in terms of the observed distribution

$$\tau_k = \frac{1}{k!}\left|\frac{d^k}{ds^k}\quad(s)\right|_{s=0}, \tag{26}$$

we may express the quantities

$$\gamma_m = \frac{1}{m!}\left|\frac{d^m}{ds^m}\ln \mathfrak{T}(s)\right|_{s=0} \tag{27}$$

in the form (see eqs. [12] and [17])

$$\gamma_m = \sum_{k=1}^{m}\sum_{(\lambda)}\frac{(-1)^{k-1}(k-1)!}{\lambda_1!\lambda_2!\ldots\lambda_i!}\left(\frac{\tau_1}{\tau_0}\right)^{\lambda_1}\left(\frac{\tau_2}{\tau_0}\right)^{\lambda_2}\ldots\left(\frac{\tau_i}{\tau_0}\right)^{\lambda_i} \tag{28}$$

for $m \geqslant 1$ and

$$\gamma_0 = \ln\ \tau_0. \tag{29}$$

Further, we have

$$\frac{1}{m!}\left|\frac{d^m}{ds^m}\ln^2 \mathfrak{T}(s)\right|_{s=0} = \sum_{k=0}^{m}\gamma_{m-k}\gamma_k, \tag{30}$$

and hence equation (25) may be rewritten in the form

$$q_m = \frac{1}{\nu r}\left[\gamma_m - \frac{1}{24}\left(\frac{\Delta r}{r}\right)^2\sum_{k=0}^{m}\gamma_{m-k}\gamma_k\right]. \tag{31}$$

The relation between the moments μ_j of $\{q_m\}$ and those of $\{\tau_k\}$,

$$M_j = \sum_{k=0}^{\infty} k^j \tau_k \qquad (j=0,\ 1,\ 2,\ \ldots), \tag{32}$$

can be easily derived from equation (24), in the same manner as equation (28) was derived from equation (12). We have for $j \geq 1$

$$\mu_j = \frac{1}{\nu r}\left| \frac{d^j}{ds^j} \ln \mathfrak{T}(e^s) - \frac{1}{24}\left(\frac{\Delta r}{r}\right)^2 \frac{d^j}{ds^j} \ln^2 \mathfrak{T}(s) \right|_{s=0}. \tag{33}$$

If we let Γ_j denote the jth semi-invariant of the observed distribution $\{\tau_k\}$,

$$\begin{aligned} \Gamma_j &= \left| \frac{d^j}{ds^j} \ln \mathfrak{T}(e^s) \right|_{s=0} \\ &= j! \sum_{k=1}^{j} \sum_{(\lambda)} \frac{(-1)^{k-1}(k-1)!}{\lambda_1!\lambda_2! \ldots \lambda_i!} \left(\frac{M_1}{1!}\right)^{\lambda_1} \left(\frac{M_2}{2!}\right)^{\lambda_2} \cdots \left(\frac{M_i}{i!}\right)^{\lambda_i}, \end{aligned} \tag{34}$$

we may rewrite equation (33) in the form

$$\mu_j = \frac{1}{\nu r}\left[\Gamma_j - \frac{1}{24}\left(\frac{\Delta r}{r}\right)^2 \sum_{k=1}^{j-1} \binom{j}{k} \Gamma_{j-k}\Gamma_k\right]. \tag{35}$$

For the first three values of j we have, explicitly,

$$\mu_1 = \frac{1}{\nu r} M_1, \qquad \mu_2 = \frac{1}{\nu r}\left\{M_2 - M_1^2\left[1 + \frac{1}{12}\left(\frac{\Delta r}{r}\right)^2\right]\right\},$$

and (36)

$$\mu_3 = \frac{1}{\nu r}\left\{M_3 - (3M_2M_1 - 2M_1^3)\left[1 + \frac{1}{12}\left(\frac{\Delta r}{r}\right)^2\right]\right\}.$$

4. *Analysis of observational data.*—In order to interpret the extensive color measures of Stebbins, Huffer, and Whitford,[9] information is needed on the intrinsic colors and distances of the stars. Values of the color excesses and the spectroscopic distance moduli of 283 stars above the main sequence were kindly provided in advance of publication by Dr. W. W. Morgan. In addition, Dr. Morgan has allowed the writer to use his provisional spectral types of a considerable number (about 350) of main-sequence B stars contained in *MWC* 621. Where no accurate spectral types were available, the color excesses and distance moduli given in *MWC* 621 were corrected statistically. The mean correction to the distance moduli of stars with HD types betweeen B0 and B5 was found to be -0.5 ± 0.3 mag. For the color excesses the correction applied was $+0.04 \pm 0.02$ mag., again nearly the same for all stars with HD types earlier than B5. From the data thus chosen, the sample to be analyzed was selected in view of the conditions required by our theory. The main question is to define a volume of space through which interstellar matter may be considered distributed homogeneously in a statistical sense. This is not a simple task, since there are reasons to expect, on the large scale, an arrangement of the interstellar matter in the galactic plane not entirely at random.[10] Existing observational evidence, however, would not seem to contradict an assumption of homogeneity in the galactic plane within 1 kiloparsec from the sun. It might appear that the lack of near-by obscuring "cloud complexes" in the region extending from $l = 160°$ to $l = 220°$ indicates nonhomogeneity in different galactic longitudes. But it may be also recalled that there are so few of such heavy clouds that large fluctuations in their numbers at different positions should be expected. In the direction normal to the galactic plane we have set, rather arbitrarily, the boundaries of our sampling region at $|z| = 100$ psc.

[9] *Mt. W. Contr.*, No. 621; *Ap. J.*, **91**, 61, 1940. This paper is referred to hereafter as "*MWC* 621."

[10] Recently W. W. Morgan, D. Osterbrock, and S. Sharpless, in *A.J.*, **57**, 3, 1952, have exhibited for the first time definite evidence suggesting an arrangement of the *H* II regions in the galactic plane similar to that observed in the Andromeda nebula.

According to Van Rhijn,[11] the color excess of a point with $|z| = 100$ psc is, on the average, about two-thirds of the value corresponding to a point with $z = 0$ at the same distance from the sun. Thus, neglecting entirely the latitude effect of the color excess, for stars with $|z| \leqslant 100$ psc, we would not expect to bias our analysis greatly. Our sample space, finally, was defined by the color excesses of all stars in *MWC* 621 within 1 kiloparsec from the sun and with $z \leqslant 100$ psc, after excluding stars with uncertain intrinsic color indices (Be type). From the collection of sample points available, two representative distance groups were selected, the characteristics of which are given in Table 1. It is noticed that, according to Van Rhijn,[12] the nearer group may be considered essentially complete. In the most distant group, II, some highly reddened stars may be missing, since they fall outside the limits of completeness of the *Henry Draper Catalogue*. The observational information relevant to our analysis has been summarized in Figure 1, where the frequency distribution of the color excesses is illustrated, and in Table 1, where the values of the first three sample means are given for each group.

TABLE 1

CHARACTERISTICS OF OBSERVED COLOR EXCESSES

	Group I	Group II
Number of stars	286	242
Distance moduli	7.0–8.5	8.6–9.9
r (psc)	375	720
Δr (psc)	250	480
$\epsilon^{-1}\,\overline{E}(r) = M_1$	11.68	19.12
$\epsilon^{-2}\,\overline{E^2}(r) = M_2$	231.2	492.2
$\epsilon^{-3}\,\overline{E^3}(r) = M_3$	6257	15,791
$\nu\mu_1$	31.14	26.6
$\nu\mu_2$	339.5	157.1
$\nu\mu_3$	3090	1404

A complete interpretation of the distribution of color excesses, on the basis of equation (31), would require the identification of the probability densities $\{\tau_k\}$ with the observed frequencies shown in Figure 1. It is recalled that the individual colors from which the histograms were derived have an over-all observational uncertainty of the order of $0^m03 = 3\epsilon$. Under these conditions it is clear that the application of equation (31) could not provide reliable results. In connection with a similar statistical problem, Chandrasekhar and Münch[13] have pointed out the misleading results which the inversion of a histogram formed from low-precision data might give. Consequently, we have chosen to characterize the distribution $\{q_m\}$ only by means of its moments. The first three sample means, given in Table 1, have been identified with the first three moments M_j of the sequence $\{\tau_k\}$.[14] From equations (36) we then determine the moments μ_j of $\{q_m\}$, in terms of the parameter ν, as given in the lower part of Table 1. The comparison of the

[11] *Op. cit.*, § 2, eq. (16).

[12] *Op. cit.*, § 2 (5).

[13] *Ap. J.*, **111**, 142, 1950.

[14] This identification of the sample means with the population means implicitly involves the assumption of independence between the distributions of sample points (early-type stars) and of interstellar matter. On the large scale it has been observed by W. Baade (*Pub. Obs. U. Michigan*, **10**, 7, 1951) that in the case of M 31 the two distributions are not independent. However, in the relatively small volumes of space we are dealing with, no strong causal connection between early-type stars and interstellar matter seems to be present.

$\nu\mu_i$'s derived for the two groups immediately reveals the bias of group II in favor of low color excesses, arising from the incompleteness referred to above.

We have discussed earlier the manner in which the mean and the variance of the distribution of color excesses of stars at a certain distance r have been interpreted in terms of the parameters ν and e_0 of Ambarzumian's model. Allowing for the spread in the distances of the sample points, it is readily seen that, instead of equations (6), we have

$$e_0 = \frac{M_2}{M_1} - M_1\left[1 + \frac{1}{12}\left(\frac{\Delta r}{r}\right)^2\right]$$

and (37)

$$(\nu r)^{-1} = \frac{M_2}{M_1^2} - 1 - \frac{1}{12}\left(\frac{\Delta r}{r}\right)^2 .$$

For our two distance groups, equations (37) give the values

$$\text{I:}\quad e_0 = 7.7\ , \qquad \nu = 4.1\ \text{kpc}^{-1}\ ,$$

$$\text{II:}\quad e_0 = 5.9\ , \qquad \nu = 4.5\ \text{kpc}^{-1}\ .$$

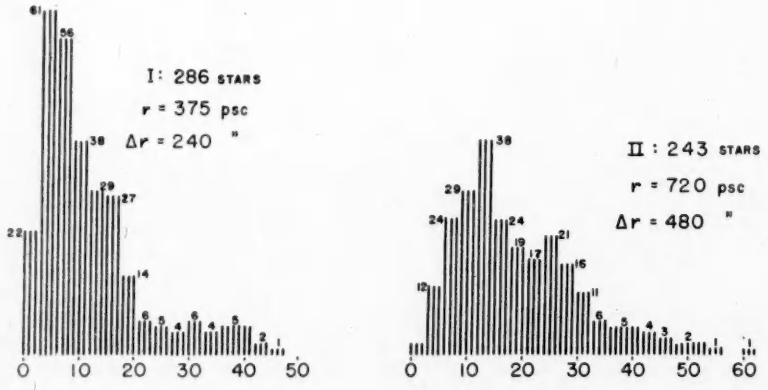

FIG. 1.—Distribution of the color excesses of stars with distance moduli $m - M$ in the intervals *I*: $7.0 \leqslant m - M \leqslant 8.5$; and *II*: $8.5 \leqslant m - M < 10.0$. The abscissae represent color excesses in units of $\epsilon = 0.01$ mag., and the ordinates give the numbers of stars with color excesses in successive intervals of spread $3\,\epsilon$.

It may be noticed, however, that the observed distributions have significantly larger skewness than these values of e_0 and ν would predict; for we have (in units of kpc^{-1})

$$\text{I:}\quad \nu\mu_3 = 3090\ \text{(observed)}\ , \qquad \nu e_0^3 = 1840\ \text{(predicted)}\ ,$$

$$\text{II:}\quad \nu\mu_3 = 1404\ \text{(observed)}\ , \qquad \nu e_0^3 = 929\ \text{(predicted)}\ .$$

These numbers suggest that the dispersion of the color excesses produced by individual clouds is significant. E. Schatzman[5] correctly called attention to the point, although the skewness shown by the fundamental data he used was greatly exaggerated by the admixture of stars of different luminosities.

A better idea of the form of the distribution of the absorbing powers of the clouds is given by the first three moments μ_1, μ_2, and μ_3. To derive their values from the data

given in Table 1, we need to know the value of ν. The most direct determination of ν would result from the frequency τ_0 of unreddened stars, if it were known with fair accuracy; equation (24) gives

$$\nu = -\frac{1}{r}\ln\tau_0\left[1-\frac{1}{24}\left(\frac{\Delta r}{r}\right)^2\ln\tau_0\right]. \tag{38}$$

If the values of τ_0 are identified with the observed frequencies of stars represented in the first block of the histograms of Figure 1, equation (38) provides the values of τ_0 given in Table 2. The agreement of the numerical values derived for the two groups is

TABLE 2

PROPERTIES OF THE DISTRIBUTION OF REDDENING MATTER

	Group I	Group II
τ_0	22/286	2/243
ν	7.2	7
μ_1	4.3	3.6
σ	0.88	0.79
γ	2.88	2.26
e_1	3.2	2.6
e_2	16.5	11.2
p	0.911	0.876
$A_1=7e_1\epsilon$	0^m22	0^m18
$A_2=7e_2\epsilon$	1^m2	0^m79
νp (kpc^{-1})	6.5	6
$\nu(1-p)$ (kpc^{-1})	0.6	1

entirely fortuitous, since the sampling errors affecting τ_0 in group II are so large that the resulting value of ν is almost meaningless. The value of τ_0 for group I, on the contrary, is reliable enough to enable us to compute the desired moments. The dispersion around the mean and the skewness of the color excesses produced by the individual clouds may then be described by the standard deviation σ and the coefficient of skewness γ:

$$\sigma = \left(\frac{\mu_2}{\mu_1^2}-1\right)^{1/2},$$
$$\gamma = (\mu_3 - 3\mu_2\mu_1 + 2\mu_1^3)(\mu_2-\mu_1^2)^{-3/2}. \tag{39}$$

The values derived for these two parameters are given in Table 2. A rough idea of the spread of the values of the absorbing powers of the clouds around their mean may be then obtained by recalling that, for a Poisson distribution, both σ and γ have the value unity. We thus see that the dispersion around the mean is less than in a Poisson law, but the skewness is larger.

In order to give a more intuitive picture of this property of the distribution $\{q_m\}$, we may follow Schatzman[5] and postulate that there are only two "kinds of clouds" producing constant color excesses e_1 and e_2 (in units of ϵ) and that they occur with probabilities p and $1-p$, respectively. We may then determine the values of e_1, e_2, and p, from the moments μ_1, μ_2, and μ_3, through the conditions

$$p\,e_1^j + (1-p)\,e_2^j = \mu_j \qquad (j=1,2,3). \tag{40}$$

This system of algebraic equations can be solved readily in the explicit form

$$p(1-p) = \frac{1}{4+\gamma^2},$$

$$e_1 = \mu_1 \left\{ 1 - \frac{\sigma}{2} [(4+\gamma^2)^{1/2} - \gamma] \right\}, \tag{41}$$

$$e_2 = \mu_1 \left\{ 1 + \frac{\sigma}{2} [(4+\gamma^2)^{1/2} + \gamma] \right\}.$$

The numerical values derived for p, e_1, and e_2 are given in the lower part of Table 2, which also gives the extinctions (in magnitudes) for visual light, A_1 and A_2, produced by the small and large clouds and their relative frequencies of occurrence along the line of sight, νp and $\nu(1-p)$, respectively. It is of some interest to remark that, although the procedure we have followed to derive the values of e_1 and e_2 is essentially different from the one followed by Schatzman, our final results are in fair agreement, especially as far as e_1 is concerned. The absorptive power of the large clouds has been reduced by about 1 mag., probably as a result of the more reliable information at our disposal regarding highly reddened stars. But this reduction might in part also be due to the rather arbitrary method followed by Schatzman of dissecting the observed color-excess distribution into two parts, one supposed to correspond to the "small clouds" and the other to the larger ones.

So far, the interpretation we have given to the color-excess distribution in terms of two kinds of clouds rests on an entirely *ad hoc* assumption. Our analysis obviously could not rule out the existence of a gradual transition from the small clouds to the larger ones. When it is recalled, however, that near-by clouds with optical thicknesses of the order of 1 mag. have been detected by the classical methods of stellar statistics,[15] it is tempting to identify them with the large clouds postulated above in our analysis. We may provide some evidence for the legitimacy of this identification by comparing the distributions of color excesses in one of the so-called "clear" regions of the Milky Way and in a region where dense clouds are known to exist. In Figure 2 we have illustrated the frequency diagrams of the color excesses for each of the following regions of our sample I: I*a*, $210° > l > 155°$; I*b*, $155° > l > 60°$; I*c*, $60° > l > -10°$; and I*d*, $350° > l > 320°$. In region I*a* no large values of E are found. In region I*b* the extensive Taurus cloud complex and those farther north in Cassiopeia and Cepheus are responsible for the large values of E. Region I*c* extends over the great rift in Aquila, but it is not affected by heavy absorption within 500 psc. Finally, in region I*d* several near-by heavy dark clouds are known to exist. If we characterize the first two moments of the respective distributions of E by the parameters e_0 and ν defined in equation (37), we derive the results given in Table 3. It can then be seen that, for the clear regions I*a* and I*c*, the values of e_0 are comparable to the value of e_1 given in Table 2. The values of e_0 derived for regions I*b* and I*d* are heavily weighted by the large clouds and cannot be compared either with e_1 or e_2.

5. *Concluding remarks.*—In the previous sections we have supposed the linear dimensions of the clouds to be so small compared with the average distance between them that they may be considered as points along the line of sight. It is thus clear that our analysis cannot provide any definite answer to questions related to the spatial extension of the hypothetical clouds. In order to study this aspect of the problem, it would be necessary to evaluate the joint probability distribution $W_2(E_1, r_1; E_2, r_2)$ for observing color excesses E_1 and E_2 at two specified points r_1 and r_2. Within the framework of the discrete-cloud model of Ambarzumian this cannot be accomplished unless

[15] Cf. J. L. Greenstein, *Harvard Ann.*, **105**, 359, 1937.

additional specific assumptions regarding the actual geometrical forms of the clouds are introduced.[16] And it is apparent that to postulate a priori any regular shape, as a sphere[17] or a circular cylinder with axis along the line of sight,[18] is a highly arbitrary and restrictive procedure. It would seem, therefore, that the simple model we have considered here is not appropriate to describe in more detail the random process underlying equa-

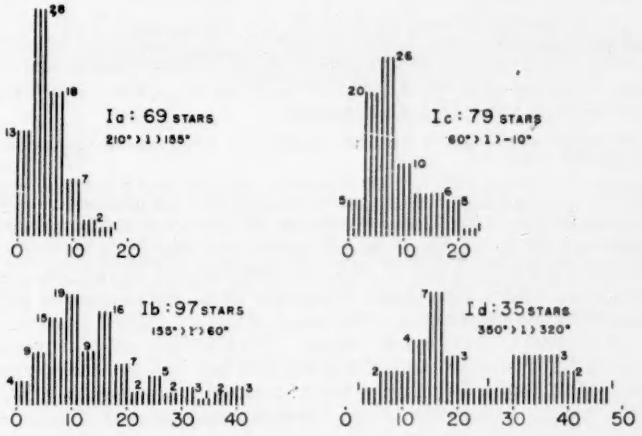

FIG. 2.—Distribution of the color excesses of stars at distances between 250 and 500 psc. and in four different regions of the Milky Way. The abscissae represent color excess in units of $\epsilon = 0.1$ mag., and the ordinates give the numbers of stars with color excesses in successive intervals of spread 3ϵ. Notice that the scale of the ordinates is not the same for all four histograms.

TABLE 3

ANALYSIS OF $E(r)$ IN VARIOUS REGIONS OF THE MILKY WAY

	REGION			
	Ia	*Ib*	*Ic*	*Id*
Gal. longitudes	210°–155°	155°–60°	60°–350°	350°–320°
No. of stars	69	97	79	35
M_1	5.30	14.3	8.15	23.34
M_2	38.12	289.0	92.48	678.1
e_0	1.68	5.45	2.89	4.84
ν	8.4	7.0	7.5	13

[16] By analyzing the numbers of diffuse nebulae per unit volume, under the assumption that no causal connection exists between nebulae and illuminating stars, Ambarzumian and Gordeladse (*Bull. Abastumani Ap. Obs.*, **2**, 37, 1937) derived a value for the mean number of clouds per unit volume N. The relation between N and ν involves a length which has been interpreted as the "radius" of a cloud. The determination of this "radius," however, is affected by a large uncertainty, and values between 1 and 50 psc are considered (cf. L. Spitzer, *Ap. J.*, **108**, 276, 1948: Ia).

[17] Cf. Schatzman, *op. cit.*

[18] Cf. V. A. Ambarzumian, *Doklady Acad. Nauk Armenian SSR*, **1**, 9, 1944; also G. E. Rusakov, *Leningrad Univ. Uchen. Zapiski*, No. 116, *Trudy Astr. Obs.*, **13**, 53, 1949.

tion (2). Chandrasekhar and Münch[19] have pointed out this shortcoming of Ambarzumian's model and have also suggested a procedure to analyze the first moment of W_2. On a later occasion we shall consider the problem in detail and show how the scale of the variations in space of the density of reddening dust can, in principle at least, be determined by analyzing the correlation coefficient between the color excesses of stars separated by a fixed distance.[20]

It is a pleasure to record my indebtedness to Dr. W. W. Morgan for allowing me to use a great deal of unpublished data regarding colors, absolute magnitudes, and spectral types of early-type stars. My thanks are also due to Dr. J. L. Greenstein for reading and criticizing a preliminary version of this paper.

[19] *Ap. J.*, **115**, 103, 1952.

[20] In a recent note (*Harvard Bull.*, No. 920, September, 1951) Dr. Bart J. Bok has critically reviewed the work so far done on the basis of Ambarzumian's model, with special reference to the series of papers by Chandrasekhar and Münch mentioned earlier. It is not the intention of the writer to discuss here in detail every argument raised by Dr. Bok. In the text of the present paper the meaning and limitations of Ambarzumian's model have been emphasized to a point that misunderstandings arising from too literal interpretations should be discounted. It would appear, however, that the essential difference between the point of view maintained by Dr. Bok and ours is that he does not accept the necessity of describing the distribution of interstellar matter statistically as a whole.

DETERMINATIONS OF COLOR CLASSES FOR 204 STARS OF LARGE PROPER MOTION

E. F. CARPENTER, A. J. DEUTSCH,* AND W. J. LUYTEN
Steward Observatory, University of Arizona, and University of Minnesota Observatory
Received April 18, 1952

ABSTRACT

This paper presents a catalogue of the colors of 204 stars of large proper motions in the Southern Hemisphere.

The colors of 204 stars of large proper motion in the Southern Hemisphere have been measured on plates taken with the 36-inch Steward reflector and a Wood replica grating arranged in the manner proposed by Whipple and Norman.[1] In this procedure the grating is mounted close to the photographic plate in the converging beam of the Newtonian focus, at such a distance as to produce a spectrum of only a few normal stellar image-diameters in length. A suitable absorption filter removes the central region of the spectral image, thus leaving two stellar images, recorded simultaneously, at the extremities of the spectrum (cf. Fig. 3 of Whipple and Norman's paper). Whipple and Norman proposed their technique as a means of rapid recognition of qualitative colors, but we have found that, if the images are measured with a conventional type of scale plate, the colors can be obtained from a single exposure with an uncertainty of only about 0.2 or 0.3 color class.

Our replica grating was made and selected by Professor R. W. Wood. It is 70 mm in diameter and has 1200 lines per inch. Most of the light is concentrated in one of the images of the first order. Unlike the grating used at Harvard, however, the blue, rather than the red, is the more efficiently concentrated, our red and blue first-order images being, respectively, about 1.7 and 4.0 mag. brighter than the corresponding faint first-order images.

Eastman spectroscopic plates types 103-*C* and 103-*E* with Wratten filters Nos. 30 and 32 were used. Filter No. 32 gives a stronger blue image than does No. 30, and equality of images occurs, respectively, at color classes g2 (for No. 32) and a8 (No. 30). For late types, No. 32 is therefore preferable, but for early types its strong blue image is inclined to be elongated. The spectral regions represented in the blue and red images are centered at about λ 4200 and λ 6300, both being a little to the violet of this with the No. 30 filter and a little to the red with No. 32.

In our installation the grating is 24 mm in front of the focal plane ($f/5$), and the separation of the red and blue image-centers is 0.22 mm. Measurement is made by means of a scale plate mounted on the wedge-carrier of a Hartmann microphotometer. Images of a fairly even intensity level were used, and color classes were established by an empirical calibration of blue and red scale differences versus known color classes. The scale readings of the two first-order red images were used as a criterion of the contrast of each plate.

We believe that this method of colorimetry warrants the enthusiasm indicated by its authors. There is, however, one source of trouble which was not anticipated, viz., the tendency of the blue images to be grayer than the red images of the same diameter on each plate. This effect vanishes for images reached in exposures of ½ minute or less. It is therefore inferred that it may arise from the relatively worse seeing of blue images

* Now of the Mount Wilson and Palomar Mountain Observatories.

[1] *Harvard Bull.*, No. 908, 1938.

TABLE 1

LPM	R.A.	Dec.	m_{pg}	C	LPM	R.A.	Dec.	m_{pg}	C
6	$0^h06^m.4$	-27°24'	12.0	m1	265	$7^h32^m.5$	-10°16'	11.5	f3
8	12.9	16 25	12.6	m7	269	38.1	17 16	13.0	g4
12	15.2	11 01	14.7	m8	274	52.9	29 11	14.4	m8
24	25.4	6 43	13.0	m2	282	8 10.6	21 23	13.0	m8
25	26.2	6 44	14.2	m8	284	11.5	32 19	14.4	m8
41	0 43.7	-31 05	14.4	m8	285	8 15.5	-34 17	14.0	m8
50	55.9	28 07	12.7	m8	292	27.2	1 34	13.0	k7
52	58.3	4 44	14.5	m7	296	38.8	23 18	13.0	m4
53	59.6	10 08	11.2	m6	297	39.7	32 48	12.5	a0
56	1 01.8	34 57	10.8	k6	299	51.6	12 56	13.0	m6
76	1 35.5	- 5 16	12.6	f1	300	8 56.6	- 6 12	11.8	k2
83	40.8	42 27	12.7	m2	313	9 22.2	36 51	15.2	m8
87	44.1	8 54	14.8	m8	320	33.8	2 36	14.6	m7
92	54.6	36 30	13.7	m8	321	33.9	21 25	12.8	m6
96	2 02.5	17 52	10.8	m8	322	36.6	39 08	12.6	m5
100	2 06.7	-16 36	11.5	m7	323	9 37.9	-40 50	12.4	m8
102	07.2	14 36	13.3	m8	324	40.3	18 59	13.6	m8
104	10.4	17 56	11.2	m6	325	41.6	17 33	14.5	m8
106	11.5	25 42	13.7	g4	327	42.6	17 58	14.0	m8
107	11.7	32 15	11.5	m8	333	56.7	46 11	12.2	m8
109	2 13.4	-12 54	14.0	m8	334	9 59.1	-30 09	12.8	m8
111	14.5	31 14	12.7	m8	336	10 09.5	2 24	12.2	m8
112	14.5	31 14	13.2	m8	337	09.8	18 21	11.8	m2
113	16.0	35 51	13.7	m8	338	10.9	35 23	14.7	m8
114	16.0	35 51	14.4	m8	341	14.4	11 41	12.4	m8
117	2 17.0	-37 01	13.8	m8	347	10 22.7	- 9 58	11.8	m5
122	37.7	34 18	14.6	m8	348	23.7	17 43	13.0	m2
133	52.0	36 06	9.5	g2	349	24.1	6 14	11.0	m
136	55.8	13 05	13.5	m7	353	37.3	6 38	12.0	m6
137	55.9	36 50	13.0	k9	354	38.2	19 05	14.1	m8
144	3 10.4	-38 18	12.0	m8	355	10 38.2	-19 05	15.3	m8
154	26.8	27 34	13.8	a9	357	43.4	18 49	12.7	m8
155	26.8	27 34	15.0	m7	358	43.5	35 05	13.6	m8
159	32.6	31 14	11.3	f6	360	46.1	29 50	14.3	m8
168	44.2	11 22	13.8	m8	361	50.1	1 50	11.0	k5
173	3 51.5	-37 12	12.8	m4	362	10 53.1	- 9 06	14.8	m8
176	4 04.5	20 58	11.0	m2	364	55.2	7 15	14.5	g1
183	15.1	26 12	13.5	m7	365	56.8	18 12	14.5	m8
190	26.7	25 16	13.5	m8	368	11 07.2	24 19	11.8	m7
192	31.1	39 52	13.6	m1	374	12.9	17 50	11.2	m8
195	4 42.8	-11 58	14.6	m5	375	11 12.9	-17 50	11.5	m8
198	51.6	17 50	12.5	m8	376	12.9	17 50	15.5	m8
201	5 00.1	19 37	12.5	m5	377	14.3	27 40	14.8	m8
202	01.2	17 26	13.0	m8	382	15.8	2 58	14.5	a4
218	45.7	36 21	11.6	m3	384	21.5	18 04	15.1	m8
234	6 19.8	-22 43	12.2	m6	386	11 25.5	- 8 53	13.0	m3
238	23.4	26 46	14.5	m5	388	29.4	40 45	13.0	m8
250	7 03.0	38 30	13.8	m8	390	32.2	23 35	12.0	m8
261	22.4	39 12	14.8	m8	391	33.1	32 14	11.5	m8
264	30.4	36 00	14.4	m8	398	44.1	13 44	12.6	m8

TABLE 1

LPM	R.A.	Dec.	m_{pg}	C	LPM	R.A.	Dec.	m_{pg}	C
402	11^h 50.8	- 7°06'	13.8	m8	577	15^h 39.5	-20°05'	12.6	m8
403	51.5	31 07	14.7	m8	585	44.3	13 25	12.2	k6
405	52.5	35 39	14.7	m5	587	57.3	34 34	15.2	m8
406	53.3	37 59	13.5	m8	593	16 11.3	28 22	13.9	m8
410	58.7	1 27	11.5	m8	597	16.8	37 26	12.0	m8
411	12 01.2	-16 17	12.4	m0	601	16 20.5	-46 36	13.4	m8
413	02.1	37 59	13.6	m8	611	32.5	30 44	13.5	m8
415	02.9	24 23	14.3	m7	612	33.3	15 04	12.0	g9
423	22.1	33 43	14.2	m8	615	37.0	45 54	13.8	m5
425	23.2	24 17	13.9	m8	624	54.4	4 17	13.8	m8
433	12 27.3	- 5 11	14.9	m8	629	17 09.3	- 1 48	12.6	m8
436	33.2	45 38	12.3	m8	630	10.3	5 03	12.7	m7
437	33.9	4 05	14.5	m8	653	39.9	16 37	13.8	m8
442	38.1	43 18	13.5	m8	661	53.2	16 24	11.0	g4
447	42.1	15 06	13.0	m8	670	18 12.3	33 43	14.8	m8
448	12 44.6	- 3 17	13.3	m7	671	18 16.7	- 5 47	13.6	m5
449	45.2	8 19	12.9	m5	674	19.4	33 24	14.0	k2
461	13 06.7	34 35	13.9	m8	679	33.5	32 34	13.8	g7
465	11.9	3 50	13.2	g9	683	41.3	30 17	14.2	m2
469	17.2	35 09	14.3	m8	688	46.7	23 54	12.4	m8
472	13 20.9	-25 38	14.5	m8	696	19 06.5	-14 50	13.4	m8
475	23.0	28 05	12.0	m8	710	46.7	11 26	14.2	m2
476	24.6	30 55	14.5	m8	714	54.0	1 10	14.1	a2
482	28.0	32 23	13.0	m8	724	20 04.3	19 33	12.7	m8
490	37.9	24 21	13.8	k5	736	18.7	6 36	12.5	m5
491	13 43.1	-17 43	13.3	m5	741	20 24.6	-27 54	12.8	m8
499	51.1	20 00	14.5	m8	746	38.7	22 31	11.0	m1
503	58.0	31 33	12.2	m8	753	51.4	2 57	11.5	k7
506	59.9	24 17	13.3	m8	754	52.7	14 15	14.5	m2
509	14 06.5	30 41	12.4	m8	758	54.1	10 37	12.7	m8
512	14 09.7	- 0 21	14.0	m7	763	21 02.2	-17 06	12.4	m8
524	18.8	0 51	13.8	m8	770	10.7	19 31	12.6	m4
527	27.0	46 42	12.5	m8	782	27.2	25 06	13.8	m3
531	30.9	9 43	12.5	m8	808	59.1	19 44	13.0	m4
536	35.6	0 36	13.2	g3	809	59.5	37 19	13.2	m8
538	14 35.9	- 3 01	14.3	m8	812	22 03.0	-38 30	14.2	k7
541	45.3	2 58	14.7	m8	822	15.6	31 13	14.2	k1
543	46.8	25 53	12.8	m8	831	23.3	21 05	13.6	k0
544	46.8	25 53	13.3	m8	840	45.4	37 04	12.8	m8
545	48.7	40 58	14.2	m0	850	23 03.3	2 26	13.8	m5
548	14 50.6	-11 22	13.7	m0	855	23 08.0	-19 28	14.7	m6
553	15 03.1	37 13	13.3	m8	861	13.1	12 38	14.1	m8
554	06.5	19 47	12.2	m9	887	45.9	27 57	14.2	m8
557	10.2	21 48	11.8	g9	895	53.2	6 25	12.5	m8
561	15.6	18 25	10.8	m8	898	57.3	34 22	13.5	m8
562	15 16.4	-12 33	13.7	m2	900	23 59.1	-35 45	13.8	m4
567	19.0	27 39	14.7	m8					
571	29.0	41 04	11.1	m8					
572	33.4	37 43	13.0	m8					
575	35.1	21 08	12.0	m7					

occasioned by the greater atmospheric refractive index for blue light. This was especially so in our case, since all stars observed were of southern declinations and some even went as far south as −40°, with corresponding maximum altitude of 17°. This effect is thus likely to be inherent in any method of colorimetry, done with telescopes of moderate or large size, in which images of different colors are directly compared in an effort to evade the erratic zero-point errors which are so troublesome with multiple exposures.

The data obtained are shown in Table 1, where the several columns give, in order, the LPM number from Luyten's catalogue,[2] the position for 1950, the estimated photographic magnitude, and the color classes derived in the present paper. Table 2 gives the

TABLE 2

LPM	*Durchmusterung*	LPM	*Durchmusterung*	LPM	*Durchmusterung*
6	CoD −27° 16	297	CoD −32° 5613	475	CoD −27° 9225
50	CoD −28 302	300	BD − 5 2678	503	CoD −31 10833
53	BD −10 216	322	CPD−38 3525	509	CoD −30 11195
56	CPD−35 110	323	CPD−40 3789	527	CPD−46 6822
83	CoD −42 594	333	CoD −45 5627	531	BD − 9 3964
96	BD −18 359	337	BD −17 3088	543	CoD −25 10553
100	BD −17 400	347	BD − 9 3070	557	CPD−21 5912
107	CoD −32 828	349	BD − 5 3063	561	BD −18 4032
111	CoD −31 909	357	BD −18 3019	571	CPD−40 7021
133	CPD−36 296	361	BD − 1 2457	585	BD −13 4246
144	CoD −38 1058	368	CoD −23 9765	597	CoD −37 10765
159	CoD −31 1454	374	BD −17 3336	612	BD −14 4454
173	CoD −37 1501	375	BD −17 3337	741	CoD −28 16676
176	BD −21 784	390	CoD −23 10062	746	BD −22 5504
218	CoD −36 2458	391	CoD −31 9113	753	BD − 3 5059
234	CoD −22 3005	436	CoD −45 7872	895	BD − 6 6318

TABLE 3

Star	R.A.	Dec.	m_{pg}	μ	C
L 796–10	0^h53^m3	−11° 46′	15.1	0″.47	f1
L 307–26	5 55.6	−46 57	12.0	0.44	m4
L 1251–1	8 20.6	+22 01	11.0	0.39	m0
BD+9°2190	9 26.6	+ 8 51	11.0	0.40	f3
BD+8°2269	9 46.4	+ 8 04	10.6	0.28	k4
L 547–27	13 58.5	−31 37	12.4	0.04	m1
L 1345–70	16 00.6	+20 45	13.9	1.55	m4
L 1277–81	17 02.1	+17 02	13.3	1.12	m4

BD, CPD, or CoD identifications for the program stars contained in these catalogues. In Table 3 are listed the color classes of eight additional proper-motion stars which are not contained in the LPM catalogue used for Table 1.

It may be recalled here that the preliminary color classes published by Luyten were obtained by estimating directly, in tenths of a magnitude, the difference in color index between the proper-motion star and a number of comparison stars of the same magnitude and then applying a correction for the expected average color index of these comparison stars, the amount of this correction depending on the apparent magnitude and the galactic latitude. While it was expected that color indices obtained in this manner would

[2] *Pub. Astr. Obs. Minnesota*, **3**, 1, 1941.

be subject to accidental errors of no more than perhaps 0.2 mag., they might well be seriously in error in obscured regions where the comparison stars could be up to a whole magnitude redder than average. This is borne out again by a comparison of these earlier approximate color classes with those derived in the present paper, as, e.g., for the stars LPM 261, 553, 597, 629, 630, and 683. On the whole, however, the two sets of determinations agree well enough to inspire confidence in both methods, though it is puzzling to find that for LPM 364 the earlier, less accurate method gave a color class "a," the newer method gives "g1," whereas the spectral class is found to be DA and the accurate color index derived from a comparison with standard magnitudes in Selected Areas yields 0.04. By and large, there seems to be no question but that the earlier and cruder color classes are systematically too early and that both the earlier and the present method fail to distinguish accurately between the different subclasses in spectral class M—witness the multitude of stars indicated to be "m8." Two stars, LPM 282 and 327, appear to be considerably redder than any of the other stars; it will be interesting to see whether future parallax determinations bear this out by indicating that these two are stars of exceptionally low luminosity.

It is a pleasure to acknowledge the financial assistance received from the Rumford Fund of the American Academy of Arts and Sciences, which enabled us to purchase the grating, and from the Gould Fund of the National Academy of Sciences, which made it possible to obtain the observations. The observations were all made in 1940-1941, and all reductions were completed in 1942. Intrusion of wartime duties has delayed publication until now.

STELLAR SPECTRA AND COLORS IN CYGNUS AT GALACTIC LATITUDE +14°

DONALD A. MACRAE
Warner and Swasey Observatory, Case Institute of Technology
Received April 10, 1952

ABSTRACT

Photographic magnitudes, colors, and spectral types of 938 stars to limiting magnitude 12.7 are given in Table 3 and Figure 1, *A–F*. The photometric data, obtained from plates taken with the Burrell telescope, are based on a sequence of stars in the field for which magnitudes and colors were determined by photoelectric means. Luminosity classes have been assigned to stars brighter than 11.2. A few stars of special interest are discussed, including one which is similar to BD+28°4211 (Op), a new carbon star, and three new variables, one of which is an S-type star.

INTRODUCTION

In fields which lie slightly outside the plane of the Milky Way the absorption is often small and uniform and reaches a maximum value in a relatively short distance. Stellar-density analyses are correspondingly more trustworthy than in the galactic plane and yield important information about the structure of the galaxy. Where the lower latitudes are unobscured, the dependence of density on distance from the galactic plane can be found. Where the absorption is complex in the lower latitudes, investigations in intermediate latitudes yield information which could not be obtained otherwise.

An observational program involving spectral classification, magnitudes, and colors has been undertaken in these regions of the Milky Way. It supplements the corresponding

TABLE 1

IDENTIFICATION OF ILF-1

Central star: BD+44°3086, HD 180551, or 45°157 in Table 3
1950 co-ordinates: $\alpha = 19^h13^m4$; $\delta = +45°5'$
Galactic co-ordinates: $l = 43°.8$; $b = +14°.2$ (*Lund Ann.*, No. 3)
Diameter of field: 3°.7
Area of field: 10.6 square degrees.
Position of center on Chart 21 of Ross-Calvert *Atlas:* 8.2 cm. west of δ Cyg, 0.4 cm north of δ Cyg

program in the galactic plane being carried out with the Burrell telescope and already well advanced.[1] The first region reported on is the present one. It is located on the north side of the Milky Way near the junction of Cygnus, Lyra, and Draco and is designated as ILF-1 (intermediate latitute field No. 1).

The position and size of the field are given in Table 1. The area shows no nonuniformity of stellar distribution which might be due to variations in the absorption characteristics. Long-exposure photographs show numerous faint galaxies. The field lies some 10° outside Hubble's zone of avoidance, which at these longitudes comes within 5° of the galactic equator on the north side. Regions LF3b[2] and LF3a (unpublished) are at the same longitudes and extend in latitude from −1° to +5°. It is well known that the north side of the Milky Way in Cygnus is relatively clear of obscuration, even in very low latitudes.

PHOTOMETRIC DATA

The photometry in the photographic region was carried out on Kodak Spectroscopic II*a*-O plates with exposures of 30 seconds and 5 seconds. The plates were always taken in

[1] McCuskey and Seyfert, *Ap. J.*, **106**, 1, 1947, and subsequent papers in the same *Journal*.
[2] Nassau and MacRae, *Ap. J.*, **110**, 40, 1949.

pairs, with the telescope reversed between plates, so that distance corrections of a linear nature were neutralized. The color equation of the magnitude system appears to be negligible, and no color corrections were applied.

A provisional photographic-magnitude sequence was established in the field by means of polar comparisons (eight pairs) and comparisons with a sequence in LF3b (three pairs). The limiting magnitude was about 1 mag. fainter than the limit of the spectral survey. These plates were measured on the Bennett fixed-aperture photometer, so that the accidental errors of the magnitudes were small. A discussion of systematic errors as determined by photoelectric measures will follow in succeeding paragraphs.

The field stars were measured on two pairs of plates by means of a graduated scale of stellar images. Discordant stars were remeasured on a third pair. Stars brighter than magnitude 11.2 were measured on three double-exposure (with telescope reversed) plates of the shorter exposure time. The mean error of a magnitude determined from a single pair of plates is ± 0.13 mag. This is an internal estimate obtained from those stars which were measured on five pairs. Accidental errors of estimation and accidental deviations made in drawing the reduction-curves for each pair of plates contribute equally to this dispersion. The measures on the five pairs of plates do not show any systematic deviations depending on the position of the star on the plate. For an index of the precision of the final magnitudes it can be assumed that the stars brighter than magnitude 8.8 were measured on three pairs, stars between 8.8 and 11.2 were measured on five pairs, and fainter stars on two pairs. The mean errors of the final magnitudes are therefore ± 0.08, ± 0.06, and ± 0.09 mag. for the three magnitude groups.

The photometry in the red region was carried out on Kodak Spectroscopic 103*a*-E plates exposed behind a Wratten No. 22 filter. The effective wave length of this combination is estimated to be 6200 A. Exposures were 60 seconds and 10 seconds, and again all plates were taken in pairs.

The provisional photored magnitudes of the same sequence stars were determined by polar comparisons[3] (8 pairs of plates) and LF3b comparisons (2 pairs of plates). These plates were also measured with the photometer.

The field stars were measured with a graduated scale of images. The same numbers of plates were used as in the photographic measures. The estimated mean error of a magnitude determination from a single pair of plates, ± 0.10 mag., is not significantly smaller than the corresponding quantity for the blue plates. Conservative estimates of the mean errors of the final magnitudes are therefore obtained if they are taken to be the same as for the photographic magnitudes of the same stars.

PHOTOELECTRIC DATA

A study of the relationship between spectral type and red index for the field stars showed evidence of systematic errors, which were attributed to the magnitude sequences. The existence of zero-point and scale errors has been demonstrated in even some of the most fundamental and carefully done photometry.[4] Dr. Gerald E. Kron at the Lick Observatory kindly agreed to furnish photoelectric observations of color and magnitude for 25 stars in ILF-1 for the purpose of eliminating the errors in the provisional sequences. He observed these stars with the Lick equipment in July, 1949. On the basis of the magnitudes supplied by Dr. Kron, small but well-determined zero-point and scale corrections were applied to the provisional photographic magnitudes of the sequence stars. The photoelectric measures also made it possible to apply similar corrections to the photored sequence. Allowance had to be made for the difference in effective wave length of the photored and the International photovisual; but, since most of Kron's stars were very

[3] Nassau and Burger, *Ap. J.*, **103**, 25, 1946.

[4] Stebbins, Whitford, and Johnson, *Ap. J.*, **112**, 469, 1950.

near to color index zero, the exact relationship was unimportant. The photographic magnitudes and red indices in Table 3 are based on the sequences corrected in this way.

There is now general agreement that the North Polar Sequence does not represent a satisfactory photometric standard. The photometric system represented by the magnitudes in Table 3 is nearly the same as the "International," but the exact relationship cannot be defined. During the summer of 1951 the photoelectric photometer of the Warner and Swasey Observatory was put into use, and a few observations of the bright sequence stars in ILF-1 were obtained. These suffice to show that the photovisual magnitudes supplied by Kron are within 0.02 mag. (independent of color) of the yellow magnitudes (V) defined by Johnson and Morgan[5] and that the color system of the colors sup-

TABLE 2

MAGNITUDE SEQUENCE

Star	m_{pg}	m_{pr}	*RI*	Spectrum
45° 167	7.49	7.53	−0.04	A2
45 157	8.07	8.13	−0.06	A0
43 41	8.03	8.06	−0.03	B9
44 231	8.11	6.78	+1.33	K0 III
45 86	9.15	8.96	+0.19	A5m
44 215	8.69	8.63	+0.06	A2
46 93	9.30	9.46	−0.16	B9
45 147	9.24	7.97	+1.27	G5 III
45 153	9.75	9.72	+0.03	A2
44 122	9.75	9.35	+0.40	F2 V
45 177	10.04	9.55	+0.49	F5 V
44 142	10.40	9.97	+0.43	F5 V
45 131	10.67	10.10	+0.57	F8 V
45 178	10.89	10.24	+0.65	G2 V
44 133	11.29	10.21	+1.08	G8 V
45 170	11.15	9.76	+1.39	G8 III
44 148	11.43	11.09	+0.34	F2 V
45 144	11.64	10.81	+0.83	G5 V
44 137	12.00	10.50	+1.50	G8 III
44 147	12.16	11.45	+0.71	G2
44 139	12.29	11.67	+0.62	G0
45 173	12.45	12.04	+0.41	F5
(23)	12.78	12.07	+0.71	G0
45 146	13.05	11.48	+1.57	G8:
45 162	12.98	11.61	+1.37	G5
(26)	.....	11.75	+1.5:	G5–8
(27)	.....	11.73	+1.6:	K
(28)	.....	12.48	+0.8:	F–G

plied by Kron satisfies the relations variously given for Eggen's "Photoelectric Studies" by Eggen himself,[6] Johnson,[7] and Johnson and Morgan.[5] A series of additional photoelectric measures is planned for the forthcoming observing season to establish these relationships in this field.

Table 2 contains, for the stars which formed the sequence, the photographic magnitudes (second col.), the photored magnitudes (third col.), the corresponding red indices (fourth col.), and the spectral types. The entries in the first column are the identification numbers on the charts, Figure 1, *A–F*. The magnitudes for these stars which are given in the catalogue (Table 3) are those determined from the field plates only.

[5] *Ap. J.*, **114**, 522, 1951.

[6] Paper VIII, *Ap. J.*, **114**, 141, 1951.

[7] *Ap. J.*, **112**, 240, 1950.

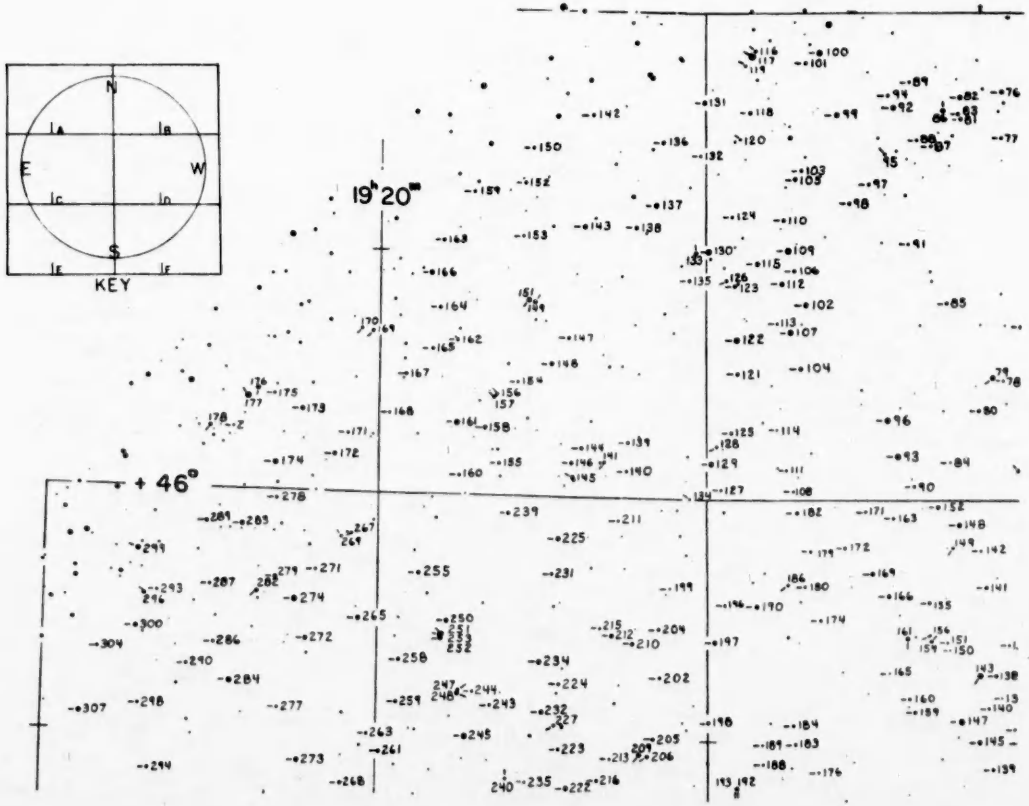

FIG. 1A–F.—Identification chart for ILF-1

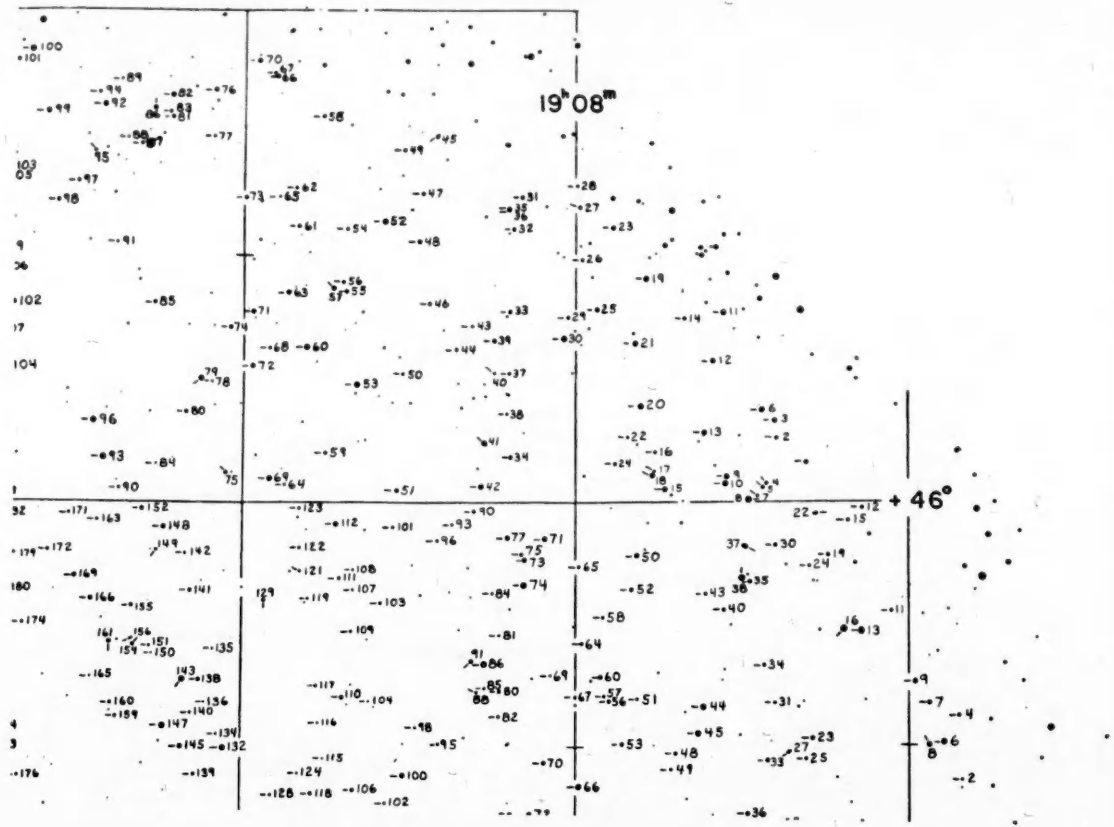

FIG. 1B–F.—Identification chart for ILF-1

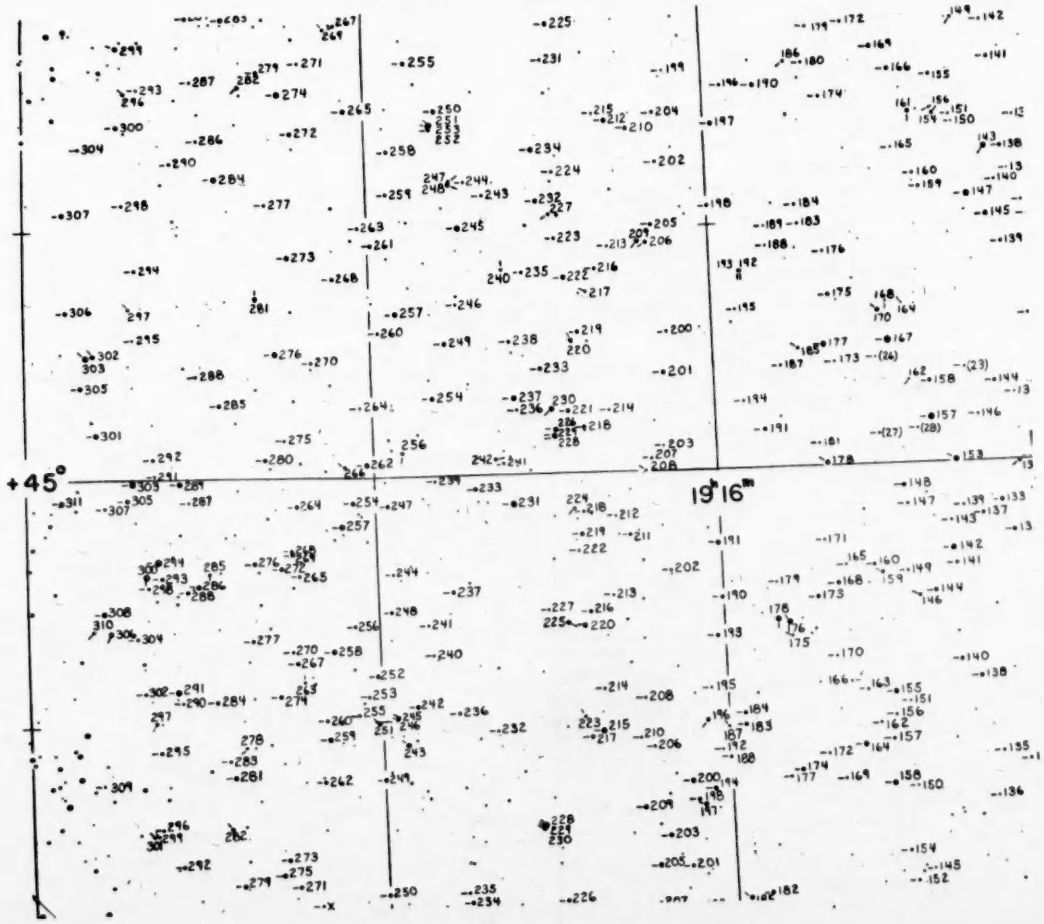

FIG. 1C–F.—Identification chart for ILF-1

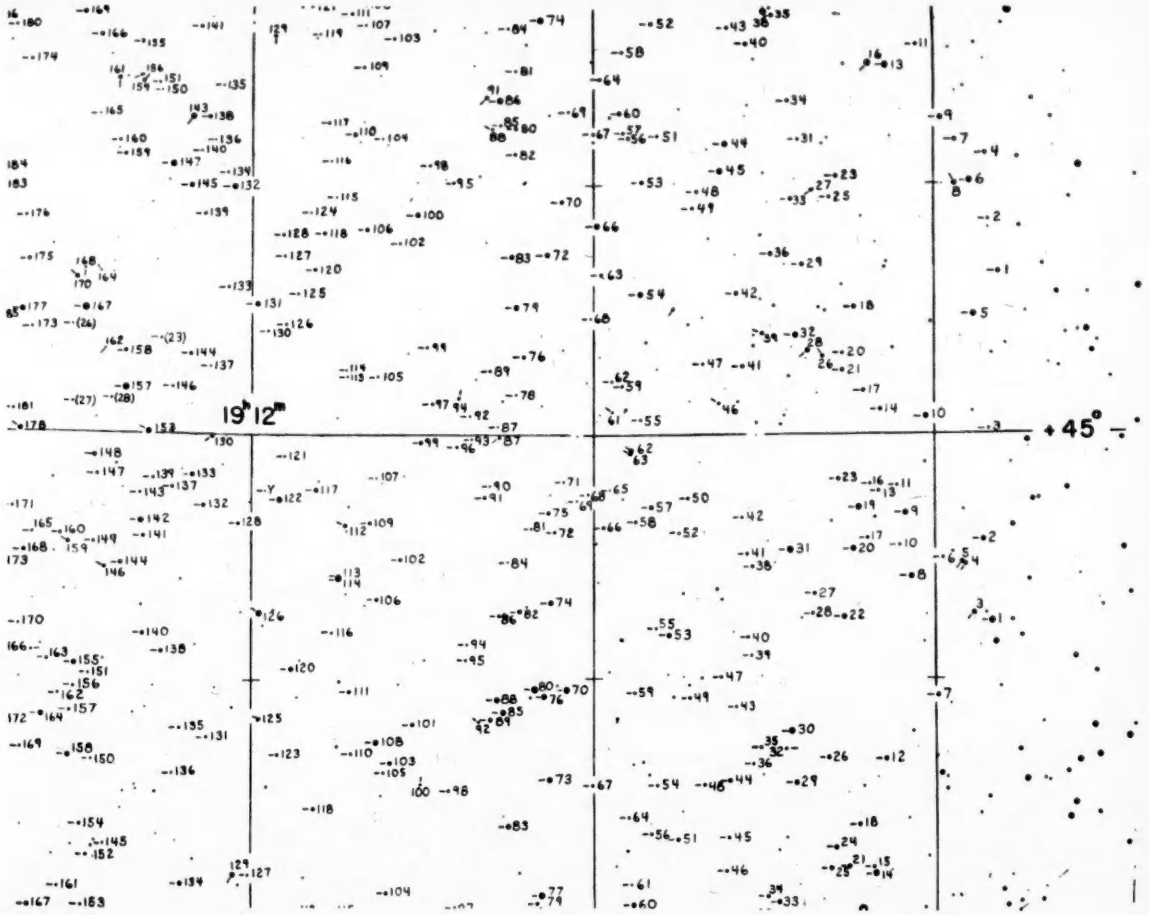

FIG. 1D–F.—Identification chart for ILF-1

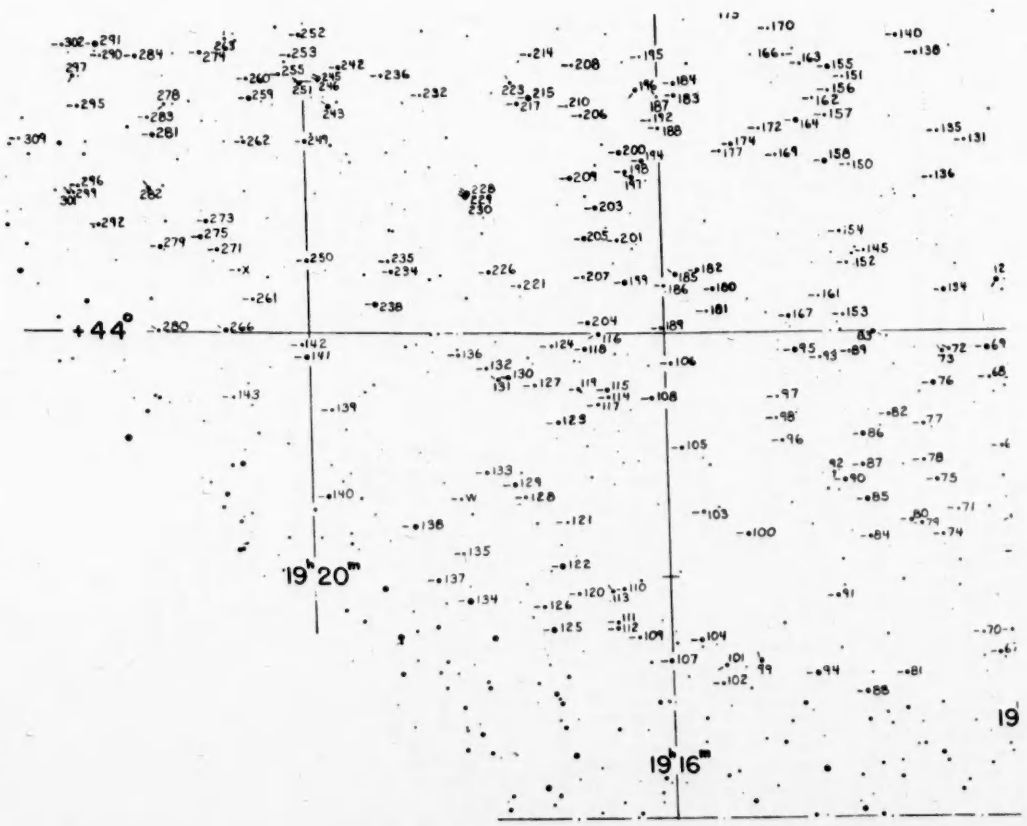

FIG. 1E–F.—Identification chart for ILF-1

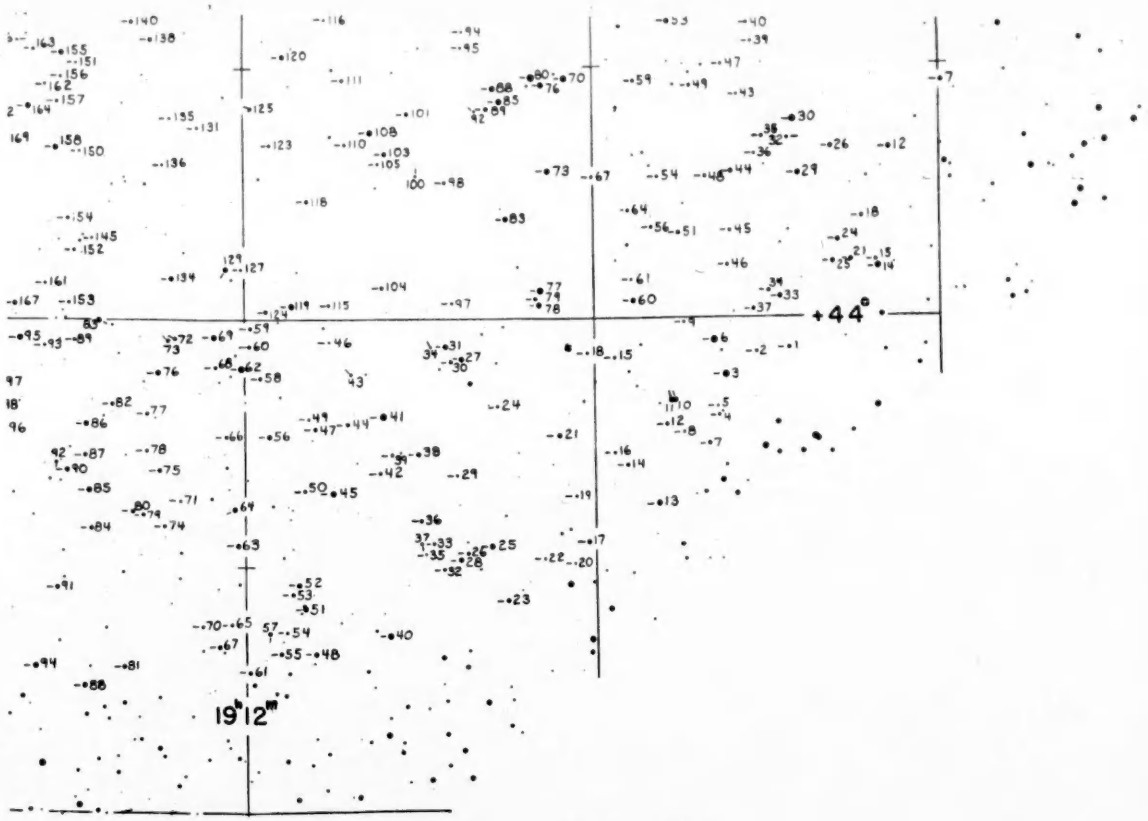

FIG. 1F–F.—Identification chart for ILF-1

SPECTRAL CLASSIFICATION

The characteristics of the objective-prism spectra taken with the Burrell telescope have been described in the previous publications of this observatory already referred to. The faint stars have been classified on three 30-minute plates (IIa-O). For the stars brighter than photographic magnitude 11.2, from two to six plates of shorter exposure have been used. Other plates taken with the 4° and 2° prisms and covering the photographic, visual, red, and infrared regions of the spectrum have been consulted to decide difficult cases, overlapping spectra, very red stars, or variables. The classification given in the catalogue represents a final estimate based on all plates. The system of classification is based on the *Atlas of Stellar Spectra*.[8] Objective-prism spectra of representative stars with Yerkes classifications were available and used as standards during the classification. For about half the stars, particularly the ones brighter than magnitude 11.2, the classification was made by direct superposition of the standards over the unknown spectrum.

All stars later than A5 and brighter than magnitude 11.2, with the exception of some difficult cases, were classified according to luminosity. The Roman numeral designations are the same as in the *Atlas*. Peculiar and metallic-line stars were also noted. For stars fainter than 11.2 mag., luminosity classes were assigned wherever possible.

The catalogue of 938 stars is believed to contain all stars in the field brighter than 12.70 photographic magnitude, and a few fainter ones. This limit is about ½ mag. fainter than that reached in LF3b. Presumably, a large part of this is due to the decrease in the scattered light of the Milky Way at this latitude.[9]

THE CHART AND CATALOGUE

The chart on which the stars are identified by number, Figure 1, *A–F*, has been reproduced from a photographic plate (blue-sensitive) taken with the Schmidt camera. The star images have been enlarged by a technique previously described.[10] Some refinements of procedure have been made which lead in this chart to a more satisfactory variation of image size with magnitude. Acknowledgment is made to Mr. D. E. Snow for carrying out the photographic procedures pertaining to the reproduction.

The key to the six sectional charts is found in Figure 1, *A*. The scale of each chart can be found conveniently from the half-degree marks on most of the hour circles. The co-ordinates are for 1950.

In the catalogue, Table 3, the following information is given for each star.

Col. 1.—The catalogue number, following the scheme of the *Bonner Durchmusterung*. If the star is in the BD catalogue, an asterisk is placed after the present catalogue number. In Table 4 will be found the BD numbers and HD numbers for the stars in the field. The letter *R* calls attention to the remarks at the end of the catalogue.

Col. 2.—The photographic magnitude.

Col. 3.—The red index, defined as the difference, photographic minus photored magnitude.

Col. 4.—The spectral type and luminosity classification. In this column, "p" stands for peculiar, "m" for a metallic-line A star, "e" for emission lines, "ov" designates difficulties due to overlapping spectra, and "ft" indicates that the star was difficult to classify because of its faintness. A metallic-line A star is an otherwise normal star which shows the G band, while a peculiar A star is one which shows lines ascribed to europium, chromium, silicon, etc.

In all columns of the catalogue a colon indicates an uncertainty.

[8] Morgan, Keenan, and Kellman (Chicago: University of Chicago Press, 1943).

[9] Henyey and Greenstein, *Ap. J.*, **93**, 70, 1941.

[10] Nassau and MacRae, *op. cit.*, p. 478.

Table 3

Observational Data for Region ILF-1

Zone + 43°

No.	m_{pg}	R. I.	Sp.	No.	m_{pg}	R. I.	Sp.	No.	m_{pg}	R. I.	Sp.
1 R	12.18:	- 0.34	Op	51*	11.24	+ 1.14	G5III	101	12.11	+ 0.17	A0
2	12.41	+ 0.49	F2	52	11.28	+ 0.42	F0	102	12.38	+ 1.82	K3III
3*	8.10	+ 0.69	F8III	53 R	12.21	+ 0.80	G8V	103*	12.05	+ 2.36	M3III
4	12.32	+ 0.48	G0:ov	54	12.58	+ 0.45	F5	104	11.51	+ 0.71	F8V
5	12.58	+ 0.70	G2:ov	55	11.94	+ 1.07	G5:	105	11.91	+ 0.61	F2III
6*	7.72	- 0.16	B8	56	11.14	+ 0.62	G0V	106	12.01	+ 2.57	M2III
7	11.92	+ 0.55	F8	57	12.03	+ 0.47	F2	107*	11.53	+ 1.09	G8V
8	12.58	+ 0.48	F2	58	11.85	+ 0.42	F0	108	11.47	+ 1.34	G8III
9	12.49	+ 0.62	G0	59	11.98	+ 0.68	G2	109	12.56	+ 0.74	G0
10	11.07	+ 1.15	G8III	60	12.09	+ 1.48	K0III	110	12.08	+ 0.50	F0
11*	10.13	+ 1.47	G8III	61	12.09	+ 1.24	G8V	111	12.22	+ 0.40	F5:ov
12	11.99	+ 1.29	G5	62*	8.80	+ 0.46	F0V	112	11.93	+ 1.68	K2III
13*	11.03	+ 1.57	G8III	63	11.04	+ 0.42	F0V	113	12.01	+ 0.87	G0
14	12.13	+ 0.68	G0	64	10.98	+ 0.37	F2V	114	12.14	+ 2.01	K2III
15	12.35	+ 1.71	G8III	65	12.38	+ 0.72	G0	115*	11.21	+ 0.69	G5V
16	12.53	+ 1.59	K0III	66	12.25	+ 0.83	G0	116*	11.42	+ 2.47	M2III
17	11.50	+ 0.69	G0V	67	11.74	+ 1.02	G8V	117	12.12	+ 0.72	F8
18	12.47	+ 1.52	K0III	68	12.18	+ 1.50	K0	118	11.25	+ 1.07	G5III
19	12.51	+ 0.65	F8	69	10.29	+ 0.03	A5	119	11.68	+ 0.71	G2
20 R	12.18:	+ 2.25::	M5IIIe	70	12.61	+ 1.60	K0III	120	12.36	+ 0.85	G0
21	11.37	+ 0.63	G2V	71	12.70	+ 0.91	F5	121	12.74	+ 0.50	F0V
22	12.63	+ 1.34	G5V	72*	12.02	+ 1.63	K0III	122*	9.64	- 0.09	A2
23	11.72	+ 0.60	F5	73	11.80	+ 0.72	F5	123*	11.57	+ 2.22	M3III
24	12.28	+ 0.34	A3	74	12.35	+ 0.93	G0	124	12.39	+ 2.14	K3III
25*	10.80	+ 0.59	F8V	75	11.65	+ 0.52	F8	125*	10.12	+ 0.77	G2V
26 R	12.23	+ 0.79	F8	76*	10.93	+ 1.51	K0III	126	12.12	+ 0.43	A5
27	10.78	+ 0.35	F0V	77	12.12	+ 0.83	G0	127 R	12.01:	+ 2.57:	M5III
28	11.13	+ 0.57	G0	78	12.24	+ 0.70	G0	128	12.38	+ 1.81	K0III
29	12.63	+ 1.67	K0III	79	12.22	+ 0.60	F2	129*	11.21	+ 2.38	M0III
30	11.93	- 0.21	B5	80	11.93	+ 0.89	G2	130*	10.84	+ 1.27	K0III
31*	10.85	+ 1.95	K3III	81	11.70	+ 0.64	F8	131	12.01	+ 1.28	G5III
32	12.35	+ 0.74	F8	82	11.87	+ 0.55	F8	132 R	12.69	+ 1.38	G8III
33	12.21	+ 2.09	M5III	83*	10.72	+ 0.15	A3	133	11.99	+ 0.56	F5
34	12.69	+ 1.52	G8III	84	11.99	- 0.50	B5	134*	9.12	+ 1.69	K2III
35	12.63	+ 1.33	G8III	85	10.64	+ 0.66	F5III	135	12.47	+ 0.87	G5
36 R	12.02	+ 0.52:	F8:	86*	10.70	+ 1.63	K2III	136*	12.18	+ 1.76	K0III
37	12.29	+ 0.63	F8	87	11.75	+ 0.31	A2	137	11.63	+ 0.42	F0V
38	11.51	+ 0.91	G2V	88 R	11.32:	+ 0.26:	A2	138*	10.52	+ 0.44	F5V
39	12.24	+ 0.72	F5	89	12.16	+ 0.75	G5V	139	12.29	+ 0.69	F8
40*	9.92	+ 0.52	F5III	90*	11.40	+ 0.58	F2	140	11.08	+ 0.67	F8V
41*	8.03	- 0.06	B9	91	11.82	+ 1.47	G8III	141*	10.43	- 0.17	B8
42	12.01	+ 0.47	F2	92	12.27	+ 0.47	F5	142	12.24	+ 0.78	G0
43*	12.32	+ 0.64	F8	93	12.35	+ 0.48	F5	143	12.63	+ 1.22	G8
44	11.90	+ 0.55	F5	94*	10.57	+ 1.34	G8III				
45*	9.76	+ 1.88	K5III	95*	10.14	+ 0.50	F5V				
								Zone + 44°			
46	12.53	+ 0.68	G0	96	12.20	+ 0.73	G0	1*	9.82	+ 1.60	K0III
47	11.79	+ 1.31	K0III	97	12.59	+ 0.97	G2	2	11.38	+ 1.30	G8III
48	11.48	+ 1.25	K0III	98	12.65	+ 0.82	G2	3	11.48	+ 1.23	G8III
49	12.61	+ 0.63	F5	99	12.38	+ 1.20	G2:ov	4*R	11.74	+ 0.59	G0V
50	12.35	+ 1.43	G5III	100*	11.37	+ 0.51	F5	5*R	11.72	+ 0.37	F2

Table 3

Observational Data for Region ILF-1

Zone + 44° (Cont'd.)

No.	m_{pg}	R. I.	Sp.	No.	m_{pg}	R. I.	Sp.	No.	m_{pg}	R. I.	Sp.
6	12.61	+ 0.59	F0	56	12.15	+ 0.90	G5	106	11.91	+ 0.68	G2
7	11.70	+ 1.28	G8III	57	11.46	+ 0.50	F2V	107	12.48	+ 0.42	F2:ov
8	10.69	+ 0.15	F0V	58	12.40	+ 1.96	K2III	108*	10.58	+ 1.26	G5III
9	10.64	+ 0.22	F2V	59	12.31	+ 0.66	F5	109	11.78	+ 1.39	K0
10	12.69	+ 1.42	G2	60*	11.17	+ 1.40	G5III	110	12.36	+ 0.88	G2
11	12.47	+ 0.55	F8	61	12.58	+ 0.68	F8	111	12.22	+ 1.58	G5III
12*	11.58	+ 1.79	K2III	62	11.88	+ 0.35	F2	112	11.48	+ 0.76	G8V
13	12.42	+ 0.54	F5	63*	11.62	+ 0.66	F5	113*R	10.80	+ 0.47	F2:ov
14*	9.23	+ 1.77	K0III	64*	12.47	+ 2.31	M2III	114*R	10.41	+ 0.39	A5:ov
15	12.42	+ 1.93	K5III	65*	12.89	+ 2.44	M0	115	12.32	+ 0.80	G5
16	12.58	+ 0.44	G0	66	12.03	+ 1.31	G8V	116	12.56	+ 0.52	F5:ft
17	12.44	+ 0.71	G0	67	12.29	+ 1.28	K2:ov	117*	11.38	+ 1.59	G8III
18*	11.99	+ 0.56	G0	68	12.49	+ 0.57	F8	118	11.92	+ 0.69	F8
19*	10.00	+ 1.42	G8III	69	12.64	+ 0.74	G5	119*	10.37	+ 1.14	G5III
20*	10.50	+ 0.29	A5p	70*	9.20	+ 0.29	A5p	120	11.22	+ 1.10	G8V
21	11.73	+ 0.58	G0	71*	12.55	+ 0.64	G0	121	12.58	+ 1.37	K2
22	11.01	+ 0.37	F0V	72	12.20	+ 1.29	G5III	122*	9.82	+ 0.44	F2V
23	11.92	+ 1.37	G8III	73 R	10.63	- 0.03	F0III	123	12.61	+ 2.41	K5
24	11.50	+ 1.92	K3III	74	10.81	+ 0.51	F8III	124	12.05	+ 1.46	G8III
25	11.69	+ 0.50	F0	75	11.80	+ 1.55	K0III	125	12.65	+ 0.81	F5
26	11.84	+ 1.50	K0III	76	10.40	+ 0.74	G2V	126*R	9.87	+ 1.13	G5V
27	12.16	+ 1.32	G5III	77*	9.22	+ 0.35	F0V	127	12.56	+ 1.76	G8
28	12.23	+ 1.22	G8III	78*	10.90	+ 1.11	G8V	128	12.12	+ 0.71	F8
29*	11.06	+ 1.35	G8III	79	12.17	+ 0.56	F2	129*	10.76	+ 0.17	A5
30*	8.78	+ 0.60	F2III	80*R	7.60	+ 0.15	A5	130	12.02	+ 1.50	G8III
31*R	8.99	+ 0.95	G0V	81	12.44	+ 1.29	G5III	131	12.45	+ 0.65	G2
32	12.33	+ 0.57	F8	82	11.22	+ 0.34	F0V	132	11.70	+ 1.04	G2III
33	11.47	+ 0.46	F2	83	10.86	+ 0.59	F8V	133	11.28	+ 1.15	G8V
34	12.05	+ 1.43	G8III	84	12.59	+ 0.25	A3	134*	11.09	+ 0.20	F0:
35	12.13	+ 0.17	A2	85*	10.15	+ 0.11	A3p	135	12.44	+ 0.64	G0
36	12.63	+ 0.59	F5	86	12.22	+ 1.37	K0III	136	12.59	+ 0.79	F8
37	11.97	+ 0.83	G0	87	12.20	+ 0.67	F8	137	12.02	+ 1.50	G8III
38	12.32	+ 0.34	F2	88*	10.38	+ 0.81	G5V	138	11.54	+ 0.41	F0
39	12.47	+ 0.56	G0	89	11.58	+ 0.72	G0	139	12.40	+ 0.81	G0
40	12.50	+ 2.00	K2	90	12.58	+ 0.83	G0	140	11.90	+ 0.82	G0
41	12.18	+ 0.41	F2	91	11.82	+ 0.47	F5	141	11.95	+ 0.52	F5
42	12.61	+ 1.24	G8V	92	12.65	+ 1.02	G2	142*	10.38	+ 0.40	F5V
43	12.68	+ 0.83	F8:	93	12.52	+ 0.67	F5	143	12.56	+ 0.70	G0
44	11.44	+ 0.58	F8	94	12.52	+ 0.37	F0	144	11.64	+ 0.70	G0V
45	12.24	+ 1.27	G5III	95	12.41	+ 0.56	F5	145	12.53	+ 0.89	G0
46	12.27	+ 0.75	F8	96	12.21	+ 0.51	F2	146	12.02	+ 0.26	A2
47	12.42	+ 0.93	G5V	97	12.43	+ 1.04	G5	147	12.16	+ 0.68	G2
48	12.16	+ 1.28	G5III	98	12.30	+ 0.66	G0	148	11.34	+ 0.46	F2V
49	12.23	+ 0.15	A2	99	11.52	+ 0.51	F2	149	12.33	+ 0.71	F5
50	12.16	+ 0.50	F8	100	12.61	+ 0.55	F5	150	12.63	+ 0.77	G5V
51*	11.78	+ 0.43	F2	101	11.77	+ 1.58	K0III	151	12.77	+ 0.36	A2:
52	12.35	+ 0.43	F5	102	11.77	+ 0.40	F2	152	12.39	+ 1.48	K0V
53	11.06	+ 0.42	F8V	103	11.60	+ 0.80	G0V	153	12.40	+ 1.34	G8
54	12.35	+ 0.75	G2	104	11.87	+ 0.47	F2	154	12.18	+ 0.70	F8
55	12.53	+ 0.53	F8	105	12.42	+ 0.77	G0	155*	10.86	+ 0.72	G0V

Table 3

Observational Date for Region ILF-1

Zone + 44° (Cont'd.)

No.	m_{pg}	R. I.	Sp.	No.	m_{pg}	R. I.	Sp.	No.	m_{pg}	R. I.	Sp.
156	12.38	+ 0.64	F5	206	12.40	+ 0.53	F8:	256	12.14	+ 0.34	A5
157	12.16	+ 0.64	F8	207	12.38	+ 0.59	F8	257*R	9.90	+ 0.32	A5
158*	10.78	+ 2.17	M0III	208	12.25	+ 0.82	G2	258*	10.63	+ 1.37	K0III
159	11.93	+ 0.50	F2	209*	10.98	+ 0.79	G5V	259*	10.83	+ 0.41	A5p
160	12.18	+ 0.56	F5	210	12.68	+ 0.73	G0:	260	12.15	+ 1.55	G8V
161	12.63	+ 0.85	G0:	211	12.22	+ 0.79	F8	261	12.30	+ 0.76	F8
162	12.51	+ 0.83	G2	212	12.79	+ 0.65	F2V	262	12.00	+ 1.28	K2III
163 R	12.21	+ 0.77	G2	213	12.69	+ 1.87	G8V	263	12.42	+ 0.67	F5
164*	10.65	+ 1.26	G5III	214	12.33	+ 0.90	G0	264	11.84	+ 0.55	F8
165	12.69	+ 0.77	F5	215*	8.70	+ 0.14	A2	265	12.29	+ 1.59	G8III
166	12.68	+ 0.70	F5	216	11.95	+ 1.58	G2III	266	11.10	+ 0.36	F0
167*	11.52	+ 1.64	K0III	217	11.39	+ 0.55	F5	267*	11.46	+ 2.07	K2III
168	11.60	+ 0.70	F5	218	12.58	+ 0.75	F8:ov	268	12.47	+ 0.37	F0:ov
169	12.45	+ 0.70	G0	219	11.43	+ 0.53	F0	269	11.52	+ 1.46	K0III
170	12.75	+ 0.41	A2	220*	10.88	+ 1.07	G5III	270	12.47	+ 1.02	G2
171	12.55	+ 0.48	F5	221	12.29	+ 0.65	F8	271*	12.00	+ 0.75	G0
172 R	12.58	+ 2.11	K0III	222	12.35	+ 0.72	F8:ov	272	11.30	+ 0.40	F2
173	11.91	+ 0.62	F5	223	12.23	+ 1.59	K0III	273*	11.54	+ 0.67	F8
174*	11.56	+ 2.21	K5III	224	12.11	+ 1.72	K0III	274	11.63	+ 0.21	A2
175	12.36	+ 0.58	F8	225	11.68	+ 0.06	B8	275	11.38	+ 1.74	K0III
176*	9.59	+ 1.41	G8III	226*	11.95	+ 1.97	K2III	276*	11.48	+ 2.12	K5III
177	12.24	+ 0.54	F5	227	12.65	+ 0.79	G0	277	12.02	+ 0.79	G0
178*	9.88	+ 1.86	K3III	228*R	9.21	+ 0.77	F8III:ov	278	12.42	+ 0.80	G0
179	12.84	+ 0.60	A:ft	229	11.97	+ 0.48	F2:ov	279	11.46	+ 0.57	F0
180	11.62	+ 1.86	K3III	230	12.18	+ 2.32	M5III	280	12.48	+ 1.38	G8
181*	12.64	+ 0.50	F5	231*	8.11	+ 1.38	K0III	281	11.12	+ 0.04	A2
182	11.45	+ 1.45	G8III	232	12.44	+ 0.58	F5	282	11.88	+ 0.42	A5
183	11.73	+ 0.08	B9	233	11.61	+ 0.75	F5III	283	12.61	+ 0.82	G0:
184	11.75	+ 1.23	G8V	234	11.94	+ 0.57	F0	284	11.65	+ 0.26	F0
185	11.11	+ 0.67	F8III	235	12.44	+ 1.01	G2:	285	12.20	+ 0.34	A5
186	12.15	+ 0.84	G0	236	11.99	+ 1.80	K3III	286	10.71	+ 0.13	A3
187	12.47	+ 0.53	A5	237	11.77	+ 1.36	G5III	287	12.63	+ 0.47	F5
188	12.22	+ 1.52	K0	238*	9.97	+ 0.57	G0V	288	11.82	+ 0.45	F2
189*	11.96	+ 1.04	G5	239	12.42	+ 1.60	G8III	289*	10.10	+ 1.30	G5III
190	11.85	+ 1.02	G5V:	240	12.67	+ 1.57	K0III	290	12.67	+ 0.55	F0
191*	10.69	+ 0.42	F0III	241	12.63	+ 1.59	K2III	291*	9.46	+ 1.12	G5V
192	12.65	+ 0.54	F5	242	11.48	+ 1.61	K0III	292 R	12.51	+ 1.32	G8III
193	11.80	+ 0.60	F5	243*	10.64	+ 1.24	K0V	293	11.83	+ 0.58	F5
194*	11.20	+ 0.64	F2V	244	12.61	+ 0.99	G0	294*	7.82	+ 1.14	K0V
195	12.76	+ 0.50	A:ft	245	12.31	+ 0.79	F5:ov	295	12.12	+ 0.48	F2
196	11.74	+ 0.51	F2ov	246	12.65	+ 0.88	F8:ov	296	12.33	+ 1.77	K0III
197*	11.13	+ 0.57	F2V	247	11.76	+ 0.45	F5	297	12.32	+ 0.82	G0
198*	11.65	+ 0.77	G2	248	12.17	+ 0.65	F0	298	12.44	+ 0.80	G0
199*	10.13	+ 1.52	K0III	249	11.50	+ 1.44	G8III	299	12.49	+ 0.77	G0
200*	10.59	+ 0.65	G0V	250	11.56	+ 0.76	F8III	300*	8.63	+ 0.13	A0
201	12.09	+ 1.53	K0III	251	11.15	+ 0.62	F8	301	12.16	+ 0.56	F5
202	12.43	+ 2.10	K0:ov	252	11.56	+ 0.54	F0V	302	12.27	+ 1.49	K2
203*	11.00	+ 0.63	F8V	253	12.44	+ 1.03	G0	303*	8.81	+ 0.45	F0V
204*	11.49	+ 2.35	K5III	254*	11.32	+ 2.39	M3III	304	12.20	+ 1.32	K0III
205*	10.84	+ 0.47	F2V	255	12.19	+ 1.84	K0III	305	11.56	+ 0.61	F2

Table 3

Observational Data for Region ILF-1

Zone + 44° (Cont'd.)

No.	m_{pg}	R. I.	Sp.
306*	11.52	+ 0.68	G0
307	12.31	+ 0.51	F5
308*	10.40	+ 1.87	K2III
309 R	12.80:	+ 2.58:	S
310	12.22	+ 1.56	K0III
311	10.78	+ 0.41	F5V

Zone + 45°

No.	m_{pg}	R. I.	Sp.
1	11.72	+ 1.40	G8III
2	12.60	+ 0.74	G2
3	12.51	+ 0.51	F5
4	12.11	+ 0.82	G2V
5*	10.60	+ 0.30	F2V
6*	10.56	+ 1.58	K0III
7*	11.96	+ 0.79	G2V
8*	11.34	+ 1.39	G8III
9*	11.14	+ 0.56	F5III
10*	11.09	+ 1.30	K0III
11	12.30	+ 0.27	F0
12	12.10	+ 0.53	F8
13*R	10.46	+ 2.01	K2III
14	11.96	+ 1.24	G5III
15	12.29	+ 1.53	K5III
16*	8.96	+ 0.20	A5
17	11.96	+ 0.48	F5
18	11.78	+ 1.42	K0III
19	12.07	+ 0.53	F8
20	12.34	+ 0.22	A5
21	12.14	+ 2.06	K5III
22	12.39	+ 0.66	F8
23	11.86	+ 0.69	G2
24	12.58	+ 1.74	K0III
25	12.23	+ 0.21	A5
26	12.22	+ 0.28	F2
27	12.36	+ 1.42	K0III
28	11.44	+ 1.63	K3III
29	11.76	+ 1.57	G8III
30	12.13	+ 1.80	K3III
31	12.64	+ 1.31	K0III
32*	10.38	+ 0.47	F5V
33	11.91	+ 0.68	G0V
34	12.24	+ 0.46	F2
35	11.74	+ 0.39	F5III
36	11.69	+ 1.05	G8V
37	11.68	+ 0.51	F5
38*	9.07	+ 0.75	F8V
39	12.11	+ 0.53	F5III
40	11.88	+ 0.59	G2
41	12.02	+ 0.73	G0V
42	11.93	+ 1.39	K0III
43	12.11	+ 0.19	F2V
44*	10.40	+ 0.38	F2III
45*	10.13	+ 0.66	G2V
46	12.42	+ 0.66	F8
47	12.58	+ 0.73	F8
48	12.16	+ 0.52	F5
49	12.36	+ 0.92	G5
50	11.40	+ 0.60	F5
51	12.40	+ 1.37	G8III
52	11.77	+ 0.38	F0
53	11.88	+ 0.26	A5p
54*	10.78	+ 1.18	G5III
55	12.52	+ 0.18	A5
56	12.07	+ 1.47	G5III
57	12.30	+ 0.25	A5
58	12.35	+ 0.49	F2
59	12.35	+ 1.47	K0III
60	11.54	+ 0.14	A2p
61	12.58	+ 0.88	G2
62	12.36	+ 0.56	F8
63	12.08	+ 0.42	A3p
64	12.07	+ 0.61	F5
65	12.16	+ 0.81	G2
66*	10.17	+ 1.56	G8III
67	12.18	+ 1.45	K2III
68	12.61	+ 0.69	F5
69	12.58	+ 0.54	F5
70	11.68	+ 1.02	G5III
71*	11.01	+ 1.72	K3III
72	10.97	+ 1.13	G5III
73*	10.99	+ 1.31	G8III
74*	9.45	+ 0.75	F8V
75	11.86	+ 0.46	F2
76	11.82	+ 0.51	F5
77	11.23	+ 0.50	F5V
78	12.49	+ 0.77	G5V:
79*	10.52	+ 1.71	K2III
80	11.99	+ 0.57	G0
81	12.47	+ 1.69	G5:
82	12.12	+ 0.28	A5
83	11.08	+ 0.58	F8III
84	12.59	+ 1.77	K2III
85	12.35	+ 0.53	F5:ov
86*	9.17	+ 0.18	A5m
87	12.63	+ 1.79	K2III
88	12.24	+ 0.71	G0
89	12.31	+ 1.58	K0III
90	12.02	+ 0.28	F0
91	11.75	+ 0.60	F5
92	12.45	+ 0.59	F5
93	12.51	+ 1.34	G5V
94 R	12.56	+ 0.80	F8
95	12.16	+ 0.48	F5
96	12.20	+ 0.76	G0
97	11.87	+ 0.42	F5
98	12.34	+ 0.95	G5
99	12.16	+ 0.79	G5
100*	10.86	+ 1.03	G8V
101	12.44	+ 1.76	G8III
102	12.19	+ 1.29	G5
103	12.24	+ 0.79	G2
104	12.68	+ 0.59	F5
105*	12.28	+ 0.78	G5
106	11.52	+ 1.52	K0
107	12.53	+ 2.22	M2III
108	12.49	+ 1.52	G5III
109	12.20	+ 0.60	F5
110*	11.36	+ 1.28	G8III
111	12.05	+ 0.12	A2
112*	10.82	+ 1.93	K3III
113	12.40	+ 0.80	G5:ov
114	12.53	+ 0.59	G0:ov
115	12.63	+ 1.85	K0III
116	12.58	+ 1.29	G5III
117	12.05	+ 0.41	F0
118	11.82	+ 1.67	K0III
119	12.53	+ 0.54	F5
120*	11.78	+ 1.41	G5III
121	12.35	+ 0.52	F2
122	12.19	+ 1.47	K0III
123	12.03	+ 0.51	F0
124	12.61	+ 0.58	F2
125	12.27	+ 2.34	M2III
126	11.93	+ 0.60	G2
127	12.16	+ 1.31	G5
128	12.14	+ 0.70	G0
129	11.97	+ 1.74	K0III
130	12.32	+ 0.97	G5
131*	10.67	+ 0.67	F8V
132*	10.01	+ 0.07	A2p
133	11.96	+ 0.50	A5
134	12.51	+ 1.01	G2
135	12.45	+ 0.78	G2
136	12.65	+ 0.79	G2
137	12.54	+ 1.41	G5
138	11.56	+ 0.68	G0V
139	11.91	+ 0.63	F8
140	12.22	+ 0.56	F0

Table 3

Observational Data for Region ILF-1

Zone + 45° (Cont'd.)

No.	m_{pg}	R. I.	Sp.	No.	m_{pg}	R. I.	Sp.	No.	m_{pg}	R. I.	Sp.
141	11.97	+ 2.34	K5III	191	11.66	+ 0.73	F2	241	12.40	+ 0.70	G2:ov
142	12.53	+ 1.01	G5	192	12.06	+ 0.36	A5	242	11.91	+ 0.58	G0
143*	9.97	+ 0.32	A5	193	12.63	+ 0.61	F2:ov	243	12.43	+ 0.74	G2
144	11.72	+ 1.00	G5V	194	12.40	+ 0.98	G5V	244	12.63	+ 1.85	K3III
145	10.93	+ 0.46	F0V	195	12.51	+ 1.51	G8III	245	9.75	+ 1.52	G8III
146	13.05	+ 1.57	G8:	196	12.20	+ 0.32	F2	246	12.48	+ 0.32	F2V
147*	9.31	+ 1.37	G5III	197*	11.18	+ 0.84	G5V	247	12.38	+ 0.62	F5:ov
148*	10.95	+ 0.58	F5V	198	11.71	+ 1.08	G8V	248*	11.05	+ 1.30	K0III
149	12.23	+ 0.59	F8	199	12.61	+ 0.41	F5:	249*	11.22	+ 1.90	K5III
150	12.58	+ 0.67	F8:ov	200	12.09	+ 0.66	G0	250*	11.24	+ 1.49	G8III
151	12.38	+ 1.15	G5	201	11.45	+ 0.85	G2V	251	11.54	+ 0.67	F5III:ov
152*	11.40	+ 1.90	G8III	202	12.27	+ 0.83	F8	252	11.93	+ 0.55	ov
153*	9.78	+ 0.11	A2	203	12.63	+ 0.54	F5:	253*	10.90	+ 1.61	K0III
154	11.64	+ 0.43	F0	204	12.12	+ 0.67	F5	254	11.15	+ 1.53	K0III
155	11.68	+ 0.49	F2	205	11.80	+ 1.67	K0III	255	11.71	+ 0.84	G5V
156	12.67	+ 0.77	G0:ov	206	11.68	+ 0.80	G2	256	11.98	+ 0.53	F0V
157*	8.01	- 0.10	A0	207	12.38	+ 1.60	G5	257*	10.55	+ 0.37	F5V
158*	11.68	+ 1.53	K2III	208	12.44	+ 0.62	G0	258	11.94	+ 0.51	F2
159	11.70	+ 0.74	F8	209*	11.04	+ 0.71	G0V	259	12.09	+ 0.51	F5
160	11.95	+ 1.58	G8III	210	11.55	+ 1.43	K0III	260	12.14	+ 0.32	A5
161	11.50	+ 1.71	K3III	211	12.68	+ 0.62	F8	261	11.70	+ 1.24	G5
162	12.98	+ 1.37	G5	212	11.22	+ 0.60	G0	262*	10.67	+ 0.17	A5
163	12.24	+ 0.83	G2	213	12.57	+ 1.34	G8III	263	12.44	+ 1.68	K0III
164	12.57	+ 1.47	K0	214	12.56	+ 0.74	F5	264	12.67	+ 0.74	F8:
165	12.56	+ 0.70	G2	215	12.62	+ 0.85	F8	265	11.19	+ 0.71	G2
166	11.24	+ 1.22	G8III	216	12.23	+ 0.79	G0V	266	12.18	- 0.11	A2:
167*	7.52	- 0.02	A2	217	12.25	+ 0.42	A3	267	12.58	+ 1.10	G5
168	12.31	+ 0.55	G0	218	11.62	+ 0.33	F2	268 R	12.00	+ 0.57	G2
169	11.18	+ 0.43	F0III	219	11.58	+ 1.31	K0V	269	12.53	+ 0.73	F8
170*	11.08	+ 1.32	G8III	220*	11.20	+ 0.48	F0III	270	12.32	+ 0.92	G5ov
171	12.05	+ 0.31	A5:	221*	11.17	+ 0.59	F2V	271	12.62	+ 0.36	A3p:
172	12.55	+ 0.61	G2	222	10.97	+ 2.08	K5III	272*	11.41	+ 1.78	K2III
173	12.40	+ 0.49	F5	223	12.27	+ 0.67	F8	273*	10.76	+ 1.48	K0III
174	12.05	+ 0.80	G5	224	12.44	+ 1.38	G5	274*	9.52	+ 0.41	F2V
175	11.40	+ 0.70	G0	225*	11.33	+ 1.40	K0III	275	12.56	+ 0.58	F2
176	12.15	+ 0.61	F5	226*R	10.71	+ 0.09	A5	276*	9.83	+ 1.55	K0III
177*	9.97	+ 0.43	F5V	227	12.21	+ 0.94	G5	277	12.36	+ 2.19	K3III
178*	11.06	+ 0.82	G2V	228	11.96	+ 0.41	ov	278	12.51	+ 1.54	K0III
179	12.19	+ 0.69	F5	229*R	11.02	+ 0.52	F2ov	279	11.88	+ 1.01	G2
180	12.18	+ 0.62	F5:	230*	10.33	+ 0.41	F5III	280	11.70	+ 0.62	F2V
181	12.58	+ 0.60	F5	231	12.25	+ 0.31	F2	281	11.58	+ 0.46	F5
182	11.68	+ 0.76	G2	232	11.28	+ 1.40	K0III	282	11.77	+ 0.52	F2
183	11.96	+ 0.53	F5	233 R	12.12	+ 0.60	A5	283*	11.22	+ 1.77	K0III
184	12.05	+ 1.97	K3III	234*	10.69	+ 1.10	G8V:	284*	10.05	- 0.26	B9
185	11.94	+ 1.54	G8III	235	12.30	+ 0.49	F2	285*	11.53	+ 0.67	G2
186	12.17	+ 0.70	F5	236	12.47	+ 2.28	K5III	286	12.44	+ 0.40	F8
187	12.33	+ 1.80	K2III	237*	10.06	- 0.13	B9	287	12.65	+ 0.67	G2
188	12.31	+ 0.48	F2	238	12.09	+ 1.93	K0III	288	12.31	+ 0.83	G2
189	12.64	+ 0.75	F8:ov	239 R	11.99:	+ 0.79:	G2	289	12.04	+ 0.62	F5
190*	11.17	+ 0.40	F5III	240	12.50	+ 1.56	K0III	290	12.34	+ 0.44	F0V

Table 3

Observational Data for Region ILF-1

Zone +45° (Cont'd.)

No.	m_{pg}	R. I.	Sp.	No.	m_{pg}	R. I.	Sp.	No.	m_{pg}	R. I.	Sp.
291	12.58	+ 0.56	F8:	31	11.82	+ 0.25	F2	81	11.84	+ 0.63	G0
292	12.01	+ 0.51	F2	32	11.96	+ 0.84	G2	82	11.03	+ 0.49	F5III
293	12.58	+ 0.80	G2	33	11.78	+ 1.55	G8III	83	12.16	+ 0.77	G0
294	11.86	+ 0.55	G0	34	11.60	+ 1.59	G8III	84	12.55	+ 0.59	G0
295	12.70	+ 1.53	K0III	35	12.01	+ 0.56	ov	85	11.97	+ 0.59	F8
296	11.91	+ 0.62	F8	36	12.51	+ 1.67	ov	86*	11.04	+ 0.14	A3
297	12.28	+ 0.46	F2	37	11.86	+ 0.48	F5	87	12.35	+ 1.04	G8V
298	12.21	+ 0.11	A2p:	38	12.34	+ 0.60	G0:	88	12.51	+ 0.65	F5
299	10.78	+ 0.58	F5III	39	11.47	+ 0.67	F8	89	12.44	+ 0.36	F2
300	11.30	+ 1.27	G8III	40	12.32	+ 0.64	F5p	90*	11.76	+ 1.70	K5III
301*	10.59	+ 0.37	F0V	41*	11.91	+ 0.62	F8III	91	12.61	+ 0.57	F5
302*	11.11	+ 0.39	F2III	42*	10.61	+ 1.43	K0III	92*	10.32	+ 0.38	F2V
303*	9.29	+ 0.48	F0p	43	12.22	+ 0.50	F2	93*	9.23	- 0.22	B9
304	12.36	+ 0.78	G2	44	12.03	+ 1.42	G8V	94	12.17	+ 0.01	A2
305*	11.28	+ 1.20	G8III	45	12.14	+ 1.52	G8III	95	12.31	+ 0.44	F2
306	11.35	+ 0.49	F5V	46	11.80	+ 0.55	F8	96*	9.63	+ 0.05	A2
307	10.69	+ 0.28	A5	47	12.15	+ 1.66	G8III	97	12.13	+ 0.15	A2
				48	11.42	+ 1.15	G8III	98 R	11.78	+ 0.13	A2
				49 R	11.96	+ 0.51	F5	99	10.80	+ 0.38	G0V
	Zone + 46°			50	12.13	+ 2.29	M3	100*	9.28	+ 0.06	A3
1	12.01	+ 1.52	G8III	51	11.46	+ 0.52	F2	101	11.78	+ 0.37	F5
2	12.21	+ 2.10	K5III	52*	10.31	+ 1.12	G8V	102*	10.34	+ 1.80	K2III
3	11.34	+ 1.30	G8III	53*R	9.90	+ 0.81	G0V	103	11.90	+ 0.35	F5
4	12.12	+ 0.54	G0	54	12.11	+ 0.55	F5	104	11.22	+ 0.32	F0
5	12.21	+ 0.56	F8	55	11.53	+ 0.47	F0	105*	11.24	+ 0.42	F5
6*	10.82	+ 1.14	G8III	56*	12.11	+ 1.97	K3III	106	11.92	+ 0.36	A5
7	12.51	+ 0.98	G5III	57	10.95	+ 0.58	F8III	107*	9.72	+ 2.12	K5III
8*	9.27	+ 2.06	K3III	58	12.12	+ 0.64	F8	108	12.16	+ 0.66	G0
9	10.89	+ 0.87	G2III:ov	59	12.03	+ 1.37	K0III	109*	7.98	+ 0.06	A2
10*	10.35	+ 0.49	F8IIIov	60*	10.18	+ 0.60	F8III	110	11.78	+ 1.20	G5III
11*	10.55	+ 0.32	F5V	61	11.95	+ 1.08	G5III	111	12.33	+ 0.64	F5
12*	11.27	+ 0.49	F2V	62	12.35	+ 1.33	G5	112	11.09	+ 0.54	F8V
13*	11.17	+ 0.73	G5V	63*	11.24	+ 1.11	G5V	113	12.58	+ 0.56	F8
14	12.22	+ 0.74	G2	64	12.09	+ 0.37	F0	114	12.50	+ 1.78	K2
15	10.76	+ 0.48	F8V	65	12.68	+ 1.39	G8	115	11.26	+ 1.37	K0III
16	12.22	+ 0.40	F2	66	11.66	+ 0.48	F8	116 R	12.20	+ 0.14	A2:ov
17	12.48	+ 0.46	F2	67	12.14	+ 0.50	G0	117*R	6.35	+ 0.50:	F5V
18*	10.70	+ 0.06	A3	68	12.21	+ 1.50	K0III	118	11.73	+ 0.82	G2
19*	10.95	+ 0.76	G2V	69*	10.36	+ 1.23	G8III	119	12.39	+ 0.94	G5
20*	10.40	+ 2.37	M0III	70 R	11.07:	+ 2.25:	M5IIIe	120	12.62	+ 0.60	F8
21*	10.99	+ 0.99	G2III	71*	11.42	+ 1.99	K2III	121	11.68	+ 0.48	F5
22	12.47	+ 0.36	A5	72*	11.18	+ 1.36	G8III	122*	9.39	+ 1.93	K5III
23	11.74	+ 1.37	G8III	73	11.94	+ 1.90	K2III	123	11.81	+ 1.01	G5
24	12.05	+ 0.52	F5	74	11.58	+ 0.94	G8V	124	12.51	+ 1.05	G5
25	11.52	+ 0.70	G0	75*	11.64	+ 1.91	K2III	125	12.02	+ 0.02	A2
26	12.05	+ 0.51	F5	76	11.82	+ 0.55	F2	126	11.92	+ 0.60	F5
27	12.09	+ 0.63	F5	77	12.61	+ 1.71	G8III	127	12.31	+ 0.41	F8:
28	12.68	+ 1.55	G5	78	12.48	+ 1.60	G8III	128	12.00	+ 0.58	F8
29	12.14	+ 0.53	F5	79*	10.58	+ 0.55	G0V	129*	10.43	+ 1.48	G8Ib
30*	10.36	+ 2.22	K5III	80	11.64	+ 0.31	F0V	130*	9.10	+ 0.31	A5p

Table 3

Observational Data for Region ILF-1

Zone + 46° (Cont'd.)

No.	m_{pg}	R. I.	Sp.	No.	m_{pg}	R. I.	Sp.	No.	m_{pg}	R. I.	Sp.
131	11.08	+ 0.56	G0V	146	11.88	+ 0.64	G0	161*	9.39	- 0.02	A3
132	12.93	+ 2.46	M5III	147	12.33	+ 1.33	K0	162	12.31	+ 1.37	G5III
133	11.48	+ 0.64	F8	148	11.46	+ 0.70	F8	163	12.11	+ 0.55	F2
134	12.59	+ 0.53	F5	149	11.47	+ 0.59	F5	164	12.09	+ 0.55	F0
135	12.14	+ 2.08	K2	150	12.64	+ 1.21	G5	165	12.19	+ 1.99	K5III
								166*	11.02	+ 2.01	K2III
136	11.66	+ 0.66	F5V	151*	10.63	+ 1.06	K0V	167	12.20	+ 0.66	G0
137*	10.59	+ 1.01	G8V	152*	12.29	+ 1.81	G8III	168	12.56	+ 0.50	G0
138	11.70	+ 0.71	G2	153	12.61	+ 0.44	F2	169	12.02	+ 0.59	F5
139	12.33	+ 1.71	G8III	154	12.49	+ 1.22	G8III	170	12.44	+ 1.04	G5
140	12.35	+ 0.45	F8	155	12.27	+ 1.63	G8III	171	12.45	+ 1.48	K0III
								172	11.64	+ 2.24	K5III
								173	11.39	+ 0.47	F5III
141	12.51	+ 1.61	G8III	156	12.50	+ 1.09	G8	174	10.70	+ 0.50	F2III
142	12.20	+ 0.83	G0	157	11.81	+ 0.82	G2	175	12.53	+ 0.37	F5:ft
143	11.17	+ 0.77	G8V	158	11.70	+ 1.45	K0III	176*	11.30	+ 0.50	F5
144	12.16	+ 1.56	G8III	159	12.52	+ 0.56	F5	177*	8.71	+ 1.14	G8III
145	11.88	+ 0.59	F8	160	12.38	+ 0.58	F5	178*	12.13	+ 2.01	K3III

REMARKS TO TABLE 3

43°
1: See remarks in the text.
20: ST Lyr. (301 d.)
26: Faint companion 320°, 8".
36: Companion 40°, 5".
53: Companion 300°, 10".
88: Double 20°, 3".
127: V475 Cyg (I) See text.
132: This is ADS 12326 200°, 10".

44°
4 and 5: Coincident BD images.
31: ADS 12065 unresolved.
73: ADS 12127 7" Color peculiar.
80: A5p?
113 and 114: Coincident BD images.
126: See ADS 12194.
163: Double elongated E-W.
172: Faint companion 340°, 10".
228: With 229 and 230 ADS 12331.
257: A5p?

44° (Cont'd.)
292: Faint companion 0°, 10".
309: See text.

45°
13: ADS 12047.
94: Double 170°, 12".
226 and 229: Coincident BD images.
233: Double 280°, 10".
239: Double, elongated N-S.
268: Faint companion 350°, 10".

46°
49: Double, elongated E-W.
53: FL Lyr (Ecl).
70: SS Lyr (352 d.).
98: Sharp H lines.
116: Companion 150°, 8".
117: Too bright. m_{pg} is based on Potsdam Pub. 17.

STARS OF SPECIAL INTEREST

A remarkably blue star, two new M-type variables, a variable of type S, and a new carbon star were found in the course of the spectral classification. The following notes pertain to these stars and to one other.

43°1.—The spectrum of this star resembles that of BD+28°4211,[11] the characteristic features of which are very weak hydrogen lines, a strong line of *He* II 4686, and extreme blueness. Although the spectrum is weak because of the faintness of the star, it is certain that it is of a very early type, and this conclusion is confirmed by its color ($RI = -0.34$). It is reasonable to suppose that the star lies well below the main sequence. Its relative proper motion does not exceed a tenth of a second of arc per annum.

TABLE 4*a*

BD AND HD EQUIVALENTS

BD	ILF-1	HD	BD	ILF-1	HD	BD	ILF-1	HD
43°			44°			45°		
3157	44° 14	178351	3093	44° 178	181067	2877	45° 245	181961
163	43 3	178821	102	44 215	181598	879	46 161	182005
164	43 6	178847	107	44 228	181777	886	45 274	182420
165	43 11	178970	109	44 231	181827	887	45 276	182441
172	44 77	179336	121	44 291	182693	893	45 303	182895
178	43 41	179817	122	44 294	182736			
181	43 45	179935	123	44 300	182780	46°		
187	43 62	180185	124	44 303	182805	2632	46 20	178990
203	44 199	181299				637	46 30	179240
207	43 122	181491	45°			640	46 52	179781
215	43 134	181778	2831	45 13	178328	641	46 53	179890
			832	45 16	178375	652	46 100	180888
44°			834	46 8	178660	653	46 102	180913
3065	44 30	178614	835	45 38	178686	656	46 107	180967
066	44 31	178613	844	45 74	179335	657	46 109	180966
071	44 70	179259	847	45 86	179458	658	46 117	181096
073	44 80	179367	856	45 132	180239	660	46 122	181117
078	44 114	179960	859	45 147	180428	662	46 130	181206
083	45 153	180476	863	46 93	180637	675	46 177	182549
086	45 157	180551	864	46 96	180657			
092	44 176	181046	865	45 167	180681			

Unlike BD+28°4211, this star has not escaped attention in the past. It was found that Parenago had announced it to be an irregular variable[12] (range 0.9 mag.), based on photographic observations in 1939. So far, the star has not received an official variable-star designation. An attempt to establish its variability was made through a survey of eight Schmidt plates (1949) and sixteen Harvard Observatory plates (1940), but no change in brightness was revealed during these intervals.

Two other faint blue stars (twelfth magnitude) appear in Table 3: 43°30 and 43°84. Both are of spectral type B5.

44°309.—This star is assigned to spectral class S. It is interesting to remark that the star was first noticed on a plate covering the red region (*F*-sensitization), where a strong band at about 6500 A sets it apart from all other stars. Merrill has remarked on the usefulness of the 6470 band as a criterion of classification for S stars.[13] The absorption spec-

[11] MacRae, Fleischer, and Weston, *Ap. J.*, **113**, 432, 1951; see also a recent paper by Greenstein, *P. A. S. P.* **64**, 256, 1952.

[12] *SVS 1021, Variable Star Bull. Acad. Sci. U.S.S.R.*, **6**, 25, 1946. [13] *Ap. J.*, **56**, 457, 1922.

trum in the photographic region near maximum light shows complex features, including the characteristic broad absorption space at λ 4640 (*ZrO*), and closely resembles the spectrum of AA Cyg. *Hδ* is clearly seen in emission. The spectrum in the infrared region (*N*-sensitization) is markedly variable, with a classification of M2 or earlier on one plate and M6 on another. The photographic magnitude at maximum is estimated to be 12.8, and the red index about 2.6 mag. The star was bright in early July, 1948, but it was at least 1½ mag. fainter in September and October of the same year.

W.—This star, so marked, will be found on the chart near 43°133. Its spectral class is M8:e, estimated from the infrared plates, with emission (*Hγ* and *Hδ*) visible in the

TABLE 4*b*

BD EQUIVALENTS

BD	ILF-1	BD	ILF-1	BD	ILF-1	BD	ILF-1
43°		44°		44°		45°	
3166	43° 13	3061	44° 19	3116	44° 267	2869	45° 197
168	44 60	062	44 18	117	44 273	870	46 129
173	44 78	063	44 20	118	44 276	871	45 209
174	43 25	064	44 29	119	45 285	872	45 220
175	43 31	067	44 51	120	44 289	873	45 222
177	43 40	068	44 64	125	44 306	874	45 225
180	43 43	069	44 63	126	44 308	875	45 234
183	43 51	070	44 65	127	44 301	876	45 244
184	44 119	072	44 73	128	44 305	878	45 248
188	44 129	074	44 85			880	45 249
189	43 72	075	44 88	45°		881	45 250
190	44 134	076	44 108	2826	45 5	882	45 253
191	43 76	077	45 105	827	45 6	883	45 257
192	43 83	079	44 117	828	45 8	884	45 272
193	43 86	080	44 122	829	45 7	885	45 273
194	43 90	081	44 Y	830	45 9	888	45 283
195	43 94	082	44 126	833	45 32	889	45 284
196	43 95	084	44 142	836	46 10	890	46 178
197	44 167	085	45 158	837	46 13	892	45 306
198	43 100	087	44 155	838	45 44		
199	44 181	088	44 158	839	45 45	46°	
200	43 103	089	44 164	840	46 18	2622	46 6
201	44 189	090	45 178	841	45 54	625	46 11
202	43 107	091	44 174	842	45 66	626	46 12
204	43 115	094	44 191	843	45 71	631	46 19
205	43 116	095	44 194	845	45 73	633	46 21
206	44 204	096	44 197	846	45 79	642	46 56
208	43 123	097	44 198	848	46 41	643	46 60
209	43 125	098	44 200	849	46 42	644	46 63
210	43 129	099	44 203	850	45 100	645	46 72
211	43 130	100	44 205	851	45 110	646	46 71
212	44 226	101	44 209	852	45 112	647	46 79
216	43 136	103	45 221	853	45 120	649	46 86
217	43 138	104	44 220	854	46 69	650	46 92
221	44 238	105	45 229	855	45 131	655	46 105
223	43 141	106	45 230	857	46 75	664	46 137
226	44 271	108	45 237	858	45 143	666	46 151
		110	44 243	860	45 148	667	46 152
44°		111	45 262	861	45 152	670	46 166
3057	44 1	112	44 254	862	46 90	674	46 176
058	44 4	113	44 257	866	45 170		
059	45 10	114	44 258	867	45 177		
060	44 12	115	44 259	868	45 190		

photographic region, although at the limit of the plate. The star is variable in brightness (July 9, 1948: $m_{pr} = 14.2$; September 13, 1948: $m_{pr} = 11.7$). The λ 7900 band[14] is seen.

X.—This star is marked near 44°271 on the chart. The temperature class is M8, but the evidence that the star is an emission-line star is not very strong. However, the photometric plates suggest that it is a variable with a small range ($m_{pr} = 11.5$). The λ 7900 band is not visible.

Y.—Marked near 44°122. This faint star ($m_{pg} = 12.9$, $RI = 1.0$ mag., spectral type G) is the only one which can reasonably be identified with BD+44°3081. No evidence of variability could be found.

Z.—Marked near 46°178. This star is a new carbon star, spectral class C5 in Keenan and Morgan's system.[15] Characteristic features are seen in the photographic region and in the infrared. No evidence of variability was found ($m_{pr} = 11.1$, $RI = 3$ mag.). The star AW Cyg, a bright carbon star, is about 1° east of this star.

Information about the following variables will be found in the catalogue: FL Lyr (46°53), SS Lyr (46°70), ST Lyr (43°20), and V 475 Cyg (43°127). No emission lines were found in the spectrum of the last-named star. Maximum magnitudes for variable stars given in Table 3 are necessarily uncertain.

I wish to express my gratitude to Dr. Kron for providing the photoelectric data. The use of his observations in the calibration of the provisional magnitudes shows that there is much to be gained by such a combination of photoelectric and photographic techniques in investigations of galactic structure.

[14] Nassau, van Albada, and Keenan, *Ap. J.*, **109**, 333, 1949.

[15] *Ap. J.*, **94**, 501, 1941.

SPECTRAL-TYPE, MAGNITUDE, AND COLOR-INDEX RELATIONS IN THE GALACTIC STAR CLUSTER IN COMA BERENICES*

HAROLD F. WEAVER
Lick Observatory and Leuschner Observatory, University of California
Received June 24, 1952

ABSTRACT

The Coma Berenices cluster is studied on the basis of new spectroscopic and photoelectric observations. Spectral types are assigned on the system of the Morgan, Keenan, and Kellman *Atlas;* a simple preliminary system of classifying metallic-line stars is proposed. Photoelectric magnitudes and colors, determined with both the 12-inch refractor and the 36-inch Crossley reflector of the Lick Observatory, are compared with magnitudes and colors determined photoelectrically by Eggen and with magnitudes determined photographically by Trumpler.

The magnitude-color, color-spectral-type, and magnitude–spectral-type diagrams determined from the new observational material are exhibited. From the first of these diagrams it appears that the majority of the fainter Coma stars (color range +0.2 to 0.6 mag.) form an extraordinarily compact sequence, in general agreement with Eggen's conclusion for these stars. However, some cluster members in this color range show much greater scatter from the compact sequence than can be accounted for by observational error. Application of a statistical test for the equality of variances shows that the scatter of the brighter main-sequence Coma stars (color $< +0.2$ mag.) about an empirical sequence line is almost, but not quite, significantly greater than the scatter observed for the fainter stars about an empirical sequence line. The stars in the upper part of the dwarf branch thus may form a less compact sequence than the fainter stars. The question of structure in the upper part of the diagram is considered in detail. It is shown that the statistical uncertainty introduced by cluster depth, observational error, and the small number of stars in the upper region of the main sequence prevents one from using the Coma cluster to determine any possible fine-structure details in the magnitude-color relation in this region of the diagram.

Preliminary discussion of the metallic-line stars shows that these objects occur in the color-magnitude range of both normal A- and F-type stars. Spectral peculiarities among the brightest cluster members are briefly described; evidence is produced to show that main-sequence stars of the same color may have different spectral types on the basis of the customary line-intensity-ratio criteria. The main sequence in the color–spectral-type diagram appears linear; the dispersion of the spectral type for a given observed color shows clearly. The magnitude–spectral-type diagram exhibits no new features in addition to those shown by the magnitude-color and color–spectral-type diagrams.

I. INTRODUCTION

The near-by galactic star clusters can serve as excellent objects for observational tests of many astrophysical hypotheses. They have played particularly important roles, for example, in the observational study of the interrelations between spectral type, magnitude, and color index. They can serve as test groups for the study of the occurrence of stars having specific peculiarities, such as "metallic-line" spectra, variable spectra, and so forth.

In view of these various possibilities, a spectroscopic program including stars in a group of the nearer galactic clusters was started a number of years ago. Specifically, the purposes of this program have been to provide adequate data (i) to detect metallic-line and other peculiar stars in galactic clusters; (ii) to study the frequency of occurrence of such peculiar objects; (iii) to obtain accurate H-R diagrams of the cluster members; (iv) to determine the relation between spectral type and color index for the cluster members; and (v) to examine the consistency, or the variation, of general spectral characteristics from cluster to cluster.

The spectroscopic observations for this program have been completed for some time. Recently, a photoelectric photometric program for the determination of magnitudes and color indices of stars in the clusters studied spectroscopically was initiated. The

* *Contributions from the Lick Observatory*, Ser. II, No. 44.

present report deals with the first cluster for which all data have been obtained. In particular, it deals with points i, iii, and iv, mentioned above, for the Coma cluster.

On the basis of common proper motion, common radial velocity, and the relationship between magnitude and spectral type, Trumpler[1] has assigned membership in the cluster to 37 stars. He classes the cluster as IIIp and describes[2] it as "a loose aggregation of relatively luminous and massive stars moving through a space containing few large but many small stars." He remarks further that, while the Coma cluster is poor compared to the Pleiades, "it is not an exceptional object. On the contrary, nearly one-half of the galactic star clusters listed and classified [by Trumpler[3]] were noted as poor (containing fewer than 50 stars) and the Coma group seems to be a typical representative of this most numerous class of clusters, which so far has been but little investigated."

II. THE OBSERVATIONAL DATA

1. ESTIMATES OF SPECTRAL TYPE AND LUMINOSITY CLASS

The spectral-type and luminosity-class estimates were made on the system of the Morgan, Keenan, and Kellman *Atlas*[4] by direct comparison of each spectrogram with a set of spectrograms of standard stars chosen from the *Atlas* list. A Hartmann spectrocomparator was used for the comparisons; an effort was made to match the densities of the cluster star and the *Atlas* star being compared.

TABLE 1

Atlas STARS USED AS STANDARDS TO DEFINE SPECTRAL TYPES

Star	MKK Type	Star	MKK Type	Star	MKK Type
α Leo	B7 V	δ UMa	A3 V	36 UMa	F8 V
δ Crv	B9 V	α Aql	A7 V	β CVn	G0 V
α Lyr	A0 V	σ Boo	F2 V	κ Cet	G5 V
α CMa	A1 V	π^3 Ori	F6 V	61 UMa	G8 V

The list of specific *Atlas* stars which, as far as possible, have been used to define the spectral types of the cluster stars is given in Table 1. These particular objects were chosen because (*a*) sufficiently accurate trigonometric parallaxes exist to permit a reliable check on their positions in the H-R diagram; and (*b*) they exhibit a relatively smooth relation between their color indices and their spectral types.

The stars listed in Table 1 do not include stars of all *Atlas* spectral types. As secondary standards for the cluster spectral types, the *Atlas* standard stars ζ UMa, A2V; g UMa, A5V; ε Cep, F0V; and ι Peg, F5V, were used.

The great majority of the spectrograms used in this survey are of dispersion 75 A/mm at $H\gamma$; only well-widened spectra were used. A few of the spectra examined for types are of 50 A/mm at $H\gamma$. Spectrograms of the two dispersions were not mixed; they were treated separately. Spectrograms of *Atlas* standard stars were available on both dispersions.

The classification criteria recommended in the *Atlas* have been generally employed. For a few stars of early A type the intensity of the K line was considered in the assign-

[1] *Lick Obs. Bull.*, **18**, 167, 1938 (No. 494). We shall designate the Coma stars by Trumpler's numbers.

[2] *Ibid.*, p. 193.

[3] *Lick Obs. Bull.*, **14**, 154, 1930 (No. 420).

[4] Morgan, Keenan, and Kellman, *An Atlas of Stellar Spectra with an Outline of Spectral Classification* (Chicago: University of Chicago Press, 1943).

ment of type. In spectrograms of the dispersion used, the *Mn* I blend at λλ 4030–4034, recommended by the *Atlas* authors, is very difficult to see.

Considerable care was taken to insure the homogeneity of the system of spectral types among the various clusters investigated. All plates of all stars in the entire series of clusters were mixed. During examination of a plate the identity of neither the star nor the cluster to which the star belonged was known to the observer. Each plate was examined independently upon two separate occasions.

Comparison of the first and second estimates of spectral type for each star showed that, for all stars except early and mid A types, there was no change between the two estimates in 60 per cent of the cases; in 30 per cent of the cases there was a change of one-half subtype (that is, from F2 to F2+, for example);[5] and in 10 per cent of the cases there was a difference of one subtype. For the early and mid A-type stars, which often possess very poor lines, these percentages were different, being 50, 40, and 10 per cent, respectively.

From a discussion of the internal agreement of 168 estimates of spectral types of 26 stars in the Coma cluster, the probable errors listed in Table 2 were found for a single spectral-type estimate.

TABLE 2

PROBABLE ERRORS FOR A SINGLE ESTIMATE OF SPECTRAL TYPE FOR PLATES OF DIFFERENT QUALITY

Plate Quality	p.e. of One Spectral-Type Estimate
Good	0.5 spectral subtype
Fair	0.6 spectral subtype
Poor	1.0 spectral subtype

The Coma cluster contains a number of metallic-line stars to which no unique spectral type can reasonably be assigned. The spectral types assigned on the basis of different criteria are conflicting. We have therefore attempted to indicate for these metallic-line stars the degree of conflict between the various spectral criteria—the degree of "metallicism"—by use of the symbols ML 0, ML 1, ML 2, ML 3. To a very pronounced metallic-line star the designation ML 3 has been assigned; to an incipient or slightly metallic-line star the designation ML 0 or ML 0–1 would be assigned. Intermediate degrees of metallicism are indicated by intermediate numerical values of the index following the letters ML.

An ML designation by itself does not, however, give an adequate description of the spectrum; it tells nothing about the strength or appearance of the hydrogen lines, or of the K line of *Ca* II, which is abnormally weak in these stars. Thus, for example, ML 0–1 might describe a star for which hydrogen and the metals were about F0 but for which the K line was A7. On the other hand ML 0–1 might describe a star for which the K-line intensity corresponds to A3, hydrogen intensity corresponds to A5, but the metals are slightly strong for either of these types.

A complete description of an ML star as seen on small or intermediate dispersion might thus require a minimum of three spectral types: one for the K line, one for the hydrogen lines, and one for the metals. Such triple designations have been used, for example, by Roman, Morgan, and Eggen.[6] Since the metallic lines in general are often not

[5] I have often assigned subtypes intermediate between the *Atlas* subtypes, as, for example, F2+. This symbolism implies that a star is halfway between *Atlas* subtypes F2 and F5. The symbol F5+ means a star is halfway between F5 and F6, and so forth. I have also assigned additional types to the A stars, such, for example, as A4, which is between A3 and A5.

[6] *Ap. J.*, **107**, 107, 1948.

consistent within themselves, in that ML stars show lines characteristic of both high and low luminosity, the specification of a type for the metals may offer some difficulties.

For the present I have found it convenient to describe the spectra of the ML stars by two symbols: (1) a spectral type indicative generally of the hydrogen-line intensity and (2) an ML symbol indicative of the degree of conflict between the hydrogen-line type and the type estimated on the basis of the metals (ordinarily later than the hydrogen type), and the type assigned on the basis of the K-line intensity (ordinarily earlier than the hydrogen type). This system, though it will undoubtedly bear revision as more is learned about the characteristics of ML stars and as more is desired from the classification, appears to give an adequate means of describing the ML stars for present purposes. The proposed classification brings out two primary aspects of any ML star: (1) it calls immediate attention to the fact that a star is a metallic-line object and indicates the degree of metallicism; (2) it indicates an approximate position of the metallic-line star among the normal stars in the H-R diagram, that is, it places the star among the normal stars of the same general range of absolute magnitude and color.

For a qualitative picture of the types of spectra designated here by the ML symbolism, Figure 1 shows reproductions of the spectra of Coma stars having the spectral designations given in the accompanying tabulation. In the present discussion no attempt will

Star (Trumpler No.)	Type	Color (Mag.)	Apparent Magnitude	Remarks
T 10.....	A4	0.00	5.94	Normal star; var. rad. vel.
T 68.....	A4 ML 1	.06	6.68	Lines show rotation effects
T 139.....	A4 ML 2	.05	6.65	
T 144.....	A4 ML 2–3	0.07	6.51	Sp. binary

be made to examine in detail the statistics of the metallic-line stars in Coma Berenices. They will be considered later in a general discussion of the metallic-line stars in all the clusters included in this survey.

2. PHOTOELECTRIC MAGNITUDES AND COLOR INDICES

The photoelectric magnitudes and color indices of the Coma stars have been determined completely anew for this investigation. A 1P21 multiplier was used with a d.c. amplifier designed by G. E. Kron and built by J. L. Smith.[7] The output of the amplifier is recorded on a Brown "Electronik" strip-chart potentiometer shunted to become a 0–1 milliammeter. The recorder was found to be linear within measuring error of the line drawn by the recording pen, except possibly at the very top of its scale (deflection >90 units). In the observations this region of the scale was never used. Checks of the amplifier, originally calibrated by the method described by Kron and Smith,[8] showed its calibration to be highly satisfactory. All observations were made with the same photomultiplier, battery voltage supply, amplifier, and recorder, but with two different telescopes and two different filter systems.

A picture of the equipment as it was used on the 12-inch telescope has been published by Eggen,[9] except that in the present observations the amplifier and recorder were those described above, not those shown in Eggen's Figure 1. In addition, in all the present work the 1P21 photomultiplier was mounted in a cylindrical cavity turned in a solid

[7] The amplifier was built for Dr. Joel Stebbins, to whom I express my thanks for its loan as well as the loan of a Brown recorder.

[8] *Ap. J.*, **113**, 324, 1951; *Contr. Lick Obs.*, Ser. II, No. 34.

[9] *Ap. J.*, **111**, 65, Fig. 1, 1950; *Contr. Lick Obs.*, Ser. II, No. 25.

piece of soft iron rather than of duraluminum, in order to avoid any possible variation in cell response caused by varying orientation of the multiplier in the earth's magnetic field.[10] On the 12-inch telescope a Corning No. 5562 filter of standard optical thickness was used for blue magnitudes; a Corning No. 3385 filter of standard optical thickness was used for yellow magnitudes.

The photometer at the Newtonian focus of the 36-inch Crossley reflector differs from that on the 12-inch telescope, in that it has a field lens. Observations at the Crossley were made in the blue with a Corning No. 5562 filter, and in the yellow with a Corning No. 3384 filter, both of standard optical thickness.

Since the color transmission-curve of the 12-inch lens is quite different from the reflectivity-curve of the aluminized Crossley mirror and since different color filters were used in the photometers, the color systems of the photometric data obtained with the two instruments are rather different.

Observing technique.—A consistent, observing technique was used throughout the entire series of observations. A typical night's observing program ran as shown in the accompanying tabulation.

Observation No.	Object Observed	Observation No.	Object Observed
1	Standard radium source	10	Standard radium source
2	Red extinction star	11	Sky
3	Sky	12	Blue extinction star
4	Blue extinction star	13	Red extinction star
5, 6, 7, 8, 9	Cluster stars (or NPS stars)	14, 15, 16, 17, 18	Cluster stars

The standard radium source was used primarily to detect any over-all sensitivity changes in the equipment throughout the night. If such changes were found (at most, they were of the order of 1 per cent), the observations were corrected for the sensitivity variations. These variations affect only the magnitudes, not the colors.

Sky readings were always taken at a high sensitivity, graphed as a function of time, read off for the times of the star observations, and reduced for amplifier sensitivity setting. This general procedure was possible, since the observations were all confined to a small area of the sky. Observations of NPS stars were made at least once each night; preferably, such observations should be made a minimum of three times, that is, at the beginning, middle, and end of each night. A rather large fraction of the observing time was spent in the extinction determination. This was deemed necessary in view of the degree of accuracy that was the final goal of the program. The extinction stars were observed five to seven times each night, and over as large a range of zenith distance ($\sim$1.4 average in sec z) as possible.

In the observations of the stars, two complete sets of deflections were made for each "observation." A typical trace is shown in Figure 2. The series of exposures made for one star thus gives: (1) dark deflection, (2) yellow deflection, (3) blue deflection, (4) dark deflection (centering of star checked at this time), (5) blue deflection, (6) Yellow deflection, and (7) dark deflection. This procedure permits an immediate and continuous check on the consistency and quality of the observations and of the night. If the two blue traces or two yellow traces or three dark traces did not agree within a small percentage of their total value, the series was repeated. Continued disagreement meant trouble with the equipment, the photometric quality of the night, or both. The observing procedure proved to be an excellent one for maintaining a complete check on the observations while they were being made.

Extinction.—Nightly extinction factors were computed by the method of conditioned

[10] Eggen, *Ap. J.*, **114**, 141, 1951; *Contr. Lick Obs.*, Ser. II, No. 37.

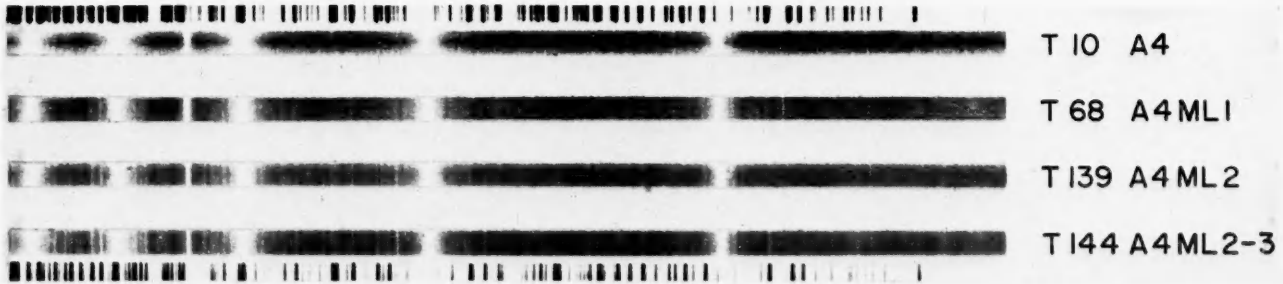

FIG. 1.—Spectra of stars illustrating the ML classification. The reproductions are from plates taken at the McDonald Observatory

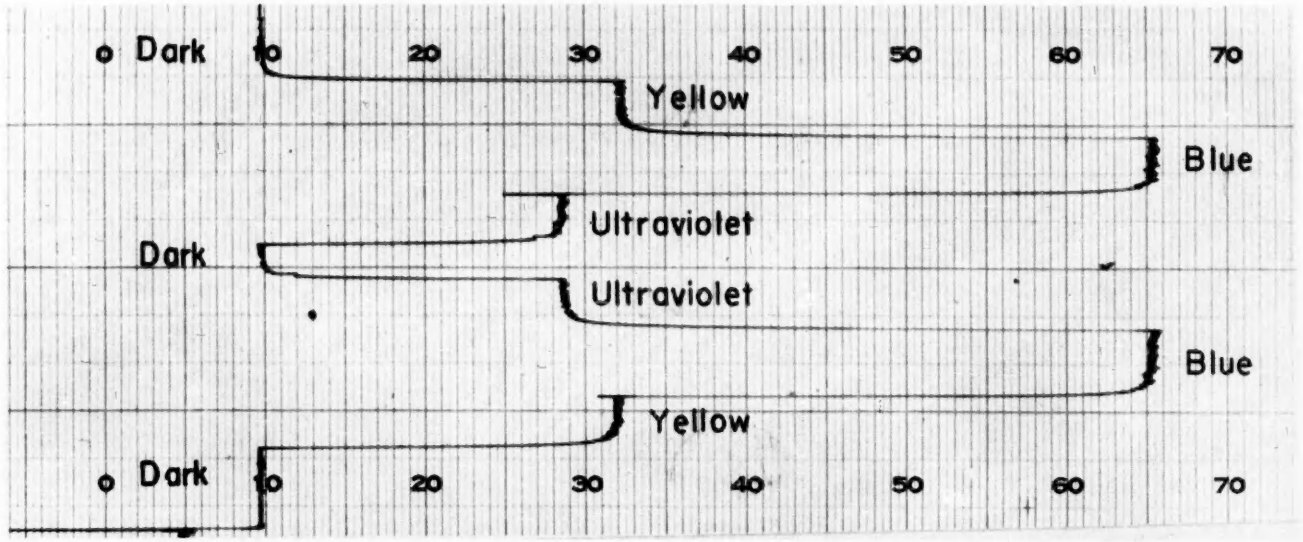

FIG. 2.—Typical photometer trace of blue extinction star. Time increases from right to left. The observations shown cover a period of time of about 5 minutes. The ultraviolet colors of the Coma stars are not considered in the present discussion; they will be discussed in a future report.

extinction coefficients.[11] Briefly, in this method the extinction coefficients are computed for each night with the assumption that the zero-atmosphere colors and magnitudes of the extinction stars are the same on all nights.

Reduction to the International System.—The nightly NPS observations were reduced in the same manner and with the same nightly extinction coefficients as the cluster stars. Night zero-point adjustments determined from, and applied to, the cluster stars have been applied to the NPS stars. Thus the cluster stars have been considered the primary objects. The NPS stars have been carried along with the cluster stars; they have not been used in any internal adjustments.

This procedure represents a departure from that followed by some observers, who do make use of NPS stars in internal adjustments. The NPS stars are generally observed in a rather different part of the sky from that in which the area stars (in this case the Coma stars) are observed. In spite of the fact that only the very best photometric nights were used for the observations reported here, it is entirely possible that between areas of the sky separated by appreciable azimuths there may exist differences in transparency.[12] Industrial areas are very asymmetrically located about Mount Hamilton, and seeing often differs from one azimuth to another. Therefore, in photoelectric photometry, as in photographic photometry, the transfer to the pole may be the weakest link

TABLE 3

COMPARISON OF P AND $P - V$ WITH $m_{pg,\,Int}$ AND C_{Int}

Star	$m_{pg,\,Int}$	P (Mag.)	Difference (Mag.)	C_{Int} (Mag.)	$P-V$ (Mag.)	Difference (Mag.)	No. of Obs.
2r	7.91	7.91	+0.00	+1.57	+1.57	0.00	6
4r	9.23	9.23	0.00	+1.02	+1.02	0.00	7
6	7.12	7.09	+0.03	+0.06	+0.04	+0.02	7
10	9.15	9.18	−0.03	+0.12	+0.15	−0.03	7

in the photometric chain; the accuracy of the polar observations is definitely less than that of the cluster stars. On apparently excellent nights on which results of very high quality are obtained for the cluster stars, small but definite systematic errors are sometimes found for the polar stars. Because of this fact, the observed magnitudes and colors of the NPS stars have been used only to transfer from instrumental magnitude and color systems to the International System.

In accordance with an informal agreement among the photometric observers at the Mount Wilson–Palomar, Washburn, and Lick Observatories, the nine NPS stars (6, 2r, 10, 4r, 13, 8r, 16, 19, 12r) that were measured by Stebbins, Whitford, and Johnson[13] were adopted as primary standards in this work. Specifically, the "International System" used for this discussion of the Coma stars is that defined by Stebbins, Whitford, and Johnson's four high-weight stars, 2r, 4r, 6, and 10, which, in essence, define their system. Photographic magnitudes on this system are denoted by the symbol P and color indices by the symbol $P-V$, as suggested by Kron and Smith.[14]

Table 3 gives for the NPS stars 2r, 4r, 6, and 10 the final values of P and $P-V$

[11] Discussed in the appendix.

[12] Eggen (*Ap. J.*, **114**, 141, 1951; *Contr. Lick Obs.*, Ser. II, No. 37) has noted extinction differences east and west of the meridian.

[13] *Ap. J.*, **112**, 469, 1950.

[14] *Ap. J.*, **113**, 324, 1951; *Contr. Lick Obs.*, Ser. II, No. 34.

derived from the present observations and compares these values with C_{Int} and $m_{\text{pg, Int}}$ given by Stebbins, Whitford, and Johnson.[15] The values P and $P-V$ have been determined from the observed values on the instrumental system through the transformation equations

$$\begin{aligned} P-V &= 0^{m}976 + 1.032C_{\text{Crossley}} \\ &\quad \pm\ 9 \quad \pm 13 \qquad \text{(p.e.)} \\ &= 0^{m}848 + 1.085C_{\text{12-inch}} \\ &\quad \pm 12 \quad \pm 46 \qquad \text{(p.e.)}\,; \end{aligned} \tag{1}$$

$$\begin{aligned} P &= m_{\text{Crossley}} + 6^{m}618 + 0.025\,(P-V) \\ &\quad \pm 15 \quad \pm 16 \qquad \text{(p.e.)} \\ &= m_{\text{12-inch}} + 5^{m}338 - 0.037\,(P-V) \\ &\quad \pm 15 \quad \pm 17 \qquad \text{(p.e.)}\,. \end{aligned} \tag{2}$$

The probable error of a single observation of P for a polar star is ± 0.035 mag., a value twice as great as the corresponding quantity for the cluster stars. The probable error for a single $P-V$ determination of a polar star is ± 0.012 mag., again a value nearly twice as large as the probable error of $P-V$ for a cluster star.

Final $P-V$ and P values for the Coma stars.—Table 4 contains all the individually observed as well as the mean values of the color indices, $P-V$, for the coma stars. Table 5 gives the individually observed and the mean photographic magnitudes, P, for the same stars. The essential computations involved in the determination of these tabulated values are as follows:

a) *Extinction*, calculated by the method of conditioned coefficients; this procedure eliminates to a very high degree of approximation possible nightly color equations.

b) *Zero-point adjustments*, applied to the instrumental system values m_0 and C_0 for the various nights; these corrections were derived in several steps from the following comparisons among the cluster stars: (i) Preliminary Crossley mean magnitude and color systems were derived from the observations of May 29/30, June 8/9, and June 9/10. Ten stars, common to the observations of each of these nights, permitted good zero-point adjustments. (ii) The zero-point adjustments necessary to put the Crossley nights June 22/23 and 25/26 on this preliminary system were determined and applied. The final mean Crossley magnitude and color systems were then formed from all observations of the five nights. (iii) The mean 12-inch magnitude and color systems were formed. The transformation equations to go from 12-inch to Crossley were derived. (The NPS stars were included in this derivation because of the long color base line they provided.) (iv) The 12-inch magnitudes and colors were transformed to the Crossley systems. The various zero-point adjustments applied are shown in Tables 4 and 5.

c) The NPS stars, which, except as noted just above, had to this point played no part in the reductions, were used to derive the transformation equations (1) and (2).

d) With the aid of equations (1) and (2) the values $P-V$ and P given in Tables 4 and 5 were derived.

Internal accuracy of the photometric results.—From the data of Tables 4 and 5 the following probable errors result. For color indices, $P-V$,

p.e. = $\pm 0^{m}0097$ for one observation with the 12-inch,
p.e. = $\pm 0^{m}0074$ for one observation with the Crossley.

[15] *Op. cit.* The magnitudes given by Stebbins, Whitford, and Johnson have not previously been published. The colors are from Seares and Joyner, *Ap. J.*, **101**, 15, 1945; *Contr. Mt. W. Obs.*, No. 701.

TABLE 4

INDIVIDUAL AND MEAN COLOR INDICES ON THE INTERNATIONAL SYSTEM

STAR	12-INCH		CROSSLEY					MEAN $P-V$
	May 27/28	May 28/29	May 29/30	June 8/9	June 9/10	June 22/23	June 25/26	
T 10	0m00	0m00	+0m01	.....	0m00	.....	.....	0m00
T 19	+ .32	+ .28	+ .30	.....	+ .28	.....	.....	+ .30
T 36	+ .33	+ .29	.....	+0m27	.....	+0m30	.....	+ .30
T 49	+ .27	+ .24	.....	+ .24	.....	+ .27	.....	+ .25
T 53	.....	.....	.....	+ .43	.....	.....	+0m43	+ .43
T 58	.....	.....	.....	+ .39	.....	.....	+ .41	+ .40
T 60	+ .05	+ .05	.....	.....	.....	+ .05	.....	+ .05
T 62	+ .06	+ .06	.....	+ .06	.....	.....	+ .06	+ .06
T 65	.....	.....	.....	+ .46	.....	.....	+ .49	+ .47
T 68	+ .06	+ .05	+ .06	.....	+ .06	+ .05	.....	+ .06
T 76	.....	.....	.....	+ .45	.....	+ .47	.....	+ .46
T 82	.....	.....	.....	+ .14	.....	.....	+ .15	+ .15
T 85	.....	.....	.....	+ .48	.....	+ .45	+ .49	+ .47
T 86	+ .40	+ .35	+ .35	.....	+ .36	.....	.....	+ .37
T 90	.....	.....	.....	+ .37	.....	.....	+ .37	+ .37
T 91	+ .38	+ .38	.....	+ .40	+ .40	.....	.....	+ .39
T 92	.....	.....	.....	+ .42	+ .41	.....	.....	+ .41
T 97	.....	.....	+ .42	+ .43	+ .44	+ .45	.....	+ .43
T 101	+ .38	+ .35	+ .34	.....	+ .34	.....	.....	+ .35
T 102	.....	.....	.....	+ .51	.....	+ .51	+ .50	+ .51
T 104	+ .11	+ .10	+ .12	+ .09	+ .11	+ .10	+ .11	+ .11
T 107	− .05	− .06	− .04	− .04	− .04	− .05	− .05	− .05
T 109	+ .15	+ .15	.....	+ .13	+ .14	.....	.....	+ .14
T 111	+ .42	+ .43	.....	+ .43	+ .44	.....	.....	+ .43
T 114*	.....	.....	+ .35	.....	+ .41	.....	.....	(+ .38)
T 118	.....	.....	+ .33	+ .35	+ .34	+ .33	.....	+ .34
T 125	+ .15	+ .14	+ .17	.....	+ .16	.....	.....	+ .15
T 130	− .04	− .04	− .02	.....	− .03	.....	.....	− .03
T 132	.....	.....	+ .59	+ .60	+ .60	.....	.....	+ .60
T 139	+ .06	+ .06	+ .06	+ .02	+ .05	+ .04	+ .04	+ .05
T 144	+ .06	+ .08	+ .09	.....	+ .06	.....	.....	+ .07
T 145	+ .09	+ .09	+ .09	+ .08	+ .08	+ .08	+ .08	+ .08
T 146	− .19	− .18	− .18	− .18	− .17	− .18	− .18	− .18
T 150	.....	.....	+ .71	+ .72	+ .71	.....	+ .70	+ .71
T 160	− .09	− .07	− .07	− .07	− .07	−0.08	− .07	− .07
T 162	.....	.....	+ .37	.....	+ .37	.....	.....	+ .37
T 183	0.00	−0.01	0.00	0.00	0.00	.....	−0.01	0.00
Zero point adjustment	−0.002	+0.002	−0.002	−0.002	+0.005	−0.002	−0.002	.....

* The $P-V$ of star T 114 is very uncertain. Only two discordant observations of its color exist; it is not known which of these is in error.

TABLE 5

INDIVIDUAL AND MEAN MAGNITUDES ON THE INTERNATIONAL SYSTEM

STAR	12-INCH		CROSSLEY					MEAN *P*
	May 27/28	May 28/29	May 29/30	June 8/9	June 9/10	June 22/23	June 25/26	
T 10	5^m92	5^m93	5^m96	.....	5^m95	.....	.....	5^m94
T 19	8.33	8.33	8.34	.....	8.34	.....	.....	8.33
T 36	8.37	8.35	.....	8^m35	.....	8^m36	.....	8.36
T 49	8.08	8.07	.....	8.06	.....	8.06	.....	8.07
T 53	.....	.....	.....	9.43	.....	.....	9^m12	9.13
T 58	.....	.....	.....	9.17	.....	.....	9.18	9.17
T 60	6.43	6.45	.....	.....	.....	6.46	.....	6.45
T 62	6.29	6.25	.....	6.27	.....	.....	6.24	6.26
T 65	.....	.....	.....	9.49	.....	.....	9.51	9.50
T 68	6.64	6.64	6.64	.....	6.65	6.64	.....	6.64
T 76	.....	.....	.....	9.47	.....	9.47	.....	9.47
T 82	.....	.....	.....	7.51	.....	.....	7.50	7.51
T 85	.....	.....	.....	9.74	.....	9.71	9.75	9.73
T 86	8.87	8.83	8.87	.....	8.86	.....	.....	8.86
T 90	.....	.....	.....	8.89	.....	.....	8.87	8.88
T 91	5.07	5.10	.....	5.10	5.12	.....	.....	5.10
T 92	.....	.....	.....	8.93	8.91	.....	.....	8.92
T 97	.....	.....	9.50	9.49	9.52	9.52	.....	9.51
T 101	8.71	8.69	8.70	.....	8.70	.....	.....	8.70
T 102	.....	.....	.....	9.81	.....	9.86	9.81	9.83
T 104	6.77	6.76	6.73	6.72	6.75	6.74	6.75	6.75
T 107	5.02	5.03	5.01	5.00	5.02	5.03	5.03	5.02
T 109	6.48	6.48	.....	6.44	6.49	.....	.....	6.47
T 111	8.53	8.54	.....	8.56	8.58	.....	.....	8.55
T 114	.....	.....	8.88	.....	8.94	.....	.....	8.91
T 118	.....	.....	8.66	8.69	8.70	8.65	.....	8.67
T 125	5.06	4.98	5.03	.....	5.03	.....	.....	5.03
T 130	4.93	4.84	4.88	.....	4.89	.....	.....	4.89
T 132	.....	.....	10.41	10.47	10.46	.....	.....	10.45
T 139	6.67	6.67	6.67	6.62	6.65	6.64	6.66	6.65
T 144	6.52	6.52	6.53	.....	6.49	.....	.....	6.51
T 145	6.66	6.66	6.67	6.60	6.63	6.64	6.64	6.64
T 146	4.99	4.99	4.96	5.01	4.98	4.99	4.99	4.99
T 150	.....	.....	10.41	10.48	10.38	.....	10.42	10.42
T 160	5.31	5.32	5.31	5.33	5.27	5.32	5.29	5.31
T 162	.....	.....	8.92	.....	8.93	.....	.....	8.93
T 183	6.19	6.19	6.21	6.24	6.18	.....	6.18	6.20
Zero point adjustment	0.00	0.00	−0.02	+0.03	0.00	+0.01	+0.01	.....

For photographic magnitudes, P,

p.e. = $\pm 0^m020$ for one observation with the 12-inch,[16]
p.e. = $\pm 0^m017$ for one observation with the Crossley.[16]

Comparisons between results with the two telescopes.—In Figure 3, *a*, the differences $(P-V)_{\text{Crossley}} - (P-V)_{\text{12-inch}}$ are shown as a function of $P-V$. The greatest difference is 0.025 mag.; the "probable difference," defined here as 0.6745 times the root-mean-square difference, is ± 0.0090 mag.

In Figure 4, *a*, the differences $P_{\text{Crossley}} - P_{\text{12-inch}}$ are plotted as a function of $P-V$. The greatest difference between the values obtained with the two instruments is 0.03 mag.; the probable difference is ± 0.011 mag.

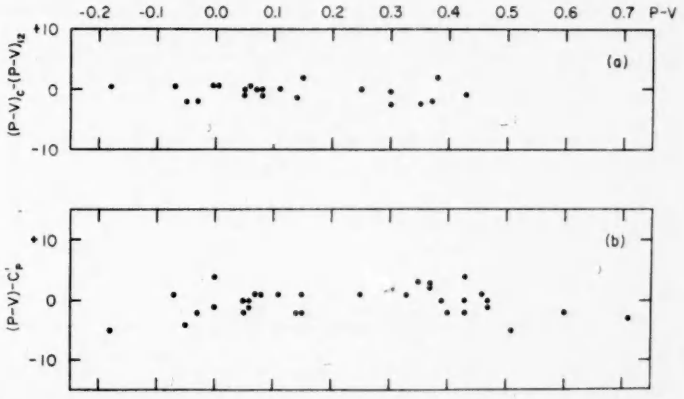

FIG. 3.—*a*, Differences $(P-V)_{\text{Crossley}} - (P-V)_{\text{12-inch}}$ as a function of $P-V$. The Crossley values are the averages of three observations, the 12-inch values are the averages of two observations. Differences are indicated in units of 0.01 mag. *b*, Differences $(P-V) - C'_p$ as a function of $P-V$. Here C'_p represents Eggen's color indices transformed to the system of the present paper by equation (3). Differences are indicated in units of 0.01 mag.

The numbers of individual observations in these comparisons are as follows: Each 12-inch value represents the mean of two observations; each Crossley value represents, on the average, the mean of three observations.

Comparisons with other observers.—There exist only two photometric series of sufficient accuracy to warrant comparison with the present results. The color indices in Table 4 can be profitably compared with the photoelectric results obtained by Eggen;[17] the magnitudes can advantageously be compared both with Eggen's results and with the photographic results obtained by Trumpler.[18]

[16] The residuals on which these values are based are not normally distributed, hence a "probable error" based on the concept of normality is a value of somewhat academic interest. For example, if two residuals in the 12-inch series of magnitudes are omitted, the "probable error" for the remaining twenty 12-inch results is only half as large as the quoted value. It seems preferable to err on the conservative side and to quote the higher values of the probable errors, which, by and large, give a rather more pessimistic view of the accuracy of the results than they may deserve. The nonnormal distribution of residuals probably is due to localized atmospheric trouble. The scatter of residuals definitely varies from night to night, again presumably, because of the atmosphere.

[17] *Ap. J.*, 111, 414, 1950; *Contr. Lick Obs.*, Ser. II, No. 27. [18] *Op. cit.*

Figure 3, *b*, gives as a function of $P-V$ the differences

$$(P-V)-C'_p,$$

where C'_p represents Eggen's color index converted to the color system of the present paper through the transformation equation,

$$C'_p = 1.098C_p - 0^m042 \qquad (3)$$
$$\pm 14 \quad \pm 5 \quad \text{(p.e.)}.$$

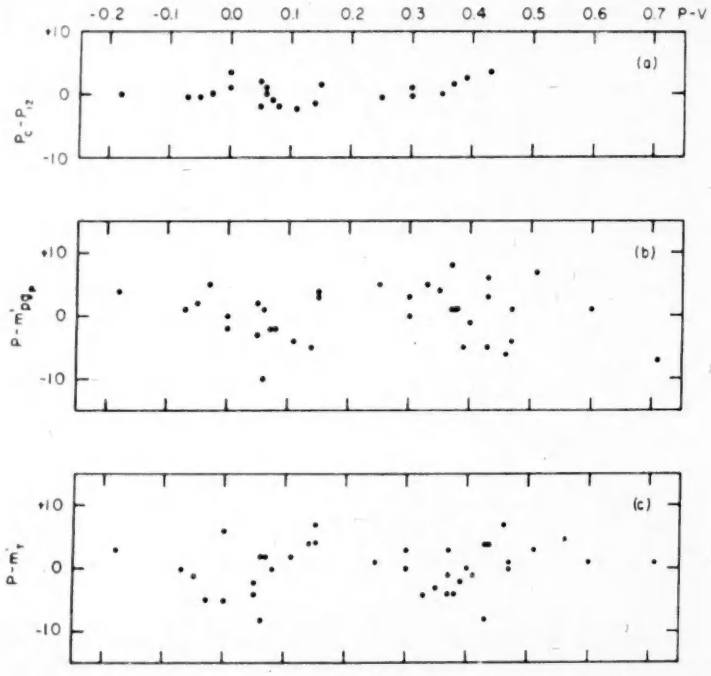

FIG. 4.—*a*, Differences $P_{\text{Crossley}} - P_{\text{12-inch}}$ as a function of $P-V$. The Crossley values are the averages of three observations, the 12-inch values are the averages of two observations. Differences are indicated in units of 0.01 mag. *b*, Differences $P - m'_{pg}$ as a function of $P-V$. Here m'_{pg} represents Eggen's magnitudes transformed to the system of the present paper by equation (4). Differences are indicated in units of 0.01 mag. *c*, Differences $P - m'_T$ as a function of $P-V$. Here m'_T represents Trumpler's magnitudes transformed to the system of the present paper by equation (6). Differences are in units of 0.01 mag.

The difference between Eggen's color system and that of Table 4 results from the fact that Eggen referred his "International System" to a set of NPS stars different from that used in this work. Probably also involved to some extent is the fact that Eggen's blue observations were made with a filter admitting much more ultraviolet than that used in the present observations. If the amount of ultraviolet light involved in two photometric systems is very different, it is possible that a transformation equation of some order higher than the first may be required. In extreme cases, it is possible that no analytic transformation exists.

In addition to the somewhat larger scatter of the points in Figure 3, *b*, there is a rather unusual pattern of residuals. The largest residuals occur at the ends of the diagram. Ordinarily, one would expect the smallest residuals to occur among the brightest stars (in this case generally among the bluest stars because of the strong correlation between color and magnitude), since these stars are observed with lowest amplifier sensitivities and the recorder traces are most nearly free of "noise." As fainter stars are observed, the measurements become less certain. This general phenomenon of smaller differences among the brighter stars and larger ones among the fainter stars is visible to some extent in Figure 3, *a*, in which the differences in color indices determined with the Crossley and the 12-inch are illustrated; it is, however, not particularly marked in the magnitude comparison of those two instruments in Figure 4, *a*.

The situation of finding the largest residuals at the extreme ranges of the diagram of Figure 3, *b*, could be changed to some extent if a nonlinear transformation were used in the comparison of the two color systems. If a smooth second-degree curve were drawn among the points of Figure 3, *b*, it would be convex upward; this is, in fact, the curvature to be anticipated if Eggen's colors were determined with a blue filter that transmitted

TABLE 6

STARS SHOWING LARGE RESIDUALS $(P - V) - C'_p$

$P-V$	Residual $(P-V)$ $-C'_p$	Star	Observed $P-V$ Values						
			12-Inch		Crossley				
			May 27/28	May 28/29	May 29/30	June 8/9	June 9/10	June 22/23	June 25/26
−0^{m}18	−0^{m}05	T 146	−0^{m}19	−0^{m}18	−0^{m}18	−0^{m}18	−0^{m}17	−0^{m}18	−0^{m}18
− .05	− .04	T 107	− .06	− .06	− .04	− .04	− .04	−0.05	− .05
0.00	+0.05	T 183	0.00	−0.01	0.00	0.00	0.00	.....	−0.01

more ultraviolet light than the blue filter used for the present observations. However, because of the scatter of points in Figure 3, *b*, it is somewhat doubtful if a second-degree transformation-curve is justified on the basis of these data alone.

The stars with large residuals in Figure 3, *b*, are identified in Table 6, in which the individual $P-V$ values obtained for these stars are also given. These stars would appear to have well-determined mean $P-V$ values. Star T 146 is listed by Deutsch[19] as a spectrum variable belonging to the chromium group. However, there appears to be no indication of magnitude or color variations in the present series of photoelectric observations. Eggen[20] has remarked that he finds the star "slightly and erratically variable in magnitude and color." Stars T 107 and T 183 are not known to be spectrum variables; there is no indication of variability in these photoelectric observations. The larger than average values of $(P-V) - C'_p$ for these stars therefore appear to be just chance variations. It is possible, however, that these larger residuals can be traced, at least in part, to the differences in the amount of ultraviolet light involved in Eggen's photoelectric system and in that of the present paper.

In Figure 4, *b*, the magnitudes P are compared with the magnitudes determined by

[19] *Ap. J.*, **105**, 283, 1947.

[20] *Ap. J.*, **112**, 141, 1950; *Contr. Lick. Obs.*, Ser. II, No. 30.

Eggen. The figure shows $P-m'_{pg_v}$ as a function of $P-V$. The quantities m'_{pg_v} are Eggen's magnitudes converted to the system of this paper by the transformation equation

$$m'_{pg_p} = -0^m130 + 1.012\, m_{pg_p} + 0.144\,(P-V) \qquad (4)$$
$$\pm 42 \quad \pm 7 \quad \pm 54 \quad \text{(p.e.)},$$

which is the most general type of linear transformation equation. The size of the magnitude scale coefficient is surprising, but it and the color coefficient are not well separated because of the strong correlation between magnitude and color in the cluster; hence the physical significance of the coefficients is somewhat doubtful. The coefficients in the expression were determined by least squares: possibly, for the present, equation (4) should be regarded simply as the most general linear expression minimizing the sum of the squares of the differences $P-m_{pg_v}$. The source of the apparent scale difference in magnitude is a question that will require further investigation. The probable difference of $P-m'_{pg_v}$ is ± 0.031 mag.

A comparison of the magnitudes P with Trumpler's photographic magnitudes m'_p is given in Figure 4, *c*, where the difference $P-m'_p$ is plotted as a function of $P-V$. The quantity

$$m'_p = -0^m533 + 1.055\, m_p - 0.005\,(P-V) \qquad (5)$$
$$\pm 38 \quad \pm 19 \quad \pm 47 \quad \text{(p.e.)}$$

is Trumpler's magnitude m_p put on the magnitude system of this paper. Trumpler's magnitudes show no color equation when compared to the present magnitudes, but they do appear to have a considerable magnitude-scale difference. The probable difference $P-m'_p$ is ± 0.027 mag. This value is in excellent agreement with that to be anticipated on the basis of Trumpler's statement:[21] "The [magnitudes of the] best determined stars have a probable error of $\pm 0^m023$, the average for the 211 stars is $\pm 0^m028$."[21] On the basis of Figure 4, *b* and *c*, and the numerical values of the probable differences, Trumpler's photographic and Eggen's photoelectric results appear to be of comparable consistency.

Compilation of data.—The final data on spectral types, magnitudes, and color indices are compiled in Table 7. In this compilation the magnitudes are the mean values in Table 5; the color indices are the mean values in Table 4.

III. DISCUSSION OF THE OBSERVATIONS

The data in Table 7 may be displayed in three different ways: (1) as a magnitude-color diagram; (2) as a color–spectral-type diagram; and (3) as a magnitude–spectral-type diagram.

1. THE MAGNITUDE–COLOR-INDEX DIAGRAM

Figure 5 shows the magnitude–color-index diagram derived from the Coma stars from the observations given in Table 7.

(i) Perhaps the most striking aspect of Figure 5 is the high degree of correlation between the magnitudes and colors of the stars that form the main sequence. The question immediately arises as to whether or not the scatter observed in the diagram is real. Do the stars form a sequence or sequences of inappreciable width, as suggested by Eggen;[22] is the observed scatter due only to observational error?

Unfortunately, the star cluster in Coma Berenices does not permit a definitive answer to this question. The distance and physical dimensions of the Coma cluster are such that cluster depth itself is enough to produce an appreciable scatter in the observed magnitudes. When the effect of cluster depth is coupled with the inevitable errors of observation and the fact that the cluster contains very few stars, it becomes quite clear that the

[21] *Op. cit.*, p. 181.

[22] *Ap. J.*, **111**, 65 and 414, 1950; *Contr. Lick Obs.*, Ser. II, Nos. 25 and 27.

Coma cluster is not a suitable object on which to base a very detailed study of the magnitude-color diagram.

Assume for the moment that the stars in the Coma cluster have identical absolute magnitudes. Such a model of the cluster has, of course, no physical reality. However, it will enable one to visualize most easily how great a spread will be introduced into the apparent magnitudes by cluster depth and also to compute the distribution of residuals that will be introduced by cluster depth.

Trumpler's investigation places the center of the Coma cluster at a distance of 75

TABLE 7

MEAN MAGNITUDES, COLOR INDICES, AND SPECTRAL TYPES

Star	*P*	*P*−*V*	Sp. Type	No. of Plates	Remarks*
T 10	5^m.94	0^m.00	A4 V	8	Var. RV; rotation
T 19	8.33	+0.30	F5 V	7	
T 36	8.36	+ .30	F2+ V	9	
T 49	8.07	+ .25	F2 V	8	
T 53	9.13	+ .43	F8+ V	9	
T 58	9.17	+ .40	G0 V	5	Var. RV ?
T 60	6.45	+ .05	A5 V	14	Rotation; slight ML tendencies?
T 62	6.26	+ .06	A4 ML 3	3	8 Comae
T 65	9.50	+ .47	G0 V	5	Var. RV ?
T 68	6.64	+ .06	A4 ML 1	11	Rotation
T 76	9.47	+ .46	G0 V	10	
T 82	7.51	+ .14	A8 ML 0–1	8	
T 85	9.73	+ .47	G0+ V	8	
T 86	8.86	+ .37	F6+ V	10	
T 90	8.88	+ .37	F5+ V	8	
T 91	5.10	+ .39	F8:p	8	Sp. binary; 12 Comae
T 92	8.92	+ .41	F6+ V	9	
T 97	9.51	+ .43			Var. RV
T 101	8.70	+ .35	F5: V	7	
T 102	9.83	+ .51	G0+ V	4	Var. RV
T 104	6.75	+ .11	A6 ML 0–1	9	Slight rotation
T 107	5.02	− .05	A4 p	7	13 Comae
T 109	6.47	+ .14	F0 V	11	ADS 8539 separation 1″; $\Delta m = 1$ mag.
T 111	8.55	+ .43	F8+ V	8	Previously unannounced dbl line binary
T 114	8.91	(+ .38)	F8 V	8	
T 118	8.67	+ .34	F6 V	9	
T 125	5.03	+ .15	F0 p	4	14 Comae; shell spectrum; rotation
T 130	4.89	− .03	A4 p	4	16 Comae
T 132	10.45	+ .60	G2+ V	8	
T 139	6.65	+ .05	A4 ML 2	4	
T 144	6.51	+ .07	A4 ML 2–3	2	Spectroscopic binary
T 145	6.64	+ .08	A4 ML 3	3	
T 146	4.99	− .18	A0 p	4	17 Comae; spectrum var.
T 150	10.42	+ .71	G8: V	4	Var. RV
T 160	5.31	− .07	A3 p	4	21 Comae *Sr* II strong; spectrum var.
T 162	8.93	+ .37	G0 V	10	
T 183	6.20	0.00	A4 ML 1–2	3	22 Comae

*"Rotation" is used to denote the fact that the spectrum lines are broad and, so far as can be told from plates of this dispersion, characteristic of a rotating star.

parsecs.[23] The cluster shows no appreciable elongation or asymmetry as projected on the sky; its limiting radius is 4°. The rather regular appearance of the cluster leads one to expect the cluster to be essentially spherical in form. In what follows, the assumption will therefore be made that the cluster is spherically symmetrical. From the cluster distance and angular diameter, the nearest point of the Coma cluster is found to be 70 parsecs from the sun, the most distant 80 parsecs. Hence the distance moduli of the near edge, center, and far edge of the cluster are

$$(m-M)_{\text{near edge}} = 4^{\text{m}}226\,,$$
$$(m-M)_{\text{center}} = 4^{\text{m}}376\,, \qquad \text{Diff.} = 0^{\text{m}}150\,;$$
$$(m-M)_{\text{far edge}} = 4^{\text{m}}516\,, \qquad \text{Diff.} = 0^{\text{m}}140\,.$$

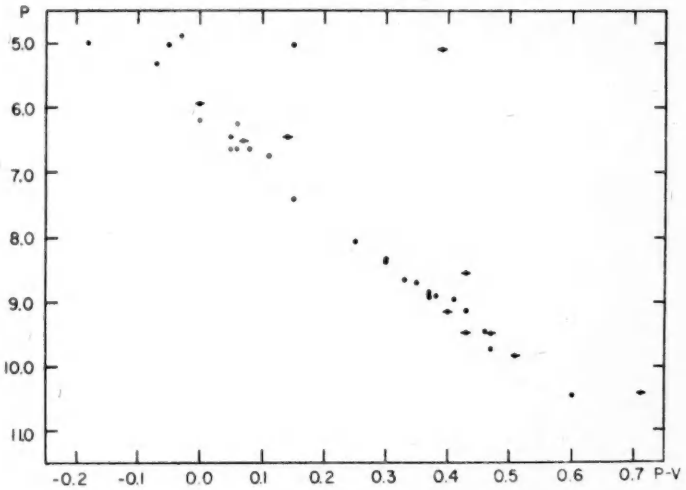

FIG. 5.—Magnitude–color-index diagram. Data are from Table 7. The open circles represent ML stars. A horizontal line through a point means that the point represents a star known or suspected to be a binary star.

A star at the most distant point of the cluster will be observed 0.14 mag. fainter than a star at the center of the cluster; a star at the nearest point will be observed 0.15 mag. brighter than a star at the cluster center. A total spread of 0.29 mag. in the apparent magnitudes of stars in the cluster can be produced by cluster depth.

Trumpler's space-density law for members of the Coma cluster can be approximated by the simple but adequate formula

$$\Phi(r) = k(1-r)\,, \qquad \Phi(r) = 0\,(r>1)\,, \tag{6}$$

where k is a parameter and r is measured in fractional parts of the cluster radius. On the basis of Trumpler's density law and the assumption of the spherically symmetrical model of the cluster, the distribution of magnitude residuals caused by cluster depth can

[23] Eggen has derived from his photoelectric observations a slightly larger value of 79 parsecs, but for the present purpose this difference is of little importance.

readily be computed. The expected distribution of residuals is illustrated[24] in Figure 6. This theoretical distribution refers, of course, only to the effects of cluster depth.

The distribution of residuals pictured in Figure 6 was derived on the basis of a hypothetical cluster model in which all stars were of the same absolute brightness. The residual distribution histogram of Figure 6 is also correct, however, for cluster stars of different brightnesses, provided that the stars form a magnitude-color sequence of zero dispersion. In this case the histogram of Figure 6 represents the theoretical distribution of residuals from the sequence line.

The effect of observational errors is to spread the distribution of residuals beyond that shown in Figure 6. Let $H(v)$ represent the distribution of residuals resulting from both cluster depth and observational errors:

$$H(v) = \int_{-\infty}^{+\infty} D(x)\,\phi(v-x)\,dx\,. \tag{7}$$

Here $D(v)$ represents the distribution of residuals caused by cluster depth and $\phi(v)$, taken as a normal frequency function,

$$\phi(v) = \frac{1}{\sigma_e\sqrt{2\pi}}\exp\left(-\frac{v^2}{2\sigma_e^2}\right), \tag{8}$$

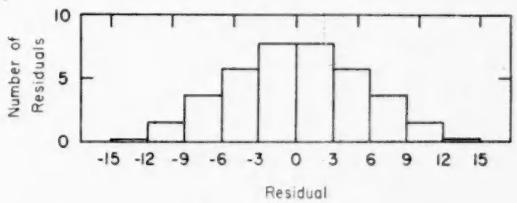

FIG. 6.—Hypothetical distribution of magnitude residuals derived from a study of the cluster depth and density function. Residuals are indicated in units of 0.01 mag.

represents the distribution of residuals in magnitude caused by observational errors in the magnitudes and colors. If σ_c^2 represents the variance of the observed colors and σ_m^2 the variance of the observed magnitudes, then

$$\sigma_e^2 = \alpha^2\sigma_c^2 + \sigma_m^2\,,$$

where α represents the slope of the line expressing the relation between magnitude and color. It is found from Figure 5 that $\alpha \leq 8.4$; hence

$$\sigma_e^2 \leq 70.56\sigma_c^2 + \sigma_m^2\,. \tag{9}$$

The greater part of the variance in $\phi(v)$ thus arises from the observational errors in the colors; the observational errors in the magnitudes play a relatively minor role. From the previous discussion of the probable errors of P and $P-V$,

$$\text{p.e. of } P \leq \pm 0^m012\,,^{25}$$

$$\text{p.e. of } P-V = \pm 0^m0052\,,$$

[24] In drawing this distribution, I have neglected the small difference of 0.01 mag. in the residuals for the nearest and farthest points of the cluster.

[25] In n. 16 attention was called to the fact that the magnitude residuals show a non-Gaussian distribution and that the residuals seemed to be distributed more compactly than would be indicated by the quoted probable errors. The value 0.012 mag. therefore represents a kind of upper limit for the numerical value of the p.e. of P.

one finds that

$$\sigma_e \leq 0^m.068 .$$

For the calculation of $H(v)$, σ_e has been put equal to 0.068 mag.

Although the distribution of residuals $D(v)$ caused by cluster depth and shown as a histogram in Figure 6 is, strictly, one of finite range, it can for many purposes be closely approximated by a Gaussian distribution with dispersion $\sigma_d = 0^m.055$. For the calculation of $H(v)$ the distribution of residuals due to cluster depth may be described by the expression

$$D(v) = \frac{N}{\sigma_d \sqrt{2\pi}} \exp\left(-\frac{v^2}{2\sigma_d^2}\right). \tag{10}$$

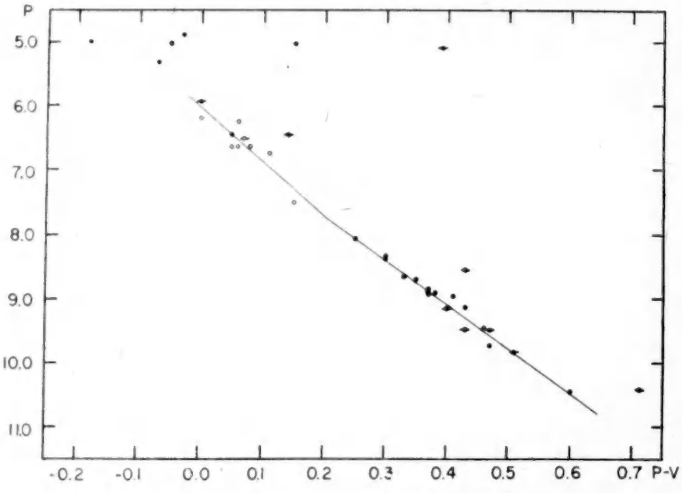

FIG. 7.—Empirical curve drawn among the points forming the main sequence. The curve shown consists of segments of two straight lines fitted to the points by least squares; it is drawn for purposes of illustration only. See text for fuller discussion.

Since $D(v)$ and $\phi(v)$ are both taken to be of Gaussian form for this calculation, $H(v)$ is also Gaussian:

$$H(v) = \frac{1}{\sigma_H \sqrt{2\pi}} \exp\left(-\frac{v^2}{2\sigma_H^2}\right), \tag{11}$$

where

$$\begin{aligned} \sigma_H &= \sqrt{(\sigma_d^2 + \sigma_e^2)} \\ &= \sqrt{[(0.055)^2 + (0.068)^2]} \\ &= 0^m.088 . \end{aligned} \tag{12}$$

It is of immediate interest to compare the predicted distribution of residuals $H(v)$ computed on the basis of observational error and cluster depth with the observed distribution of residuals $O(v)$ about some sequence line. Such a comparison cannot be made without some additional calculations. We possess no a priori knowledge of the shape and position of any magnitude-color-sequence line for the Coma stars. However, on the hypothesis that such a sequence line does exist, one can make use of the Coma data to estimate the sequence line. In Figure 7 is shown a sequence that has been put

among the points of Figure 5 for purposes of illustration; it consists of segments of two straight lines[26] fitted to the points of Figure 5 by least squares. The two line segments are joined at $P-V \sim +0^m.2$. The observed distribution $O(v)$ is given by the distribution of observed points about these line segments.

For the compilation of residuals from this empirical sequence, the double-line binary T 111, the close visual double T 109, and the spectroscopic binary T 150, which lies very high above the main sequence, have been omitted from consideration. All other stars (28 in number) fainter than $P = 5^m.5$ are included. The six stars brighter than $P = 5^m.5$, and which have been omitted, are all objects that have peculiar spectra. Certainly some (and possibly all) of these six stars are giants that do not enter into a discussion of the main sequence. Since several stars marked "var. RV" or "var. RV?"

TABLE 8

OBSERVED AND PREDICTED MAGNITUDE RESIDUALS

Mag. Limits	No. of Residuals (Obs. *minus* Curve)	Theoretical $H(v)$	Mag. Limits	No. of Residuals (Obs. *minus* Curve)	Theoretical $H(v)$
$+0^m.24$			$-0^m.03$		
	2.5	0.1		4.5	3.3
+ .21			− .06		
	1	0.3		2	2.6
+ .18			− .09		
	1.5	0.7		1	1.9
+ .15			− .12		
	0.5	1.2		0	1.2
+ .12			− .15		
	1	1.9		1	0.7
+ .09			− .18		
	2.5	2.6		1	0.3
+ .06			− .21		
	0	3.3		1	0.1
+ .03			− .24		
	2.5	3.7		1	0.1
+ .00			−0.27		
	5	3.7			
−0.03					

are included among the objects used in the compilation of residuals and since some of these supposedly double stars lie below, while others lie above, the sequence line, it is likely that the true dispersion is slightly larger than that observed.

In Table 8 the observed distribution of residuals, $O(v)$, and the theoretical distribution, $H(v)$, are tabulated. Comparison shows that the two distributions are not well matched. The dispersion, σ_0, of $O(v)$ is found to be 0.137 mag., while the dispersion of $H(v)$, σ_H, is 0.088 mag. The form of $O(v)$ is somewhat different from that of $H(v)$; it is, in fact, almost flat. There is little tendency for $O(v)$ to taper down at the ends of its range.

The general form and the dispersion of $H(v)$, the theoretical distribution of residuals, are well established. It is unlikely on physical grounds that the cluster is to any degree elongated toward the sun and hence that σ_d has been grossly underestimated. The standard deviations of the mean errors of P and $P-V$ are less than 10 per cent of the

[26] These lines represent the regression lines of magnitude on color, not the structural relation between magnitude and color.

computed quantities; the probability that σ_e has been underestimated by a factor of nearly 2 is therefore vanishingly small. All indications are that the points forming the main sequence in Figure 7 scatter about the empirical sequence line more than is predicted on the basis of cluster depth and observational error. The main sequence as a whole, while it is decidedly narrow, does not lend support to the hypothesis of a zero-dispersion sequence.

There is some indication in Figure 7 that the points in the diagram may not cluster to the same degree about the two line segments forming the empirical main sequence. For the two line segments separately it is found that

$$\sigma_0\,(\boldsymbol{P}-\boldsymbol{V}>+0^{\mathrm{m}}2) = 0^{\mathrm{m}}108\,,$$

$$\sigma_0\,(\boldsymbol{P}-\boldsymbol{V}<+0^{\mathrm{m}}2) = 0^{\mathrm{m}}181\,.$$

Under the assumption that the parent-populations are normally distributed, one finds, through use of the F-test[27] for the equality of variances, that the probability that the two groups of stars are homogeneous (that is, that they have been drawn from the same parent-population) is somewhat greater than 0.05. On the basis of the customary statistical criteria of significance, the difference between the two σ's is thus not significant, though it is great enough to arouse suspicion that possibly the brighter stars and the fainter stars differ in some of their characteristics.

The majority of the fainter Coma stars ($\boldsymbol{P}-\boldsymbol{V} > +0^{\mathrm{m}}2$) cluster remarkably closely around the empirical sequence line. The value of σ_0 for the fainter stars is controlled primarily by four objects that have large residuals (≥ 0.16 mag.). On the basis of the hypothetical distribution of residuals $H(v)$, 1.4 stars would be expected with residuals ≥ 0.16 mag. Two stars are observed with residuals ≥ 0.22 mag.; on the basis of theory, 0.2 star would be expected to possess a residual of such size. Of these two stars having quite large residuals, T 97 is of particular interest. It lies 0.22 mag. below the empirical sequence line, yet is a spectroscopic binary with a radial-velocity range >60 km/sec. The primary star in T 97 must be considerably fainter than the other Coma stars of the same color.

Star T 92, on the other hand, lies 0.22 mag. above the empirical main sequence; Trumpler's[1] radial-velocity measurements indicate that it is a constant-velocity object. Stars T 92 and T 97 differ in color by only 0.02 mag.; they must differ in magnitude by considerably more than 0.5 mag.

Thus, while the majority of the fainter Coma stars appear to form a very narrow sequence, not all the stars conform to this rule. Some stars appear to scatter considerably about the empirical sequence line.

The brighter stars of the main sequence ($\boldsymbol{P}-\boldsymbol{V} < 0^{\mathrm{m}}2$) may possibly have a greater dispersion than the fainter stars. In his study of the Coma cluster, Eggen has suggested that the brighter stars fall onto two sequences of inappreciable dispersion which are, in some regions of the magnitude-color diagram, separated by only 0.3 mag. No such separation of the stars into sequences is evident in the magnitude-color diagram derived from the present series of observations and exhibited in Figure 5. This difference in result between Eggen's observations and those of the present paper arises primarily because of the rather large and erratic differences between Eggen's colors, C_p, and the present colors, $\boldsymbol{P}-\boldsymbol{V}$. These differences are particularly marked, it will be recalled, among the brighter stars.

The observational detection and unambiguous separation of sequences of the closeness of those postulated by Eggen is a problem of some difficulty; the cluster to serve as a subject for testing the hypothesis of separate sequences among the brighter stars must be very carefully chosen. The Coma cluster is not a suitable object for making a test of

[27] The F-test of the equality of two variances will be found discussed in many statistics textbooks; see, for example, Dixon and Massey, *Introduction to Statistical Analysis* (New York: McGraw-Hill Book Co., Inc., 1951), chap. viii.

Eggen's hypothesis. The dispersion of $H(v)$, caused by cluster depth and observational errors, coupled with the small number of stars in the upper part of the diagram precludes the use of the Coma cluster as a suitable object for the study of any possible fine structure in the magnitude-color diagram.

Ordinarily, it might be assumed that, if $H(v)$ has a dispersion of only 0.088 mag., as found in this investigation, two sequences separated by 0.3 mag. could readily be

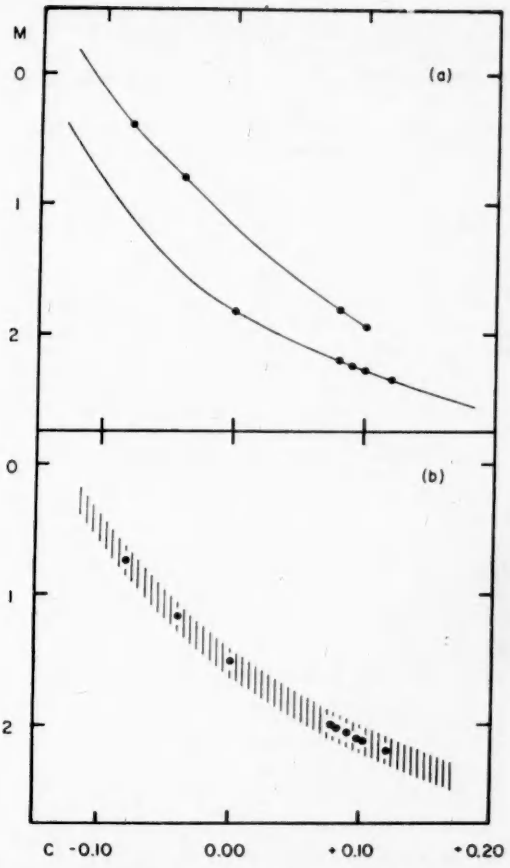

FIG. 8.—*a*, Hypothetical two-sequence, zero-dispersion model population. *b*, Hypothetical one-sequence model with cosmic dispersion. Half the population is found within the shaded area.

established as separate entities. If a large number of stars is available, this assumption is quite correct. However, the problem of delineating any possible sequences on the basis of only a few points is of a very different nature from that of delineating them if a large sample of points is available. If only a few points are available, the assumption that sequences separated by 0.3 mag. can readily be established if $\sigma_H = 0.088$ is not correct. The difficulties involved may be best illustrated by the use of a few examples.

In Figure 8, *a*, is shown a model population of nine stars that are located on two se-

quences of zero dispersion. The sequence lines are Eggen's;[28] the stars are placed on these sequences in the same relative positions in which Eggen suggests[17] that they are found in the Coma cluster. For convenience, the population represented in Figure 8, *a*, will be termed a "two-sequence model." In Figure 8, *b*, is shown a model population that lies along a sequence in which "cosmic dispersion" exists. In this model the stars are normally distributed about a sequence line. This sequence line, which is the center line of the shaded area in Figure 8, *b*, defines the mean of the two lines in the two-sequence model, Figure 8, *a*. In Figure 8, *b*, the shaded area, which has been drawn so that half the stars will fall within it, has a width of $\pm$ one "cosmic probable error." The cosmic dispersion has been taken as 0.16 mag. This value, coupled with $\sigma_H = 0^m088$, gives the observed value $\sigma_0 = 0^m181$ found from Figure 7 for this region of the diagram. Figure 8, *b*, pictures what may be called a "one-sequence model."

Nine stars having the same colors as those in Figure 8, *a*, are shown schematically along the center line of the shaded area of Figure 8, *b*. Actually, of course, if one is given

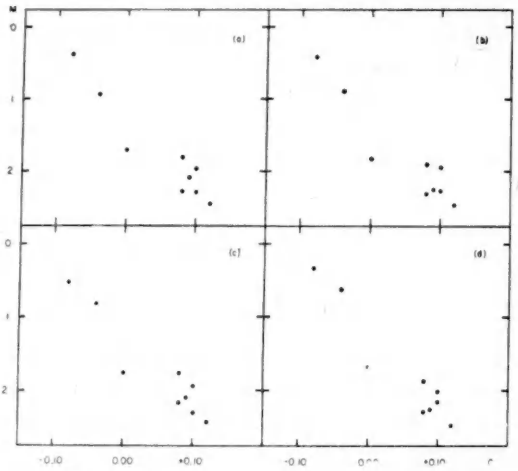

FIG. 9.—*a*, *b*, *c*, *d*, Synthetic samples drawn from the two-sequence population

the color of a star in the one-sequence model, the absolute magnitude of the star is not uniquely specified. For a given color the absolute magnitude of a star in the one-sequence model is a chance variable whose distribution is Gaussian with a dispersion of 0.16 mag.

Assume, now, that the nine stars in the two-sequence model are "observed." The σ of one observation is 0.088 mag., which is caused by cluster depth and observational errors. Four such samples (or synthetic observation series) for the two-sequence model were constructed[29] in the customary manner with the aid of tables of random-sampling numbers.[30] The four series are shown in Figure 9, *a*, *b*, *c*, and *d*. Analogous "synthetic observation series" have been constructed for the one-sequence model; these are shown in Figure 10, *a*, *b*, *c*, and *d*.

[28] *Ap. J.*, **112**, 141, 1950; *Contr. Lick Obs.*, Ser. II, No. 30.

[29] The problem of the construction of such random samples from an infinite parent-population is discussed in many texts on statistics; see, for example, Kendall, *The Advanced Theory of Statistics* (London: Charles Griffin & Co., 1947), **1**, 193. An example that is the complete counterpart of the one considered here is treated by Kendall on p. 195.

[30] The table by Kendall and Babington Smith, *J.R. Stat. Soc.*, **101**, 147, 1939, has been used.

The eight diagrams of Figures 9 and 10 do not constitute a mathematical proof, but they give clear visual indications that the identification of sequences separated by only a few tenths of a magnitude is a problem of very great difficulty when only a small sample of stars is available. It is doubtful whether an investigator confronted only with these diagrams could deduce with any precision the characteristics of the model from which the samples were drawn. In the case of the two-sequence model, diffculties are in some instances encountered in assigning stars to the proper sequence even if one has exact knowledge of the positions of the two hypothetical sequence lines in the diagram. On the basis of some samples from the one-sequence model one might be tempted to assign two-sequence characteristics to the parent-population. Figures 9 and 10 make it clear that very great caution must be exercised in the interpretation of observational results for star clusters containing few members.

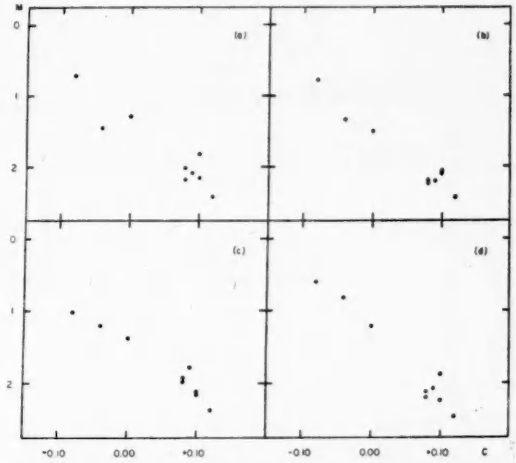

FIG. 10.—*a*, *b*, *c*, *d*, Synthetic samples drawn from the one-sequence model population

In the case of a small sample, details of the two-sequence model are badly obliterated by an observational error as great as 0.088 mag. This particular value, it will be recalled, is made up of two components, one due to cluster depth, $\sigma_d = 0^m055$, and the other due to observational errors in the magnitudes and colors, $\sigma_e = 0^m068$. Most of this latter error arises from the observational error of $P-V$ (see eq. [9]). Possibly with improved methods and equipment and even better photometric skies than were available for the present work, σ_e could be reduced in size.[31] If σ_e were reduced to zero, the actual scatter of points in Figure 9, *a*, *b*, *c*, and *d* would be reduced by $100 \times (0.088 - 0.055)/0.088 = 37$ per cent. The scatter in Figure 10, *a*, *b*, *c*, and *d* would be reduced by a negligible amount of 7 per cent. For Figure 9, *a*, *b*, *c*, and *d* the reduction of σ_H by 37 per cent would mark an important step toward a more certain interpretation of the two-sequence samples. However, even with this reduction of scatter, the accurate interpretation of a small sample of stars for the two-sequence model might not be easy. Cluster depth is thus a definite complication that makes the Coma cluster, which contains very few stars, an unsuitable object for the study of any possible fine structure in the magnitude-color diagram.

[31] Primarily this would involve determining P–V to three decimals, with probable errors of the general order of ± 0.001 or ± 0.002 mag.

(ii) A second feature of interest in the color-magnitude diagram in Figure 5 is the distribution of metallic-line stars in magnitude and color. The sample of ML objects in Coma is very small, and it does not permit one to make any very definite statements about their distribution in either magnitude range or color range. It might be pointed out tentatively, however, that (1) the less pronounced cases of metallicism appear to occur throughout the entire range of color or magnitude in which ML objects are found. The more pronounced cases of metallicism tend to occur near the middle of this magnitude-color range. (2) The ML stars occur in a magnitude and color range that includes normal stars of types A and F. (3) Not all stars that occur in the magnitude-color range in which ML stars are found are ML stars. The greater amount of statistical material provided by the ML stars in all the clusters studied on this program will permit these questions to be more thoroughly discussed at a later time.

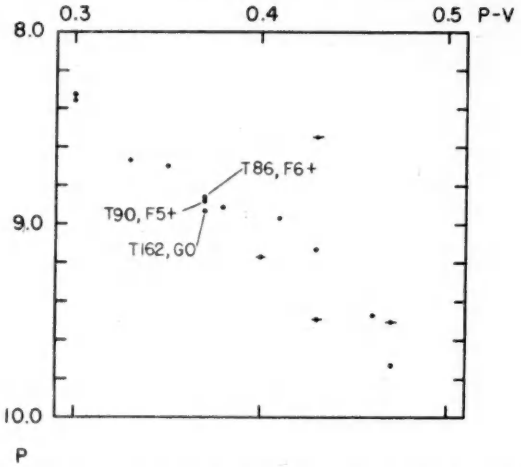

FIG. 11.—Detail of a portion of the magnitude-color diagram. Stars known or suspected to be binaries are marked with horizontal lines.

(iii) It appears that stars of essentially the same color may have spectral types that are rather different. A detailed section of the color-magnitude diagram is shown in Figure 11. The group of three stars at approximately $P = 8^m9$, $P-V = +0^m37$, furnishes a good example of this phenomenon of different spectral types for stars of the same luminosity and color. Table 9 gives the individual observations of magnitudes and colors for these three stars. Enlargements of the spectra of star T 90, F5+, and star T 162, G0, which are taken as examples, are shown in Figure 12. The greatest intensity difference appears in the hydrogen lines, of which $H\delta$ is shown in the enlargement. Hydrogen is noticeably stronger in T 90 than in T 162. Since the spectral type is determined from the ratios $4045/H\delta$ and $4227/H\gamma$, T 90 is assigned an earlier type than T 162. Such differences in spectral types for stars that are essentially the same in absolute magnitude and color cannot fail to have a marked influence on the magnitude-spectral-type and the color-spectral-type diagrams. In both diagrams scatter will be introduced by the lack of perfect correlation between color and spectral type.

(iv) The group of six stars brighter than $P = 5.5$ are all objects of peculiar spectra.

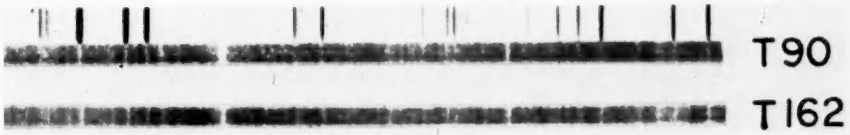

FIG. 12.—Enlargements of spectra of stars T 90 and T 162, showing that to stars of the same color different spectral types may be assigned on the basis of line-intensity ratios. The spectral type is determined by the ratios 4045/$H\delta$ and 4227/$H\gamma$. The hydrogen lines differ appreciably in intensity in the two stars; the intensities of the metals do not differ similarly.

Star T 146 is included in Deutsch's[32] catalogue of spectrum variables. Morgan[33] has reported intensity variations in lines of *Cr* II and *Sr* II for this star.

Star T 160 has been found by Morgan[33] to have *Sr* II, λ 4215, variable in intensity. Deutsch[32] very strongly suspects that the K line as well as a number of other lines change intensity. The amplitudes of variation are small, however, and could not be conclusively established by Deutsch. Eggen[20] finds the star to be slightly variable in magnitude and color.

TABLE 9

OBSERVED COLOR INDICES AND MAGNITUDES OF STARS T 86, T 90, AND T 162

Star	May 27/28	May 28/29	May 29/30	June 8/9	June 9/10	June 25/26	Mean	Eggen*
	(*P*−*V*) 12-Inch		(*P*−*V*) Crossley				*P*−*V*	C'_p
T 86	0^{m}40	0^{m}35	0^{m}35	.....	0^{m}36	.....	0^{m}37	0^{m}34
T 90	.....	.....	.....	0^{m}37	.....	0^{m}37	0.37	0.34
T 162	.....	.....	0.37	.....	0.37	.....	0.37	0.35
	P 12-Inch		*P* Crossley				*P*	m'_{pg_p}
T 86	8.87	8.83	8.87	.....	8.86	.....	8.86	8.87
T 90	.....	.....	.....	8.89	.....	8.87	8.88	8.85
T 162	.....	.....	8.92	.....	8.93	.....	8.93	8.95

* The values quoted for Eggen have been converted to the system of the present paper by eqs. (3) and (4).

TABLE 10

COMA STARS BRIGHTER THAN $P = 5^m5$

No.	Sp. Type	*P*	M_p^*	*P*−*V*	No.	Sp. Type	*P*	M_p^*	*P*−*V*
T 91	F8:p	5^{m}10	+0^{m}70	+0^{m}39	T 130	A4p	4.89	+0.49	−0.03
T 107	A4p	5.02	+0.62	−0.05	T 146	A0p	4.99	+0.59	−0.18
T 125	F0p	5.03	+0.63	+0.15	T 160	A3p	5.31	+0.91	−0.07

* The absolute magnitudes have been computed under the assumption that the cluster distance is 75 parsecs.

Stars T 107 and T 130 are rather similar to each other in their spectral characteristics, and, although they exhibit various individual intensity differences in certain lines, they are generally similar to T 125, which is the late-type shell star, 14 Comae, discussed by Struve and Swings.[34] On the basis of the spectrograms used in this study, the underlying spectrum of star T 125 appears later than A5, as assumed by Struve and Swings. In Table 7 the star has been classified F0p. Incidentally, it is noteworthy that star T 125 is not a dwarf, as was suggested by Struve and Swings in the study of the shell spectrum, but is a giant that falls in the Hertzsprung gap.

Star T 91, 12 Comae, has been listed by Trumpler as having a composite spectrum of

[32] *Ap. J.*, **105**, 283, 1947. [33] *Ap. J.*, **76**, 275, 1932. [34] *Ap. J.*, **94**, 291, 1941.

types gF4 + A. The spectroscopic orbit of the F-component has been determined by Miss Vinter Hansen.[35] She and J. H. Moore made a careful search for lines of the second component, hypothetically of type A, but were unable to find any. Cesco and Sahade[36] made a similar search on four plates taken with the 500-mm Cassegrain quartz spectrograph at the McDonald Observatory, but they found no certain evidence of lines of the secondary component except possibly in the K line, which showed an anomalous velocity. The lines of T 91 are very shallow and have a curious veiled appearance. The magnitude difference between the primary and secondary must be slight, in view of the great amount of veiling. Unless the early-type star is essentially lineless—and this does not seem to be the rule for the bright early-type stars in Coma—the lines of the secondary should be visible.

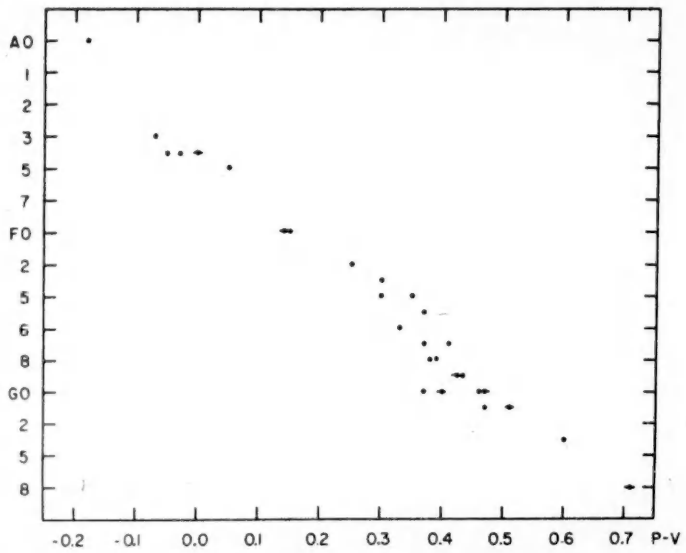

FIG. 13.—Color–spectral-type relation of stars in the Coma cluster. Stars known or suspected to be binaries are indicated by horizontal lines.

If the secondary component is of early type and is veiling the lines of the *F*-component, which appears to be the case from an examination of the spectrum, then in the estimate of the spectral type some allowance must be made for the reduced intensity of the metals of the *F*-component lines and the increased intensity of the hydrogen lines. Making such allowances, one arrives at a somewhat later type for T 91 than has generally been assigned. In Table 7 the type F8:p has been provisionally assigned to star T 91.

2. THE COLOR-INDEX–SPECTRAL-TYPE RELATION

The correlation between color index and spectral type for the Coma stars is shown graphically in Figure 13. A portion of the scatter of points in the figure can be accounted for on the basis of slight observational inaccuracies of spectral types, of the order of a fraction of one subclass. However, the scatter is too great to be attributed entirely to this cause. As mentioned in the discussion of the color-magnitude diagram, there appear to be real and significant differences in spectral type for stars of the same or essentially the same color index.

[35] *Lick Obs. Bull.*, **19**, 101, 1940 (No. 504). [36] *Ap. J.*, **99**, 317, 1944.

The interesting question of whether or not the intrinsically brighter stars (the six stars of peculiar spectra discussed above) follow the same color–spectral-type relation as the intrinsically fainter stars unfortunately cannot be adequately answered because of the small number of stars available. There may be an indication that the earlier-type brighter stars are slightly bluer than the trend indicated for the intrinsically fainter stars of the same spectral type. The data for Figure 13 are, however, too few in number to permit us to draw any statistically valid conclusions about this question.

3. THE APPARENT-MAGNITUDE–SPECTRAL-TYPE RELATION

The relation between apparent magnitude and spectral type is shown graphically in Figure 14, which does not include metallic-line stars, since their spectral types are am-

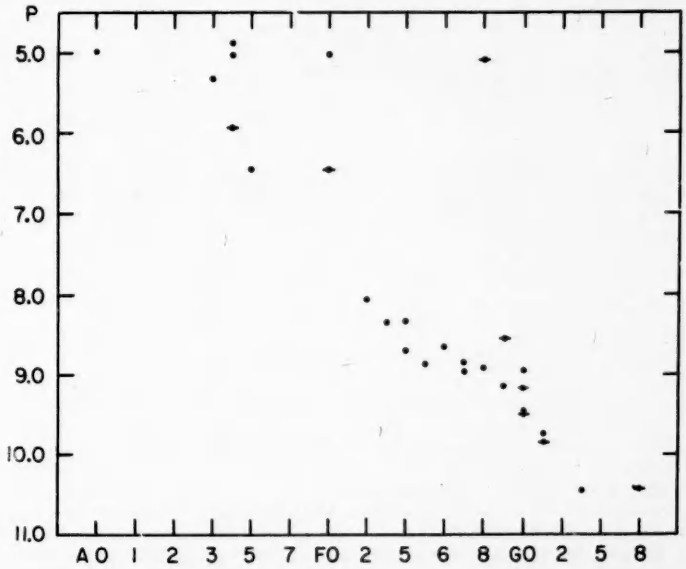

FIG. 14.—Magnitude–spectral-type relation of stars in the Coma cluster. Stars known or suspected to be binaries are indicated by horizontal lines.

biguous. No new features are illustrated by this diagram, which shows a very close resemblance to the magnitude–spectral-type diagram published by Trumpler.[37]

As a consequence of the essential linearity of the color-index–spectral-type relation, Figure 13, the magnitude–spectral-type relation closely resembles the magnitude-color relation (Fig. 5). The points defining the magnitude–spectral-type relation, however, scatter more than the points defining the magnitude-color relation. This increased scatter arises, first, because spectral type cannot be so accurately estimated as color index can be measured and, second, because of the nonperfect correlation between color and spectral type as assigned on the basis of line-intensity ratios.

It is a pleasure to thank Dr. Joel Stebbins for checking some of the reductions of the observations made with the Crossley reflector and for several valuable criticisms of the various drafts of this report.

[37] *Op. cit.*, p. 192.

APPENDIX

1. *Nightly extinction coefficients.*—Practical atmospheric extinction calculations are based upon two assumptions, which appear, for reasonable ranges of air mass, to be adequate for the needs of present-day photometry: (*a*) the atmosphere is homogeneous in any horizontal layer; (*b*) The color-extinction and magnitude-extinction coefficients are linear functions of the zero-atmosphere color of a star.

Assumption *a* leads to the equation

$$C_0 = C_z - \kappa \sec z \,, \tag{13}$$

where C_0 is the zero-atmosphere color of the star, C_z is the color observed at zenith distance z, and κ is the color-extinction coefficient for the particular star observed and for a particular night.

By assumption *b*,

$$\kappa = \kappa_0 - \kappa_1 C_0 \,, \tag{14}$$

where κ_0 and κ_1 are coefficients depending upon the physical properties of the atmosphere for a particular night. Combining equations (13) and (14), we find

$$C_0 = \frac{C_z - \kappa_0 \sec z}{1 - \kappa_1 \sec z} \,. \tag{15}$$

Observations of a specified blue star and a specified red star made on a particular night over an appreciable range of z permit the evaluation of κ_0 and κ_1. By application of equation (15), then, the zero-atmosphere color of any star can be found.

Using an obvious notation, one can write quite analogously for magnitudes:

$$m_0 = m_z - \mu \sec z \,, \tag{16}$$

$$\mu = \mu_0 - \mu_1 C_0 \,, \tag{17}$$

and hence

$$m_0 = m_z - (\mu_0 - \mu_1 C_0) \sec z \,. \tag{18}$$

The coefficients μ_0 and μ_1 can be evaluated from the same observations of the blue and red extinction stars used to evaluate κ_0 and κ_1. For any star for which C_0 can be found, m_0 can thus be found also. The method and equations described here have been used, for example, by Stebbins, Whitford, and Johnson.[38]

2. *The method of conditioned coefficients.*—If the same two extinction stars are observed on many nights (as was the case for the cluster program), extinction method 1 is not entirely satisfactory, in that it fails to make full use of all available information. In particular, it does not make full use of the fact that the zero-atmosphere colors and magnitudes of the extinction stars are constants[39] and should have the same numerical values each night. In method 1 the zero-atmosphere colors and magnitudes of the extinction stars are determined from each night's observations. If these nightly values, which are inevitably affected by observational errors, are used in the calculation of κ_0 and κ_1, μ_0 and μ_1, slight inconsistencies are introduced in the computed values of these extinction coefficients. These slightly inconsistent coefficients have the effect of introducing small nightly color equations and zero-point variations in the magnitudes and colors of all the stars observed. These small but nevertheless significant nightly differences can be eliminated by a careful discussion of each night's results. It is more convenient, however, to remove them entirely, or at least very nearly entirely, at the beginning of the calculations by handling the extinction problem by another method.

In extinction method 2, in which nightly differences are effectively eliminated, the extinction calculation proceeds in two steps:

a) From equations (13) and (15) C_0 and m_0 for the blue and red extinction stars for each night's observations are computed by the method of least squares. Mean values of $\bar{C}_0$ and $\bar{m}_0$ are formed for each extinction star from all the observations.[40]

[38] *Ap. J.*, 112, 469, 1950. [39] Provided, of course, that the extinction stars are not variable.

[40] For the determination of $\bar{m}_0$ the observations of the standard radium source must be used to adjust the over-all sensitivity of the equipment for each night to some mean value. The taking of the mean $\bar{m}_0$ has physical significance only if this sensitivity adjustment is made.

b) With $\bar{C}_0$ and $\bar{m}_0$ determined, equations (13) and (15) may be used in the form[41]

$$\kappa \sec z = C_z - \bar{C}_0 , \tag{19}$$

$$\mu \sec z = m_z - \bar{m}_0 . \tag{20}$$

From these expressions κ and μ are next determined for each night by the method of least squares. In this second calculation the zero-atmosphere colors and magnitudes are fixed; they are the mean values found in step *a*. With the newly computed κ's and μ's, the numerical values of κ_0, κ_1, μ_0, and μ_1 are computed for each night from equations (14) and (17). In these calculations the mean values of $\bar{C}_0$ and $\bar{m}_0$ are used rather than the nightly values.

When the values κ_0, κ_1, μ_0, and μ_1 are available, the zero-atmosphere colors and magnitudes are computed for all stars by equations (15) and (18). Values of κ_0, κ_1, μ_0, and μ_1 obtained by methods 1 and 2 for seven nights of observations are shown in Table 11.

TABLE 11

EXTINCTION COEFFICIENTS

METHOD	12-INCH		CROSSLEY				
	May 27/28	May 28/29	May 29/30	June 8/9	June 9/10	June 22/23	June 25/26
1 (κ_0)	+0^{m}107	+0^{m}110	+0^{m}080	+0^{m}117	+0^{m}127	+0^{m}083	+0^{m}123
1 (κ_1)	− .024	− .029	− .044	− .038	− .037	− .041	− .019
1 (μ_0)	+ .270	+ .257	+ .215	+ .330	+ .337	+ .227	.....
1 (μ_1)	− .044	− .064	− .049	− .035	− .044	− .039	.....
2 (κ_0)	+ .107	+ .113	+ .097	+ .118	+ .120	+ .097	+ .120
2 (κ_1)	− .024	− .027	− .036	− .034	− .032	− .031	− .028
2 (μ_0)	+ .287	+ .317	+ .270	+ .355	+ .320	+ .257	+ .337
2 (μ_1)	−0.043	−0.053	−0.037	−0.035	−0.035	−0.030	−0.035

Experience with the observations reported here has shown that extinction method 2 is highly satisfactory in practice. Analysis of all observed magnitudes and colors showed no night variations in these quantities depending on color after extinction method 2 was employed in the reductions. However, small variations in zero point from one night to another do remain, even with method 2. A maximum zero-point variation of 0.005 mag. in color was found for the five-night Crossley observations reported here.[42] Zero-point variations in magnitude from night to night are of no primary importance; they mainly reflect changes in absolute sensitivity of the photoelectric equipment. However, the proper determination of the magnitude zero-point adjustments that are required poses some delicate problems in the reduction of observations. The application of zero-point corrections in both colors and magnitudes is of considerable importance in any series of observations in which each star is not observed each night.[43]

[41] Here the $\bar{m}_0$ refers to the mean $\bar{m}_0$ reduced to the value that would be observed for the particular over-all sensitivity of the equipment for the specific night. This nightly value of $\bar{m}_0$ can be readily derived from the mean $\bar{m}_0$ found in step (*a*) and from the deflections observed for the standard radium source for the specific night as compared to the standard sensitivity (or radium source deflection) on which the mean $\bar{m}_0$ is based.

[42] That color equations are more nearly eliminated than zero-point differences is not surprising. The extinction stars represent, presumably, the extremes of color observed. By forcing agreement between objects of such extreme color, any essentially second-order color effects are rather completely eliminated. In zero point this is not the case. Here, in essence, the average of two values is being compared with the average of all values observed. Naturally, the average of the total number of observations is the more precise, and hence zero-point adjustments must be made.

[43] Although only color and zero-point corrections have been discussed, one can imagine even further corrections that might be applied, such, for example, as corrections for size of diaphragm (if the photometer diaphragm were changed during the course of a series of observations), and possibly seeing.

PRAESEPE: MAGNITUDES AND COLORS*

HAROLD L. JOHNSON
Yerkes and McDonald Observatories
Received June 28, 1952

ABSTRACT

Magnitudes and colors in ultraviolet, blue, and yellow light have been measured for 133 physical members of the Praesepe cluster and for 17 nonmembers in the same field. A comparison with the photographic photometry of Haffner and Heckmann shows the latter work to be extraordinarily good. Two color-magnitude diagrams are given, and the relation between the two color indices is discussed.

Photoelectric measures at the approximate effective wave lengths, 3500 A, 4300 A, and 5550 A, have been made on 133 known members of the Praesepe cluster and on 17 field stars in the region. The total number of observations, including those for tying the cluster into the standard system, is 544. The average number of observations per star is 2.9, except for the two cluster standards which were observed much more. The observations were made in two seasons: winter, 1950–1951, and winter-spring, 1952.

The observations were made and reduced in the manner described by Johnson and Morgan.[1,2] Tests of the linearity and scale of the photometric equipment are also described there. The cluster standards were each observed at least once every 1½ hours on each night, and empirical corrections, computed on the assumption that the standard stars are always the same, were applied to all observations. The magnitudes and colors of these cluster standards were determined on the fundamental system[2] by special observations on 22 different nights. The relative internal probable errors between stars in the cluster are given in Table 1. The probable errors for the tie-in with the fundamental system are given in Table 2.

TABLE 1

RELATIVE PROBABLE ERRORS FOR ONE OBSERVATION

	V (Mag.)	p.e. $B-V$ (Mag.)	$U-B$ (Mag.)
$V<13$.....	±0.007	±0.005	±0.010
$V>13$.....	±0.010	±0.010	±0.020

TABLE 2

PROBABLE ERRORS OF THE TIE-IN WITH THE FUNDAMENTAL SYSTEM

	V (Mag.)	$B-V$ (Mag.)	$U-B$ (Mag.)
p.e.....	±0.006	±0.003	±0.008

The results of all observations are listed in Table 3, where the first column contains the number of the star assigned by Klein-Wassink;[3] the second, third, and fourth, the observed values of V, $B-V$, and $U-B$, respectively, while the last column gives the number of independent observations on each star. In five cases the star has no Klein-Wassink number, and that of Hertzsprung[4] (H) is given. In one case the number is that of Vanderlinden[5] (VL). The table is divided into two sections: members and nonmembers of the cluster. The first section, physical members, contains all the stars observed which were considered by Klein-Wassink[3] to be members of the cluster from their proper mo-

*Contributions from the McDonald Observatory, University of Texas, No. 214.

[1] *Ap. J.*, **114**, 522, 1951.

[2] *Ap. J.*, in press.

[3] *Groningen Pub.*, No. 41, 1927.

[4] *A.N.*, **205**, 71, 1917.

[5] *Étude de l'amas de Praesepe* (Gembloux, 1935).

Table 3a

Colors and Magnitudes of Praesepe Stars

Cluster Members

Star (KW)	V	B-V	U-B	n	Star (KW)	V	B-V	U-B	n
32	11.85	+0.775	+0.389	2	286	8.02	+0.190	+0.127	5
45	8.25	+0.251	+0.093	2	288	10.69	+0.593	+0.093	2
48	12.33	+0.913	+0.642	3	292	8.18	+0.304	+0.087	3
50	6.75	+0.190	+0.112	3	295	9.37	+0.416	+0.008	5
52	12.28	+0.903	+0.650	3	300*	6.30	+0.172	+0.161	3
58	11.26	+0.671	+0.193	3	301	11.17	+0.655	+0.191	2
70	11.31	+0.801	+0.412	2	304	11.52	+0.741	+0.511	5
79	12.11	+0.865	+0.536	4	309	11.63	+0.765	+0.354	4
90	10.90	+0.699	+0.220	2	313	12.20	+0.834	+0.568	3
100	10.55	+0.583	+0.091	4	318	8.65	+0.291	+0.081	1
114	8.14	+0.209	+0.113	1	322	10.87	+0.679	+0.198	6
124	9.00	+0.321	+0.029	4	323	7.30	+0.224	+0.090	1
127	10.90	+0.596	+0.087	4	325	10.61	+0.608	+0.089	3
142	9.31	+0.492	+0.019	2	326	11.54	+0.716	+0.282	3
143	8.51	+0.228	+0.092	1	328	6.85	+0.205	+0.149	4
146	9.39	+0.404	-0.001	1	332	9.55	+0.434	+0.004	1
150	7.45	+0.255	+0.137	2	334	11.02	+0.725	+0.273	4
154	8.50	+0.251	+0.072	5	335	11.05	+0.351	+0.168	2
155	9.42	+0.412	+0.011	2	340	8.48	+0.259	+0.075	2
162	10.58	+0.573	+0.065	3	341	10.30	+0.520	+0.028	3
164	11.51	+0.704	+0.259	4	344	12.09	+0.861	+0.524	3
172	12.55	+0.945	+0.697	4	348	6.78	+0.168	+0.140	6
181	10.47	+0.588	+0.080	2	350*	8.71	+0.325	+0.112	2
183	12.34	+1.001	+0.759	4	363	12.43	+0.932	+0.857	3
198	12.35	+0.975	+0.774	3	365	10.18	+0.645	+0.192	1
203	7.73	+0.219	+0.095	1	370	9.04	+0.380	+0.045	1
204	6.67	+0.249	+0.147	2	371	10.11	+0.505	+0.052	3
207	7.87	+0.197	+0.112	3	375*	8.35	+0.208	+0.053	2
208	10.56	+0.585	+0.090	3	385*	7.92	+0.241	+0.101	1
209	12.74	+0.975	+0.792	4	392	10.72	+0.595	+0.099	6
212*	6.59	+0.959	+0.724	5	399	10.93	+0.624	+0.132	3
217	10.23	+0.513	+0.016	1	403	11.71	+0.780	+0.390	6
222	10.11	+0.489	-0.003	5	411	9.32	+0.389	-0.024	3
224*	7.32	+0.195	+0.142	3	416	9.59	+0.412	+0.004	1
226	8.89	+0.321	+0.045	3	417	12.36	+0.894	+0.599	5
227	9.49	+0.414	-0.011	3	418	10.47	+0.565	+0.059	3
229	7.54	+0.250	+0.124	3	421	10.17	+0.516	+0.021	1
232*	9.23	+0.389	-0.002	5	425	11.42	+0.526	+0.031	1
236	10.30	+0.506	-0.001	4	428*	6.90	+0.963	+0.740	4
239*	9.67	+0.443	-0.017	5	429	8.53	+0.297	+0.071	2
246	12.06	+0.856	+0.499	3	430	12.04	+0.846	+0.516	5
250*	9.79	+0.466	+0.002	1	432	11.05	+0.646	+0.190	1
253*	6.39	+0.983	+0.827	std	434	11.41	+0.726	+0.252	2
256	12.64	+1.016	+0.884	3	445	7.98	+0.208	+0.098	3
257	11.01	+0.785	+0.377	1	448	12.15	+0.977	+0.561	4
265	11.98	+0.814	+0.451	3	454	9.88	+0.465	+0.007	1
265	6.31	+0.006	+0.019	std	458	9.71	+0.551	+0.064	1
268	9.39	+0.477	+0.002	1	459*	9.23	+0.387	+0.011	2
271	8.81	+0.322	+0.062	5	460	12.10	+0.896	+0.625	5
275	9.96	+0.534	+0.079	5	466	10.99	+0.649	+0.161	2
276	7.54	+0.180	+0.151	5	471	12.15	+0.853	+0.534	3
279*	7.70	+0.201	+0.153	3	472	9.77	+0.447	-0.012	4
282	10.08	+0.507	+0.013	5	474	12.12	+0.986	+0.768	4
283*	6.44	+1.021	+0.902	5	476	11.82	+0.760	+0.356	3
284	6.78	+0.261	+0.129	2	488	11.44	+0.733	+0.312	3

Table 3a Continued

Cluster Members

Star (KW)	V	B-V	U-B	n	Star (KW)	V	B-V	U-B	n
492	12.13	+0.859	+0.549	3	576*	13.70	+0.812	+0.401	3
498	11.73	+0.768	+0.337	3	577*	14.68	+1.470	+1.257	3
508	10.77	+0.594	+0.099	3	H 3*	13.78	+1.221	+1.215	2
514	12.33	+0.921	+0.657	4	H 139*	13.92	+1.265	+1.222	1
537	11.65	+0.762	+0.355	4	H 262*	14.19	+1.451	+1.196	2
542	11.72	+0.782	+0.396	3	H 274*	13.55	+1.167	+1.089	2
553	10.15	+0.447	-0.010	3	H 306*	13.57	+1.181	+1.139	2
559*	14.01	+1.272	+1.196	3	VL 135*	6.58	+0.674	+0.253	5
560*	13.97	+1.289	+1.261	2					
561*	14.41	+1.376	+1.242	3					
566*	14.94	+1.484	+1.099	4					
568*	14.11	+0.777	+0.366	2					
572*	14.61	+0.953	+0.688	3					
574*	13.83	+1.201	+1.141	2					
575*	14.29	+1.353	+1.219	2					

Table 3b

Field Stars

Star (KW)	V	B-V	U-B	n	Star (KW)	V	B-V	U-B	n
94	7.83	+0.479	+0.064	1	361	11.87	+0.589	-0.003	2
108	10.01	+1.009	+0.779	2	377*	6.73	+0.104	+0.052	1
134	10.14	+0.893	+0.517	2	407*	8.50	+1.050	+0.917	1
138	11.18	+0.276	+0.072	1	433	11.05	+0.424	+0.002	1
149	12.37	+0.455	-0.047	3	443	10.65	+0.918	+0.659	1
190	9.09	+1.273	+1.406	1	446	13.22	+1.119	+0.970	2
192	10.95	+0.251	+0.081	2	462	10.99	+0.548	+0.055	2
250	9.78	+0.384	+0.079	1					
273	12.35	+0.265	+0.062	2					
321	11.72	+0.318	-0.015	2					

tions. Also included in this section are a number of stars found to be members by Haffner and Heckmann.[6] The second section contains a few nonmembers that were observed.

It is of considerable interest to compare these new observations with those of Haffner and Heckmann.[6] The effective wave length of their red point is considerably greater than 5500 A, and an approximate transformation facilitates the comparison. For this purpose we shall assume linear transformations and determine the coefficients from the stars brighter than $V = 7.0$. The resultant equations are

$$(B-V)_H = +0.167 + 0.609 C_H , \tag{1}$$

$$V_H = m_{6450} - 0.027 + 0.273 C_H , \tag{2}$$

where the subscript H designates values by Haffner and Heckmann or values computed from them. On the basis of observations of NPS stars,[1] the color index on the International System, *assuming a linear transformation*,[7] is

$$C_{\text{int}} = +0.958 + 1.090 C_y . \tag{3}$$

Since $C_y = (B-V) - 1.040$,[2]

$$C_{\text{int}} = -0.176 + 1.090\,(B-V) , \tag{4}$$

or

$$B-V = +0.161 + 0.917 C_{\text{int}} . \tag{5}$$

NOTES TO TABLE 3

212 The spectral type by Morgan is K0 III.
224 ADS 6915 A. The spectrum shows double lines (Adams *et al.; Ap. J.*, **81**, 187, 1935).
232 The spectral type by Morgan is F2.
239 The spectral type by Morgan is F6 V.
250 Visual double, 9^m8–15^m, 12″, 50°.
253 The spectral type by Morgan is K0 III.
279 Spectroscopic binary (*Lick Obs. Pub.* No. 18).
283 The spectral type by Morgan is K0 III. Visual double, 6^m4–14^m, 13″, 164°.
300 Double-line spectroscopic binary (*Lick Obs. Pub.* No. 18).
350 Visual double, 8^m7–15^m, 12″, 321°.
375 Spectroscopic binary (Mt. Wilson, private communication to Haffner and Heckmann).
385 ADS 6931. The radial velocity of the brighter component is variable (*Lick Obs. Pub.* No. 18).
407 Long-period variable.
428 The spectral type by Morgan is K0 III.
459 The spectral type by Morgan is F4.
559 Probable member, according to Haffner and Heckmann.
560, 561, 566 See note for No. 559.
568 Certain member, according to Haffner and Heckmann.
572, 574 See note for No. 568.
575 See note for No. 559.
576 See note for No. 568.
577 See note for No. 559.
H 3, H 139, H 262, H 274, H 306 See note for No. 568.
VL 133 Proper motion: -0^s029, $-0''018$ (Boss 2282). Radial velocity: $+35.8 \pm 2.9$ km/sec (*Lick Obs. Pub.* No. 18).

[6] *Göttingen Veröff.*, Nos. 55, 1937, 66 and 67, 1940.

[7] See H. L. Johnson, *Ap. J.*, **116**, 272, 1952, for a discussion of the validity of such transformations.

Haffner and Heckmann have set the zero point for C_H at the zero point for the International color indices; the very good agreement between the values of $B-V$ obtained from equations (1) and (5) for $C_H = C_{int} = 0$ shows that there can be no significant errors in the zero points for the colors of either Haffner and Heckmann or myself. Haffner and Heckmann give -0.03 ± 0.02 (m.e.) mag. as the zero-point correction for m_{4270} to IPg; their method of setting the zero point of m_{6450} gives essentially the same correction for their red magnitudes. Equation (2), for $C_H = 0$, agrees with this correction better than one might expect from the errors of the two series. These agreements in zero points with

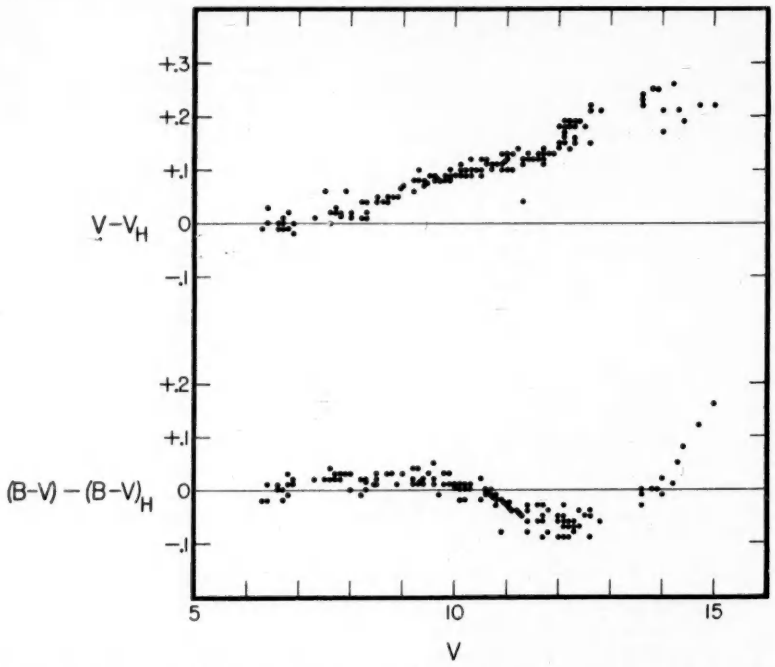

FIG. 1.—Comparisons of the photoelectric observations with the photographic ones of Haffner and Heckman.

respect to the fundamental system (via the NPS) are very good, especially when one considers that linear transformations have been used.[7]

Comparisons between the values determined from equations (1) and (2) and the values of V and $B-V$ from Table 3*a* are shown in Figure 1. While there appear to be magnitude errors in Haffner and Heckmann's work, the accuracy of their photographic photometry is extraordinary. Some of the field stars in Table 3*b* whose colors and magnitudes differ greatly from those for the Praesepe main sequence also deviate appreciably ($\sim$0.1 mag.) from the principal sequences of Figure 1. This fact, with the systematic deviations shown by Figure 1, shows that equations (1) and (2) do not completely describe the relations between the two photometric series.

A total of 60 known cluster members were not observed photoelectrically but were observed by Haffner and Heckmann. Their values for these stars have been transformed by equations (1) and (2), corrected as indicated by Figure 1, and listed in Table 4. As

Table 4

Praesepe Stars observed by Haffner and Heckmann

Cluster Members

Star (KW)	V	B–V	Star (KW)	V	B–V	Star (KW)	V	B–V
9	11.39	+0.82	257	12.83	+0.98	456	12.59	+0.91
16	9.16	+0.51	244*	9.98	+0.62	478	9.68	+0.43
25	11.53	+0.71	258	10.24	+0.57	495	9.94	+0.66
27	11.45	+0.74	267	13.13	+1.05	496	9.56	+0.52
30	11.40	+0.72	272	12.68	+1.05	515	10.13	+0.51
31	9.73	+0.57	287	10.41	+0.60	533	11.56	+0.95
34	9.47	+0.45	293	9.85	+0.47	534	7.53	+0.22
38	8.69	+0.33	297	11.59	+0.87	535	12.65	+0.94
40	7.79	+0.22	299	13.20	+1.08	536	9.42	+0.51
47	9.32	+0.50	336	11.45	+0.74	538	8.62	+0.38
49	10.55	+0.60	349	12.17	+0.87	540	11.00	+0.71
55	11.38	+0.86	353	12.35	+0.93	541	10.69	+0.66
60	12.95	+0.97	367	10.70	+0.69	543	11.42	+0.75
141	12.38	+0.91	368	11.50	+0.72	544	12.44	+0.95
182	10.51	+0.68	390	12.95	+1.07	546	11.60	+0.76
184	11.59	+0.91	396	9.83	+0.46	549	10.11	+0.51
196	10.73	+0.65	401	12.96	+1.04	551	12.71	+0.96
213	11.78	+0.76	415	13.09	+1.07	552*	8.56	+0.09
218	9.36	+0.44	439	9.45	+0.39	VL 166*	7.54	+0.24
236	11.87	+0.99	449	7.91	+0.21	VL 1236*	9.84	+0.47

NOTES TO TABLE 4

244 W UMa variable, TX Cnc.
377 ADS 6930. Spectroscopic binary (*Lick Obs. Pub.* No. 18).
552 Algol-type variable, S Cnc.
VL 166 Proper motion: −0".0026, −0".019 (*Yale Trans.*, Vol. **10**, 1934, reduced to PGC system.) Radial velocity: +30 km/sec (Mt. Wilson, private communication to Haffner and Heckmann).
VL 1236 Proper motion: −0".0023, −0".024 (*Yale Trans.*, Vol. **10**, 1934), reduced to the PGC system.

in Table 3, the star numbers are those of Klein-Wassink,[3] except for two stars whose numbers are those of Vanderlinden (*VL*).[5]

The color-magnitude diagram, V versus $B-V$, for cluster members is shown in Figure 2. The large dots designate stars observed photoelectrically; the small dots, those transformed from the work of Haffner and Heckmann. The extreme narrowness of the main sequence for $B-V > +0.3$ is evident. As is suggested by Haffner and Heckmann, the few stars scattered above the main sequence probably are binaries. All the stars below the main sequence are cluster members according to the proper motions.

The distance modulus of Praesepe can be determined by comparing the Praesepe main sequence with near-by dwarfs having large parallaxes.[2] The distance modulus so deter-

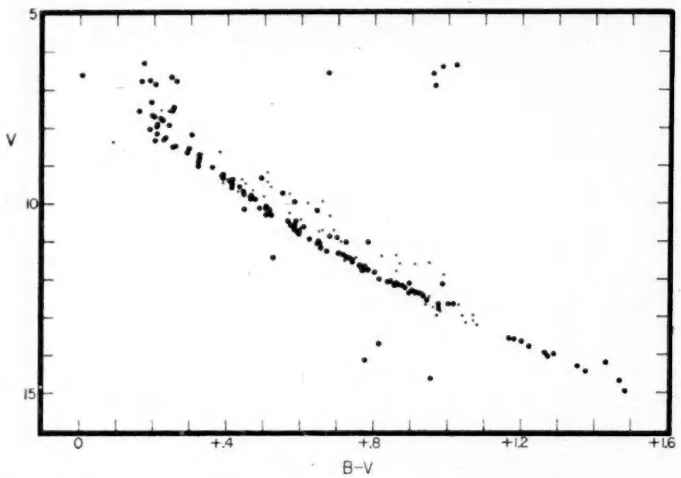

FIG. 2.—V versus $B-V$ for Praesepe. The large dots represent photoelectric observations, while the small dots represent values transformed from the work of Haffner and Heckmann.

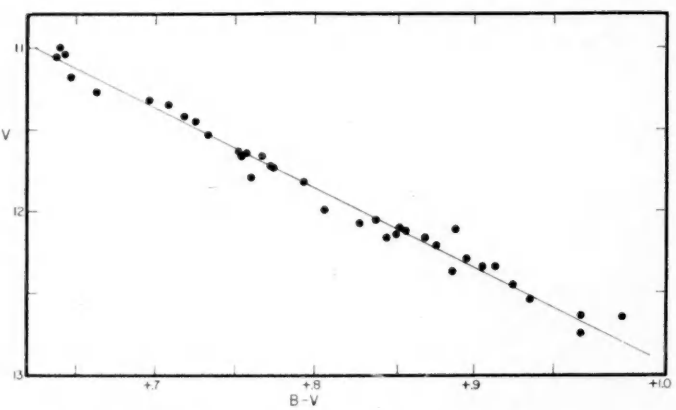

FIG. 3.—V versus $B-V$ for the narrowest portion of the Praesepe main sequence

TABLE 5

MAGNITUDE SCATTER IN PRAESEPE

Source of Error	p.e. (Mag.)	Source of Error	p.e. (Mag.)
V	± 0.005	Total	± 0.022
$B-V$	$\pm .015$	Observed	± 0.040
Depth of cluster	± 0.015		

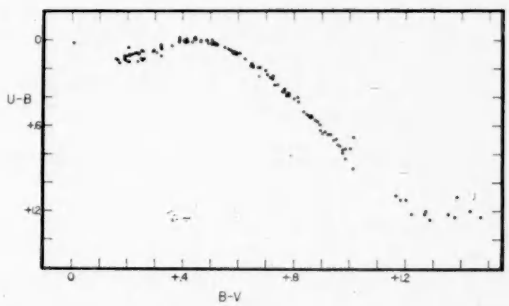

FIG. 4.—$U-B$ versus $B-V$ for Praesepe. The open circles designate the five yellow giants

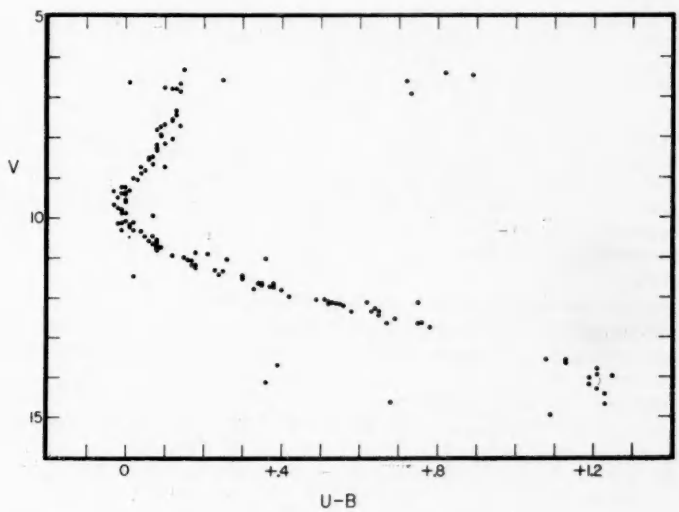

FIG. 5.—V versus $U-B$ for Praesepe

mined is 6.2 ± 0.1 (p.e.) mag, and there seem to be no significant systematic differences in shape between the Praesepe main sequence and that defined by the near-by stars for $B-V > +0.4$.

In Figure 3 is plotted, greatly magnified, the narrowest portion of the main sequence of Figure 2. Only photoelectric observations have been used, and all stars lying more than 0.2 mag. above the main sequence have been omitted. The straight line drawn through the plotted points appears to be satisfactory, and the probable error of the deviations of the points from the line is, in terms of V, ±0.040 mag. If we are to interpret this result in terms of cosmic dispersion, we must make an estimate of all other possible sources of scatter. The three important sources of scatter, other than possible cosmic dispersion, are: errors in V; errors in $B-V$ (multiplied by 5—the slope of the line in Fig. 3); and scatter due to the finite depth of the cluster in the line of sight. The probable errors due to V and $B-V$ are given in the first two rows of Table 5; they have been determined from the individual observations of the stars plotted in Figure 3. According to Trumpler,[8] the diameter of the cluster is 90′, which corresponds, on the assumption that the cluster is spherical, to a maximum scatter in V of ±0.03 mag. It seems unlikely that the probable error of this scatter will exceed ±0.015 mag., and this value has been given in the third row of Table 5.

It seems likely that the dispersion in this narrowest section of the Praesepe main sequence is larger than that due to observational errors and the depth of the cluster, but this does not necessarily mean that the cosmic dispersion is finite. There are enough probable double stars in Praesepe having comparable components to make it likely that a number of the stars plotted in Figure 3 have secondary components of sufficient brightness to affect our result. We can, however, give an approximate upper limit to the cosmic dispersion here: ±0.03 (p.e.) mag. in V. Unless the distribution of binaries changes considerably, the cosmic dispersion is definitely greater than this value for the bluer main-sequence stars in Praesepe.

Figure 4 shows a plot of $U-B$ versus $B-V$. The effect of absorption in the Balmer continuum for the A stars ($U-B = B-V = 0$ at A0 V)[2] is quite apparent. Another effect producing an apparent increase in ultraviolet intensity with decreasing temperature shows among the late K and early M stars in the lower-right-hand corner of the diagram. For $B-V > +0.4$, the relation between $U-B$ and $B-V$ coincides with that determined from near-by main-sequence stars.[2] This fact shows that the amount of reddening material in front of, or within, the cluster is negligible. The extreme narrowness of the Praesepe main sequence (see Fig. 2) also argues against any internal reddening. The variable reddening correlated with distance from the center of the cluster found by Wallenquist[9] must, as he suggests, be due to some systematic error of unknown origin.

Figure 5 gives the color-magnitude diagram, V versus $U-B$. The large effect of the hydrogen absorption in the A stars is again apparent. The main sequence is, as in Figure 2, quite narrow.

To recapitulate, the following important points have been discussed:

1. The photographic work of Haffner and Heckmann on Praesepe is amazingly accurate. The zero points of the present work with respect to the fundamental system are confirmed by their work.
2. The distance modulus of the Praesepe cluster is found to be 6.2 ± 0.1 (p.e.) mag.
3. The shape of the Praesepe main sequence does not differ significantly from that defined by near-by dwarf stars having large trigonometric parallaxes.
4. For one portion of the Praesepe main sequence, the upper limit for cosmic dispersion in magnitude is ±0.03 (p.e.) mag.

[8] *Lick Obs. Bull.*, **14**, 154, 1930.

[9] *Uppsala Astr. Obs. Medd.*, No. 100 = *Ark. f. Astr.*, Vol. **1**, No. 10, 1949.

NOTES

THE REACTION RATE OF THE PROTON-PROTON CHAIN

Recent progress in experimental nuclear physics now makes possible fairly accurate calculations of the rate of the proton-proton reaction chain. This chain of thermonuclear reactions, starting with the formation of a deuteron from the collision and beta-decay of two protons, has the net result of converting four H^1-atoms into one He^4-atom, releasing a fraction of 7×10^{-3} of the rest-mass energy into thermal energy. The aim of this note is to present the results of recent calculations[1] in a form suitable for astrophysical applications to main-sequence stars.

These calculations were carried out on the assumption of an accurate Maxwellian distribution of thermal energies for a constant temperature T (in 10^{6}° K), uniform density ρ (in grams per cubic centimeter), and uniform concentration (by mass) x_H of hydrogen. It is now well established[1] that, for values of T, ρ, and x_H corresponding to conditions in the interior of main-sequence stars,[2] the reactions making up the overwhelming bulk of the proton-proton chain are the following.

$$H^1 + H^1 \rightarrow D^2 + e^+ + \nu + 0.42 \text{ Mev}, \qquad 8 \times 10^9 \text{ years}, \tag{1}$$

$$H^1 + D^2 \rightarrow He^3 + \gamma + 5.5 \text{ Mev}, \qquad 4 \text{ seconds}, \tag{2}$$

$$He^3 + He^3 \rightarrow He^4 + 2H^1 + 13 \text{ Mev}, \qquad 3 \times 10^5 \text{ years}. \tag{3}$$

The calculated mean reaction times[3] for $T = 15$ and $\rho x_H = 100$ (approximate central conditions for the sun) are also given in the above equations. The probable errors in the calculated reaction rates are about 25 per cent for the first reaction, about 50 per cent for the second reaction, and a factor of about three for the last reaction.

The rate of the reaction chain as a whole and hence the rate of energy production are controlled by the first and slowest reaction. Its rate was calculated[1] using the latest data on the beta-decay constant[4] and an accurate calculation of the relevant matrix element.[5] At temperatures T in the neighborhood of a temperature T_0 (in 10^{6}° K), the rate of energy production ϵ can be expressed in the form

$$\epsilon = \epsilon_0 \frac{\rho x_H^2}{100} \left(\frac{T}{T_0}\right)^n \text{ erg/gm sec}. \tag{4}$$

Calculated values of ϵ_0 and n for four values of T_0, typical of central temperatures of various main-sequence stars, are given in Table 1.

[1] E. E. Salpeter, *Phys. Rev.*, **88** (in press).

[2] The reaction chain is completed exclusively by means of reaction (3) only if the electron gas is non-degenerate. This is the case if the density ρ is of the order of 10^3 gm/cm^3 or less, which is certainly the case in main-sequence stars. But for densities of the order of 10^6 gm/cm^3 most He^3 nuclei undergo an inverse beta-decay, absorbing high-energy electrons from the degenerate Fermi gas. For applications to white dwarf stars see T. D. Lee, *Ap. J.*, **112**, 561, 1950.

[3] The mean life of hydrogen is *one-half* of the reaction time for reaction (1).

[4] G. L. Trigg, *Phys. Rev.*, **86**, 506, 1952. The large increases in both the calculated values and the accuracy of this reaction rate are mainly due to equivalent increases for the beta-decay constant as deduced from observed beta-decays.

[5] E. Frieman and L. Motz, *Phys. Rev.*, **83**, 202, 1951, and private communication.

Under conditions of dynamic equilibrium the concentrations (by mass) of deuterium (x_D) and of He^3 (x_3) adjust themselves so that the rates of creation and destruction are equal for each nuclear species. Values of x_D and x_3, calculated from the various reaction rates, are also given in Table 1. The probable errors are about 25 per cent for ϵ_0, about 50 per cent for x_D, and about a factor of 3 for x_3. It should be noted that the concentrations of deuterium and He^3 (except at very low temperatures) are very small, which is

TABLE 1

RATE* OF ENERGY PRODUCTION ϵ_0, EXPONENT OF THE VARIATION WITH TEMPERATURE n, CONCENTRATIONS (BY MASS) x_D AND x_3, FOR DEUTERIUM AND He^3, RESPECTIVELY, FOR VARIOUS TEMPERATURES T

T (in 10^6 ° K)	ϵ_0 (in Ergs/gm/Sec)	n	x_D/x_H	x_3/x_H
5	0.24	6.0	5.6×10^{-17}	0.13
8	3.1	5.0	4.1×10^{-17}	0.008
15	50	4.0	3.0×10^{-17}	4×10^{-5}
30	530	3.0	2.3×10^{-17}	1.0×10^{-6}

* See eq. (4).

not in disagreement with spectroscopic observations[6] on stellar atmospheres. But the terrestrial concentrations of deuterium are *enormously* larger than the calculated equilibrium values given in Table 1. This seems to suggest that the material from which the earth was formed could not have come from the interior of a main-sequence star.

E. E. SALPETER

LABORATORY OF NUCLEAR STUDIES
CORNELL UNIVERSITY
ITHACA, NEW YORK
July 23, 1952

THE MOTIONS OF HIGH-VELOCITY INTERSTELLAR CLOUDS

The discovery by C. S. Beals[1] of the multiple components of interstellar H and K lines has usually been taken as proving the existence of discrete interstellar clouds. The most complete data on the motions of these clouds are due to W. S. Adams[2] and have recently been thoroughly discussed by A. Blaauw,[3] who has remarked upon the asymmetry in the velocity distribution of the interstellar K-line components. The origin of the small high-velocity interstellar clouds which give rise to this asymmetry is not yet known, and it was thought possible that an investigation of their motions might throw light on that problem.

For this purpose those stars from Table 2 of Adams' paper were considered which show "high-velocity" interstellar lines; that is, lines indicating residual velocities (corrected for a solar motion of 20 km/sec) greater than or equal to 15 km/sec. There are 68 such stars in all, but for the purpose of this investigation Nova Aquilae 1945 was omitted, and so were the faint components of three binaries whose interstellar spectra are, in each case, very similar to those of their brighter companions. The remaining 64 stars were separated into three categories, according to the sign of the residual velocities

[6] J. L. Greenstein, *Ap. J.*, **113**, 531, 1951.

[1] *M.N.*, **96**, 661, 1936.

[2] *Ap. J.*, **109**, 354, 1949.

[3] *B.A.N.*, No. 436, 1952.

associated with their high-velocity interstellar-line components. Category I comprises 41 stars in whose spectra the high-velocity interstellar components show residual velocities which are all negative; category II comprises 18 stars showing interstellar components, all indicating positive residual velocities. Category III comprises the remaining five stars, each of which shows several high-velocity interstellar components with residual velocities, some of which are positive and some negative. There is a pronounced asymmetry in the motions of the high-velocity clouds, in the sense that most of them are moving toward the sun. The asymmetry is apparent, too, in the difference, cloud velocity *minus* star velocity, and it appears that most of these clouds are moving away from the stars in whose spectra their absorption lines are observed. This asymmetry is not an effect of galactic rotation, for only 13 of the stars considered lie in that half of the galactic plane where the rotation may be expected to give rise to negative residual velocities.

Table 1 shows the number of the stars considered which have normal spectra, the number of Be stars, the number of cBe stars, and the number of Bp stars in each category. The spectral types are taken from Adams' paper. The ratio of the number of stars in category I to the number in other categories is, for stars with normal spectra, 38:12, while for stars with spectral peculiarities this ratio is 3:11.

TABLE 1

Spectral Type	Number of Stars in Each Category		
	I (Residual Velocities All Negative)	II (Residual Velocities All Positive)	III (Residual Velocities both Positive and Negative)
Normal	38	11	1
Be	3	2	3
cBe	.....	5	.....
Bp	.....	.....	1
Total	41	18	5

It is clear not only that most of these stars belong to category I but that categories II and III contain a far higher percentage of stars with spectral peculiarities than does category I. The preponderance of negative residual velocities for these high-velocity clouds is not compatible with the usually assumed random motions of interstellar clouds. Blaauw suggests[3] that "perhaps part of the observed negative velocities may not be of interstellar origin but have some connection with the star itself." The correlation of positive residual velocities with spectral peculiarities certainly suggests that at least some interstellar clouds are more closely associated with the stars than has hitherto been assumed or, alternatively, that some of the components of multiple lines may not be due to truly interstellar clouds at all. However, it is to be noted that in those cases where the correlation suggests a connection between cloud and star, the motion of the cloud is not such as to give rise to the observed asymmetry. This correlation depends rather strongly on the accepted spectral types of a few stars, but the preponderance of negative residual velocities appears well established.

Leonard Searle

Princeton University Observatory
August 1, 1952

A NEW INFRARED BAND SYSTEM OF *FeO**

In the course of some spectroscopic studies on the combustion of carbon monoxide containing a small quantity of iron pentacarbonyl, there was observed an intense band system in the near infrared. The spectrum extends from 7000 to 15,000 cm^{-1} (about 0.7–1.4 μ) and can be attributed to the *FeO* molecule.

The spectra were recorded with a Perkin-Elmer Model 12C spectrometer equipped with a dense flint-glass prism and an Eastman Kodak lead sulphide detector. The spectral band passed by the spectrometer for a 20 μ slit varied from 20 cm^{-1} at 7000 cm^{-1} to 50 cm^{-1} at 14,000 cm^{-1}. The combustion took place over a water-cooled burner with a rectangular slot of dimensions 0.46 × 44 mm.

Figure 1 shows a tracing of the spectrum as recorded over this region. Some sixty bands can be measured at low dispersion in this system, and Table 1 lists the frequencies, in cm^{-1}, for the maxima of the bands.

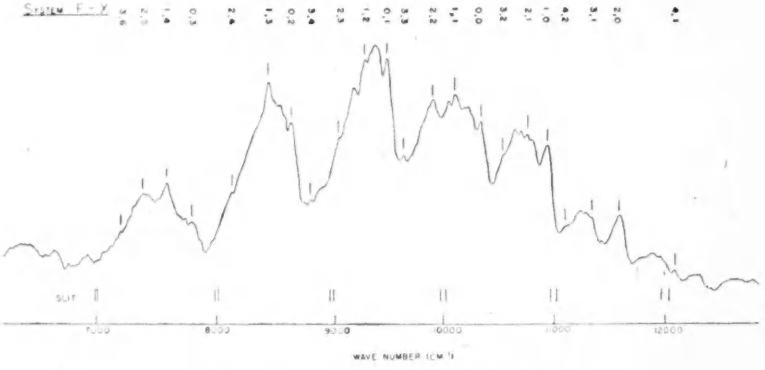

FIG. 1.—Infrared emission spectrum of *FeO*

A number of the bands, as indicated in Figure 1, can be arranged in a vibrationa array. The mean value of the upper-state frequency difference, $\nu' = 651$ cm^{-1}, belongs to no previously reported system of *FeO*. The mean frequency difference of the lowe state, $\nu'' = 864$ cm^{-1}, agrees well with the value of 875 cm^{-1} determined by Delsemm and Rosen[1,2] for the ground state. With the thermal method of excitation used, the intensity of this new system is of the same order of magnitude as that of the strong yellow system, a further indication that we are dealing with a resonance transition of the *FeO* molecule. The system reported by Malet and Rosen[2,3] in the region 10,000–15,000 cm^{-1} appears to be the weaker short-wavelength portion of our system. Some of their bands, denoted by (*R*), fit into our vibrational scheme and are included in Table 1.

* Supported in part by the ONR. Presented at the American Physical Society meeting at Washington, D.C., May, 1952.

[1] A. Delsemme and B. Rosen, *Bull. Soc. sci. Liége*, **1945**, p. 70.

[2] B. Rosen, *Nature*, **156**, 570 (1945).

[3] L. Malet and B. Rosen, *Bull. Inst. r. Col. Belg.*, **1945**, p. 377.

Lines of the system also occur on plates of the iron arc photographed by Kiess in the region 9000–11,000 A with 15,000 and 7500 lines per inch gratings. Grating spectra of our source, in both the infrared and the yellow, are being taken and measured. The grating measurements of the prominent lines at 9220.42, 9223.94, and 9672.71 A are in

TABLE 1

INFRARED BANDS OF *FeO*

Wave Number (cm^{-1})	Wave Length (μ)	Intensity	Assignment	Wave Number (cm^{-1})	Wave Length (μ)	Intensity	Assignment
13459 (*R*)	0.7428	.....	6, 1	9747	1.0257	30	.....
13000 (*R*)	0.7690	.....	4, 0	9631	1.0380	28	3, 3
12313	0.8119	.....	3, 0	9473	1.0553	54	0, 1
12147 (*R*)	0.8230	.....	4, 1	9387	1.0650	55	.....
12002	0.8320	2	.....	9355	1.0687	56	.....
11945	0.8369	3	.....	9311	1.0737	53	.....
11882	0.8414	4	5, 2	9254	1.0803	52	1, 2
11798	0.8474	3	.....	9160	1.0914	41	.....
11741	0.8515	3	.....	9082	1.1008	32	.....
11598	0.8620	14	2, 0	9026	1.1076	27	2, 3
11436	0.8742	6	3, 1	8891	1.1244	21	.....
11350	0.8808	14	.....	8781	1.1385	17	3, 4
11304	0.8844	14	.....	8719	1.1466	17	.....
11234	0.8899	14	4, 2	8593	1.1634	38	0, 2
11138	0.8976	11	.....	8531	1.1719	39	.....
11099	0.8998	10	.....	8492	1.1773	42	.....
10962	0.9120	32	1, 0	8432	1.1856	44	.....
10807	0.9251	33	.....	8390	1.1916	48	1, 3
10766	0.9286	34	2, 1	8294	1.2054	36	.....
10708	0.9336	35	.....	8164	1.2246	26	2, 4
10655	0.9383	35	.....	8060	1.2404	17	.....
10593	0.9438	31	.....	7743	1.2911	12	0, 3
10547	0.9479	29	3, 2	7700	1.2983	12	.....
10332	0.9676	38	0, 0	7652	1.3065	13	.....
10257	0.9747	38	.....	7552	1.3238	22	1, 4
10221	0.9781	41	.....	7481	1.3364	16	.....
10175	0.9825	41	.....	7433	1.3450	17	.....
10105	0.9893	44	1, 1	7396	1.3517	18	.....
10046	0.9951	42	.....	7360	1.3583	18	.....
9947	1.0051	38	.....	7307	1.3682	15	2, 5
9896	1.0102	43	2, 2	7257	1.3776	12	.....
9851	1.0149	39	.....	7219	1.3849	9	.....
9794	1.0208	35	.....	7187	1.3910	8	.....

fair agreement with and may account for three unidentified faint solar lines in the sun's spectrum.[4] As a resonance transition of *FeO*, the system may be a prominent feature of late-type stellar spectra.

A. M. BASS
W. S. BENEDICT

NATIONAL BUREAU OF STANDARDS
June 23, 1952

[4] H. D. Babcock and C. E. Moore, "The Solar Spectrum λ 6600 to λ 13495," *Pub. Carnegie Inst. Washington*, No. 579, 1947.

RADIAL VELOCITIES OF Z SCULPTORIS, ξ PHOENICIS, AND β CRUCIS

The present note reports on the results of the spectrographic observations of Z Sculptoris, ξ Phoenicis, and β Crucis with the Bosque Alegre reflector. All the spectrograms—except one of the ξ Phe, which was kindly secured by Dr. J. Landi Dessy—were obtained by Sahade with the Wood-grating spectrograph, which gives a dispersion of about 42 A/mm. All the plates—36 for Z Scl, 31 for ξ Phe, and 21 for β Cru—were measured by Albarracín. As a check, Sahade has remeasured 7 plates of Z Scl, 3 of ξ Phe, and 9 of β Cru. The star lines used for Z Scl and ξ Phe are listed in Table 1; for β Cru we have

TABLE 1

STELLAR LINES USED FOR THE RADIAL-VELOCITY DETERMINATIONS

Z SCULPTORIS		ξ PHOENICIS		Z SCULPTORIS		ξ PHOENICIS	
Element		Element		Element		Element	
Hζ	3889.05	*H*15	3711.97	*Hδ*	4101.74	*Ca* II	3933.66
Ca II	3933.66	*H*14	3721.94	*Ca* I	4226.73	*Sr* II	4077.71
Ca II	3968.47	*H*13	3734.37	*Fe* I	4250.46	*Hδ*	4101.74
Fe I	4005.25	*H*12	3750.15	*Fe* I	4260.48	*Sr* II	4215.52
Fe I	4045.82	*H*11	3770.63	*Hγ*	4340.47	*Hγ*	4340.47
Fe I	4063.60	*H*10	3797.90	*Fe* II	4351.76	*Mg* II	4481.23
Fe I	4071.74	*H*9	3835.39	*Fe* I + *Ti* I	4404.75	*Hβ*	4861.33
Sr II	4077.71	*Hζ*	3889.05	*Mg* II	4481.23		

used the wave lengths given by Kühlborn[1] in his study on early B-type stars. It has not been possible, of course, to measure all the lines on each of the corresponding plates, but the minimum of lines measured were 6 for Z Scl, 6 for ξ Phe, and 9 for β Cru.

Z SCULPTORIS[2]

This star was observed in 1946, 1947, 1948, and 1950, and it was included on the program because Schneller's *Katalog* for 1939 indicated that a variation in brightness from 6.3 to 7.6 mag. had been detected and that the type of variation was *unbekannt*. Quoting S. Gaposchkin,[3] "This star was suspected of variability by Thome (*Córdoba Results*, **17**, XII, 1894) and Pickering at first concluded that there was a photographic variation; later, however, he stated that there was no variation (*Harvard Ann.*, **46**, 232, 1903). The star is too bright for successful study on the patrol plates but a discussion of over five hundred estimates leads to the conclusion that the variation, if any, is inappreciable with the accuracy that we can attain, the probable error of the median magnitude being 0.05 magnitude." Gaposchkin's value for the photographic magnitude of Z Scl is 7.60 ± 0.05 mag.

The spectral type of Z Scl (Fig. 1) is around F8V, and the radial velocity obtained from our material is −13.8 ± 0.6 (p.e.) km/sec; the scatter of our results is probably not significant.

ξ PHOENICIS[4]

ξ Phe was included on the program because it had been announced as an eclipsing variable; after our observations were made, it turned out that there had been a mistake in the greek letter and that the announcement did not actually mean to refer to ξ Phe.

[1] *Veröff. U.-sternw. Berlin-Babelsberg*, Vol. **12**, Part I, 1938.

[2] $\alpha = 0^h37^m5$; $\delta = -34°14'$ (1950.0). GC 789 = CD−34°224 = CPD−34°56 = HD 3735 (Sp. F8).

[3] *Harvard Ann.*, **115**, 225, 1950.

[4] $\alpha = 0^h39^m5$; $\delta = -56°47'$ (1950.0). GC 830 = BS 183 (5.83 mag.) = CD−57°137 = CPD −57°143 = HD 3980 (Sp. F0p).

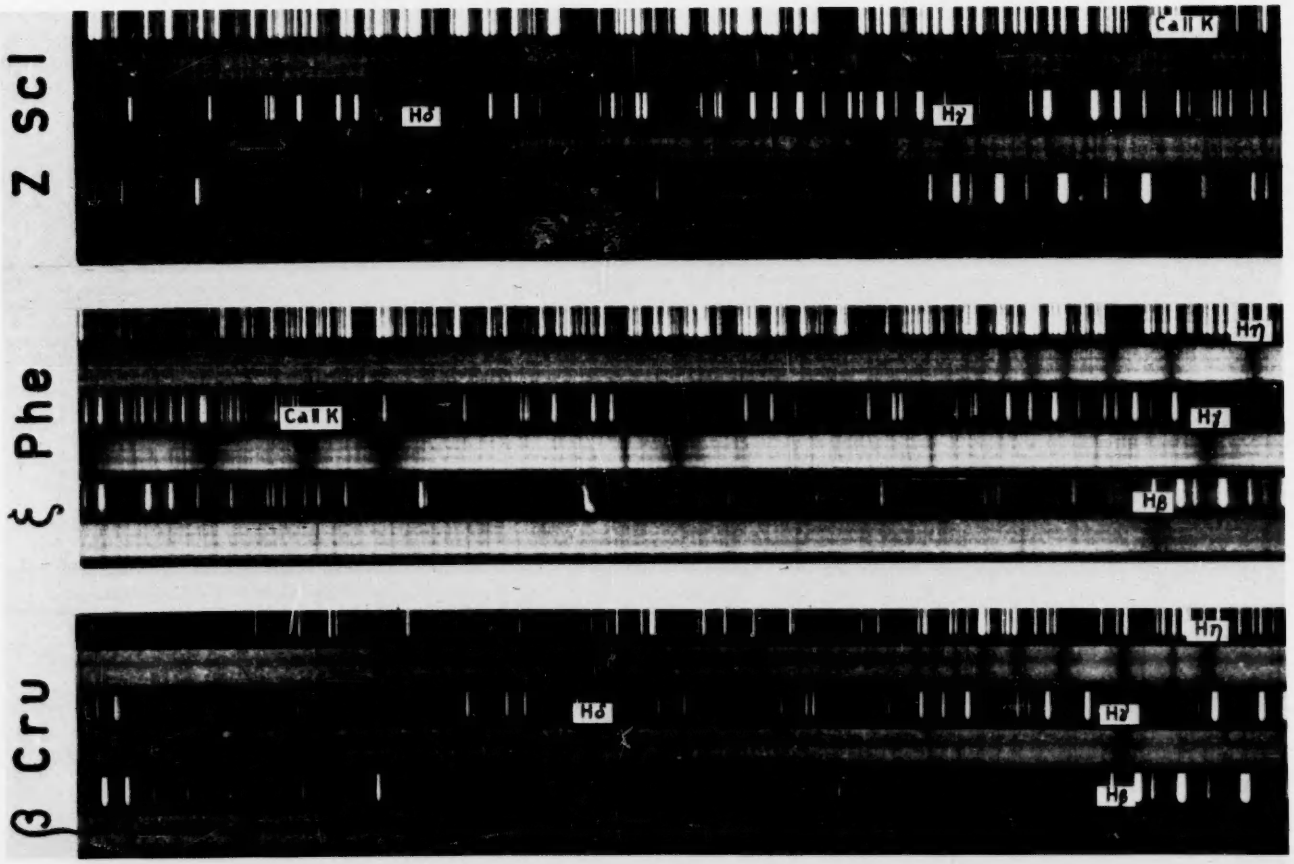

FIG. 1.—Positive enlargements of spectra of Z Scl, ξ Phe, and β Cru

The spectrographic material was obtained in the interval July–September, 1949, and there is an additional plate secured in 1946 for surveying purposes. The *Henry Draper Catalogue* remarks that "the spectrum is very peculiar, and resembles the composite type in combining strong *H* lines with several intense solar lines. The strontium lines 4077.9 and 4215.7, and the double silicon line 4128.1, 4131.1 are specially well marked." Actually, ξ Phe is a peculiar star of around A8 spectral type (Fig. 1), which belongs to the "strontium-europium" group. Outstanding absorption lines, besides those of *H* and *Ca* II, are the *Sr* II 4077 and 4215 lines, λ 4290, and *Mg* II 4481. High-contrast plates of ξ Phe will be obtained in order to publish a list of wave lengths and identifications.

The radial velocity of ξ Phe, as derived from our material, is $+7.1 \pm 0.6$ (p.e.) km/sec, a value which agrees, within expected limits from the probable errors, with the one quoted in Moore's *General Catalogue of Radial Velocities*,[5] namely, $+9.8 \pm 0.8$ (p.e.) km/sec. The latter value was determined as a mean from several measures of four plates taken in Chile with a linear dispersion of about 20 A/mm.

The scatter of our velocities is probably not significant; furthermore, the mean values for *H* and for the other elements are practically the same. However, it seems in order to mention that, on one plate which yields a mean radial velocity as high as +20 km/sec, three *H* lines give $+36 \pm 2.2$ (p.e.) km/sec and the rest of the elements (four lines), $+9 \pm 2.2$ (p.e.) km/sec, while from a plate taken immediately after, under the same conditions, we have +4 km/sec for the mean value, 0 ± 2.8 (p.e.) km/sec for five *H* lines, and $+9 \pm 2.4$ (p.e.) km/sec for the rest of the elements (three lines).

The plates were examined for variation in line intensities, and no strong evidence for the existence of such a phenomenon was found.

β CRUCIS[6]

The second brightest star of the Southern Cross was spectrographically observed at Bosque Alegre in 1946, 1947, and 1950, because of the remark in the *Henry Draper Catalogue* that on one plate "4387.8 and 4471.8 appear to be slightly bright on the edge of the greater wave length" and because it had been announced by W. H. Wright[7] as having variable radial velocity with a range of 19 km/sec. The plates on which Wright's report was based—10 in number—had been taken in the years 1904, 1905, 1907, and 1909. The results from them are listed in the Lick *Catalogue of Stellar Radial Velocities*,[8] together with those from 46 later spectrograms; the mean value from all this material, namely, $+20.0 \pm 0.5$ (p.e.) km/sec, was adopted in Moore's *General Catalogue of Radial Velocities*[9] only as a provisional radial velocity of β Cru.

The radial velocities obtained from our material are listed in Table 2; their mean value is $+10 \pm 1.0$ (p.e.) km/sec. The probable error of the individual radial velocities is of the order of ±2.0 km/sec, and therefore the scatter shown by our measures is somewhat large, the range being of the order of the one previously announced. However, all the available values for the radial velocities of β Cru (those appearing in Moore's *Catalogue* and ours) do not suggest any period for representing them. The fact that the mean values from the material considered by Moore and from our material differ by an amount larger than is consistent with the probable errors affecting them would seem to support the hypothesis that β Cru actually shows variation in velocity. The possibility that the difference may arise from the different values in the wave lengths adopted by the Lick

[5] *Lick Obs. Pub.*, **18**, 5, 1932.

[6] $\alpha = 12^h44^m8$; $\delta = -59°25'$ (1950.0). GC 17374 = BS 4853 (1.50 mag.) = HD 111123 (Sp. B1).

[7] *Lick Obs. Bull.*, **5**, 176, 1909. The reference is quoted in Moore's *Third Catalogue of Spectroscopic Binary Stars* (*Lick Obs. Bull.*, No. 355, 1924).

[8] *Lick Obs. Bull.*, **16**, 188, 1928. The linear dispersion of the spectrograms was either 10 or 20 A/mm.

[9] *Op. cit.*, p. 103. The revised spectral type quoted is B1s.

people and by us for the comparison and the stellar lines was considered, and it was concluded that the possibility is out of the question.

The spectral type of β Cru (Fig. 1) is B1, and the luminosity class around IV; there is not the least trace of emission on our plates, even on two F plates taken in order to

TABLE 2

RADIAL VELOCITIES OF β CRUCIS

Date	U.T.	Radial Velocity (Km/Sec)	No. of Measures	No. of Lines Measured
1946 Mar. 28	7:00	+24	2	11
28	7:20	0	2	10
Apr. 22	6:14	+12	2	11
23	6:44	+ 8	1	10
July 18	21:54	− 2	2	14
1947 Mar. 14	6:13	+11	1	10
July 2	22:34	+13	1	13
4	22:12	+ 1	4	13
5	22:25	+ 8	2	12
6	22:02	+ 3	4	12
7	22:07	+13	2	16
25	0:37	+ 1	3	22
26	22:24	+10	1	9
27	22:19	+ 2	1	12
28	22:35	+13	2	26
Aug. 6	22:31	+10	1	11
10	22:44	+ 8	2	15
1950 Feb. 3	8:45	+15	2	11
Aug. 5	22:38	+16	2	13
5	22:50	+23	3	12
6	0:28	+13	1	9

cover the *Hα* region. The Balmer series is seen up to *H*16, a fact which suggests for β Cru a luminosity class[10] which agrees with the one derived by considering Morgan, Keenan, and Kellman's[11] criteria.

Note added in proof.—When this paper was in press, we received a copy of Schneller's third volume of *Geschichte und Literatur des Lichtwechsels der veränderlichen Sterne* (Berlin: Akademie-Verlag, 1952), from which we learned that Hoffmeister has concluded from observations made by him (Mitt. über veränderliche Sterne, No. 13; Kl. Veröff. Berlin-Babelsberg, No. 27) that Z Scl is not variable.

JORGE SAHADE
JULIO ALBARRACÍN

OBSERVATORIO ASTRONÓMICO
CÓRDOBA, ARGENTINA
July 10, 1952

[10] Unsöld and Struve, *Ap. J.*, **91**, 365, 1940.

[11] *An Atlas of Stellar Spectra* (Chicago: University of Chicago Press, 1943).

ERRATA

In *Ap. J.*, **116**, 220, 1952, equation (10) should read $K = \frac{1}{2}(V_{max} - V_{min})$.

JOHN B. IRWIN

The FACE of the MOON

BY RALPH B. BALDWIN

An answer, in terms of the meteorite theory, to the question of how the moon came to exist in its present form.

The study of the moon—a mirror for the study of the earth.

256 pages. 6¾"×9¼". Illustrated. $5.00.

THE UNIVERSITY OF CHICAGO PRESS

New Model!

35-mm. EXAKTA "VX"

Single Lens Reflex Camera

One lens both for viewing and picture taking assures perfect sharpness, accurate exposure, maximum depth of field, and instant interchange for color. You always see the exact image before you take the picture—whether the subject is an inch or a mile away, whether it is microscopic or planetary, whether it is moving or stationary. Instantly interchangeable lenses permit selection of wide angle, close-up, copy and telescope photography. With f2.8 Zeiss Tessar "T" Coated Lens with Pre-Set Diaphragm Control . . . . . $269.50 cut included

Write Dept. 1100 For Free Booklet "X"

NATURE PHOTOGRAPHY WITH MINIATURE CAMERAS by Alfred M. Bailey (Denver Museum of Natural History). This eminent explorer and scientist displays his finest Exakta photographs and others along with explanatory material. 35 full page photographs, 64 pages 50c

EXAKTA CAMERA COMPANY
45 W. 29th St. New York 1, N.Y.

A Completely Revised Edition

THE ATMOSPHERES OF THE EARTH AND PLANETS

By GERARD P. KUIPER

Important new material has been added to make this edition the most modern and complete monograph on planetary atmospheres.

Additions include:

—Information recently obtained in V-2 flights about our upper air and the *x*-ray spectrum of the sun.

—Identification of the strong red and infrared emissions of the night sky.

—A new determination of the cosmic abundances of the chemical elements.

—A derivation of the exact temperature in the upper stratosphere.

—A determination of the age of meteorites.

—A discussion of the presence of nitrous oxide in the lower atmosphere and its connection with the life cycle.

—A reconstruction of the conditions leading to the escape of the "proto-atmosphere."

—A new section on Jovian planets.

—A development of the atmospheric conditions on Mars.

Paperbound $3.50 *Clothbound $5.00*

THE UNIVERSITY OF CHICAGO PRESS
5750 ELLIS AVENUE CHICAGO 37, ILLINOIS

IMPORTANT BOOKS IN THE HISTORY OF ASTRONOMY

THE ARYABHATIYA OF ARYABHATA
An Ancient Indian Work on Mathematics and Astronomy

Translated with Notes by WALTER EUGENE CLARK

Aryabhata's work, which was composed in A.D. 499, is probably the earliest preserved Indian mathematical and astronomical text bearing the name of an individual author; the earliest Indian text to deal specifically with mathematics; and the earliest preserved astronomical text from the third or scientific period of Indian astronomy. This is the first complete translation from the Sanskrit of this historical document.

120 pages 7½ × 5¼ $2.50

LATIN TREATISES ON COMETS BETWEEN 1238 and 1368 A.D.

By LYNN THORNDIKE

This volume publishes for the first time the Latin texts of important tracts on comets observed between 1238 and 1368 A.D. Among the treatises are works by Aegidius of Lessines, Gerardus de Silteo, Peter of Limoges, Geoffrey of Meaux, and John of Legnano. As a summary of the Aristotelian doctrine of comets, the commentaries of Thomas Aquinas and of Albertus Magnus on Aristotle's *Meteorology* are included in English translation.

286 pages 6 × 9 *Index* $5.00

THE SPHERE OF SACROBOSCO AND ITS COMMENTATORS

By LYNN THORNDIKE

A critical edition of the Latin text, together with an English translation, of the SPHERE of John of Sacrobosco—for centuries the best and best known manual of astronomy by a Western author. Also included is the hitherto unpublished commentary by Robert of England, with an English translation. In addition, the commentary of Cecco d'Ascoli and the commentary ascribed to Michael Scot are made available for the first time outside of rare books printed in abbreviated Latin.

506 pages 6 × 9 *Index* $10.00

THE UNIVERSITY OF CHICAGO PRESS